EURASIP Journal on Wireless Communications and Networking

Femtocell Networks

Guest Editors: Ismail Guvenc, Simon Saunders, Ozgur Oyman, Holger Claussen, and Alan Gatherer

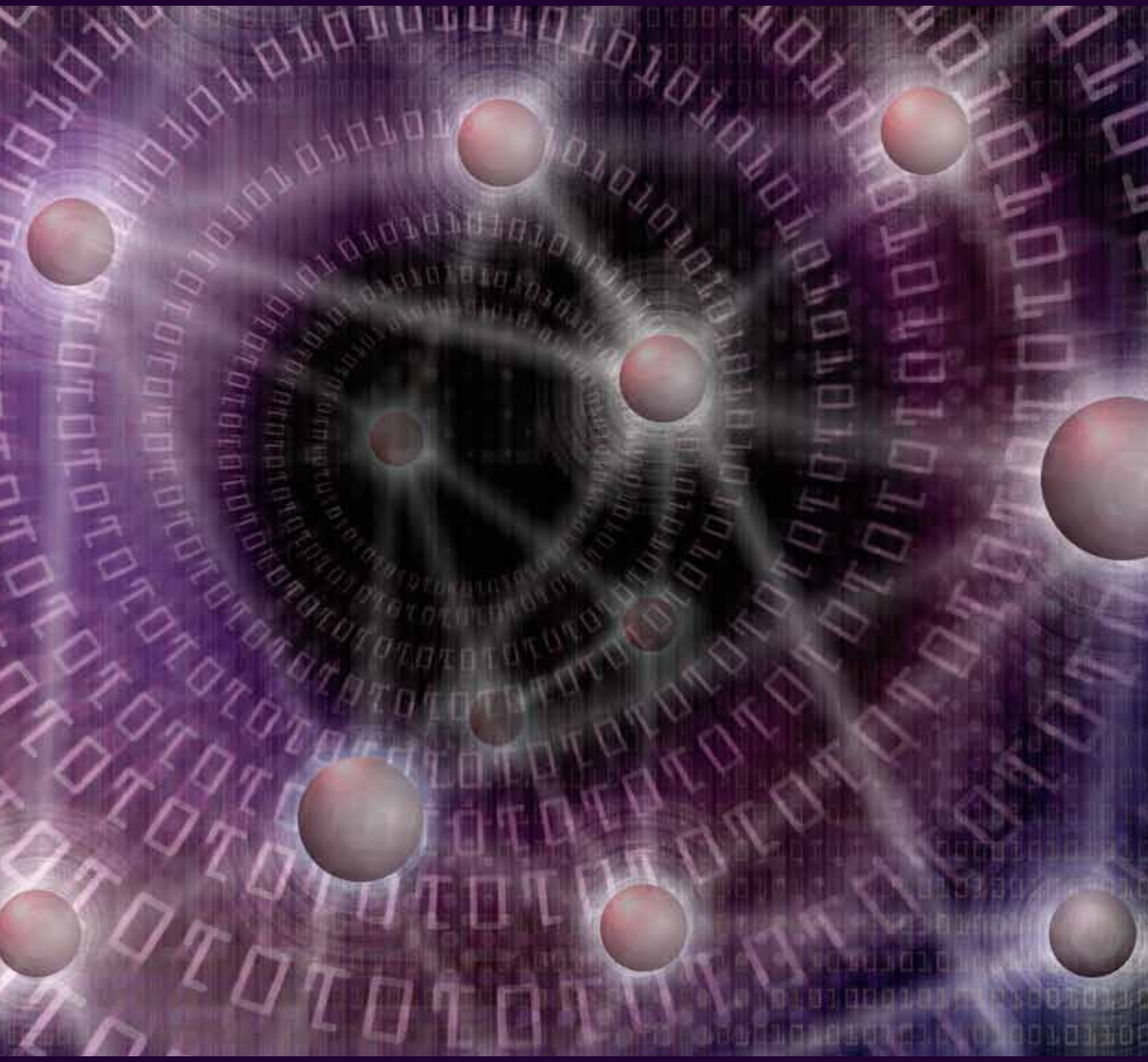

Femtocell Networks

EURASIP Journal on
Wireless Communications and Networking

Femtocell Networks

Guest Editors: Ismail Guvenc, Simon Saunders,
Ozgur Oyman, Holger Claussen, and Alan Gatherer

Contents

Femtocell Networks, Ismail Guvenc, Simon Saunders, Ozgur Oyman, Holger Claussen, and Alan Gatherer
Volume 2010, Article ID 367878, 2 pages

On Uplink Interference Scenarios in Two-Tier Macro and Femto Co-Existing UMTS Networks, Zhenning Shi, Mark C. Reed, and Ming Zhao
Volume 2010, Article ID 240745, 8 pages

A Semianalytical PDF of Downlink SINR for Femtocell Networks, Ki Won Sung, Harald Haas, and Stephen McLaughlin
Volume 2010, Article ID 256370, 9 pages

Intracell Handover for Interference and Handover Mitigation in OFDMA Two-Tier Macrocell-Femtocell Networks, David López-Pérez, Alvaro Valcarce, Ákos Ladányi, Guillaume de la Roche, and Jie Zhang
Volume 2010, Article ID 142629, 15 pages

Interference Mitigation by Practical Transmit Beamforming Methods in Closed Femtocells, Mika Husso, Jyri Hämäläinen, Riku Jäntti, Juan Li, Edward Mutafungwa, Risto Wichman, Zhong Zheng, and Alexander M. Wyglinski
Volume 2010, Article ID 186815, 12 pages

Joint Power Control, Base Station Assignment, and Channel Assignment in Cognitive Femtocell Networks, John Paul M. Torregoza, Rentsen Enkhbat, and Won-Joo Hwang
Volume 2010, Article ID 285714, 14 pages

A Bayesian Game-Theoretic Approach for Distributed Resource Allocation in Fading Multiple Access Channels, Gaoning He, Mérouane Debbah, and Eitan Altman
Volume 2010, Article ID 391684, 10 pages

Dynamic Resource Partitioning for Downlink Femto-to-Macro-Cell Interference Avoidance, Zubin Bharucha, Andreas Saul, Gunther Auer, and Harald Haas
Volume 2010, Article ID 143413, 12 pages

Best Signal Quality in Cellular Networks: Asymptotic Properties and Applications to Mobility Management in Small Cell Networks, Van Minh Nguyen, François Baccelli, Laurent Thomas, and Chung Shue Chen
Volume 2010, Article ID 690161, 14 pages

Hindawi Publishing Corporation
EURASIP Journal on Wireless Communications and Networking
Volume 2010, Article ID 367878, 2 pages
doi:10.1155/2010/367878

Editorial
Femtocell Networks

Ismail Guvenc,[1] Simon Saunders,[2] Ozgur Oyman,[3] Holger Claussen,[4] and Alan Gatherer[5]

[1] *Wireless Access Laboratory, DOCOMO USA Communications Laboratories, Palo Alto, CA 95051, USA*
[2] *Femto Forum, Guildford, UK*
[3] *Wireless Communications Laboratory, Intel Corporation, Santa Clara, CA 95054, USA*
[4] *Autonomous Networks and System Research Department, Alcatel-Lucent Bell Labs, Dublin 15, Ireland*
[5] *CTO of Baseband SoC at Huawei Technologies, Plano, TX 75075, USA*

Correspondence should be addressed to Ismail Guvenc, iguvenc@docomolabs-usa.com

Received 3 May 2010; Accepted 3 May 2010

Femtocells are small cellular base stations that may be deployed in residential, enterprise, or outdoor areas. They utilize the available broadband connections of the users (e.g., cable or DSL) and typically have a coverage radius on the order of ten meters or more. Due to their various advantages, recently there has been a growing interest in femtocell networks both in academia and in industry. Two of the main advantages of these networks include staggering capacity gains for next generation broadband wireless communication systems and the elimination of the dead-spots in a macrocellular network. Due to very short communication distances, femtocell networks offer significantly better signal qualities compared to the current cellular networks. This makes high-quality voice communications and high data rate multimedia type of applications possible in indoor environments. Small-size coverage also implies a reasonably accurate location capability without any sophisticated positioning protocol, which implies a wide range of promising applications within the domain of location-based services.

Despite several benefits, this new type of technology also comes with its own challenges, and there are important technical problems that need to be addressed for successful deployment and operation of these networks. Standardization efforts related to femtocell networks in 3GPP and IEEE are ongoing with full speed. In the meanwhile, there is also a growing interest in the academia towards fully exploiting the benefits of this promising technology. The goal of this special issue was to solicit high-quality unpublished research papers on design, evaluation, and performance analysis of femtocell networks. Based on the submitted manuscripts, eight manuscripts have been accepted, which will be summarized briefly in this editorial letter.

Probably the most important problem in femtocell networks is the presence of interference between neighboring femtocell networks and between the femtocell networks and the macrocell network. Our special issue opens with two papers that investigates the interference characteristics in femtocell networks. In "*On uplink interference scenarios in two-tier networks*", the authors Z. Shi et al. investigate uplink interference characteristics in a two-tier UMTS networks where a large number of femtocells are randomly deployed in the coverage area of a macrocellular network sharing the same carrier. Two severe interference scenarios are analyzed using simulations and it is shown that under these conditions both the femtocell and macrocell throughput is significantly reduced if no interference mitigation techniques are employed. In addition different interference mitigation techniques are discussed that can help to reduce this degradation.

In the second paper, Sung et al. derive the probability density function of the downlink signal-to-interference-plus-noise ratio (SINR) for neighboring femtocell networks in their paper titled "*A semi-analytical PDF of downlink SINR for femto-cell networks*". Their realistic mathematical model considers uncoordinated locations and transmission powers of base stations (BSs) which reflect accurately the deployment of randomly located femtocells in an indoor environment, also taking into account practical propagation models. Moreover, the accuracy of the resulting analysis on the SINR PDF is validated in the paper via Monte Carlo simulations. The benefit of this contribution is that the derived PDF can be easily calculated by employing standard numerical methods, obviating the need for time consuming simulation efforts.

After discussion of interference characteristics and statistics for different scenarios within the first two papers, the remaining papers in the special issue mostly focus on handling the interference problems in femtoecell networks. In the third paper titled "*Intracell handover for interference and handover mitigation in OFDMA two-tier macrocell-femtocell networks*", Perez et al. deal with the interference problems through intracell handover and power control techniques, which reduce the outage probability of the macrocell users that are in the vicinity of femtocell networks. Number of handover attempts and thus network signaling are also decreased with the proposed intracell handover methods.

Another approach to deal with the interference is to suppress it using multiple antenna techniques such as beamforming methods. In the article "*Interference suppression by practical transmit beamforming methods in closed femtocells*" by Husso et al., the authors utilize the availability of a control-only connection between a user equipment (UE) and an interfering femtocell base station (FBS) for interference suppression purposes. A simple two neighboring femtocell scenario is considered where the interfered UE requests the interfering FBS to replace its beamforming vector appropriately so that interference power directed to the interfered UE is minimized. While this reduces beamforming gain for a user connected to the interfering FBS, if used intelligently, it may prevent outages at neighboring femtocells with minimum performance degradation of the own users of the interfering FBS.

Efficient resource allocation techniques also carry critical importance for alleviating the impact of interference in femtocell networks. In "*Joint power control, base station assignment, and channel assignment in cognitive femtocell networks*" by Torregoza et al., the authors integrate cognitive radio and femtocell network technologies for developing joint power control, base station assignment, and channel assignment methods for femtocell networks. In order to address this complex problem, they define a multiobjective optimization framework with mixed integer variables; a pareto optimal solution is found through weighted sum approach, and the framework is shown to be both stable and converging. The results in the paper show that as the number of users in the network increases, significant gains can be obtained in the aggregate throughput when the proposed approach is deployed.

In a different paper titled "*Bayesian game-theoretic approach for distributed resource allocation in fading multiple access channels*" by He et al., a Bayesian game-theoretic model is developed to design and analyze the resource allocation problem in multiuser fading multiple access channels (MAC), where the users are assumed to selfishly maximize their average achievable rates with incomplete information about the fading channel gains. The major result of the paper is that it proves that there exists exactly one Bayesian equilibrium in such a game. Further studies on the network sum-rate maximization problem are also presented in this contribution considering symmetric user coordination strategies.

In "*Dynamic resource partitioning for downlink femto-to-macro-cell interference avoidance*" by Z. Bharucha et al., the problem of femtocell to macrocell interference for the downlink in LTE is addressed through dynamic resource partitioning, where femtocells are denied access to radio resources used by macro-UEs in their vicinity. The proposed coordination is achieved by using the downlink high interference indicator messages that are configured based on macro-UE measurements and sent by the eNB over the wireline backbone to HeNBs if required. It is demonstrated through simulations that in the investigated closed-access femtocell scenario the capacity of affected macro-UEs in vicinity of a femtocell can be increased by up to tenfold for a sacrifice of 4% of the overall femtocell downlink capacity.

Finally, in "*Extremal signal quality in cellular networks: asymptotic properties and applications to mobility management in small cell networks*", V. M. Nguyen et al. investigate the critical issues of extremal signal quality and mobility management in small-cell networks accounting for the characteristics of high density and randomness of small cells. Considering the asymptotic regime as the number of cells tends to infinity, the paper utilizes extreme value theory to derive the distribution of the extremal signal quality and establishes an analytical model to find the optimal number of cells to be scanned for maximizing the data throughput, leading to an optimized random cell scanning scheme.

We would like to take this opportunity to express our gratitude to the Editor-in-Chief of EURASIP Journal of Wireless Communications and Networking, Dr. Luc Vandendorpe, for giving us the opportunity to initiate this special issue; the editorial staff at Hindawi Publishing for their tremendous assistance during the progress of the special issue; the anonymous reviewers for their detailed and timely reviews which helped us to select the best papers among the submitted papers; and all the authors who considered our special issue for submitting their papers. We hope that you will enjoy reading this special collection of high-quality articles on femtocell networks and also hope that these papers will trigger new research ideas and directions for the successful deployment of this new technology.

Ismail Guvenc
Simon Saunders
Ozgur Oyman
Holger Claussen
Alan Gatherer

Hindawi Publishing Corporation
EURASIP Journal on Wireless Communications and Networking
Volume 2010, Article ID 240745, 8 pages
doi:10.1155/2010/240745

Research Article

On Uplink Interference Scenarios in Two-Tier Macro and Femto Co-Existing UMTS Networks

Zhenning Shi,[1] Mark C. Reed,[2,3] and Ming Zhao[2,3]

[1] *Alcatel Lucent-Shanghai Bell, China*
[2] *NICTA, Canberra Research Laboratory, Locked Bag 8001, Canberra ACT 2601, Australia*
[3] *The Australian National University, Australia*

Correspondence should be addressed to Mark C. Reed, mark.reed@nicta.com.au

Received 4 September 2009; Revised 30 November 2009; Accepted 2 March 2010

Academic Editor: Holger Claussen

A two-tier UMTS network is considered where a large number of randomly deployed Wideband Code Division Multiple Access (WCDMA) femtocells are laid under macrocells where the spectrum is shared. The cochannel interference between the cells may be a potential limiting factor for the system. We study the uplink of this hybrid network and identify the critical scenarios that give rise to substantial interference. The mechanism for generating the interference is analyzed and guidelines for interference mitigation are provided. The impacts of the cross-tier interference especially caused by increased numbers of users and higher data rates are evaluated in the multicell simulation environment in terms of the noise rise at the base stations, the cell throughput, and the user transmit power consumption.

1. Introduction

Recent decades have witnessed an unprecedented growth in the achieved data rate and the quality of service (QoS) in wireless communications.

A coarse breakup on the increased capacity reveals that most cellular throughput improvement comes from better area spectrum efficiency. Mobile broadband communication solutions with high spectral efficiency are needed for indoors where demands for higher data rate services and better coverage are growing, for example, residential or office scenarios. It is difficult to provide this coverage and data throughput by macro-cellular networks. This forms the basic foundation that motivates the recent emerging femtocell architecture. Femtocells are essentially an indoor wireless access points for connectivity to the networks of wireless cellular standards. It serves home users with low-power, short-range base stations such as the 3GPP definition of a Home NodeBs (HNB). By enhancing the capacity and coverage indoors, where a majority of user traffic originates, HNBs also bring substantial benefits to the macronetwork as the macrocell resources can be redirected to outdoor subscribers. In addition, femtocell deployment can bring substantial cost savings to operators by reducing operational costs (OPEX) and capital costs (CAPEX) as well as the churn rate from subscribers.

The introduction of femtocells gives rise to a number of technical challenges [1], for example, the IP interface to the backhaul network, closed or open access, synchronization and interference. Due to the scarcity of the radio spectrum resources, femtocells are likely to share the same carriers with the existing macrocells, which may cause interference across the two cellular layers. In particular, operators have concerns on the impact of femtocells onto the macrocells. To this end, an in-depth analysis on interference problems is needed. A comprehensive description of interference cases that exist in the uplink and downlink of the two-tier hybrid networks is given in [2]. These cases are conceptually illustrated through the simple models consisting of a couple of cells, and the analytical results of the basic scenarios are summarized together with the guidelines for interference mitigation. In the downlink, the deployment of femtocells may create multiple dead zones in the macrocell. The cochannel interference can be mitigated by using cognitive radio and adaptive power management techniques in the home base stations [2, 3].

In [4], a stochastic geometry model is employed to characterize the air interface statistics in large-scale hybrid networks, and Poisson-Gaussian sources are used to approximate the interference within and between the tiers. This approach allows the analysis to reflect the randomness of the network. However, it is assumed in [4] that users in both layers are under good coverage from their serving nodes, which may not always be the case in realistic scenarios. In [5] the femtocell capacity is shown in terms of the deployment of femtocells, user distribution in femtocells as well as the user excursion into neighbouring femtocells. In [6], the authors study the effect of access policy on a macro cellular network with embedded femtocells and suggest it should be adaptive to specific scenarios and the perspective of all participants in the system. It is found that by allowing a limited access to the femtocells, the similar QoS level to that of the macro-only scenario and much improved throughputs for all subscribers can be achieved.

In [1], a femtocell configuration is shown to improve the spectral efficiency of the network by orders of magnitude. In [4], time hopping and directional antenna are proposed to interference and further increase the capacity. A utility-based power control method is proposed in [7] to mitigate the cross-tier interference at the expense of a reasonable degradation in the femtocell SINR. Nevertheless, it is based on the assumption that the user penetration between layers is not severe, that is, the users from one layer are not likely to come within the vicinity of the NodeBs in the other layer and cause substantial cross-tier interference. We note that if open access is not supported for femtocells, user penetration inevitably leads to an adverse condition for both femtocells and macrocells. This calls for more research efforts in this area.

In this paper, we consider the uplink (UL) interfering scenarios in the WCDMA femtocells with a macronetwork overlay. The motivation for focusing on the uplink is to better understand the noise-rise onto the macro base stations and to understand what improved sensitivity at the femtocell would mean to overall system performance. To be in line with the current approach, we consider the closed subscriber group (CSG) femtocell where the home network is only accessible by a limited number of subscribers. We assume a shared carrier for femto and macronetworks, whereby the options of frequency and time hopping [4] and dedicated carriers for femtocells are excluded. In particular, two interference scenarios that UE penetration triggers in the uplink, that is, what we refer to as the "Kitchen Table problem" and "Backyard problem", are studied to show the cases that may cause a service disruption in the system of interest. The analysis is conducted in a large-scale system and takes into account other interfering sources [2] in the network air interface. It also provides a comprehensive study on how different interfering causes are inextricably linked and take effects jointly. In this paper, the interference mitigation techniques are considered to enable the network operation even in the extreme cases.

The paper is organized as follows. In Section 2, two uplink interfering scenarios under consideration are described, together with, the system parameters used in the system analysis. In Section 3, the noise rise at macro NodeBs (MNB)

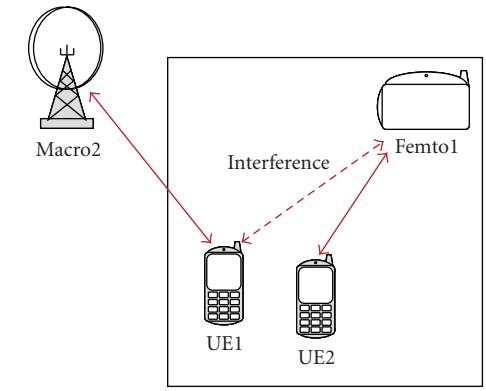

(a) Kitchen Table UE

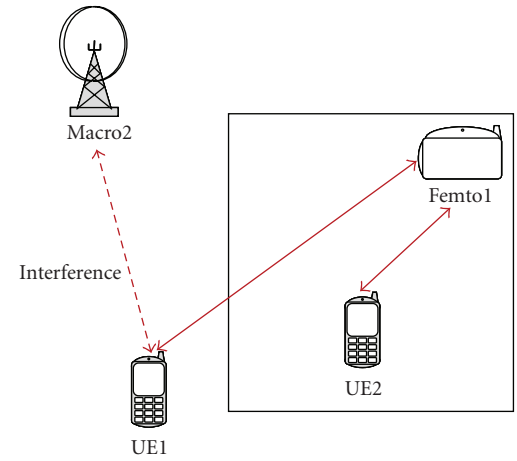

(b) Backyard UE

Figure 1: Illustrative examples of two interfering scenarios in the femtocell uplink.

is formulated and serves as a basis to separate the interfering sources in the uplink. A number of interference management techniques tackling the intercell and intracell interference are then presented. In Section 4, system simulation results are presented for suburban and urban scenarios to show the interference effect on both the macro and femto layers. Conclusions are summarized in Section 5.

2. System Model

2.1. Uplink Interfering Scenarios. Femtocells can support high data rate services since the transmitter and receiver are very close to each other and the resultant transmit power is very low. However, this is no longer the case when uncoordinated subscribers come to the vicinity of the femtocell HNB. Diagram in Figure 1(a) illustrates the scenario [2], where one macrocell and one femtocell coexist. Subscriber UE 1 is connected to the macrocell and termed as the MUE, while subscriber UE 2 camps on the femtocell and is referred to as the HUE. In this case, UE 1 enters into the household of the femtocell and causes strong interference at HNB. At the (macro-) cell-edge location, the interference becomes overwhelming as UE 1 transmit power

is close to the maximum. This MUE causes the case, what we call the Kitchen Table user (KTU) problem, where on a kitchen table there could be both femto connected and macro connected terminals. The macroconnected terminals generate high interference due to the short distance between them and the affected HNB.

The other scenario that causes noticeable uplink interference takes place when the HUE, that is, the users on the femtocells, moves outside the household and continues the femtocell service. Since the femto-connected user's signal now penetrate through the home residence, the HUE has to transmit at a much higher power level than its indoor counterparts. Classified as Scenario D in [2], we name this user the Backyard User (BYU), and thus it generates the BYU problem discussed in the paper. In Figure 1(b), both users are connected to the femtocell, while UE 2 is inside the house where the HNB coverage is good, and the other user, UE 1, is on the edge of the HNB coverage. UE 2 introduces significant interference onto the Macro layer as well as to neighbouring femtocells. In the cases where the femtocell under consideration is close to the macrocell site, the noise rise from UE 1 at the macro NodeB can be significant.

The KTU and BYU problems are two extreme cases which may bring a disruption to the network service. Although the primary victims of BYU and KTU scenarios are the macro NodeB (MNB) and HNB, respectively, our analysis shows that they are not independent but rather inextricably linked, that is, one problem may enhance the other. To understand this, let us look at an example where the KTU and BYU problems happen simultaneously in the femtocell, that is, there is a KTU close to the HNB while an HUE outside of the house. In this case, the backyard HUE has to further increase the power to overcome the interference from the uncoordinated KTU. By doing so, it aggravates the resource constraint in the uplink by adding more interference at the macrobase station. Keeping this in mind, our study aims to reveal the joint effect of these two issues, rather than study them in separate scenarios.

2.2. System Simulation Assumptions. In this section, we introduce the cellular environments where the uplink of the hybrid network is studied. In Table 1, simulation parameters of macrocells and femtocells are specified for suburban and urban scenarios, respectively. The following assumptions are stipulated in the system model:

(i) A three-tier 37 macro-cell structure is considered for macronetwork where the macro NodeB of interest is in the center and the frequency reuse factor is one.

(ii) All mobiles terminals are uniformly distributed in the macrocells and femtocells, except that the outdoor HUEs are on the femtocell boarder and at the nearest side to the macrocell base station.

(iii) Directional antennas (sectorisation) are employed at the macro base stations to increase the capacity while omni-directional antennas are employed at the femto HNBs.

(iv) The residential home penetration loss is 10 dB.

(v) Outdoor HUE penetration, that is, the percentage of BYUs in the total population of HUEs, conforms to those in [8].

(vi) Indoor MUE penetration refers to the percentage of the KTUs in the total population of MUEs.

(vii) For macrocell service, only voice calls are used. While for femto cells, three types of services are specified in Table 2, ranging from the voice call to medium data rate services.

(viii) Perfect power control is assumed at both macro base stations and femtocell HNBs (Here HUE power is determined to guarantee the assigned data service under the power cap.).

3. Uplink Interference Management

As the uncoordinated UEs get close to nonserving NodeB, they typically introduce at these NodeBs interference that is significant w.r.t. the noise floor. Interference from a few such aggressors may cause service disruption in the affected cell. Even in cases where the services can be maintained, it is achieved at the cost of higher power consumption for UE. This in turn would deteriorate the services in other neighbouring NodeBs, that is, it forms a closed loop with positive feedback that makes the situation even worse. In this paper, the cost function to optimize is the Rise over Thermal (RoT) at macro base stations and HNB.

Assuming that the transmitted signals over the wireless link are primarily subject to the propagation loss, and that the downlink pathloss is the same as that in the uplink, the RoT at macro NodeB caused by a scheduled HUE is given by [9] as follows:

$$\mathrm{RoT}_{\mathrm{MNB}} = \Delta_P + \Delta_N + \rho_{\mathrm{HNB}} + \mathrm{RoT}_{\mathrm{HNB}} + \tau - \Delta, \quad (1)$$

where $\Delta_P = P_{\mathrm{HNB,max}} - P_{\mathrm{MNB,max}}$ is the difference between NodeB transmission power, $\Delta_N = N_{\mathrm{HNB}} - N_{\mathrm{MNB}}$ is the difference on the noise figures of NodeBs, ρ_{HNB} is the required carrier-interference-ratio (CIR) at HNB, $\mathrm{RoT}_{\mathrm{HNB}}$ is the receive interference (w.r.t. to noise floor) at HNB, τ is the average transmission power increase due to fast power control and Δ denotes the coverage difference at the position of HUEs between femto and macro cells. The RoT of HNB caused by an uncoordinated MUE (In this paper, we focus on the noise rise caused by femto-to-macro interference or vice versa, to highlight the impacts of femto deployment as well as simplify the analysis.) is given by

$$\mathrm{RoT}_{\mathrm{HNB}} = P_{\mathrm{MUE}} - L_{\mathrm{MUE\text{-}HNB}} - N_{\mathrm{HNB}}, \quad (2)$$

where P_{MUE} is the transmission power of the MUE and $L_{\mathrm{MUE-HNB}}$ is the pathloss between the MUE and the affected HNB. RoT leads to degradation in the receiver sensitivity, hence needs to be minimized. In the following, we present a number of techniques that mitigate the RoTs at NodeBs.

3.1. HNB Power Management. Typically good femtocell downlink coverage can be achieved more easily when

Table 1: System Parameter for Macro and Femtocells.

	Suburban scenario	Urban scenario
Macrocell parameters		
Macrocell Radius	1 km	500 m
Max. Macro NB Transmit Power	43 dBm	43 dBm
Maximum Indoor MUE (Kitchen Table User) Transmit Power	24 dBm	18 dBm
Maximum Outdoor MUE Transmit Power	14 dBm	8 dBm
Number of Sectors per Cell	3	6
Data Rate per MUE	15 kbps	15 kbps
Spreading Factor for MUE	128	128
Number of MUEs per km^2	26	229
Relative power of control channel	−6 dB	−6 dB
Asynchronous Uplink	Yes	Yes
Duty cycle for voice call	100%	100%
MUE Indoor Penetration	10%	10%
Femtocell parameters		
Femtocell Radius	15 m	10 m
Max. HNB Transmit Power	20 dBm	20 dBm
Shielding (Penetration) Loss	10 dB	10 dB
Area percentage occupied by HNB	2.4%	3%
Number of HUEs per HNB	2	2
Number of HUEs per km^2	68	190
Spreading factor for HUE	variant	variant
Duty cycle for data service	100%	100%
HUE Outdoor Penetration	20%	10%
HNB RoT threshold	12 dB	12 dB
Propagation loss model		
Macrocell	$133 + 35\log_{10}(d)$ dB	
Femtocell	$98.5 + 20\log_{10}(d)$ dB	
Voice	15 kbps	15 kbps
Low Rate Service	120 kbps	60 kbps
Medium Rate Service	360 kbps	120 kbps

femtocell location approaches the macrocell border. In these cases, a low transmit power by HNB suffices for the range of a normal residence. On the other hand, the HNB coverage is weak when the femtocell is close to the macro cell site due to the strong macro downlink interference. A fixed HNB power setup is suboptimal as it fails to provide constant femtocell coverage across the macrocell, and it may introduce excessive interference to the macrocell.

Adaptive HNB power is an effective means to minimize the impact on the macrocell while keeping a satisfying coverage within the femtocell. To this end, common pilot channel can be used to measure the downlink channel and an appropriate HNB power is determined. In [3], a mobility event-based algorithm is used in managing HNB pilot power to minimize the unwanted handover events of UEs when HNB is in operation. Employment of the adaptive scheme substantially reduces the HNB power consumption, which corresponds to a reduction on Δ_P in (1) and leads to a decreasing $\mathrm{RoT}_{\mathrm{MNB}}$ in turn.

Since femtocell deployment is not planned but rather random in nature, zero-touch self-configuration is preferred. To this end, a Network Listen Mode (NLM) is needed at HNB to scan the network air interface [10].

3.2. Handover Outdoor HUE to the Macrocells. Outdoor HUEs may generate severe inference at the macro base stations. This can be clearly seen in (1) where as the HUE moves to the femto cell border, the downlink coverage by the macro NodeB can be much better than that of the serving HNB, that is, Δ is small, while the resultant RoT at MNB increases. A viable solution is to handover the HUE to the macro layer. On one hand, this removes the outdoor HUEs from the serving HNB, and relieves the Backyard Problem. On the other hand, HUEs added onto the macro layer consume the system resources that would be otherwise allocated to MUEs. HUE handover techniques can be determined by evaluating the signal quality of the downlink CPICH channel of the serving HNB, w.r.t. that from nearby macro base stations.

3.3. Inter-Frequency Switch for MUEs in the Dead Zone. Femto deployment generates coverage holes called dead zones inside the macrocell. Macro UE in the dead zone undergoes tremendous cross-layer interference from the HNBs in the downlink and may experience a service disruption. On the other hand, macro UE inside the dead zone causes severe interference to the femtocell uplink transmission. This can be observed in (2) where $\mathrm{RoT}_{\mathrm{HNB}}$ dramatically increases when $L_{\mathrm{MUE\text{-}HNB}}$ is small. In this case, switching of the MUEs inside the dead zone, that is, Kitchen Table UEs, to another carrier or Radio Access Technique (RAT) can effectively mitigate the problem in both femtocells and macrocells, given that the operator has alternative carriers.

3.4. Adaptive Uplink Attenuation. On average, the transmission power of femto HUEs is below that of macro UEs, due to the much shorter transmission range. Nevertheless, the dynamic range of a receiver frontend (RF) is large at the HNB and can cope with strong interference from uncoordinated UEs in extreme cases. If the noise figure N_{HNB} is fixed, the interference caused by uncoordinated Kitchen Table MUE results in a substantial noise rise $\mathrm{RoT}_{\mathrm{HNB}}$. This in turn reduces the uplink throughput (number of users) that the HNB can support significantly [8, 11]. To resolve the problem, an additional UL attenuation gain is proposed for the receiver RF at the HNB to deal with the surging interference [8, 11].

We study the problem by assuming that the femtocells affected by Kitchen Table User can be anywhere, rather than

Table 2: Impact on macrocell throughput and range.

	Data rate	Receiver mode	Macro rate reduction in [%]		Increase in the number of macro-BS in [%]	
			Urban	Suburban	Urban	Suburban
Case 1	Medium	Conv.	3.3	3.7	0.4	0.2
Case 2	Medium	Conv.	40.0	25.9	50.9	15.9
Case 2	Medium	Adv.	10.0	3.7	0.4	0.2
Case 3	Voice	Conv.	3.3	3.7	0.4	0.2
Case 3	Low	Conv.	13.3	7.4	0.4	0.2
Case 3	Medium	Conv.	53.3	37.0	87.6	28.5
Case 4	Mix	Conv.	30.0	18.5	25.1	7.6
Case 4	Mix	Adv.	10.0	3.7	0.4	0.2

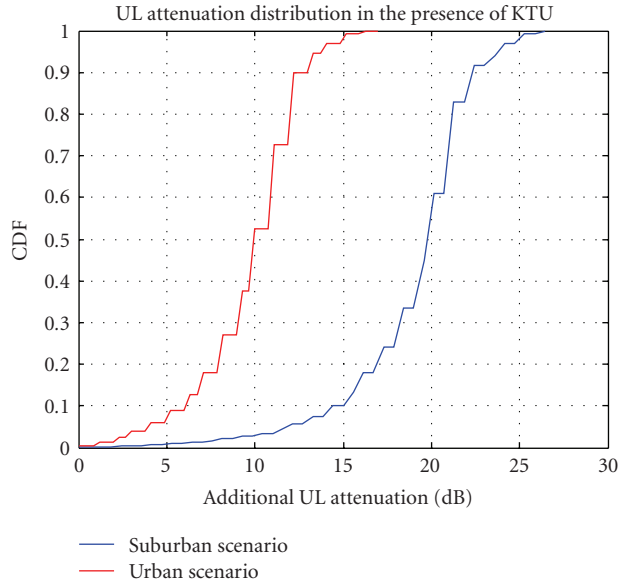

Figure 2: Distribution of adaptive UL attenuation gain when there is Kitchen Table MUE.

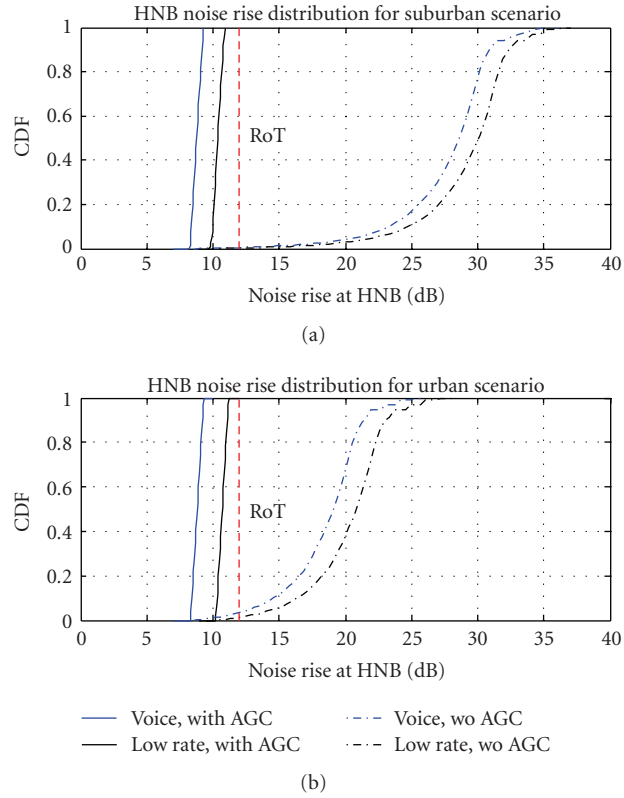

Figure 3: Distribution of rise over thermal (RoT) in a femtocell with nonconnected UE penetration.

on a few isolated points in the macro cell [2]. Depending on their positions in the macrocell, the effect of Kitchen Table MUEs on the femto cell is different, reflected by the distribution of the UL attenuation gain over a wide range. Figure 2 shows the distribution of the UL attenuation gain employed at the home NodeB RF frontend. It is observed that in suburban scenarios the attenuation gain can be as high as 30 dB, while in more than 90% of the cases the HNB receiver needs to attenuate the incoming signals by more than 15 dB. This number drastically decreases in urban areas, where only a marginal percentage of HNBs need to execute an additional attenuation gain of 15 dB. By doing so, the extravagant noise rise caused by the nonconnected UEs can be effectively controlled within the system-defined RoT threshold, which is marked as the red dashline in Figure 3.

It should be noted that using a large attenuation gain may increase the battery drain of the femto-connected terminals, reduce femtocell range, and cause additional interference onto neighboring femtocell HNBs and macro base stations. Therefore, it should be adaptive to the interference in the radio environment and applied only when it is necessary.

3.5. Downgrade Service of HUE. Under the strong interference from the Kitchen Table MUEs, the HUE can reduce the data rates of its services to relax the power requirements. This mechanism eliminates the unnecessary interference to other cochannel users but will compromise data throughput. In this paper, we let HUEs tune to the service of the highest supportable data rate if they can not achieve the target data rate. Moreover, HUE transmission power is capped at a maximum power of 21 dBm to avoid creating excessive interference.

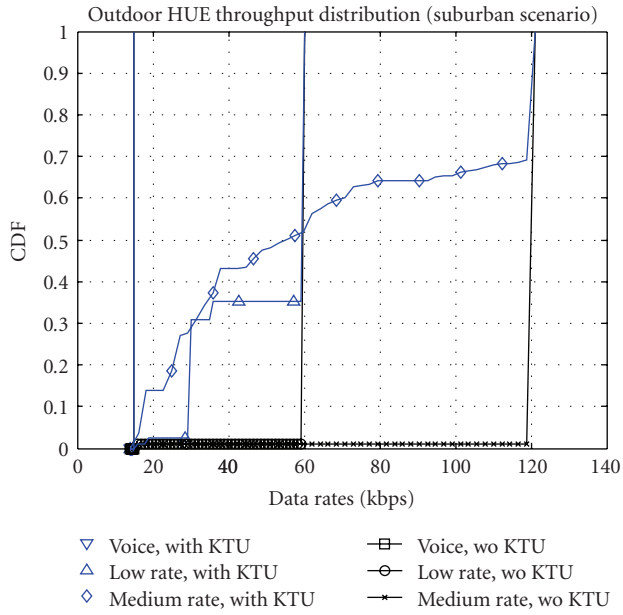

Figure 4: Distribution of outdoor HUE throughput in the presence of Kitchen Table MUEs.

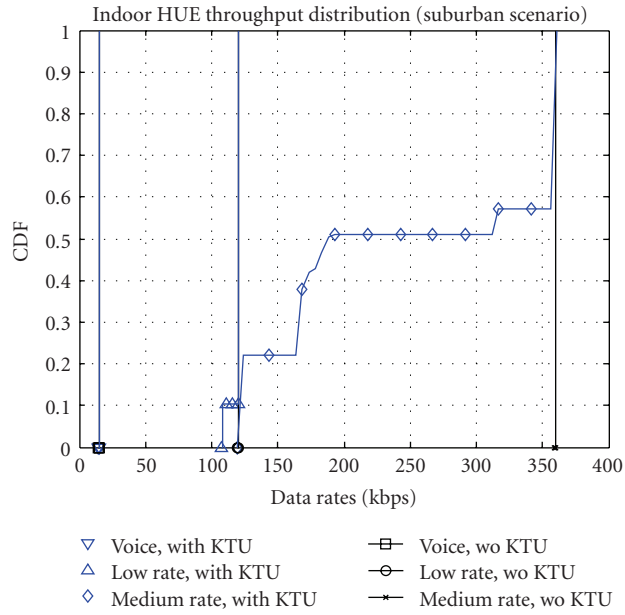

Figure 5: Distribution of indoor HUE throughput in the presence of Kitchen Table MUEs.

3.6. Improved Femtocell Receiver Sensitivity. Application of advanced methods to improve the femtocell sensitivity will reduce the transmit power from Femto-connected UEs. Different techniques can be used to achieve this including antenna diversity, interference cancellation, enhanced signal processing in synchronization, and channel estimation and equalization [12–14]. This not only enhances the performance in the femtocell, but also reduces the interference introduced to the macro layer as will be seen in the presented results.

4. Simulation Results

In this section, simulations are conducted in a femto-macro hybrid network specified in Section 2 to show the impacts of the femtocell deployment. The direct consequence of the Kitchen Table problem is to generate substantial noise rise at the affected HNBs and degradation in the HUE throughput. The increase in the HUE transmit power is shown as a result of the desensitized HNB receiver. The impact in the macro layer is studied by observing the noise rise and data throughputs in the macrocell. Unless specified otherwise, we use the parameters in Table 1 in all simulations. Adaptive power management is assumed at the home NodeBs such that a constant coverage is maintained for femtocells. The uplink attenuation technique in Section 3.4 is employed to mitigate the impact of the severe cross-tier interference.

Due to the strong interference of a macro-connected user, the Kitchen Table problem deteriorates the femtocell user performance significantly. Figures 4 and 5 show the rate distribution of three types of HUE services when there is Kitchen Table MUE against that in the absence of Kitchen Table MUEs. In suburban areas, it can be seen that for low data rate, around 35% of outdoor HUEs are served below the target rate of 60 kbps, while the ratio jumps to 68%

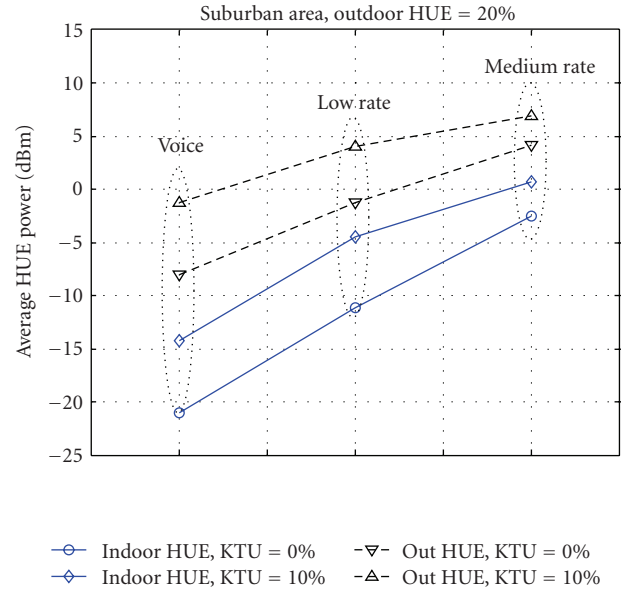

Figure 6: Average transmit power of HUEs in suburban scenario.

for medium data rate, reflecting a drastic degeneration in the uplink throughput. On the other hand, target rates can be easily achieved in cases where there is no Kitchen Table User. For indoor HUEs, the relative reduction is smaller in the presence of Kitchen Table UE. Nevertheless, the ratio of services staying below the target rate is still 57% for the medium rate service.

There is typically enough headroom in the femtocell UE transmit power due to the short transmission range. However, this is no longer the case when the Kitchen Table problem or Backyard problem occurs. Figure 6 shows the average transmission power of indoor and outdoor HUEs

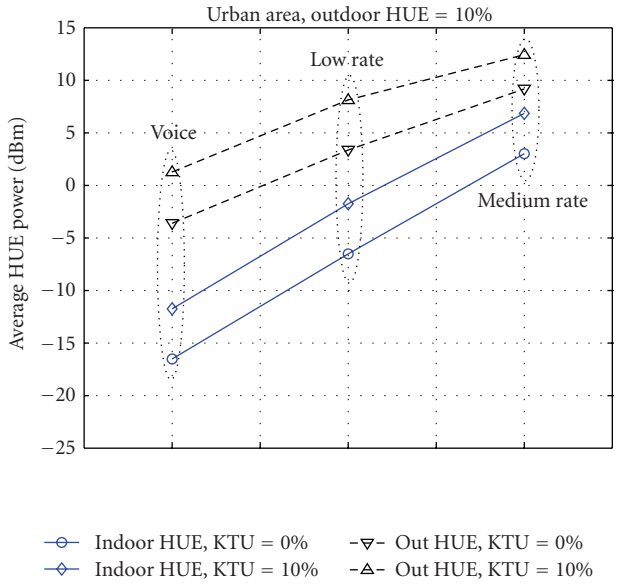

Figure 7: Average transmit power of HUEs in urban scenario.

in the suburban scenario. It can be seen that even though the outdoor HUEs are on services of lower data rates, their power consumption is typically 5~15 dBm higher than that of the indoor counterparts. This can be explained by noting that outdoor HUEs have to use extra transmit power to compensate for the more significant pathloss, including the building penetration loss. It is also observed that the presence of Kitchen Table MUEs leads to a drastic increase on the power consumption for affected femtocell users. Figure 7 shows the average power for HUEs in urban scenario, which has a similar trend to that in suburban scenario.

The Kitchen Table problem is considered as the worst scenario for the HNB where the uncoordinated MUEs introduce significant interference into the femtocell uplink. Nevertheless, from (1) it can be seen that a noise rise in the femtocell can also affect the macro-NodeB, since HUEs in the femto cells need to boost up their transmission power to improve the received signal quality at the HNB. In [2], this is classified as an undesired UE noise rise at non-serving NodeBs. To clearly show the impacts of HUEs, jointly with Kitchen Table and Backyard problems on the macrocell, four test cases are defined as follows.

(i) *Case* 1. *No Kitchen Table or Backyard Problem*. All HUEs stay inside their homes and are under good coverage of the serving HNB, while all MUEs are outside the femtocell households.

(ii) *Case* 2. *Backyard Problem Only*. A number of HUEs are on the femtocell edge (specified for suburban and urban scenarios), while macro UEs stay clear of the femtocell households.

(iii) *Case* 3. *Joint Kitchen Table and Backyard Problems*. A number of HUEs are at the femtocell edge and some MUEs are inside the units with femtocells. The percentage of outdoor HUEs and indoor MUEs is specified in Table 1.

(iv) *Case* 4. *Mixed Service*. The break up of indoor and outdoor HUE services is 70%, 20%, and 10% for voice calls, low rate services, and medium-rate services, respectivlely.

In the simulations, a baseline system equipped with conventional receiver techniques is considered. Table 2 includes the reduction in macrocell throughput due to the introduction of femtocells. It can be seen from that in Case 1, with neither Kitchen Table nor Backyard problems, interference from femtocells is tolerable and causes a marginal loss in the macrocell. The rate loss is below 5% in both urban and suburban scenarios.

In Case 2, which embodies the Backyard User problem only, the macro throughput loss increases substantially, especially for services of higher data rates. The rate reduction caused by medium rate femtocell services is 40% and 26% for urban and suburban scenarios, respectively. Results for voice and low data rates show marginal performance degradation in Cases 1 and 2, and hence omitted from the table.

Case 3 takes into account both Kitchen Table and Backyard problems, hence represents the worst scenario for the hybrid radio network. While a rate loss of no more than 15% is observed in macrocell for low rate femtocell services, the throughput compromise jumps to 53% and 37% for medium rate services, in suburban and urban scenarios. It indicates that the capacity increase in femtocells may trigger substantial macrocell performance degradation if severe Kitchen Table and Backyard problems exist.

Case 4 represents a service portfolio that is akin to the realistic traffic in the femtocell. In this case, macrocell throughput reduction can be up to 30% and 18% in urban and suburban scenarios, while improvements in receiver sensitivity are able to mitigate the problem by a great extent. We consider advanced techniques that can improve the sensitivity of the single user decoding chain by a couple of dBs and are able to cancel 80% of the intracell interference (In [14], it is shown that around 2 dB improvement in receiver sensitivity can be achieved for a moderately loaded UMTS by employing data-aided channel estimation. Using the soft interference cancellation (SIC), 80% of interfering power can be removed if the BER in the previous decoding iteration is below 0.05).

To better understand the consequence of the femtocell coexistence onto the macrocell, the increase in the MNB number is included in the right-most columns in Table 2. It can be seen that for Case 4 traffic, much more operator infrastructure is needed to maintain sufficient QoS with conventional receiver techniques. While the degradation becomes negligible if advanced signal processing is employed.

It is also observed that compared to the macrocells in suburban areas, macrocells deployed in the urban scenario are more subjected to the interference from the femtocells. This is because the urban macrocells have a much smaller range and the base station is closer to the femtocells. Moreover, due to the higher density of femtocell populations and the fact that the HUEs are more likely to be at the cell edge (refer to Table 1), urban macro base stations are

interfered by more users in the femto layer, especially those causing strong interference.

5. Conclusion

The new wireless configuration using femtocells is an appealing application to enhance the indoor service in residential areas, hot spots, and macro cellular environments, while reducing operator costs. Due to the randomness of femtocell deployments, it is crucial to understand the impacts of femtocells on the existing networks and try to minimize these effects. In this paper, we consider a hybrid network with coexisting femto and macrocells, and provide a comprehensive study on the impacts of deploying a large number of femtocells in the shared spectrum with macro cells. In particular, two severe interference scenarios caused by penetration of nonconnected UE to the other layer are analyzed. Our analysis considers a large cellular network and discusses a number of interference management schemes to improve the situation. We show through simulation that the Kitchen Table problem is the worst case scenario and on average 57% of indoor and 68% of outdoor HUEs cannot achieve the target throughput. Due to such strong interference from uncoordinated MUE, the HUE consumes 5∼10 dB more power than it normally needs. Such HUE power boosting also produces undesired noise rise at macro BS. Our results show that up to 53% and 37% macrocell throughput reductions are observed at macro BS in suburban and urban scenarios, respectively. Together with these simulation results, guidelines for minimizing the impacts of embedded femtocells on the underlying macrocells are presented.

Acknowledgments

Z. Shi was with NICTA and affiliated with the Australian National University when the work was done. He is currently with Alcatel-Lucent Shanghai Bell. M. C. Reed and M. Zhao are with NICTA and affiliated with the Australian National University. NICTA is funded by the Australian Government as represented by the Department of Broadband, Communications and the Digital Economy and the Australian Research Council through the ICT Centre of Excellence program.

References

[1] V. Chandrasekhar, J. G. Andrews, and A. Gatherer, "Femtocell networks: a survey," *IEEE Communications Magazine*, vol. 46, no. 9, pp. 59–67, 2008.

[2] "Interference management in UMTS femtocells," *Femto Forum White Paper*, December 2008.

[3] H. Claussen, L. T. W. Ho, and L. G. Samuel, "Self-optimization of coverage for femtocell deployments," in *Proceedings of the 7th Wireless Telecommunications Symposium (WTS '08)*, pp. 278–285, Pomana, Calif, USA, April 2008.

[4] V. Chandrasekhar and J. G. Andrews, "Uplink capacity and interference avoidance for two-tier cellular networks," in *Proceedings of the IEEE Global Telecommunications Conference (GLOBECOM '07)*, pp. 3322–3326, Washington, DC, USA, November 2007.

[5] D. Das and V. Ramaswamy, "On the reverse link capacity of a CDMA network of femto-cells," in *Proceedings of the IEEE Sarnoff Symposium*, pp. 1–5, Princeton, NJ, USA, April 2008.

[6] D. Choi, P. Monajemi, S. Kang, and J. Villasenor, "Dealing with loud neighbors: the benefits and tradeoffs of adaptive femtocell access," in *Proceedings of the IEEE Global Telecommunications Conference (GLOBECOM '08)*, pp. 1–5, New Orleans, La, USA, December 2008.

[7] V. Chandrasekhar, J. G. Andrews, T. Muharemovic, Z. Shen, and A. Gatherer, "Power control in two-tier femtocell networks," *IEEE Transactions on Wireless Communications*, vol. 8, no. 8, pp. 4316–4328, 2009.

[8] R4-082309, "Text proposal for HNB TR25.9xx: guidance on UL interference testing," *picoChip Designs, Airvana, AT&T, ip.access and Vodafone*.

[9] R4-080154, "Simulation results for Home NodeB to Macro NodeB uplink interference within the block of flats scenario," *Ercisson*.

[10] J. Edwards, "Implementation of network listen modem for WCDMA femtocell," in *Proceedings of the IET Seminar on Cognitive Radio and Software Defined Radios: Technologies and Techniques*, pp. 1–4, London , UK, September 2008.

[11] R4-080154, "HNB and macro uplink performance with adaptive attenuation at HNB," *Qualcomm Europe*.

[12] A. Lampe, "Iterative multiuser detection with integrated channel estimation for coded DS-CDMA," *IEEE Transactions on Communications*, vol. 50, no. 8, pp. 1217–1223, 2002.

[13] R. Otnes and M. Tuchler, "Iterative channel estimation for turbo equalization of time-varying frequency-selective channels," *IEEE Transactions on Wireless Communications*, vol. 3, no. 6, pp. 1918–1923, 2004.

[14] Z. Shi and M. C. Reed, "Iterative maximal ratio combining channel estimation for multiuser detection on a time frequency selective wireless CDMA channel," in *Proceedings of the IEEE Wireless Communications and Networking Conference (WCNC '07)*, pp. 1002–1007, Hong Kong, March 2007.

Hindawi Publishing Corporation
EURASIP Journal on Wireless Communications and Networking
Volume 2010, Article ID 256370, 9 pages
doi:10.1155/2010/256370

Research Article

A Semianalytical PDF of Downlink SINR for Femtocell Networks

Ki Won Sung,[1] Harald Haas,[2] and Stephen McLaughlin (EURASIP Member)[2]

[1] *KTH Royal Institute of Technology, 164 40 Kista, Sweden*
[2] *Institute for Digital Communications, The University of Edinburgh, King's Buildings, Edinburgh EH9 3JL, UK*

Correspondence should be addressed to Ki Won Sung, sungkw@kth.se

Received 31 August 2009; Revised 4 January 2010; Accepted 17 February 2010

Academic Editor: Ozgur Oyman

This paper presents a derivation of the probability density function (PDF) of the signal-to-interference and noise ratio (SINR) for the downlink of a cell in multicellular networks. The mathematical model considers uncoordinated locations and transmission powers of base stations (BSs) which reflect accurately the deployment of randomly located femtocells in an indoor environment. The derivation is semianalytical, in that the PDF is obtained by analysis and can be easily calculated by employing standard numerical methods. Thus, it obviates the need for time-consuming simulation efforts. The derivation of the PDF takes into account practical propagation models including shadow fading. The effect of background noise is also considered. Numerical experiments are performed assuming various environments and deployment scenarios to examine the performance of femtocell networks. The results are compared with Monte Carlo simulations for verification purposes and show good agreement.

1. Introduction

Signal-to-interference and noise ratio (SINR) is one of the most important performance measures in cellular systems. Its probability distribution plays an important role for system performance evaluation, radio resource management, and radio network planning. With an accurate probability density function (PDF) of SINR, the capacity and coverage of a system can be easily predicted, which otherwise should rely on complicated and time-consuming simulations.

There have been various approaches to investigate the statistical characteristics of received signal and interference. The other-cell interference statistics for the uplink of code division multiple access (CDMA) system was investigated in [1], where the ratio of other-cell to own-cell interference was presented. The result was extended to both the uplink and the downlink of general cellular systems by [2]. In [3], the second-order statistics of SIR for a mobile station (MS) were investigated. In [4, 5], the prediction of coverage probability was addressed which is imperative in the radio network planning process. The probability that SINR goes below a certain threshold, which is termed outage probability, is another performance measure that has been extensively explored. The derivation of the outage probability can be found in [6–8] and references therein.

While most of the contributions have focused on a particular performance measure such as coverage probability or outage probability, an explicit derivation of the probability distribution for signal and interference has also been investigated [9, 10]. In [9], a PDF of adjacent channel interference (ACI) was derived in the uplink of cellular system. A PDF of SIR in an ad hoc system was studied in [10] assuming single transmitter and receiver pair.

In this paper, we derive the PDF of the SINR for the downlink of a cell area in a semianalytical fashion. A practical propagation loss model combined with shadow fading is considered in the derivation of the PDF. We also consider background noise in the derivation, which is often ignored in the references. Uncoordinated locations and transmission powers of interfering base stations (BSs) are considered in the model to take into account the deployment of femtocells (or home BSs) [11] in an indoor environment. It has been suggested that femto BSs can significantly improve system spectral efficiency by up to a factor of five [12]. It has also been found that in closed-access femtocell networks macrocell MSs in close vicinity to a femtocell greatly suffer from high interference and that such macrocell MSs cause destructive interference to femtocell BSs [13]. Thus, an accurate model for the probability distribution of the SINR

assuming an uncoordinated placement of indoor BSs can be vital for further system improvements. In spite of the recent efforts for the performance evaluation of femtocells, most of the works relied on system simulation experiments [12–17]. To the best of our knowledge, the PDF of SINR for the outlined conditions and environment has not been derived before.

Since shadow fading is generally considered to follow a log-normal distribution, the PDF of the sum of log-normal RVs should be provided as a first step in the derivation of the SINR distribution. During the last few decades numerous approximations have been proposed to obtain the PDF of the sum of log-normal RVs since the exact closed-form expression is still unknown [18–23]. So far, no method offers significant advantages over another [18], and sometimes a tradeoff exists between the accuracy of the approximation and the computational complexity. We adopt two methods of approximation proposed by Fenton and Wilkinson [19] and Mehta et al. [20] which provide a good balance between accuracy and complexity. The performance of both methods is examined in various environments and a guideline is provided for choosing one of the methods.

The derivation of SINR distribution in this paper is semi-analytical in the sense that the PDF can be easily calculated by applying standard numerical methods to equations obtained from analysis. Numerical experiments are performed to investigate the effects of standard deviation of shadow fading, the number of interfering BSs, wall penetration loss, and transmission powers of BSs. The results obtained are also validated by comparison with Monte Carlo simulations.

The paper is organised as follows. In Section 2, the PDF of the downlink SINR is derived. Numerical experiments are performed in various environments and the results are compared with Monte Carlo simulations in Section 3. Finally, the conclusions are provided in Section 4.

2. Derivation of the PDF of Downlink SINR

The derivation of the PDF of downlink SINR is divided into two parts. First, the SINR of an arbitrary MS is expressed depending on its location in Section 2.1. Methods of approximating the sum probability distribution of log-normal RVs are discussed and adopted in the SINR derivation. Second, the PDF of SINR unconditional on the location of the MS is derived in Section 2.2.

2.1. Location-Dependent SINR. Let us consider a femtocell which will be termed the cell of interest (CoI). The CoI is assumed to be circular with a cell radius R. We assume the MSs in the CoI to be uniformly distributed in the cell area. An arbitrary MS m is considered whose location is (r_m, θ_m), where $0 \le r_m \le R$ and $0 \le \theta_m \le 2\pi$. The MS m receives interference from L BSs that are a mixture of femto and macro-BSs. The network is modelled using polar coordinates where the BS of the CoI is located at the center and the location of the jth interfering BS is denoted by $(r_b(j), \theta_b(j))$. In a practical deployment of femtocell systems, the placement of BSs in a random and uncoordinated fashion is unavoidable and may generate high interference scenarios and dead spots particularly in an indoor environment.

Let P_s^t be the transmission power of the BS in the CoI. It is attenuated by path loss and shadow fading. Let X_s be the RV which models the shadow fading. It is generally assumed that X_s follows a Gaussian distribution with zero mean and variance $\sigma_{X_s}^2$ in dB. Thus the received signal power at the MS m from the serving BS, P_s^r, is denoted by

$$P_s^r = P_s^t G_b G_m C_s {r_m}^{-\alpha_s} \exp(\beta X_s), \tag{1}$$

where G_b and G_m are antenna gains of the BS and the MS, respectively, C_s is constant of path loss in the CoI, α_s is path loss exponent of CoI, and $\beta = \ln(10)/10$. The $\ln(\cdot)$ denotes natural logarithm. P_s^r can be rewritten as follows:

$$P_s^r = \exp[\ln(P_s^t G_b G_m C_s) - \alpha_s \ln r_m + \beta X_s]. \tag{2}$$

Note that an RV $Y = \exp(V)$ follows a log-normal distribution if V is a Gaussian distributed RV. Thus, P_s^r follows a log-normal distribution conditioned on the location of MS m. The PDF of P_s^r is given by

$$f_{P_s^r}(z \mid r_m, \theta_m) = \frac{1}{z\sigma_s\sqrt{2\pi}} \exp\left[\frac{-(\ln z - \mu_s)^2}{2\sigma_s^2}\right], \tag{3}$$

where $\mu_s = \ln(P_s^t G_b G_m C_s) - \alpha_s \ln r_m$ and $\sigma_s^2 = \beta^2 \sigma_{X_s}^2$.

Let I_j^r be the received interference power from the jth interfering BS. By denoting P_j^t as the transmission power from the jth BS, I_j^r results in

$$I_j^r = P_j^t G_b G_m C_j d_{mb}(j)^{-\alpha_j} \exp\left(\beta X_j\right), \tag{4}$$

where C_j and α_j are the path loss constant and exponent, respectively, on the link between the jth BS and MS m, and X_j is a Gaussian RV for shadow fading with zero mean and variance $\sigma_{X_j}^2$ on the link between the jth BS and MS m. Note that the transmission power of each interfering BS can be different since an uncoordinated femtocell deployment is considered. Path loss parameters and standard deviation of shadow fading can also be different in each BS in practical systems. The distance between MS m and the jth interfering BS is $d_{mb}(j)$, which is obtained from

$$d_{mb}(j) = \left[r_m^2 + r_b(j)^2 - 2 r_m r_b(j) \cos(\theta_m - \theta_b(j))\right]^{1/2}. \tag{5}$$

In a similar fashion to P_s^r, I_j^r follows a log-normal distribution with PDF given by

$$f_{I_j^r}(z \mid r_m, \theta_m) = \frac{1}{z\sigma_j\sqrt{2\pi}} \exp\left[\frac{-\left(\ln z - \mu_j\right)^2}{2\sigma_j^2}\right], \tag{6}$$

where $\mu_j = \ln(P_j^t G_b G_m C_j) - \alpha_j \ln d_{mb}(j)$ and $\sigma_j^2 = \beta^2 \sigma_{X_j}^2$.

Background noise can be regarded as a constant value by assuming the constant noise figure and the noise temperature. Let N_{bg} be the background noise power at MS m, given by

$$N_{bg} = kTW\varphi, \tag{7}$$

where k is the Boltzmann constant, T is the ambient temperature in Kelvin, W is the channel bandwidth, and φ is the noise figure of the MS. In order to make N_{bg} mathematically tractable, we introduce an auxiliary Gaussian RV X_n with *zero* mean and *zero* variance so that N_{bg} can be treated as log-normal RV with parameters of $\mu_n = \ln(kTW\varphi)$ and $\sigma_n = 0$. Note that N_{bg} has a constant value, and this is accounted for by the fact that the defined RV has zero variance. This particular definition is useful for the determination of the final PDF. By introducing X_n, N_{bg} can be rewritten as follows:

$$N_{bg} = kTW\varphi \exp(X_n) = \exp[\ln(kTW\varphi) + X_n]. \quad (8)$$

Let us consider a system with no interference arising from the serving cell such as an OFDMA or a TDMA system. The downlink SINR of MS m is denoted by γ_m, which is given by

$$\gamma_m = \frac{P_s^r}{\sum_{j=1}^{L} I_j^r + N_{bg}} = \frac{P_s^r}{\Upsilon}. \quad (9)$$

In (9), Υ denotes the sum of the interference powers and the background noise power. Since all of I_j^r and N_{bg} are log-normally distributed, Υ is the sum of $L + 1$ log-normal RVs. Note that the exact closed-form expression is not known for the PDF of the sum of log-normal RVs. The most widely accepted approximation approach is to assume that the sum of log-normal RVs follows a log-normal distribution. Various methods have been proposed to find out parameters of the distribution [19–21].

Let $Y_1, \ldots, Y_M$ be M independent but not necessarily identical log-normal RVs, where $Y_j = \exp(V_j)$ and V_j is a Gaussian distributed RV with mean μ_{V_j} and variance $\sigma_{V_j}^2$. The sum of M RVs is denoted by Y such that $Y = \sum_{j=1}^{M} Y_j$. Approximations assume that Y follows a log-normal distribution with parameters μ_V and σ_V^2.

The Fenton and Wilkinson (FW) method [19] is one of the most frequently adopted approximations in literature. It obtains μ_V and σ_V^2 by assuming that the first and second moments of Y match the sum of the moments of Y_j. It should be noted that the FW method is the only approximate method that provides a closed-form expression of μ_V and σ_V^2 [20]. Let us denote μ_n as μ_{L+1} and σ_n as σ_{L+1}. From [19], the PDF of Υ conditioned on the location of MS m is given as follows:

$$f_\Upsilon(z \mid r_m, \theta_m) = \frac{1}{z\sigma_\Upsilon\sqrt{2\pi}} \exp\left[\frac{-(\ln z - \mu_\Upsilon)^2}{2\sigma_\Upsilon^2}\right], \quad (10)$$

where μ_Υ and σ_Υ^2 are given by

$$\sigma_\Upsilon^2 = \ln\left[\frac{\sum_{j=1}^{L+1} \exp\left(2\mu_j + \sigma_j^2\right)\left(\exp\left(\sigma_j^2\right) - 1\right)}{\left[\sum_{j=1}^{L+1} \exp\left(\mu_j + \sigma_j^2/2\right)\right]^2} + 1\right],$$
$$\mu_\Upsilon = \ln\left[\sum_{j=1}^{L+1} \exp\left(\mu_j + \frac{\sigma_j^2}{2}\right)\right] - \frac{\sigma_\Upsilon^2}{2}. \quad (11)$$

In spite of its simplicity, the accuracy of the FW method suffers at high values of $\sigma_{V_j}^2$. This means that the method may break down when an MS experiences a large standard deviation of shadow fading from interfering BSs. Thus, we adopt another method of approximating the sum of log-normal RVs which gives a more accurate result at a cost of increased computational complexity.

The method proposed in [20], which is called MWMZ method in this paper after the initials of authors, exploits the property of the moment-generating function (MGF) that the product of MGFs of independent RVs equals to the MGF of the sum of RVs. The MGF of RV Y is defined as

$$\Psi_Y(s) = \int_0^\infty \exp(-sy) f_Y(y) dy. \quad (12)$$

By the property of MGF,

$$\Psi_Y(s) = \prod_{j=1}^{M} \Psi_{Y_j}(s). \quad (13)$$

While the closed-form expression for the MGF of log-normal distribution is not available, a series expansion based on Gauss-Hermite integration was employed in [20] to approximate the MGF. For a real coefficient s, the MGF of the log-normal RV Y is given by

$$\hat{\Psi}_Y(s; \mu_V, \sigma_V) \triangleq \sum_{j=1}^{M} \frac{w_j}{\sqrt{\pi}} \exp\left[-s \exp\left(\sqrt{2}\sigma_V a_j + \mu_V\right)\right], \quad (14)$$

where w_j and a_j are weights and abscissas of the Gauss-Hermite series which can be found in [24, Table 25.10]. From (13), a system of two nonlinear equations can be set up with two real and positive coefficients s_1 and s_2 as follows:

$$\sum_{j=1}^{M} \frac{w_j}{\sqrt{\pi}} \exp\left[-s_i \exp\left(\sqrt{2}\sigma_V a_j + \mu_V\right)\right] = \prod_{j=1}^{M} \hat{\Psi}_{Y_j}\left(s_i; \mu_{V_j}, \sigma_{V_j}\right), \quad i = 1, 2. \quad (15)$$

The variables to be solved by (15) are μ_V and σ_V. The right-hand side of (15) is a constant value which can be calculated with known parameters.

By employing (15), μ_Υ and σ_Υ^2 in (10) can be effectively obtained by standard numerical methods such as the function "fsolve" in Matlab. The coefficient $\mathbf{s} = (s_1, s_2)$ adjusts weight of penalty for inaccuracy of the PDF. Increasing $\mathbf{s}$ imposes more penalty for errors in the head portion of the PDF of Y, whereas smaller $\mathbf{s}$ penalises errors in the tail portion. Thus, smaller $\mathbf{s}$ is recommended if one is interested in the PDF of poor SINR region, while larger $\mathbf{s}$ should be used to examine statistics of higher SINR.

As shown in (3), the received signal power, P_s^r, follows a log-normal distribution. The sum of the received interference and the background noise power, Υ, was also approximated as a log-normal RV. Thus, the SINR of the MS m, γ_m, is the ratio of two log-normal RVs, which also follows

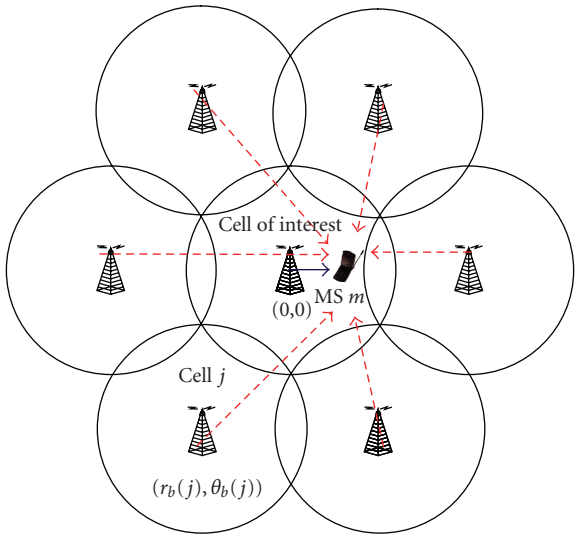

Figure 1: Locations of the CoI and the interfering BSs.

Table 1: Simulation parameters.

Parameter	Value
Cell radius	50 m
Path loss exponent	3.68
Path loss constant	43.8 dB
Center frequency	5.25 GHz
Channel bandwidth	10 MHz
MS noise figure	7 dB
BS transmission power	20 dBm
BS antenna gain	3 dBi
MS antenna gain	0 dBi
Number of interfering cells	6
Frequency reuse factor	1

Table 2: Kullback-Leibler Distance between the simulation and the analysis ($\times 10^{-4}$).

σ_{X_s} and σ_{X_j} [dB]	FW method	MWMZ method
3	6.00	6.98
4	3.66	4.34
5	11.32	6.05
6	35.70	8.81
7	90.50	12.29
8	186.87	16.24
9	324.10	21.23
10	489.04	26.13

a log-normal distribution. From (3) and (10), the PDF of γ_m is shown as

$$f_{\gamma_m}(z \mid r_m, \theta_m) = \frac{1}{z\sigma_{\gamma_m}\sqrt{2\pi}} \exp\left[\frac{-\left(\ln z - \mu_{\gamma_m}\right)^2}{2\sigma_{\gamma_m}^2}\right], \quad (16)$$

where $\mu_{\gamma_m} = \mu_s - \mu_Y$ and $\sigma_{\gamma_m}^2 = \sigma_s^2 + \sigma_Y^2$.

2.2. The PDF of Downlink SINR in a Cell. Up to this point, the PDF of the downlink SINR has been derived conditionally on the location of the MS m. Let us denote the location of MS m by ρ. Since it is assumed that MSs are uniformly distributed within a circular area, the PDF of ρ, $f_\rho(r_m, \theta_m)$, is as follows:

$$f_\rho(r_m, \theta_m) = \frac{r_m}{\pi R^2}. \quad (17)$$

From (16) and (17), the joint distribution of the SINR and the MS location is

$$f_{\gamma_m,\rho}(z, r_m, \theta_m) = f_{\gamma_m}(z \mid r_m, \theta_m) f_\rho(r_m, \theta_m) = \frac{r_m}{z\sigma_{\gamma_m} R^2 \sqrt{2\pi^3}} \exp\left[\frac{-\left(\ln z - \mu_{\gamma_m}\right)^2}{2\sigma_{\gamma_m}^2}\right]. \quad (18)$$

Let γ be the RV of the downlink SINR of an MS in an arbitrary location within a circular cell area. The PDF of γ can be obtained by integrating $f_{\gamma_m,\rho}(z, r_m, \theta_m)$ over r_m and θ_m. Thus, we get

$$f_\gamma(z) = \int_0^R \int_0^{2\pi} \frac{r_m}{z\sigma_{\gamma_m} R^2 \sqrt{2\pi^3}} \exp\left[\frac{-\left(\ln z - \mu_{\gamma_m}\right)^2}{2\sigma_{\gamma_m}^2}\right] d\theta_m dr_m. \quad (19)$$

Note that μ_{γ_m} in (19) is a function of (r_m, θ_m). We employ numerical integration methods to obtain the final PDF.

3. Numerical Results

The PDF of downlink SINR derived in (19) is calculated numerically and compared with a Monte Carlo simulation result in order to validate the analysis. We consider the nonline of sight (NLOS) indoor environment at 5.25 GHz as specified in [25, page 19] to be the basic environment for the comparison. The path loss formula is given as follows:

$$\mathrm{PL}(d) = 43.8 + 36.8 \log_{10}\left(\frac{d}{d_0}\right), \quad (20)$$

where d_0 is a reference distance in the far field. The interfering BSs are assumed to be femto BSs located on the same floor of a building throughout the experiments. However, interference scenarios such as femto BSs in different floors or outdoor macro-BSs can be easily examined by employing appropriate path loss models. The basic parameters used for the comparison are summarised in Table 1.

We assume that all interfering BSs are located at the same distance from the serving BS as shown in Figure 1. Cells are assumed to overlap each other to consider a dense deployment of the femto BSs. Although it is unlikely that the interfering BSs are in regular shapes in practical deployments, it is useful to consider this topology for examining the effects of parameters such as standard deviation of shadow fading, the number of BSs, wall penetration loss, and transmission power of BSs. It should be emphasised that the

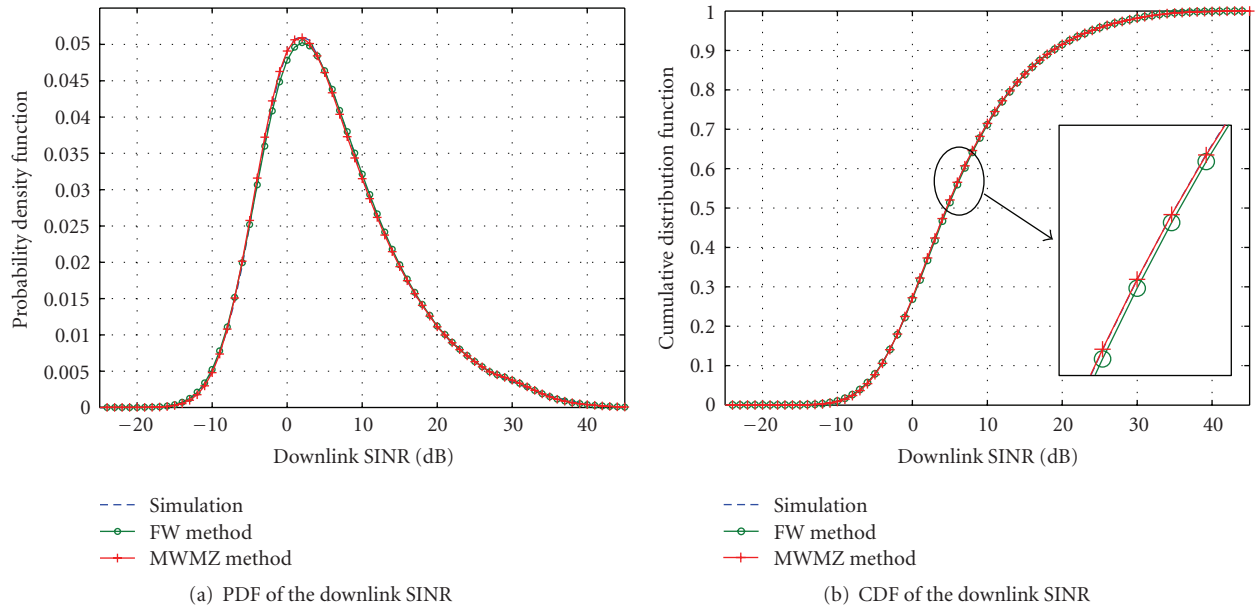

(a) PDF of the downlink SINR (b) CDF of the downlink SINR

Figure 2: A comparison of the PDF and CDF obtained by the analysis with the result of Monte Carlo simulation ($\sigma_{X_s} = \sigma_{X_j} = 3.5$ dB).

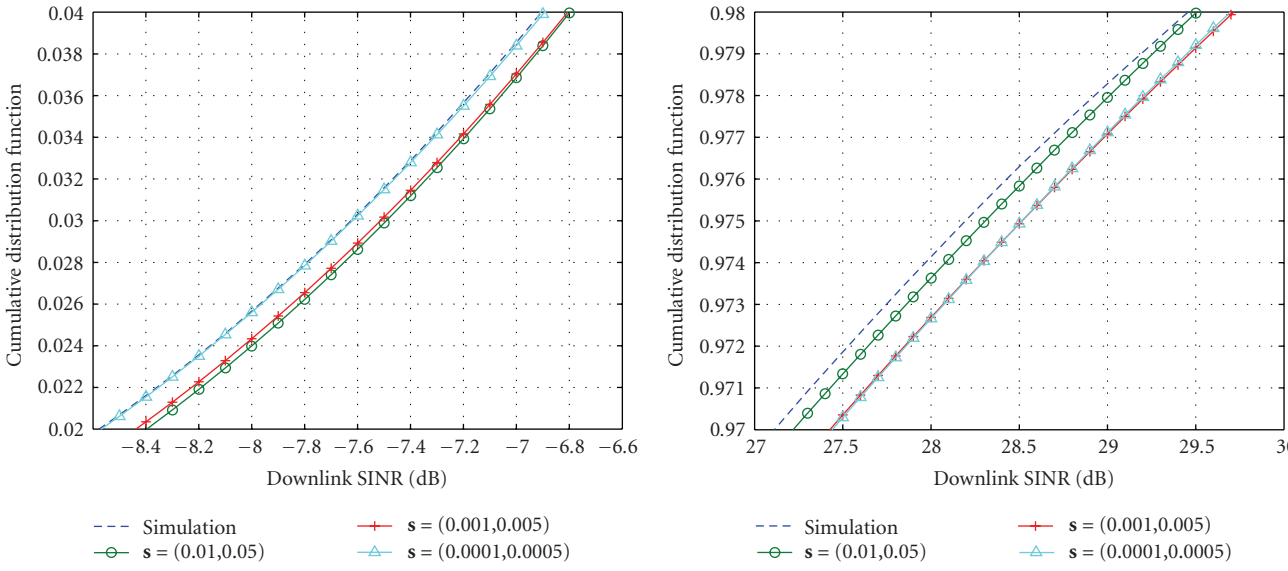

(a) Tail portion of the CDF (b) Head portion of the CDF

Figure 3: Impact of **s** on the performance of MWMZ method: tail and head portions of CDF ($\sigma_{X_s} = \sigma_{X_j} = 3.5$ dB).

PDF derived in Section 2 can effectively take into account irregular locations and transmission powers of BSs.

The result of the comparison is illustrated in Figure 2 where the PDFs derived by FW and MWMZ methods are compared with the Monte Carlo simulation result in Figure 2(a) and the cumulative distribution functions (CDFs) of the PDFs are depicted in Figure 2(b). The standard deviation of shadow fading, σ_{X_s} and σ_{X_j}, is considered to be 3.5 dB since it represents a typical value in an indoor office environment according to the measurement results in [25]. It is observed that the numerically obtained PDFs from both of the methods are in good agreement with the Monte Carlo simulation.

The impact of the parameter **s** on the performance of MWMZ method is shown in Figure 3 where the tail portion of the CDF (low SINR region) is depicted in Figure 3(a) and the head portion of the CDF (high SINR regime) is illustrated in Figure 3(b). Smaller **s** tends to give more accurate match in low SINR region while resulting in larger error in high SINR region. $\mathbf{s} = (0.01, 0.05)$ is chosen in the experiments since it brings about relatively small difference from simulations throughout the whole SINR region.

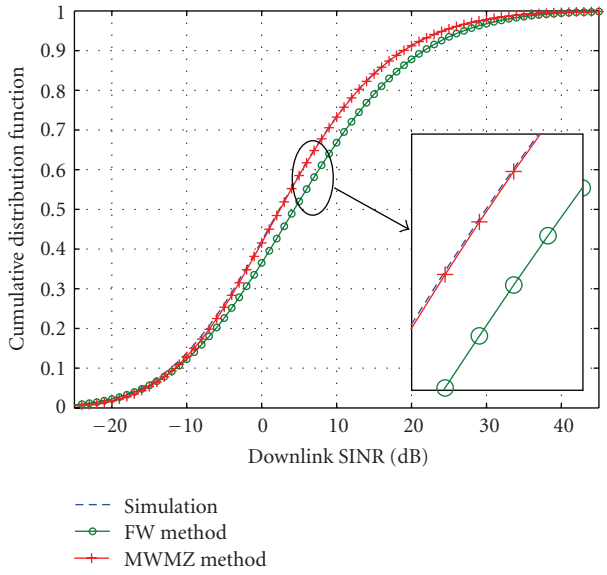

Figure 4: A comparison of the CDF obtained by the analysis with the result of Monte Carlo simulation ($\sigma_{X_s} = \sigma_{X_j} = 8.0$ dB).

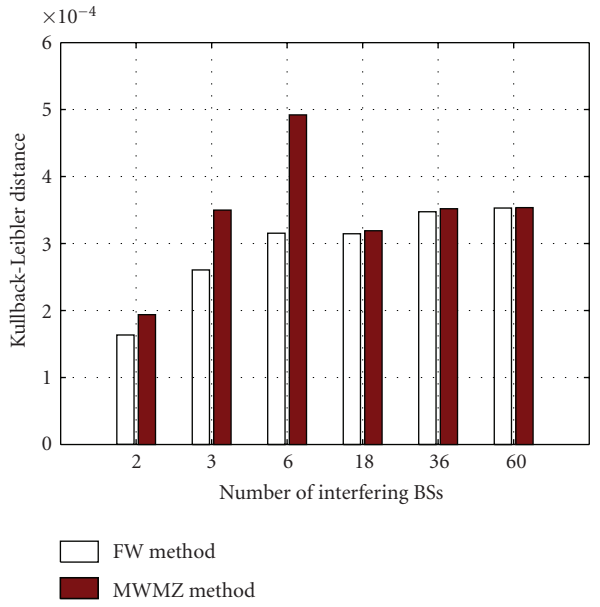

Figure 5: Kullback-Leibler Distance between simulation and analysis ($\sigma_{X_s} = \sigma_{X_j} = 3.5$ dB).

Figure 4 shows the CDFs when the standard deviation of shadow fading is 8.0 dB. While the SINR obtained by MWMZ method is still in good agreement with the simulation result, the difference between the analysis and the simulation is apparent in case of FW method. It means that FW method cannot be used in an environment where high shadow fading is experienced by MSs. In order to quantify the effect of shadow fading standard deviation, we introduce *Kullback-Leibler Distance* (KLD) which is a measure of divergence

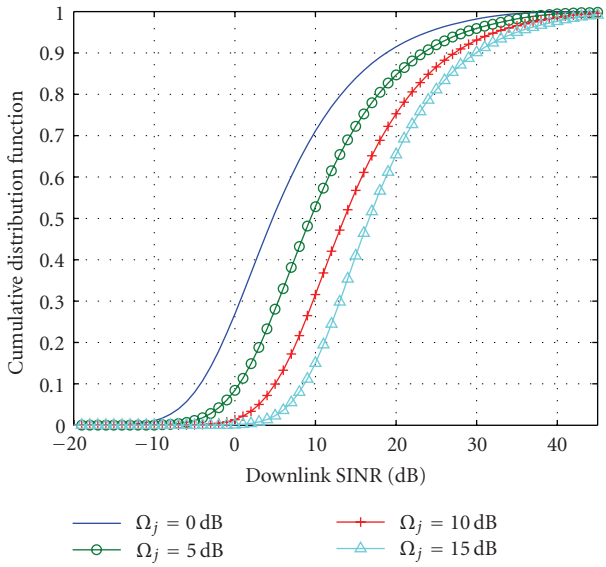

Figure 6: Effect of wall penetration loss on CDF of SINR (FW method, $\sigma_{X_s} = \sigma_{X_j} = 3.5$ dB).

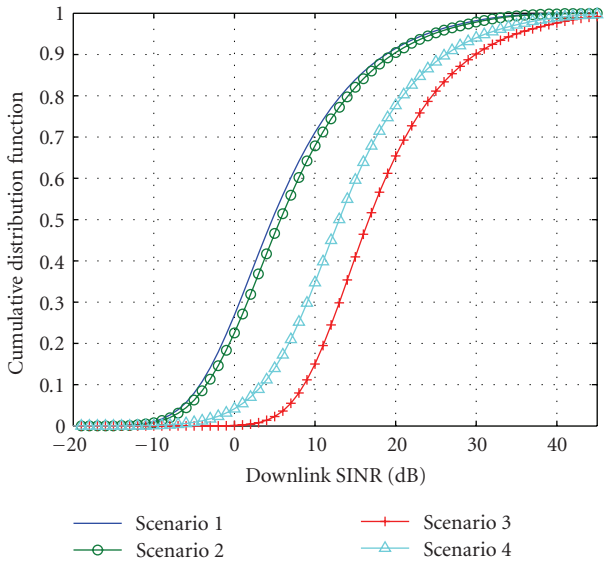

Figure 7: Effect of different wall penetration losses on CDF of SINR (FW method, $\sigma_{X_s} = \sigma_{X_j} = 3.5$ dB).

between two probability distributions [26]. For the two PDFs $p(x)$ and $q(x)$ the KLD is defined as

$$D(p\|q) = \int p(x)\log_2\frac{p(x)}{q(x)}dx. \tag{21}$$

The KLD is a nonnegative entity which measures the difference of the *estimated* distribution $q(x)$ from the *real* distribution $p(x)$ in a statistical sense. It becomes zero if and only if $p(x) = q(x)$. Table 2 presents the KLD for various standard deviations of shadow fading by assuming that the simulation results represent the true PDFs of SINR. It is shown in the table that the KLD of FW method soars when

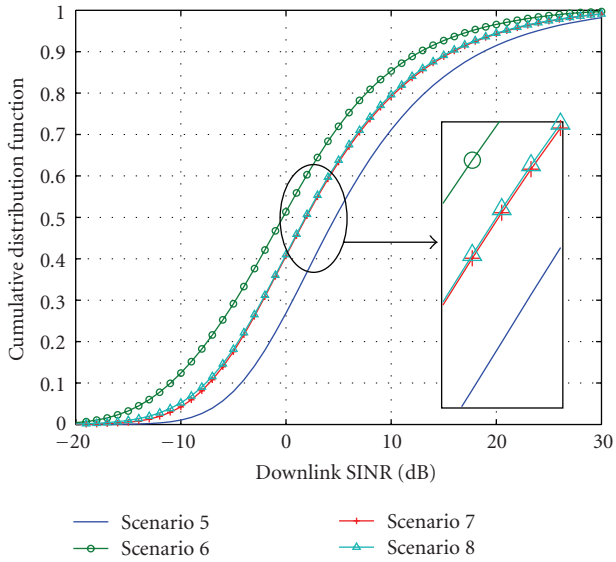

Figure 8: CDF of SINR with uncoordinated BS transmission power (FW method, $\sigma_{X_s} = \sigma_{X_j} = 3.5$ dB).

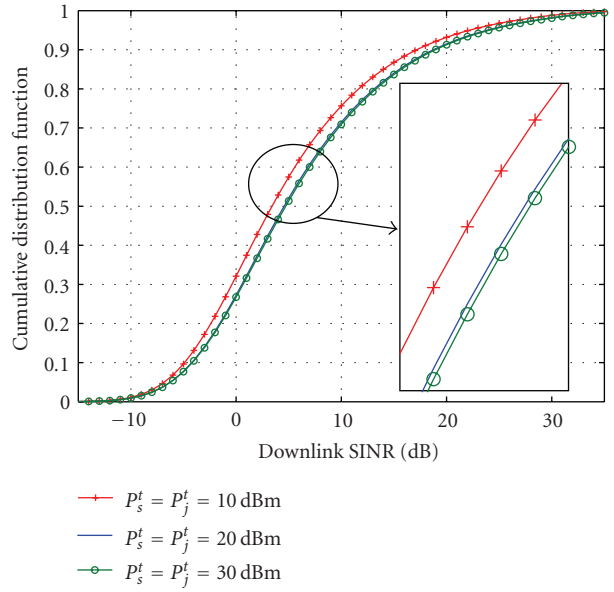

Figure 9: Effect of BS transmission power and background noise on CDF of SINR (FW method, $\sigma_{X_s} = \sigma_{X_j} = 3.5$ dB).

the standard deviation of shadow fading is higher than 6 dB. This implies that the range of standard deviation in which FW method can be adopted is between 3 dB and 6 dB, which is a typical range of shadow fading in an in-building environment [14, 25]. On the contrary, the MWMZ method maintains an acceptable level of the KLD even for the high shadow fading standard deviation. FW method is preferred if both of the methods are applicable due to its simplicity.

The effect of the number of interfering BSs is examined in Figure 5. It is known that the sum of log-normal RVs is not accurately approximated by a log-normal distribution as the number of summands increases [22]. This means that the derived SINR may not be accurate for a large number of interfering BSs. Figure 5 shows the KLD of FW and MWMZ methods compared to simulation results when L is between 2 and 60. An impairment in the accuracy is not observed as L increases, which means that the derivation of SINR in this paper is useful for the practical range of interfering BSs in the downlink of cellular systems.

The numerical results so far have focused on the verification of the derived PDF. Now we investigate the performance of femtocell network in various environments. An important observation in Figure 2 is that the probability of the SINR below 2.2 dB (a typical threshold for binary phase shift keying (BPSK) to achieve reasonable BER performance [27]) is about 0.38 for the parameters in Table 1. In other words, the outage probability is around 38%. This means that a dense deployment of femtocells in a building results in unacceptable outage, unless intelligent interference avoidance and interference mitigation techniques are put in place.

Clearly isolation of a cell by wall penetration loss is an inherent property of indoor femtocell networks which can be utilised as a means of interference mitigation. Let Ω_j be the wall penetration loss between the CoI and the interfering BS j. The effect of Ω_j is examined in Figure 6 where Ω_j is assumed to be identical for all interfering BSs. It is shown that Ω_j has significant impact on the SINR of the femtocell. The outage probability drops to 3.7% when $\Omega_j = 10$ dB and to 0.5% when $\Omega_j = 15$ dB. This result implies that the implementation of the femtocell network is viable without complicated interference mitigation method if the wall isolation between BSs is provided.

In Figure 7, different wall losses, Ω_j, are considered. We examine the following scenarios:

(i) scenario 1: $\Omega_1 = \cdots = \Omega_6 = 0$ dB,

(ii) scenario 2: $\Omega_1 = \cdots = \Omega_5 = 0$ dB and $\Omega_6 = 15$ dB,

(iii) scenario 3: $\Omega_1 = \cdots = \Omega_6 = 15$ dB,

(iv) scenario 4: $\Omega_1 = \cdots = \Omega_5 = 15$ dB and $\Omega_6 = 0$ dB.

It is shown that scenarios 1 and 2 give similar performance. This means that the isolation from one or few BSs does not result in the performance improvement when the CoI is not protected from the majority of interfering BSs. On the contrary, a considerable difference is observed between scenarios 3 and 4. Significant degradation in the SINR is caused by one BS which is not isolated by the wall.

Similar behaviours are observed in Figure 8 where different BS transmission powers are considered. The effect of the uncoordinated power is examined by considering the following scenarios where $P_s^t = 20$ dBm:

(i) scenario 5: $P_1^t = \cdots = P_6^t = 20$ dBm,

(ii) scenario 6: $P_1^t = P_2^t = P_3^t = 30$ dBm and $P_4^t = P_5^t = P_6^t = 10$ dBm,

(iii) scenario 7: $P_1^t = P_2^t = P_3^t = 25\,\text{dBm}$ and $P_4^t = P_5^t = P_6^t = 20\,\text{dBm}$,

(iv) scenario 8: $P_1^t = 30\,\text{dBm}$ and $P_2^t = \cdots = P_6^t = 20\,\text{dBm}$.

Figure 8 shows the CDFs of SINR by FW method with the assumption that $\Omega_j = 0\,\text{dB}\ \forall j$. It is observed that scenario 6 results in the worst SINR. This means that the higher transmission powers of a few BSs result in significantly decreased SINR. However, reduced transmission power in only a subset of neighbouring BSs does not necessarily improve the SINR because the predominant interference largely depends on the BSs which use high transmission powers. A similar trend is shown when comparing scenario 7 and scenario 8. The SINR performance is worse in scenario 8 than in scenario 7 for the same reason.

Finally, the effects of the BSs transmission power and the background noise are shown in Figure 9. If the transmit power drops below a certain level, a change in the PDF can be observed. For 10 dBm transmit power, for example, a noticeable impairment of the SINR can be seen. This is because the noise power remains the same regardless of the transmission power. In the case of increased transmission power, however, little change in the SINR distribution is observed. This means that the SINR is already interference limited with a transmission power of 20 dBm. Thus, the increase in the transmit power of BSs does not result in an improvement as expected.

4. Conclusion

In this paper, the PDF of the SINR for the downlink of a cell has been derived in a semianalytical fashion. It models an uncoordinated deployment of BSs which is particularly useful for the analysis of femtocells in an indoor environment. A practical propagation model including log-normal shadow fading is considered in the derivation of the PDF. The PDF presented in this paper has been obtained through analysis and calculated through standard numerical methods. The comparison with Monte Carlo simulation shows a good agreement, which indicates that the semianalytical PDF obviates the need for complicated and time-consuming simulations. The results also provide some insights into the performance of the indoor femtocells with universal frequency reuse. First, significant outage can be expected for a scenario where femto BSs are densely deployed in an in-building environment. This highlights that interference avoidance and mitigation techniques are needed. The isolation offered by wall penetration loss is an attractive solution to cope with the interference. Second, the SINR can be worsened by uncoordinated transmission powers of BSs. Thus, a coordination of BSs transmission power is needed to prevent a significant decrease in SINR.

Acknowledgment

This work was supported by the National Research Foundation of Korea, Grant funded by the Korean Government (NRF-2007-357-D00165).

References

[1] A. J. Viterbi, A. M. Viterbi, and E. Zehavi, "Other-cell interference in cellular power-controlled CDMA," *IEEE Transactions on Communications*, vol. 42, no. 4, pp. 1501–1504, 1994.

[2] M. Zorzi, "On the analytical computation of the interference statistics with applications to the performance evaluation of mobile radio systems," *IEEE Transactions on Communications*, vol. 45, no. 1, pp. 103–109, 1997.

[3] F. Graziosi, L. Fuciarelli, and F. Santucci, "Second order statistics of the SIR for cellular mobile networks in the presence of correlated co-channel interferers," in *Proceedings of the 53th IEEE Vehicular Technology Conference (VTC '01)*, pp. 2499–2503, Rhodes, Greece, May 2001.

[4] V. Koshi, "Coverage uncertainty and reliability estimation for microcellular radio network planning," in *Proceedings of the 51th IEEE Vehicular Technology Conference (VTC '00)*, pp. 468–472, Tokyo, Japan, May 2000.

[5] D. Stachle, "An analytic method for coverage prediction in the UMTS radio network planning process," in *Proceedings of the 61th IEEE Vehicular Technology Conference (VTC '05)*, pp. 1945–1949, Stockholm, Sweden, May-June 2005.

[6] M. Pratesi, F. Santucci, F. Graziosi, and M. Ruggieri, "Outage analysis in mobile radio systems with generically correlated log-normal interferers," *IEEE Transactions on Communications*, vol. 48, no. 3, pp. 381–385, 2000.

[7] M. Pratesi, F. Santucci, and F. Graziosi, "Generalized moment matching for the linear combination of lognormal RVs: application to outage analysis in wireless systems," *IEEE Transactions on Wireless Communications*, vol. 5, no. 5, pp. 1122–1132, 2006.

[8] F. Berggren and S. B. Slimane, "A simple bound on the outage probability with lognormally distributed interferers," *IEEE Communications Letters*, vol. 8, no. 5, pp. 271–273, 2004.

[9] H. Haas and S. McLaughlin, "A derivation of the PDF of adjacent channel interference in a cellular system," *IEEE Communications Letters*, vol. 8, no. 2, pp. 102–104, 2004.

[10] A. Mudesir, M. Bode, K. W. Sung, and H. Haas, "Analytical SIR for self-organizing wireless networks," *EURASIP Journal on Wireless Communications and Networking*, vol. 2009, Article ID 912018, 8 pages, 2009.

[11] V. Chandrasekhar, J. G. Andrews, and A. Gatherer, "Femtocell networks: a survey," *IEEE Communications Magazine*, vol. 46, no. 9, pp. 59–67, 2008.

[12] Z. Bharucha and H. Haas, "Application of the TDD underlay concept to home nodeB scenario," in *Proceedings of the 7th IEEE Vehicular Technology Conference (VTC '08)*, pp. 56–60, Singapore, May 2008.

[13] Z. Bharucha, I. Ćosović, H. Haas, and G. Auer, "Throughput enhancement through femto-cell deployment," in *Proceedings of the IEEE 7th International Workshop on Multi-Carrier Systems & Solutions (MC-SS '09)*, pp. 311–319, Herrsching, Germany, May 2009.

[14] H. Claussen, "Performance of macro—and co-channel femtocells in a hierarchical cell structure," in *Proceedings of the 18th IEEE International Symposium on Personal, Indoor and Mobile Radio Communications (PIMRC '07)*, Athens, Greece, November 2007.

[15] J. Espino and J. Markendahl, "Analysis of macro—femtocell interference and implications for spectrum allocation," in *Proceedings of the 20th IEEE International Symposium on Personal, Indoor and Mobile Radio Communications (PIMRC '09)*, pp. 13–16, Tokyo, Japan, September 2009.

[16] A. Valcarce, G. D. L. Roche, A. Jüttner, D. Lopez-Perez, and J. Zhang, "Applying FDTD to the coverage prediction of wiMAX femtocells," *Eurasip Journal on Wireless Communications and Networking*, vol. 2009, Article ID 308606, 13 pages, 2009.

[17] M. Yavuz, F. Meshkati, S. Nanda, et al., "Interference management and performance analysis of UMTS/HSPA+ femtocells," *IEEE Communications Magazine*, vol. 47, no. 9, pp. 102–109, 2009.

[18] N. C. Beaulieu and Q. Xie, "An optimal lognormal approximation to lognormal sum distributions," *IEEE Transactions on Vehicular Technology*, vol. 53, no. 2, pp. 479–489, 2004.

[19] L. F. Fenton, "The sum of log-normal probability distributions in scatter transmission systems," *IRE Transactions on Communications Systems*, vol. 8, no. 1, pp. 57–67, 1960.

[20] N. B. Mehta, J. Wu, A. F. Molisch, and J. Zhang, "Approximating a sum of random variables with a lognormal," *IEEE Transactions on Wireless Communications*, vol. 6, no. 7, pp. 2690–2699, 2007.

[21] S. C. Schwartz and Y. S. Yeh, "On the distribution function and moments of power sums with log-normal components," *The Bell System Technical Journal*, vol. 61, no. 7, pp. 1441–1462, 1982.

[22] S. S. Szyszkowicz and H. Yanikomeroglu, "On the tails of the distribution of the sum of lognormals," in *Proceedings of the IEEE International Conference on Communications (ICC '07)*, pp. 5324–5329, Glasgow, UK, June 2007.

[23] H. Nie and S. Chen, "Lognormal sum approximation with type IV pearson distribution," *IEEE Communications Letters*, vol. 11, no. 10, pp. 790–792, 2007.

[24] M. Abramowitz and I. A. Stegun, "Handbook of mathematical functions with fomulas," in *Graphs, and Mathematical Tables*, Dover, New York, NY, USA, 9th edition, 1972.

[25] IST-4-027756 WINNER II, "D1.1.2 v1.2 WINNER II Channel Models," February 2008, http://www.ist-winner.org/WINNER2-Deliverables/D7.1.5_Final-Report_v1.0.pdf.

[26] T. M. Cover and J. A. Thomas, *Elements of Information Theory*, D. L. Schilling, Ed., Wiley Series in Telecommunications, John Wiley & Sons, New York, NY, USA, 1st edition, 1991.

[27] A. Persson, T. Ottosson, and G. Auer, "Inter-sector scheduling in multi-user OFDM," in *Proceedings of the IEEE International Conference on Communications (ICC '06)*, vol. 10, pp. 4415–4419, Istanbul, Turkey, June 2006.

Hindawi Publishing Corporation
EURASIP Journal on Wireless Communications and Networking
Volume 2010, Article ID 142629, 15 pages
doi:10.1155/2010/142629

Research Article

Intracell Handover for Interference and Handover Mitigation in OFDMA Two-Tier Macrocell-Femtocell Networks

David López-Pérez, Alvaro Valcarce, Ákos Ladányi, Guillaume de la Roche, and Jie Zhang

Centre for Wireless Network Design (CWiND), University of Bedfordshire, D109 Park Square, Luton LU1 3JU, UK

Correspondence should be addressed to David López-Pérez, david.lopez@beds.ac.uk

Received 29 August 2009; Accepted 17 December 2009

Academic Editor: Ismail Guvenc

There are two main access policies (open and closed) to Femtocell Access Points (FAPs), being closed access the customers favorite. However, closed access is the root cause of crosstier interference in cochannel deployments of two-tier networks (i.e., macrocells and femtocells). Further, the effect of this problem is remarkably serious in the downlink of outdoor users not subscribed to any femtocell. Open access has been considered as a potential solution to this problem. However, this increases signaling in the network due to the elevated number of HandOvers (HOs) that mobile users have to perform. Therefore, this paper proposes an interference avoidance technique based on the use of Intracell HandOvers (IHOs) in Orthogonal Frequency Division Multiple Access (OFDMA) femtocells. It is shown that a proper combination of IHO and power control techniques reduces the outage probability for nonsubscribers compared with that of closed and open access. In addition, the impact of several network parameters such as the femtocell penetration is also considered in the analysis.

1. Introduction

Open access has been regarded [1] as a feasible solution to the problem of cross-tier interference in two-tier networks. Nevertheless, open access femtocell deployments are hardly practical due to the elevated number of required handovers. Indeed, when outdoor users are allowed to connect to any available cell (i.e., macrocell or femtocell) it is likely that due to the nomadic nature of these users, their connections would be continuously transferred between adjacent femtocells, or between femtocells and the umbrella macrocell. Furthermore, it is also well known [2] that HOs are not always successful and connections might be dropped as a consequence of HO failure. Additionally, the excessive signaling that emanates from an open access femtocell tier increases the complexity of the access network and introduces the need for large and powerful femtocell gateways.

1.1. Terminology. In order to clarify the concepts used throughout this article, the terminology to be applied is presented in the following. First, the main femtocell access policies are described.

(i) *Open access*: all clients of an operator have the right to connect to any of the femtocells of the operator.

(ii) *Closed access* also referred to as *Closed Subscriber Group* (*CSG*): only certain clients (subscribers) of an operator are allowed to connect to the given femtocell. The list of these clients is regulated by the femtocell owner.

(iii) *Hybrid access*: part of the femtocell resources is operated in open access, while the remaining follow a CSG approach [3]. This translates into a preferential access for subscribers and a limited access for other users.

In addition, in a closed and hybrid access, mobile users are classified as follows.

(i) *Subscribers*: these are the rightful users of a femtocell.

(ii) *Nonsubscribers*: these are users that are not registered in any nearby femtocell and therefore, they can only connect through the macrocell tier.

Moreover, the types of interference in two-tier networks are classified as follows.

(i) *Cross-tier interference*: this is caused by an element of the femtocell tier to the macrocell tier and vice versa.

(ii) *Cotier interference*: this takes place between elements of the same tier, for example, between neighboring femtocells.

Finally, note that variables in lower case represent magnitudes in natural units, while upper case indicates logarithmic scale, that is, dB.

1.2. Related Work. In order to cope with the previously mentioned problems, automatic pilot power control has been proposed in [4] as a possible solution for Code Division Multiple Access (CDMA) femtocells. However, this approach could lead to insufficient indoor coverage. In similar way, dynamic antenna patterns have also been suggested in [5], at the expense of a slightly more complex hardware in the FAPs. Furthermore in [6], a decentralized OFDMA resource allocation scheme was presented that optimizes the Area Spectral Efficiency (ASE) by applying spectrum fragmentation. However, this approach limits the maximum achievable instantaneous throughput regardless of the interference.

1.3. Contribution. It is because of the previously described drawbacks of open access that the closed access femtocell approach still seems appealing to most mobile network operators. Hence, novel solutions to the interference problem caused by CSG femtocells are still needed. In this article, a HO and interference mitigation technique based on the use of IHO for OFDMA femtocells operating in CSG mode is proposed. IHOs are widely used in Global System for Mobile communication (GSM) networks, where users are changed from channels with low-signal quality to channels that are in better conditions. The objective of this work is to apply the same concept to OFDMA subchannels, similarly as is done in GSM, in order to mitigate cross-tier interference.

In Section 2, interference is described in the context of two-tier networks. In Section 3, the notation used and several key concepts are presented. In Section 4, the IHO approach proposed in this article is depicted. In Section 5, the dynamic system-level simulation used in order to verify the performance of the IHO approach is summarized. In Section 6, a performance comparison in terms of network outages and throughput between closed, open access and IHO is given. Finally, in Section 7, the conclusions are drawn.

2. Interference in Two-Tier Networks

In two-tier networks, the severity of interference depends on two main factors: the strategy used for allocating the spectral resources to the tiers and the method used for accessing the femtocells [7]. A discussion on this topic follows.

2.1. Impact of the Spectrum Assignment on Network Performance

2.1.1. Assignment of Spectral Bands. Operators having more than one licensed spectral band have the following options for spectrum allocation [8].

(i) *Dedicated spectrum:* in this approach, a spectral band is assigned to the macrocell tier, while a different one is assigned to the femtocell tier. In this way, cross-tier interference is completely avoided, since both tiers operate at different frequencies. However, this results in a low spectral efficiency, since the cells in one tier can only access a subset of the overall frequency resources.

(ii) *Shared spectrum:* this approach reaches a higher spectral efficiency because both tiers access all resources. Nevertheless, in such configuration, cross-tier interference occurs, which could degrade the overall network performance unless interference is efficiently handled.

(iii) *Partially shared spectrum*: this is an intermediate solution. In this approach, the macrocell tier has access to all spectral bands, while femtocells operate only in a given subset. The main advantages of this approach are

(a) better spectral efficiency than with dedicated spectrum.

(b) reduction of cross-tier interference, when compared to a shared approach, since macrocell users creating or suffering from large cross-tier interference can be moved to the dedicated macrocell spectrum.

It is to be noticed that deploying a two-tier network using more than one carrier introduces a notable problem of battery drain in the User Equipment (UE), especially in the dedicated and partially shared approaches. In this case, femtocell subscribers connected to the macrocell tier perform a continuous search for the femtocell carrier, which is highly energy-consuming from the radio-interface point of view. Once the femtocell subscribers find the femtocell carrier, they synchronize to it and check, in the case of CSG access, their connectivity rights. Furthermore, if the femtocell subscriber is not allowed to connect to the CSG femtocell, its UE must resynchronize to the macrocell carrier, which supposes a new search, and therefore a further battery consumption.

Since not all operators have more than one spectral band to divide between tiers, and because the shared spectrum approach is more challenging from the technical point of view (it results in a better spectral efficiency, at the expense of having to mitigate cross-tier interference), the rest of this article focuses on the single carrier case.

2.1.2. Assignment of OFDMA Subcarriers. In OFDMA, the spectrum is divided into orthogonal subcarriers that are then

Table 1: Performance comparison.

	Subchannels allocation	
	Orthogonal	Cochannel
Average macrocell tier throughput (Mbps)	2.68	1.71
Average femtocell tier throughput (Mbps)	170.27	190.70
Average network throughput (Mbps)	172.95	192.41

Throughput analysis in a residential area (Figure 3) covered by 64 OFDMA femtocells and 1 macrocell, using a 5 MHz bandwidth. 4 indoor users are connected to each femtocell and 4 outdoor users move freely in the streets.

bundled into groups called subchannels (Wireless Interoperability for Microwave Access (WiMAX)) or resource blocks (LTE). Therefore, operators owning one spectral band and deploying a two-tier OFDMA network have different choices to allocate subchannels to the macrocell and femtocell tiers [9].

(i) *Orthogonal assignment.* A fraction of the subchannels is used only by the macrocells, while the rest of them are used exclusively by the femtocells.

(ii) *Cochannel assignment.* All macrocells and femtocells can access all subchannels.

It must also be mentioned that in [10], a hybrid approach has been proposed in which femtocells far from a macrocell use a cochannel assignment, whereas the close femtocells apply an orthogonal approach.

As explained in the previous section and in a similar way to the shared spectrum approach, a cochannel assignment of subchannels results in a larger spectral efficiency as long as cross- and cotier interference are efficiently mitigated, for example, by using self-organization techniques. To illustrate this, Table 1 shows the results of a system-level simulation of a two-tier OFDMA network (scenario shown in Figure 3) using the self-organization approach presented in [11]. The experiment verifies that the performance of a cochannel assignment in terms of network throughput is better than that of an orthogonal assignment, mainly due to the better frequency reuse.

2.2. Impact of the Access Method on Network Performance

2.2.1. Interference in Closed Access. With closed access, nonsubscribers can receive severe jamming from nearby femtocells. Even if the femtocell pilot power is larger than that of the nearest macrocell, nonsubscribers are not allowed to use the femtocell and are thus interfered in the downlink. Moreover, nonsubscribers transmitting with high power can cause interference in the uplink of nearby femtocells. The most challenging case of cross-tier interference, in this case, occurs when a nonsubscriber enters a house hosting a CSG femtocell. Then, in the downlink, the interference from the FAP is much stronger than the macrocell carrier, thus jamming the visitor. Similarly, the visitor can jam the uplink of the FAP.

2.2.2. Interference in Open Access. With this access method, nonsubscribers can also connect to femtocells. Therefore, the problem of a nonsubscriber passing by or entering a house where a femtocell is deployed is nonexistent. Hence, open access reduces the impact of cross-tier interference, which can be verified by the experiments presented in Table 2. However, open access has two major drawbacks.

(i) Femtocells are paid by subscribers, who are not keen on accepting nonsubscribers as users of their own femtocells. It is thus expected that operators would reduce the fees paid by subscribers or provide them with other advantages to make these type of femtocells more appealing.

(ii) Since all users can make use of the femtocells, the number of HOs and thus signaling increase in the network. It is also to be noticed that there is a chance that a HO will fail. According to [2], there is a 2% probability that a HO results in a dropped call. Therefore and as it is verified in Table 2, open femtocells can create outages.

Furthermore, in large deployments (high femtocell densities) of open access femtocells, even if a nonsubscriber is connected to a femtocell, the aggregate of all cotier interference coming from neighboring femtocells can disrupt its service (Table 2). It is to be noticed that cotier interference is also a problem in closed access.

As a conclusion, it is to be noticed that both access methods have drawbacks: CSG increases cross-tier interference, whereas open access increases the number of HOs [12]. In this article, the use of Intracell Handovers (IHOs) is proposed in order to cope with both issues.

3. Preliminaries

In the following, the notation used in the rest of the article is presented. Moreover, the concepts of neighboring cell list, measurement report, channel quality indicator, and handover are introduced.

3.1. Neighboring Cell List and Measurement Report. In order to select the best serving cell when the UE is idle, or to aid the HO procedure when the UE is active, the UE measures continuously the RSSs of the pilot channels of the neighboring cells. In order to simplify and speed up the task of the UE when monitoring the air interface, the serving cell periodically broadcasts to its UEs the list of cells and pilot channels that they must measure. This list is known as the Neighboring Cell List (NCL). After receiving the NCL, the UE performs (every period of duration T_{MR}) the appropriate measurements, and reports back the results to its serving cell, which then decides whether to start a new HO procedure or to take no action.

In two-tier networks, the NCL of a macrocell not only contains neighboring macrocells, but also open femtocells. Therefore, nonsubscribers must report back the RSSs of the pilot channels not only from all neighboring macrocells, but also from open femtocells.

Table 2: Performance comparison.

	Access method	
	Closed	Open
Outages due to HO failure	—	54
Outages due to interference	702	5
Average macrocell tier throughput (Mbps)	2.24	4.62
Average femtocell tier throughput (Mbps)	158.94	169.33

Outage and throughput analysis in a residential area (Figure 3) covered by 64 OFDMA femtocells and 1 macrocell using a 5 MHz bandwidth. 4 indoor users are connected to each femtocell and 8 outdoor users move in the streets.

Nevertheless, the case of CSG femtocells is different from open access. In order to minimize the impact of femtocell deployments on the existing macrocell tier, macrocells do not provide information about CSG femtocells in their neighboring cell list to the UEs. However, UEs perform an autonomous search to detect CSG femtocells [13].

3.2. Channel Quality Indicator. By using the Channel Quality Indicator (CQI), a UE can also report periodically, for example, at most every 2 ms in LTE networks, to its serving cell its signal quality in terms of Signal to Interference plus Noise Ratio (SINR), as well as the signal qualities of a given subset of resource blocks (usually the ones with better conditions). This CQI is used by the Medium Access Control (MAC) layer for channel-dependent scheduling and rate control, but it can also be used to trigger a HO when the UE reports a low SINR.

Furthermore, let us mention that in several wireless standards, such as WiMAX and LTE, the user equipment has the capability of estimating the instantaneous SINR in all subcarriers [14, 15].

3.3. Network Definition. Let us define a two-tier OFDMA network as a set of:

(i) $N + M$ cells $\{C_0, \ldots, C_i, \ldots, C_{N+M-1}\}$ with:

  (a) N femtocells $\{F_0, \ldots, F_n, \ldots, F_{N-1}\}$,
  (b) M macrocells $\{M_0, \ldots, M_m, \ldots, M_{M-1}\}$,

(ii) $X + Y$ users $\{\mathrm{UE}_0, \ldots, \mathrm{UE}_z, \ldots, \mathrm{UE}_{X+Y-1}\}$ with:

  (a) X subscribers $\{\mathrm{UE}_0^s, \ldots, \mathrm{UE}_x^s, \ldots, \mathrm{UE}_{X-1}^s\}$,
  (b) Y nonsubscribers $\{\mathrm{UE}_0^{ns}, \ldots, \mathrm{UE}_y^{ns}, \ldots, \mathrm{UE}_{Y-1}^{ns}\}$,

(iii) K subchannels $\{0, \ldots, k, \ldots, K-1\}$,

where the NCL of cell C_i contains J different cells (macrocells and femtocells) and it is denoted by $\mathcal{N}_i = \{N_0, \ldots, N_j, \ldots, N_{J-1}\}$.

3.4. Handover. In cellular networks, a HO is triggered when the RSS ($\mathrm{RSS}_{i,z}^{\mathrm{pilot}}$) of the pilot signal from a serving cell C_i at a mobile UE_z is lower than that of a neighboring cell N_j ($\mathrm{RSS}_{j,z}^{\mathrm{pilot}}$). These signal strength measurements are signal levels averaged over time using measurement reports. This averaging is necessary in order to cope with fading. Moreover, when a mobile user is located in between cells, it could happen that its transmission is ping-ponged from cell to cell. In order to avoid this effect, a hysteresis margin for the HO decision is also used. Furthermore, an umbrella cell system is normally deployed to minimize the large number of HOs incurred by high-speed users.

Then, if the HO condition is met, the serving cell C_i establishes communication with the target cell N_j and a HO is performed. However, in two-tier networks, performing a HO is not always the best choice or a possible option at all, because

(i) in closed access, it is not allowed that a nonsubscriber hands over from its serving cell to a CSG femtocell.

(ii) in open access, it is preferred to keep a mobile user connected to a macrocell than hand it over continuously and repeatedly between adjacent open femtocells. In this case, the mobile user speed must be considered.

In order to overcome these drawbacks, and the limitations imposed by closed and open access (CSG increases cross-tier interference, whereas open access increases the number of HO), the following IHO approach is proposed.

4. Intracell Handover in Femtocell Networks

The IHO is a special type of HO in which the source and target cell is the same one. The purpose of IHO is to transfer a user from a channel, which may be interfered or faded, to a clearer or less-faded channel. IHO is used, for example in GSM networks, where it is triggered when a UE reports a large RSS, but a low Received Signal Quality (RSQ) due to interference and/or fading.

The main idea of the proposed approach is that when a nonsubscriber that is connected to a macrocell suffers from cross-tier interference due to a nearby femtocell, the macrocell itself performs an IHO if possible, or casts an IHO in all interfering femtocells otherwise.

Without loss of generality respect to the IHO approach, the rest of this article focuses only on the DownLink (DL).

4.1. Triggering an IHO. When the SINR of a nonsubscriber UE_y^{ns} connected to macrocell M_m in subchannel k is smaller than a given threshold $\mathrm{SINR}_y^{\mathrm{IHO}}$, the serving macrocell M_m requests a measurement report from nonsubscriber UE_y^{ns}. In this measurement report, nonsubscriber UE_y^{ns} indicates the RSS of its serving macrocell M_m in subchannel k ($\mathrm{RSS}_{m,y}^k$), as well as the RSSs of its neighboring cells N_m in such subchannel k ($\mathrm{RSS}_{j,y}^k$).

Note that the neighboring cells of UE_y^{ns} are identified by the NCL provided by macrocell M_m to nonsubscriber

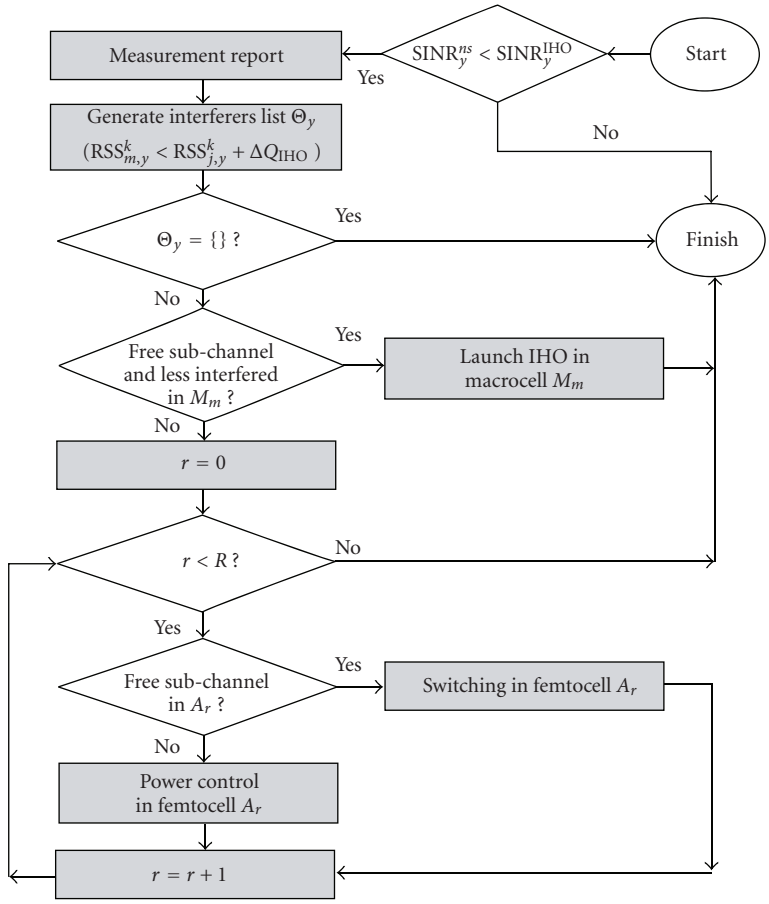

Figure 1: Intracell Handover approach.

UE_y^{ns}, and that they can be both macrocells and femtocells. Nevertheless, for the sake of simplicity it is assumed that the macrocell tier has been deployed using network planning and optimization tools, for example, base station location [16], automatic frequency planning [17], and thus macrocell intercell interference can be disregarded.

After receiving this measurement report, macrocell M_m compares its $RSS_{m,y}^k$ with the other reported $RSS_{j,y}^k$. Thereafter, macrocell M_m triggers an IHO only if condition (1) is verified by a neighboring cell N_j, and this neighboring cell is a femtocell F_n.

$$RSS_{m,y}^k < RSS_{j,y}^k + \Delta Q_{IHO} \quad \forall N_j \in \mathcal{N}_m, \tag{1}$$

where ΔQ_{IHO} denotes an interference protection margin. If ΔQ_{IHO} is too low, the nonsubscriber UE_y^{ns} may suffer from interference before the IHO is launched, and its service could be dropped. Contrarily, if ΔQ_{IHO} is too large, the IHO may be triggered to solve a nonexistent problem, thus increasing the signaling overhead in the network. Therefore, ΔQ_{IHO} must be carefully selected in order to launch the IHO before the nonsubscriber falls into outage, while minimizing the signaling overhead.

Thus, if femtocell F_n verifies (1), it is considered as a cross-tier interferer of nonsubscriber UE_y^{ns} in subchannel k, and therefore an IHO is triggered. Note that the set of all interfering femtocells of nonsubscriber UE_y^{ns} verifying (1) is denoted by $\theta_y = \{A_0, \ldots, A_r, \ldots, A_{R-1}\}$.

Thereafter launching the IHO, it can be performed either in the serving macrocell M_m or in all interfering femtocells θ_y. In order to minimize the signaling overhead, it is preferred to perform this IHO in the serving macrocell M_m than in all interfering femtocells θ_y. However, this is not always possible due to traffic load or interference conditions in the macrocell M_m.

In the following, the conditions that are taken into account to decide whether an IHO is performed in the serving macrocell or in all interfering femtocells are presented, as well as the taken actions.

4.2. Performing the IHO in the Macrocell. An IHO is launched in the serving macrocell M_m only if

(i) there is at least one free subchannel h to which nonsubscriber UE_y^{ns} can be reallocated to (switching),

(ii) and the interference suffered by subchannel h is lower than the one suffered by the assigned subchannel k.

In the case that there are more than one available subchannels in macrocell M_m, nonsubscriber UE_y^{ns} is switched to the subchannel h that suffers the least interference. This

subchannel h is selected by macrocell M_m according to the CQIs reported by nonsubscriber UE_y^{ns}. In order to do this, macrocell M_m can instruct nonsubscriber UE_y^{ns} to perform measurements on unused subchannels, and report back their signal quality over the pilot reference symbols using the CQI.

It is to be mentioned that if no subchannel fulfills these requirements, the IHO is not performed in the serving macrocell M_m, but in all interfering femtocells $A_r \in \theta_y$.

4.3. Performing the IHO in the Femtocells. If the IHO cannot be performed in the macrocell, it is attempted in all interfering femtocells verifying condition (1). In this case, the macrocell establishes communication with these femtocells (Section 4.4) and initiates an IHO in them. The signaling overhead caused by these communications is analyzed in Section 6.5. Moreover, and according to the availability of subchannels in the interfering femtocell A_r, the IHO procedure differs. When there are available subchannels in femtocell A_r, a subchannel *switching* process is carried out, whereas when there are no available subchannels in femtocell A_r, a *power control* procedure is executed. Figure 1 summarizes this sequence of actions. Both procedures are introduced next.

4.3.1. Switching Approach for IHO in the Femtocells. *Switching* is only possible when there is at least one available subchannel h in the interfering femtocell $A_r \in \theta_y$. Then, the femtocell subscriber UE_x^s, which is currently connected to subchannel k, is transferred to subchannel h. In this way, subchannel k is liberated, thus avoiding cross-tier interference to nonsubscriber UE_y^{ns}. Note that if there are more than one available subchannels in femtocell $A_r \in \theta_y$, subscriber UE_x^s is switched to the subchannel h with best conditions according to its CQIs. In order to do this, femtocell A_r can instruct subscriber UE_x^s to perform measurements on unused subchannels, and report back their signal quality over the pilot reference symbols using the CQI.

4.3.2. Power Control for IHO in the Femtocells. If there are no free subchannels in the interfering femtocell $A_r \in \theta_y$, then one option would be to disconnect UE_x^s from subchannel k for a period of time ΔT_{IHO} in order to avoid cross-tier interference towards nonsubscriber UE_y^{ns}. However, this would decrease the throughput of femtocell $A_r \in \theta_y$, which is undesired. Note that this approach, called subchannel *forbidding*, is not part of the proposed IHO algorithm, but will be used for comparison in the following.

Then, instead of disconnecting UE_x^s from subchannel k, the power transmitted by $A_r \in \theta_y$ in subchannel k is reduced for a period of time ΔT_{IHO}. In this way, cross-tier interference towards the nonsubscriber UE_y^{ns} is mitigated.

The primary objective of this power control algorithm (illustrated in Figure 2) is to manage cross-tier interference, while the secondary objective is to maximize the femtocell throughput. In this way, the reduction of the throughput of femtocell $A_r \in \theta_y$ is minimized compared to that of the forbidding approach presented above.

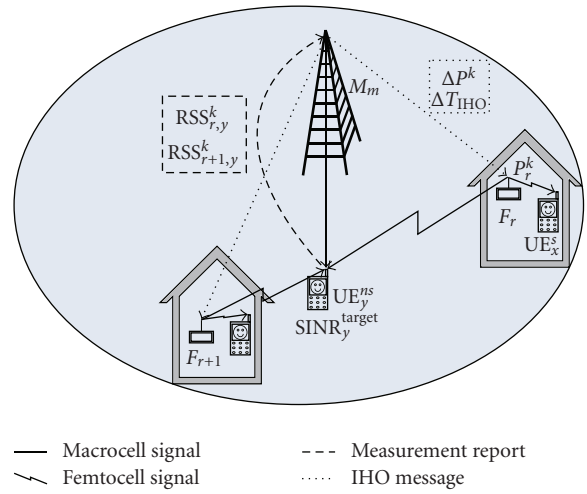

Figure 2: Power control algorithm for IHO.

The target of this distributed power control is to set the power P_r^k, with which all interfering femtocells $A_r \in \theta_y$ transmit in subchannel k, to a value $P_r^{'k}$ that ensures a certain signal quality $\text{SINR}_y^{\text{target}}$ to nonsubscriber UE_y^{ns}.

In order to guarantee such $\text{SINR}_y^{\text{target}}$, the maximum interference $i_y^{\max}$ that nonsubscriber UE_y^{ns} can tolerate is

$$i_y^{\max} = \frac{\text{rss}_{m,y}^k}{\text{sinr}_y^{\text{target}}} - \sigma, \tag{2}$$

where σ denotes the background noise.

Then, macrocell M_m asks all interfering femtocells $A_r \in \theta_y$ to decrease their transmit power in subchannel k from p_r^k to $p_r^{'k}$ so that $i_y^{\max}$ is respected for nonsubscriber UE_y^{ns}. Furthermore and in order to avoid unfair power decrease requests among femtocells, the power decrease is weighted by macrocell M_m using the RSS reported by nonsubscriber UE_y^{ns} from each interfering femtocell $A_r \in \theta_y$ according to

$$p_r^{'k} = \underbrace{i_y^{\max} \cdot \frac{\text{rss}_{r,y}^k}{\sum_{\forall r} \text{rss}_{r,y}^k}}_{i_{r,y}^{\max}} \cdot \underbrace{\frac{p_r^k}{\text{rss}_{r,y}^k}}_{pl_{r,y}^k}, \tag{3}$$

where $i_{r,y}^{\max}$ is the maximum interference that femtocell $A_r \in \theta_y$ is allowed to cause to nonsubscriber UE_y^{ns} and $pl_{r,y}^k$ is the path loss between them. Then, (3) simplifies to

$$P_r^{'k} = P_r^k - \Delta P^k, \tag{4}$$

where

$$\Delta P^k = 10 \cdot \log_{10}\left(\frac{\sum_{\forall r} \text{rss}_{r,y}^k}{i_y^{\max}}\right) \tag{5}$$

being ΔP^k the power reduction in decibels requested for subchannel k, which is computed by macrocell M_m and passed on (Section 4.4) to all interfering femtocells $A_r \in \theta_y$.

Finally, it can occur that if femtocell A_r is already transmitting with too little power in subchannel k or if

$\text{SINR}_y^{\text{target}}$ is too high, the power decrease request ΔP^k might have the same effect as switching off subchannel k. In this case, subchannel k is *forbidden* in femtocell A_r for a period of duration ΔT_{IHO}, avoiding cross-tier interference towards nonsubscriber UE_y^{ns}. However, it must be mentioned that subscriber UE_x^s is only disconnected from subchannel k if it can afford it, that is, UE_x^s has allocated more subchannels or carries a service where delay is not crucial, for example, best effort, nonreal-time service.

Let us also indicate that the decrease in the femtocell throughput when forbidding a subchannel is statistically small, since this type of IHO is performed only from time to time when the femtocell is fully loaded and a nonsubscriber passes by the femtocell proximities.

Moreover, it is worth mentioning that a femtocell can generally afford to liberate a subchannel during a short period of time to avoid the outage of a mobile outdoor nonsubscriber. For instance, a WiMAX femtocell with 5 MHz bandwidth can achieve 12 Mbps in the downlink. Since a femtocell can only be accessed simultaneously by at most 4 users and subchannel forbidding is only triggered when the femtocell is fully loaded (otherwise, there would be available subchannels to switch to), then in order to fully use all available subchannels, it is likely that the femtocell users are not only using VoIP (12.2 kbps) or video (256 kbps), but also other intensive best effort services, for example, peer to peer. Then, they can afford to free a subchannel for a short period of time in favor of avoiding a nonsubscriber outage.

4.4. Macrocell and Femtocell Communication. In order to initiate an IHO in a femtocell, the macrocell needs to communicate with it. This communication could be established over the following.

(i) The backhaul connection using the core network infrastructure, for example, Radio Access Network Application Part (RANAP) in Universal Mobile Telecommunication System (UMTS) and $S1$ in LTE [18].

(ii) A direct interface between macrocells and femtocells. This solution has synergies with LTE, which has defined an $X2$ interface for signaling between eNodeBs.

(iii) The user, who could relay data from a macrocell to a femtocell and vice versa. This solution is suggested by the authors of [9].

Given the state of the art of mobility management in LTE femtocells, and because no $X2$ interface has been standardized yet for HeNodeBs, the exchange of messages between macrocells and femtocells is more likely to be implemented over the backhaul connection. This can be done in a similar way as proposed approaches for macro to femto and femto to macro HOs, using the femtocell Gateway (GW) [19].

Since this communication is out of the scope of this paper, it is not analyzed in detail in the following sections. However, the signaling overhead originated in the system due to the IHO approach is analyzed in Section 6.5.

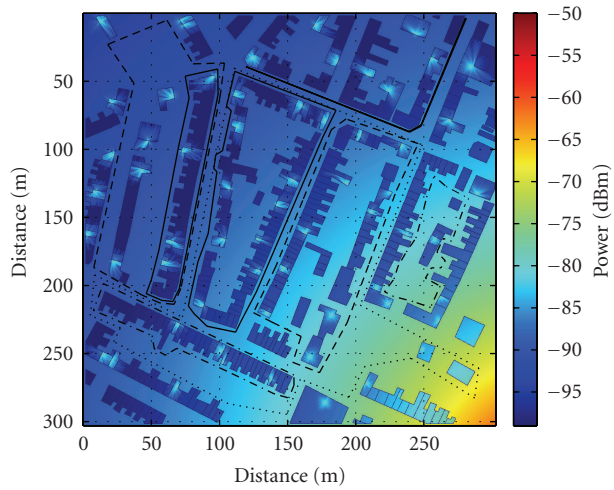

Figure 3: Received power per OFDMA subcarrier (OFDMA-512 system) in a residential area covered by 1 macrocell and 64 femtocells. Each femtocell premises contains several indoor users, while 8 pedestrian users are located outdoors, being their routes also indicated.

5. Experimental Setup

To evaluate the performance of the proposed IHO approach, dynamic system-level simulations have been used.

The scenario under scrutiny is a residential area with a size of 300×300 m in the town of Luton (U.K.), containing 438 premises of which around 400 are dwelling houses. 64 of these were selected to potentially host an indoor femtocell. Assuming that 3 operators with equal customer share provide services in this area, these 64 femtocells represents an approximate 50% femtocell penetration. Besides these femtocells, the scenario also contains one outdoor macrocell. Note that experiments were carried out with different femtocell penetrations: 50% (= 64 femtocells), 25% (= 32 femtocells) and 12.5% (=16 femtocells). The setup with 64 femtocells is illustrated in Figure 3, while the parameters of the simulation are shown in Table 3.

In this experimental evaluation, the different types of customers follow a well-defined behavior.

(i) Subscribers are located inside the houses with femtocell and do not move.

(ii) Nonsubscribers are located outdoors and move along predefined paths according to the pedestrian mobility model based on [20].

5.1. Propagation Model. For the path-loss predictions two different propagation models were used

(i) The macrocell coverage prediction was performed using the model proposed in [21]. This is an empirical model based on macrocell measurements in an urban environment at a frequency of 3.5 GHz.

Table 3: Simulation parameters.

Parameter	Value	Parameter	Value
Scenario size	300 m × 300 m	Macro Antenna Gain	0 dBi
Simulation time	800 s	Macro Antenna Pattern	Omni
Macrocells	1	Macro cable loss	3 dB
Femtocells	16, 32, 64	Femto TX Power	10 dBm
Nonsubscribers	4, 8	Femto Antenna Gain	0 dBi
Subscribers	4, 8 per femto	Femto Antenna Pattern	Omni
Carrier	3.5 GHz	UE Antenna Pattern	Omni
Bandwidth	5 MHz	UE Body Loss	0 dB
Duplexing	TDD 1 : 1	UE Noise Figure	7 dB
DL symbols (T_{DL})	19	UE Average Speed	1.1 m/s
UL symbols (T_{UL})	18	T_{MR}	50 ms
Preamble symbols	2		
Overhead symbols	11		
Frame duration	5 ms	$\mathrm{SINR}_y^{\mathrm{IHO}}$	3 dB
Subcarriers (SC)	512	$\mathrm{SINR}_y^{\mathrm{target}}$	10 dB
$\mathrm{SC}_{\mathrm{pilot}}$	48	ΔQ_{IHO}	3 dB
$\mathrm{SC}_{\mathrm{data}}$	384	ΔT_{IHO}	10 s
Subchannels (K)	8	Outage Threshold	200 ms
Thermal Noise Density	−174 dBm/Hz	Macro Path Loss	Empirical
Macro TX Power	43 dBm	Femto Path Loss	FDTD

(ii) The femtocell downlink coverages were predicted with a Finite-Dierence-Time-Domain-(FDTD) based model [22] calibrated with indoor-to-outdoor measurements at a frequency of 3.5 GHz.

The Root Mean Square Errors (RMSEs) of the macrocell and femtocell models are 8 dB and 6 dB, respectively.

5.2. System Level Simulation. An event-driven dynamic system-level simulation is used to model the operation of this two-tier OFDMA network. In this case, the life of the network through time is modeled as a series of events. For instance, an event happens when a user changes its position, when an IHO is launched, and so forth.

Because traffic modeling is out of the scope of this article, it is assumed that a user is allocated in each OFDMA frame to only 1 subchannel having T_{DL} OFDM symbols. Under this assumption, the SINR and throughput per user and other statistics are computed at regular time intervals.

This system-level simulation supports Adaptive Modulation and Coding (AMC). The different Radio Access Bearers (RABs), together with their SINR thresholds and efficiencies are shown in Table 4. Note that a UE cannot transmit when its SINR is lower than the SINR threshold of the lowest RAB defined in the network, that is, 2.88 dB.

Following the behavior of real-time services, a user is considered to be in outage when it cannot transmit for a given period of time. In this case, this period of time is fixed to 200 ms as recommended by [23] for VoIP applications.

Further information about this system-level simulator such as channel modeling, interference modeling, throughput calculation, and so forth. can be found in [11].

Table 4: RABs (Modulation and coding schemes).

RAB	Modulation	Code rate	SINR threshold	Efficiency
1	QPSK	1/2	2.88	1.00
2	QPSK	3/4	5.74	1.50
3	16QAM	1/2	8.79	2.00
4	16QAM	3/4	12.22	3.00
5	64QAM	1/2	15.88	4.00
6	64QAM	3/4	17.50	4.50

5.3. Closed and Open Access Implementation. In the closed access simulations, nonsubscribers are always connected to the macrocell. These are likely to suffer from outage when they pass close to a femtocell that is making use of the same subchannel. It is assumed that after this type of outage, the nonsubscriber reestablishes its connection or call as soon as its SINR is larger than the SINR threshold of the lowest RAB defined in the network.

In open access simulations, outdoor users are always connected to the best server regardless of whether it is the macrocell or a femtocell. This case, outdoor users send a measurement report to their serving cell based on its NCL on a regular basis (T_{MR}). This indicates the RSSs of pilot channels of neighboring cells. Then, a hard HO is performed if the RSS of the strongest neighboring cell is larger than the one of the current server. It is to be noted that the HO procedure is carried out by the network and that there is a 2% probability that it fails, resulting in a dropped call. Then, it is assumed that after this type of outage, a nonsubscriber reestablishes connection immediately.

Table 5: Outages of nonsubscribers.

ΔQ_{IHO} (dB)	−1	0	1	2	3
12.5% penetration	35	1	0	0	0
25% penetration	80	16	2	0	0
50% penetration	356	143	49	6	0

6. Results

First of all, let us mention that the IHO threshold $\text{SINR}_y^{\text{IHO}}$ has been set to 3 dB, which is a value slightly larger than that of the lowest RAB defined in the system, that is, 2, 88 dB. In this way, the IHO is launched before the user cannot achieve any RAB, and it falls into outage, that is, the user cannot transmit for more than 200 ms.

6.1. Effect of Parameter ΔQ_{IHO}. Table 5 summarizes the network performance in terms of the outage of nonsubscribers, when using IHOs with different values of the interference protection margin ΔQ_{IHO}. The simulations have been carried out with different number of femtocells in order to analyze the impact of the femtocell penetration on ΔQ_{IHO}. It has been observed that if ΔQ_{IHO} is low, for example, $\Delta Q_{\text{IHO}} = 0$, a large number of outages occur. The reason is that the IHOs are launched either too late, when the nonsubscriber is already in outage, or they are not even launched. Moreover, when the femtocell penetration grows, the interference protection margin ΔQ_{IHO} needed to fight outages is larger. For example, $\Delta Q_{\text{IHO}} = 2$ is sufficient in the case of a 25% penetration, whereas $\Delta Q_{\text{IHO}} = 3$ is needed in the case of a 50% penetration. This is due to the fact that with larger femtocell penetrations, the aggregate of cotier interference from neighboring femtocells towards a nonsubscriber grows. Therefore, the IHO must be launched when lower increases in interference are detected. Finally, it is worth mentioning that if ΔQ_{IHO} is too large, an IHO will be launched to try to solve a problem (cross-tier interference) that does not even exist, increasing thus signaling, which is undesired.

In view of the results of Table 5, $\Delta Q_{\text{IHO}} = 3$ dB is assumed in the rest of the article because it is seen to guarantee outage avoidance in all cases.

6.2. Effect of Parameter ΔT_{IHO}. Figure 4 shows the sample scenario used to illustrate the performance in terms of SINR of a nonsubscriber, when it moves across the scenario. In this case, the performance of the IHO approach with different values of ΔT_{IHO} is compared to that of closed access.

First of all, let us note that in closed access, when a nonsubscriber moves close to femtocells A or B (Figure 4(a)), it is jammed due to cross-tier interference (Figure 4(b)). This is assuming that femtocells A and B are using all available subchannels. Thus, the nonsubscriber falls into outage, since its SINR is smaller than that of the minimum RAB defined for a period longer than 200 ms.

However, when using the IHO approach and the SINR of the nonsubscriber decreases, an IHO is launched in both femtocells A and B. Then, these femtocells stop using the subchannel used by the nonsubscriber. In this way, cross-tier interference towards the nonsubscriber is mitigated, and the outage is thus avoided.

Moreover, it can be seen in Figures 4(b) and 4(c) that if ΔT_{IHO} is not finely tuned, femtocells A and B begin to use the forbidden subchannel before the nonsubscriber moves out of their coverage area. In this case, new IHO must be launched in the femtocells in order to avoid the nonsubscriber outage, increasing thus the signaling overhead in the network.

However, if ΔT_{IHO} is finely tuned (see Figure 4(d)), femtocells A and B will not use the forbidden subchannel until the nonsubscriber is out of their coverage domain. Since a pedestrian walks at an average speed of 1.1 m/s and because the femtocell radius is estimated to be 10 m [22], $\Delta T_{\text{IHO}} = 10$ s has been proven to be appropriate to force only one IHO per femtocell in a residential scenario with mobile pedestrians.

6.3. Effect of Power Control. Figure 5 illustrates the performance in terms of SINR of the nonsubscriber moving along the route defined in Figure 4(a). The IHO approach with and without power control is compared here to closed access. In this case, the macrocell and femtocells are fully loaded. Therefore, an IHO based on subchannel switching is not possible.

When the IHO approach is applied without power control, that is forbidding interfering femtocells from using the subchannel employed by the nonsubscriber, the SINR of such nonsubscriber grows notably due to the avoidance of cross-tier interference (Figure 5(a)). However, this is at the expense of reducing the femtocell throughput, since a subchannel is forbidden (Figure 5(b)).

Contrarily, when the IHO approach is used with power control, subchannels are not forbidden, but the power applied to it is reduced. This is done in a controlled manner in order to protect the nonsubscriber. As a result, the SINR of the nonsubscriber is not as large as when forbidding the subchannel, but the outage is avoided and the femtocell throughput is enhanced with respect to the forbidding case. Figure 5(b) shows a case in which power control does not recover the full throughput capacity compared to CSG, but provides a gain with respect to the forbidding approach. In this case, this throughput gain is about 250 kbps, which is enough to hold real-time services such as VoIP (12.2 kbps).

6.4. Closed, Open and IHO Comparison. In this section, the performance of the IHO approach compared to that of the closed and open access is analyzed. This has been done under different femtocell penetrations (12,5%, 25%, and 50%), and traffic loads in both the macrocell and femtocells (50% (4 users) and 100% (8 users)). There are 8 subchannels available for transmission.

The different setups are as follows.

Setup. Macrocell and femtocells are both half loaded (4 users). Under these conditions, IHOs based on subchannel switching are mostly launched in the macrocell (see Table 6 for results).

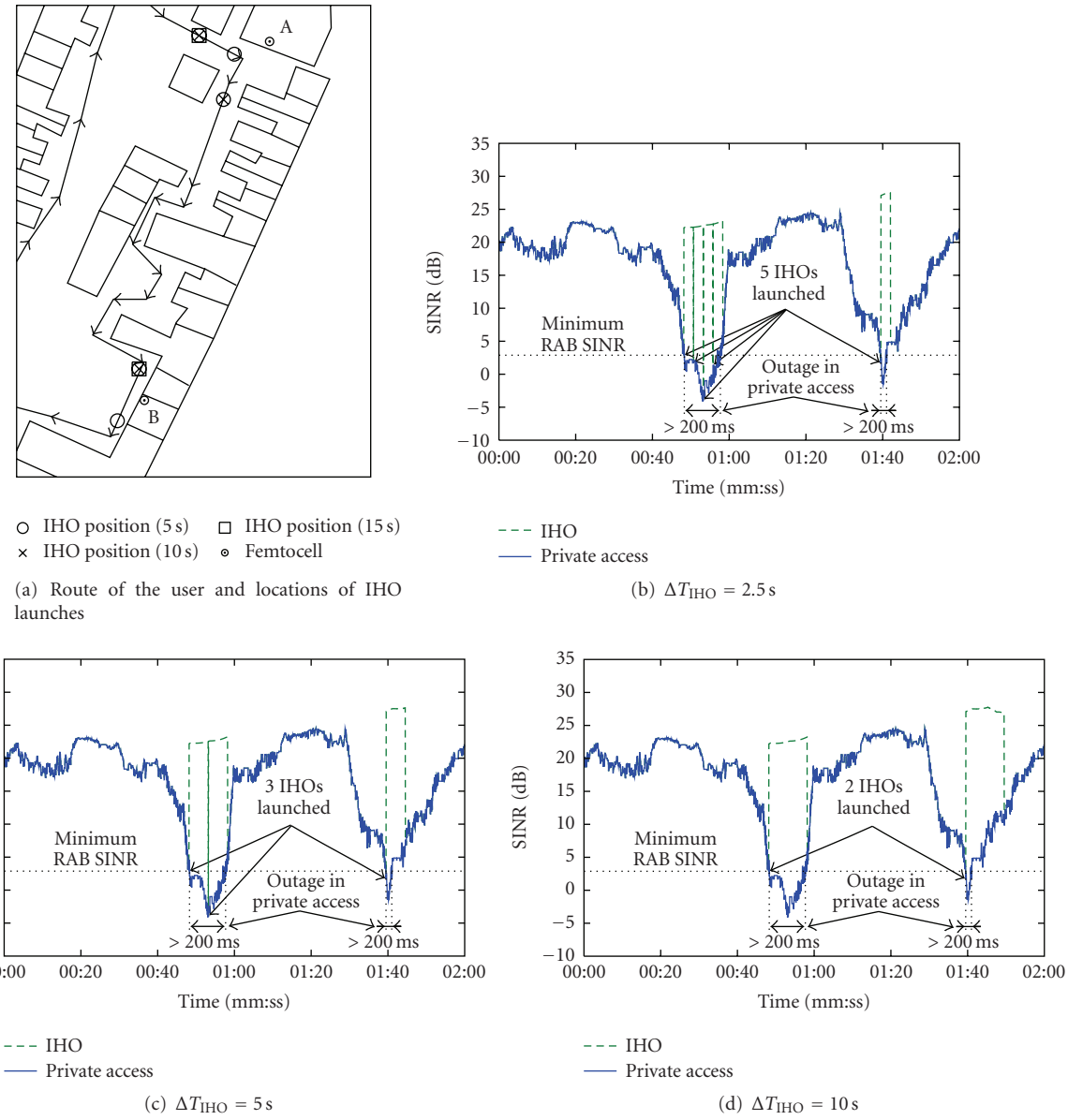

(a) Route of the user and locations of IHO launches

(b) $\Delta T_{\text{IHO}} = 2.5\,\text{s}$

(c) $\Delta T_{\text{IHO}} = 5\,\text{s}$

(d) $\Delta T_{\text{IHO}} = 10\,\text{s}$

Figure 4: Performance comparison of CSG and IHO for a mobile nonsubscriber ($\Delta Q_{\text{IHO}} = 3\,\text{dB}$).

Setup. Macrocell is fully loaded (8 users), whereas the femtocells are half loaded (4 users). IHOs based on subchannel switching are mostly launched in the femtocells (see Table 7 for results).

Setup. Macrocell and femtocells fully loaded (8 users) and IHO implemented without power control. This case, subchannels are forbidden in the femtocells (see Table 8).

Setup. Macrocell and femtocells fully loaded (8 users) and IHO implemented with power control under different $\text{SINR}_y^{\text{target}}$ for the nonsubscribers (see Table 9).

The analysis follows next with regard to different performance metrics.

6.4.1. Number of HO and IHO Attempts. First of all, let us note that in the CSG case, HOs are not allowed. Then, this value is neglected in the result tables.

It is to be mentioned that in all setups with open access, the number of HOs increases with the femtocell penetration. The more femtocells a nonsubscriber finds along its route, the more hand-ins and hand-outs must be carried out. Furthermore, the number of HOs also increases with the number of nonsubscribers.

Similarly, the number of IHOs also increases with the femtocell penetration and the nonsubscriber density. However, the number of IHOs launched is significantly less than the triggered HOs for open access in the same period of time. The reason behind this is that a unique IHO is

Table 6: Performance comparison for Setup 1 (800 s simulation).

Femtocell penetration		12.5%			25%			50%	
Access method	Closed	Open	IHO	Closed	Open	IHO	Closed	Open	IHO
HO attempts	—	243	6	—	606	86	—	1084	193
Average HO attempts into femtocells	—	7.63	0	—	9.78	0.03	—	12.36	0.44
HO attempts into macrocell	—	121	6	—	293	85	—	393	165
Outages due to HO failure	—	2	0	—	12	0	—	21	0
Outages due to interference	69	0	0	224	0	0	299	5	0
Total nonsubscribers tier throughput [Mbps]	2.35	2.69	2.66	1.77	2.62	2.44	1.29	2.45	2.13
Total subscribers tier throughput [Mbps]	44.91	47.33	46.08	91.14	93.70	92.71	166.94	172.46	166.33

IHO approach switching subchannels in the macrocell. Handover, outage and throughput analysis in a residential area (300×300 m) covered by several femtocells and 1 macrocell, using a 5 MHz bandwidth. Each house hosting a femtocell contains 4 indoor users. Furthermore, 4 users were located outdoors and demanding one OFDMA subchannel each. Note that the system level simulation is dynamic and the users move throughout the scenario.

Table 7: Performance comparison for Setup 2 (800 s simulation).

Femtocell penetration		12.5%			25%			50%	
Access method	Closed	Open	IHO	Closed	Open	IHO	Closed	Open	IHO
HO attempts	—	462	35	—	1090	80	—	2554	178
Average HO attempts into femtocells	—	14.14	2.19	—	17.88	2.50	—	28.03	2.78
HO attempts into macrocell	—	231	0	—	518	0	—	760	0
Outages due to HO failure	—	7	0	—	21	0	—	54	0
Outages due to interference	134	1	0	352	2	0	702	5	0
Total nonsubscribers tier throughput [Mbps]	4.53	5.07	5.09	3.66	4.95	4.95	2.24	4.62	4.59
Total subscribers tier throughput [Mbps]	42.24	43.06	42.24	87.07	90.00	87.99	158.98	169.33	160.18

IHO approach switching subchannels in the femtocells. Handover, outage and throughput analysis in a residential area (300×300 m) covered by several femtocells and 1 macrocell, using a 5 MHz bandwidth. Each house hosting a femtocell contains 4 indoor users. Furthermore, 8 users were located outdoors and demanding one OFDMA subchannel each. Note that the system level simulation is dynamic and the users move throughout the scenario.

needed to mitigate the cross-tier interference coming from one femtocell, while in open access two HOs are required (one hand in and one hand out). In addition, the HO is done based on the pilot signal, which is always transmitted, while the IHO only happens if the nonsubscriber and the interferer are utilizing the same subchannel (it does not always occur). Moreover, in this case and due to the multi-path effects, the coverage provided by the femtocells is not continuous. As a consequence, a nonsubscriber moving at low motion can hand over several times from the macrocell to the same open femtocell and vice versa. In order to mitigate this effect, a HO margin, which ensures that the HO is performed only if the neighboring cell is stronger by a given threshold than the server, could be considered. Nevertheless, in this way, the outages due to cross-tier interference would increase. In this case, a perfect HO is considered (as many HOs as needed are done), since the target is to compare open access and the IHO approach based on the number of outages, but not on the signaling overhead.

6.4.2. Outages Due to Interference. In all setups, closed access deployments are severely affected by cross-tier interference, resulting this in a large number of outages. As soon as a nonsubscriber walks near a femtocell using the same subchannel, the nonsubscriber falls into outage. This confirms the need of novel approaches for interference avoidance in two-tier networks.

In the case of open access, the number of outages due to interference are notably reduced compared to that of closed

Table 8: Performance comparison for Setup 3 (800 s simulation).

Femtocell penetration		12.5%			25%			50%	
Access method	Closed	Open	IHO	Closed	Open	IHO	Closed	Open	IHO
HO attempts	—	462	231	—	1090	533	—	2554	1130
Average HO attempts into femtocells	—	14.44	14.44	—	17.88	16.66	—	28.03	17.67
HO attempts into macrocell	—	231	0	—	518	0	—	760	0
Outages due to HO failure	—	7	0	—	21	0	—	54	0
Outages due to interference	284	1	0	746	2	0	1117	5	0
Total nonsubscribers tier throughput [Mbps]	3.60	4.24	4.63	2.15	3.43	4.06	1.07	2.28	3.08
Total subscribers tier throughput [Mbps]	82.40	83.65	80.29	180.05	183.44	175.05	316.48	327.38	307.38

IHO approach without power control, but forbidding subchannels in the femtocells. Handover, outage and throughput analysis in a residential area (300×300 m) covered by several femtocells and 1 macrocell, using a 5 MHz bandwidth. Each house hosting a femtocell contains 8 indoor users. Furthermore, 8 users were located outdoors and demanding one OFDMA subchannel each. Note that the system level simulation is dynamic and the users move throughout the scenario.

Table 9: Performance Comparison for Setup 4 (800 s simulation).

Femtocell penetration		12.5%			25%			50%	
Access method	IHO 10dB	IHO 15dB	IHO Forbid.	IHO 10dB	IHO 15dB	IHO Forbid.	IHO 10dB	IHO 15dB	IHO Forbid.
HO attempts	325	234	231	743	534	533	1491	1135	1130
Average HO attempts into femtocells	20.31	14.63	14.44	23.22	16.69	16.06	23.38	17.77	17.67
HO attempts into macrocell	0	0	0	0	0	0	0	0	0
Outages due to HO failure	0	0	0	0	0	0	0	0	0
Outages due to interference	0	0	0	0	0	0	0	0	0
Total nonsubscribers tier throughput [Mbps]	4.18	4.45	4.63	3.24	3.75	4.06	2.26	2.75	3.08
Total subscribers tier throughput [Mbps]	81.55	80.62	80.29	177.77	175.75	175.05	312.10	308.82	307.38

IHO approach without forbidding subchannels, but with power control in the femtocells. Handover, outage and throughput analysis in a residential area (300×300 m) covered by several femtocells and 1 macrocell, using a 5 MHz bandwidth. Each house hosting a femtocell contains 8 indoor users. Furthermore, 8 users were located outdoors and demanding one OFDMA subchannel each. Note that the system level simulation is dynamic and the users move throughout the scenario.

access. This is because nonsubscribers are allowed to connect to the strongest cell, turning the strong interferer into their best server. However, when the femtocell penetration grows, some cases of outage due to interference also appear. This is because even if the nonsubscriber is connected to the strongest femtocell, the aggregate of cotier interference from neighboring femtocells can disrupt its service, thus creating outage. It is to be noted that the signal strength of a femtocell outdoors is in the same order of magnitude as the signal strength of a neighboring femtocell located few meters away and therefore, if the femtocell penetration is large, cotier interference is a problem.

In the case of IHO, however, the number of outages due to interference is always zero. The number of outages, in this case, does not depend on the femtocell penetration, since the IHO approach is able to "switch off" all existing interferers independently of their number and position.

6.4.3. Outages Due to HO Failure. In open access, the number of HO failures increases with the femtocell penetration and the nonsubscriber density. Let us remember that according to [2], there is a 2% probability that a HO attempt results in a dropped call (outage). The more HO attempts,

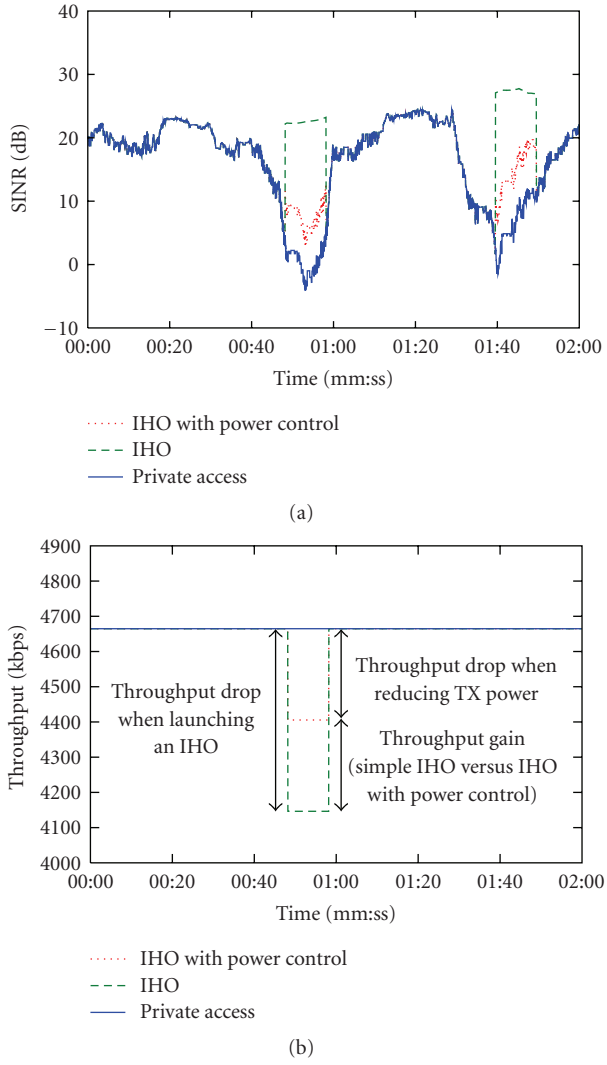

Figure 5: SINR level of a mobile nonsubscriber.

the more HO failures. Nevertheless, the number of outages due to HO failure in open access is much smaller than due to interference in CSG.

6.4.4. NonSubscriber Throughput. In all setups, open access deployments achieve a larger throughput for nonsubscribers than closed access. This is because in open access, nonsubscribers always connect to the strongest cell (macrocell or femtocell), which mitigates cross-tier interference and provides larger RABs. Moreover, the total nonsubscriber throughput in the IHO approach is also always larger than that of closed access due to cross-tier interference mitigation.

When comparing open access and the IHO approach, two issues must be highlighted.

(1) When the IHOs are performed in the macrocell (subchannel switching (Table 6)), the total nonsubscriber throughput in open access is always larger than in the IHO approach.

(2) When the IHOs are performed in the femtocells (subchannel switching (Table 7), forbidding (Table 8) or power control (Table 9)), the total nonsubscriber throughput in open access is always lower than in the IHO approach.

The reason behind this is that in the IHO approach, in the first case, the macrocell just changes the interfered subchannel of the nonsubscriber to another with less interference. However, in the second case, all interfering femtocells stop using such subchannel, thus increasing notably the signal quality and throughput of the nonsubscriber.

It is also to be noticed that in all setups and for all techniques, the larger the femtocell penetration, the lower the total nonsubscriber throughput. This is again due to interference reasons: the more femtocells, the larger the interference, and therefore, the lower the SINR of the nonsubscribers, which is thus translated into a reduction of the nonsubscribers throughput.

6.4.5. Subscribers Throughput. Open access deployments achieve a larger throughput for subscribers than closed access and the IHO approach. This is due to the fact that when a nonsubscriber connects to a femtocell, a subchannel is released in the macrocell. This way, cross-tier interference towards subscribers is reduced, and the throughput of femtocells close to the macrocell is enhanced.

Let us now compare closed access with IHO.

(1) When the IHO is based on subchannel switching either in the macrocell (Table 6) or in the femtocells (Table 7), the total subscriber throughput is slightly better in the IHO approach.

(2) When the IHO is based on subchannel forbidding (Table 8) or power control (Table 9) in the femtocells, the total subscriber throughput is higher in closed access than in the IHO approach.

The reason is that when the IHO is based on subchannel forbidding or power control, the interfering subchannel is either banned from femtocell use or its allocated power is reduced for a period of time. This causes a throughput loss for the subscribers. On the contrary, in closed access, subscribers are always connected to the same subchannel (no power variation) and thus their throughput is not reduced.

It is also to be noticed that in all setups and for all techniques, the larger the femtocell penetration, the larger the total subscriber throughput. This is because the more femtocells, the larger number of connected users in the femtocell tier. However, the average throughput per subscriber does not depend on the femtocell penetration, as it does in the nonsubscribers tier. This is because the effects of cotier interference indoors are smaller than outdoors, namely due to the shield provided by the house walls.

6.4.6. Power Control Behavior. Table 9 presents the performance of IHO with subchannel forbidding compared to that of IHO with power control. Table 9 also shows results for IHO with power control using different $\mathrm{SINR}_y^{\mathrm{target}}$ values.

This experimental evaluation shows, in agreement with the results presented in Figure 5(b), that when power control is used, the reduction of the femtocell throughput is less compared to that of subchannel forbidding. However, it occurs at the expense of decreasing the nonsubscribers throughput, since the interfering subchannels are not turned off.

It is also to be mentioned that the lower the $\mathrm{SINR}_y^{\mathrm{target}}$ value, the lower the reduction of the femtocell throughput. However, it occurs at the expense of reducing the nonsubscriber throughput, since they are only allowed to achieve lower signal qualities.

6.5. Signaling Overhead Due to IHO. The IHO approach implies the following signalin.

(i) A measurement report in order to indicate the RSSs of the neighboring cell in subchannel k, and trigger the IHO.

(ii) An IHO message in order to indicate to the interfering femtocell A_r the reduction of power ΔP^k that has to be applied to subchannel k, and for how long (ΔT_{IHO}).

The size of a measurement report is

$$R \cdot (d_{\mathrm{ID}} + d_{\mathrm{RSS}}), \tag{6}$$

where R denotes the number of interfering femtocells ($|\theta_y|$), d_{ID} indicates the number of bits required to encode the identity of a neighboring cell, and d_{RSS} represents the number of bits required to encode the RSS of a neighboring cell.

The size of an IHO message is

$$d_k + d_{\Delta P} + d_{\Delta T_{\mathrm{IHO}}}, \tag{7}$$

where d_k denotes the number of bits required to encode the identifier of the subchannel, while $d_{\Delta P}$, and $d_{\Delta T_{\mathrm{IHO}}}$ are the number of bits required to encode ΔP^k and ΔT_{IHO}, respectively.

Let us assume that 3 bits are used to encode k (there are 8 subchannels), while 8 bits (256 levels) are used for d_{ID}, d_{RSS}, $d_{\Delta P}$ and $d_{\Delta T_{\mathrm{IHO}}}$. Therefore, the number of required bits per measurement report and IHO message are 512 and 19, respectively. Note that an average of 32 interfering femtocells are considered in this calculation, which is the maximum NCL size in UMTS networks.

The measurement report is triggered when the SINR of a nonsubscriber UE_y^{ns} connected to macrocell M_m in subchannel k is smaller than a given threshold $\mathrm{SINR}_y^{\mathrm{IHO}}$. In the worst case scenario (Setup 4 (Table 9)), when having a femtocell penetration of 50% and using $\mathrm{SINR}_y^{\mathrm{IHO}} = 3\,\mathrm{dB}$ and $\mathrm{SINR}_y^{\mathrm{target}} = 10\,\mathrm{dB}$, an average of 23.38 IHOs have been triggered per femtocell (simulation time = 800 s). Therefore

(i) the average uplink bandwidth required to carry 23.38 measurement reports per femtocell in 800 s is 14.96 bps,

(ii) the average downlink bandwidth required to carry 23.38 IHO messages per femtocell in 800 s is 0.56 bps.

These values are negligible compared to the capacity of the downlink and uplink of current OFDMA standards such as LTE or WiMAX. Therefore, it can be concluded that only a small fraction of the whole available bandwidth is needed for signaling overhead.

Finally, it is to be noted that the signaling required for an IHO is lower than for a HO. When performing a HO, all packets stored in the source cell, which belong to the user that is to be handed over, has to be transferred from the source cell to the target cell (implying a large overhead). However, in the IHO approach, in the worst case scenario, the macrocell has to indicate to the interfering femtocells only the reduction of power that has to be applied to a given subchannel and for how long.

7. Conclusions

The results of the system-level simulations show the following evidence about this type of residential scenarios.

Conclusion 1. The main problems of open access are the risk of outage due to HO failure and the high signaling introduced in the network. On the other hand, CSG femtocells introduce serious jamming problems (dropped call) to macrocell users in the downlink.

Conclusion 2. Open access has always an overall better throughput performance than the one of closed access.

Conclusion 3. When the femtocell penetration is large, the aggregate of the interference of nearby femtocells might be enough to cause outage to outdoor users, who will not be able to take advantage of the open access.

Then, it has been shown that by applying an intracell handover approach to OFDMA two-tier networks, the following occurs.

Conclusion 4. Downlink cross-tier interference to nonsubscribers decreases compared to CSG deployments. This is made evident from the number of outages due to interference shown in Tables 6, 7, 8, and 9 (results).

Conclusion 5. Handover attempts and thus network signaling decrease with respect to the open access case. Furthermore, the risk of outage due to handover failure is removed as it can be seen in the tables of results.

Conclusion 6. In order to avoid macrocell deterioration due to femtocell deployment, FAPs must be flexible when limiting the throughput of their own subscribers. The interference reduction of nonsubscribers should thus have more priority than the maximization of subscribers throughput. Therefore, a trade-off between these two objectives must be always achieved. Moreover, due to the nature of the services used by subscribers, the impact of subchannel forbidding is, in average, not too crucial for femtocell connectivity.

Conclusion 7. In order to reduce signaling, IHOs are attempted in the macrocell before they are attempted in nearby femtocells. However, it has been observed that femtocell-based IHOs result in higher throughput gains than macrocell ones. This is because a femtocell IHO removes fully the cross-tier interference while a macrocell IHO selects a less interfered subchannel which is not necessarily free of cross-tier interference.

Conclusion 8. Power control helps to handle cross-tier interference, while limiting the impact to subscribers when subchannel switching is not possible.

To summarize, the IHO approach presented in this article has better performance than CSG in terms of outage and throughput of nonsubscribers in all tested femtocell penetration conditions. The throughput of nonsubscribers is slightly below than that of open access in most cases, except for large femtocell penetrations, in which the IHO approach outperforms open access (Table 8). However, the network signaling is lower in case of IHO, and thus the risk of HO failure is practically nonexistent, avoiding outage.

Acknowledgments

This work is supported by the EU FP6 project on 3G/4G Wireless Network Design "RANPLAN-HEC" with Grant no. MEST-CT-2005-020958 and EU FP6 "GAWIND" with Grant no. MTKD-CT-2006-042783.

References

[1] H. Claussen, "Co-channel operation of macro- and femtocells in a hierarchical cell structure," *International Journal of Wireless Information Networks*, vol. 15, no. 3-4, pp. 137–147, 2008.

[2] H. Claussen, L. T. W. Ho, and L. G. Samuel, "An overview of the femtocell concept," *Bell Labs Technical Journal*, vol. 13, no. 1, pp. 221–246, 2008.

[3] A. Valcarce, D. López-Pérez, G. de la Roche, and J. Zhang, "Limited access to OFDMA femtocells," in *Proceedings of the IEEE Personal, Indoor and Mobile Radio Conference (PIMRC '09)*, Tokyo, Japan, September 2009.

[4] H. Claussen, L. T. W. Ho, and L. G. Samuel, "Self-optimization of coverage for femtocell deployments," in *Proceedings of the 7th Annual Wireless Telecommunications Symposium (WTS '08)*, pp. 278–285, April 2008.

[5] H. Claussen and F. Pivit, "Femtocell coverage optimization using switched multi-element antennas," in *Proceedings of the IEEE International Conference on Communications (ICC '09)*, pp. 1–6, June 2009.

[6] V. Chandrasekhar and J. G. Andrews, "Spectrum allocation in two-tier networks," to appear in *IEEE Transactions on Communications*.

[7] J. Zhang and G. de la Roche, *Femtocells:Technologies and Deployment*, John Wiley & Sons, New York, NY, USA, 2010.

[8] J. D. Hobby and H. Claussen, "Deployment options for femtocells and their impact on existing macrocellular networks," *Bell Labs Technical Journal*, vol. 13, no. 4, pp. 145–160, 2009.

[9] D. López-Pérez, A. Valcarce, G. de la Roche, and J. Zhang, "OFDMA femtocells: a roadmap on interference avoidance," *IEEE Communications Magazine*, vol. 47, no. 9, pp. 41–48, 2009.

[10] G. Guvenc, M.-R. Jeong, F. Watanabe, and H. Inamura, "A hybrid frequency assignment for femtocells and coverage area analysis for co-channel operation," *IEEE Communications Letters*, vol. 12, no. 12, pp. 880–882, 2008.

[11] D. López-Pérez, A. Ladányi, A. Jüuttner, and J. Zhang, "OFDMA femtocells: a self-organizing approach for frequency assignment," in *Proceedings of the IEEE Personal, Indoor and Mobile Radio Conference (PIMRC '09)*, Tokyo, Japan, September 2009.

[12] G. de la Roche, A. Valcarce, D. López-Pérez, and J. Zhang, "Access control mechanisms for femtocells," *IEEE Communications Magazine*, vol. 48, no. 1, pp. 33–39, 2010.

[13] 3GPP, "UE autonomous search function for CSG cell," R2-091128, February 2009.

[14] IEEE, "IEEE standard for local and metropolitan area networks part 16: air interface for fixed and mobile broadband wireless access systems," Tech. Rep. 802.16, October 2004.

[15] 3GPP, "Radio resource control (RRC); protocol specification, (release 8)," Tech. Rep. Ts 25.331, April 2008.

[16] E. Amaldi, A. Capone, and F. Malucelli, "Planning UMTS base station location: optimization models with power control and algorithms," *IEEE Transactions on Wireless Communications*, vol. 2, no. 5, pp. 939–952, 2003.

[17] S.-E. Elayoubi, O. Ben Haddada, and B. Fourestié, "Performance evaluation of frequency planning schemes in OFDMA-based networks," *IEEE Transactions on Wireless Communications*, vol. 7, no. 5, pp. 1623–1633, 2008.

[18] H. Holma and A. Toskala, *WCDMA for UMTS-HSPA Evolution and LTE*, John Wiley & Sons, New York, NY, USA, 4th edition, 2007.

[19] L. Wang, Y. Zhang, and Z. Wei, "Mobility management schemes at radio network layer for LTE femtocells," in *Proceedings of the 69th IEEE Vehicular Technology Conference (VTC '09)*, Barcelona Spain, April 2009.

[20] C. Bettstetter, "Smooth is better than sharp: a random mobility model for simulation of wireless networks," in *Proceedings of the 4th ACM International Workshop on Modeling, Analysis and Simulation of Wireless and Mobile Systems*, pp. 19–27, Rome, Italy, 2001.

[21] A. Valcarce, H. Krauss, J. Hauck, M. Buchholz, and F. Aguado, "Empirical propagation model for WiMAX at 3.5 GHz in an urban environment," *Microwave and Optical Technology Letters*, vol. 50, no. 2, pp. 483–487, 2008.

[22] A. Valcarce, G. de la Roche, Á. Jüttner, D. López-Pérez, and J. Zhang, "Applying FDTD to the coverage prediction of WiMAX femtocells," *EURASIP Journal on Wireless Communications and Networking*, vol. 2009, Article ID 308606, 13 pages, 2009.

[23] NGMN, "NGMN radio access performance evaluation methodology," A White Paper by the NGMN Alliance, January 2008.

Hindawi Publishing Corporation
EURASIP Journal on Wireless Communications and Networking
Volume 2010, Article ID 186815, 12 pages
doi:10.1155/2010/186815

Research Article

Interference Mitigation by Practical Transmit Beamforming Methods in Closed Femtocells

Mika Husso,[1] Jyri Hämäläinen,[1] Riku Jäntti,[1] Juan Li,[1] Edward Mutafungwa,[1] Risto Wichman,[1] Zhong Zheng,[1] and Alexander M. Wyglinski[2]

[1] *Department of Communications and Networking, Helsinki University of Technology, P.O. Box 3000, 02015 TKK, Espoo, Finland*
[2] *Department of Electrical and Computer Engineering, Worcester Polytechnic Institute, Worcester, MA 01609-2280, USA*

Correspondence should be addressed to Mika Husso, mika.husso@tkk.fi

Received 21 December 2009; Accepted 3 April 2010

Academic Editor: Ismail Guvenc

We present an analysis of a femtocellular communications network and the impact of cochannel interference on link performance. Furthermore, we propose a method whereby user terminals can maintain a controlonly connection to an adjacent femtocell for interference mitigation purposes. Specifically, we provide an emphasis on suboptimal but practical methods that rely on transmit beamforming. Our numerical results demonstrate that even simple multiantenna methods can be effectively used to suppress co-channel interference provided that control channel connection between interfering femto-base station and user terminal is allowed.

1. Introduction

The emergence of new data-intensive wireless services coupled with an increase in the number of multimedia-enabled user equipments, such as smartphones, has forced mobile operators to examine new ways for increasing coverage, achieve requested data rates, and to lower the capital and operating costs (CAPEX and OPEX) of their mobile networks. One approach for filling-in coverage holes and increasing data rates has been the utilization of relatively small cellular access sites. Femtocells provide a practical solution that has recently been generating considerable interest among both academic and industrial communities. The potential cost reduction of up to 70 percent per annum in operator's network functions [1], combined with the prediction of 95 percent annual market growth in the following years [2], makes the femtocell concept a particularly lucrative option for most mobile operators.

The standardization process of femtocells launched in August 2007 via the 3rd Generation Partnership Project (3GPP) is still under way. Until now, 3GPP has published both technical reports [3] and technical specifications [4, 5] focusing on end-to-end and UTRAN architectures, respectively. Simultaneously with the 3GPP activities, the IEEE 802.16 standardization group has discussed femtocellular networking and related products. More recently, in June 2009, the Femto Forum and the WiMAX Forum agreed on collaborating with respect the development of a WiMAX Femtocell Access Point (WFAP) specifications addressing a wide range of topics such as end-to-end QoS, power optimization, and mobility management.

Concurrent with participating in standardization work, major vendors have been active in femtocell product development. The first wave of femtocell products hit the market in 2008 and several product launches are expected. For the vendors, femtocells represent significant potential for additional revenue should they prove successful.

Although femtocells provide significant benefits for mobile operators and users alike, their introduction comes with great many new challenges (see, e.g., [6]). Among these is the interference between macro and femtocells, as well as between individual femtocells. Furthermore, the effect of interference needs to be studied separately for downlink and uplink. To mitigate the interference-related problems, several approaches have been proposed including, but not limited to, open access, dedicated band deployment, transmit power optimization, interference cancelation, adaptive antennas, and MIMO schemes.

In the first phase of femtocell deployment, closed subscriber group (CSG) configurations (see [3]) are expected to be widely used due to security, billing, and contractual concerns. In a CSG configuration, the femto base station (FBS) only serves users who are a member of a particular CSG. We refer to this configuration when using the term "closed femtocell", and it is emphasized that the CSG prevents any handover attempts from users that are not included in the CSG. For this reason, it is important to develop methods for alleviating cochannel interference in private femtocells.

In this paper, we present a method for transmit beamforming-based interference control utilizing multiple antennas in the FBS in conjunction with a control-only connection established between user equipment (UE) and interfering FBSs. It is shown through the analysis and simulation that even simple and practical transmit beamforming methods can be used to effectively suppress the interference in adjacent FBSs.

The paper is structured as follows: Section 3 discusses the general system model and corresponding assumptions. Investigated transmit beamforming methods are described in Section 4 and the performance analysis is outlined in Section 5. Concluding remarks are presented in Section 6.

2. What Are Femtocellular Communications?

Femtocellular communications have been proposed as a possible solution for satisfying the rapid increase in demand for wireless access [7, 8]. Conventional wireless access networks that are currently deployed at a metropolitan scale, such as cellular telephony networks, are beginning to reach their theoretical capacity limits in terms of the number of supported end-users as well as overall data rates. This is mainly due to the explosive growth of the "smartphone" market, which requires mobility, ubiquitous wireless coverage, and support for high-data rate applications, for example, web-browsing, email, and streaming multimedia content. Furthermore, one of the key technical challenges with conventional cellular telephony networks is their intermittent coverage within indoor environments, which tends to be impaired due to the often poor wireless propagation environment [9, 10].

The femtocellular communications concept attempts to solve the issues of both limited wireless capacity and poor indoor coverage while complementing existing cellular telephony networks operating simultaneously in the same geographical vicinity. This is achieved by having the end-users setup indoor femtocellular access points using an approach similar to establishing a WLAN access point [11], for example, WiFi hotspot, where the wireless access point is connected to a wired communications infrastructure commonly available in dense urban population centers, for example, DSL, fiber-to-the-home, cable. The femtocellular access point provides the end-user with excellent wireless signal strength and coverage relative to a conventional cellular base station that may be located several kilometers away. The transmission range of a femtocellular access point is on the order of tens of meters. Furthermore, due to the limited transmission range, the high degree of frequency reuse will enable greater wireless capacity in terms of users and bandwidth [12].

Although femtocellular communication networks possess several similarities with WLAN deployments, including transmission range, access point setup, and supported bandwidths, femtocellular communication networks also possess several substantial differences such as the following.

(*i*) *Centralized Network Architecture.* The network operations of each femtocellular access point can be controlled by the wireless service provider in order to seamlessly integrate the femtocellular communication networks with each other, as well as with the conventional cellular telephony networks. Network operations such as hand-offs of wireless devices between different femtocellular access points, or between a femtocellular access point and a conventional cellular telephony base station, can only be supported by a femtocellular communication network [13]. It should be pointed out that most WLAN customer premises equipment usually operate locally and do not directly coordinate their operations with other WLAN access points or a conventional cellular telephony base station.

(*ii*) *Cellular Telephony Access.* Femtocellular access points can be viewed as an extension of the conventional cellular telephony base stations, although the former possesses a significantly lower transmission range to help ensure minimal interference with other femtocellular access points as well as the conventional cellular telephony base stations themselves. Consequently, femtocellular access points support the same transmission frequency ranges as conventional cellular telephony networks [14]. Note that conventional WLAN customer premises equipment normally does not support these frequency ranges.

(*iii*) *Home Network Connectivity.* Femtocellular access points possess the potential for an end-user to be informed of situations at the indoor premises based on the information generated by multiple wireless devices connected to the femtocellular access point, which can subsequently relay information to the cellular telephony device of the end-user. Similarly, the end-user can control appliances at the premises using the cellular telephony device as the interface and having the femtocellular access point relay control information to the respective wireless devices. Note that the other wireless devices connected to the femtocellular access point may or may not be cellular telephony devices, for example, WiFi, Bluetooth, infrared.

Consequently, femtocellular communication networks have the potential to provide the end-users with adequate wireless coverage and bandwidth while simultaneously having them be connected to the overall centralized network of the wireless service provider.

3. System Model

3.1. Interference Scenario. An FBS is a small cellular basestation with a transmission power that is less than or

comparable with a user terminal's transmission power. Considering Third Generation (3G) High-Speed Packet Access (HSPA) networks, the FBS contains some radio network controller functionalities and it is designed for use in residential or small business environments. The FBS device is about the same size as a typical digital subscriber line (DSL) or cable modem device and provides indoor wireless coverage to mobile terminals whilst using the existing broadband Internet connection (xDSL, fiber, cable, etc.) for connectivity to a remote femto-gateway.

However, residential broadband connections are not engineered to provide carrier-grade quality-of-service (QoS) guarantees at levels that would typically be demanded in conventional dedicated leased lines for macrocell backhaul. As a result, fast and accurate centralized control of femtocells is not possible. Therefore, horizontal handovers between femtocells are difficult to arrange, and vertical handover to overlaying macrocell is supported instead. Furthermore, due to privacy reasons the femtocell access can be restricted to household members. In 3GPP terminology, members of the group that are allowed to access to the femtocell form a CSG.

The femtocell deployments will be characterized by uncontrollability. Since the average user cannot be expected to possess adequate skills to optimally configure the air interface of the femtocell, then auto-configurability becomes crucial [15] as well as the ability of the femtocell to operate under heavy cochannel interference. The cochannel interference will be difficult to avoid through usage of different carriers especially in HSPA since the operation bandwidth is fixed at 5 MHz and many mobile operators possess licenses for only a very limited number of carriers.

Different interference scenarios related to femtocellular access have been listed in [3] whereby references to preliminary 3GPP investigations in different cases have been provided. Interference scenarios can be divided into two main categories: first, there are scenarios where interference occurs between femtocells. Second, there are scenarios where interference occurs between femtocells and macrocells. Other dimensions that are used for scenario definition are distinctions between cochannel and adjacent channel interference as well as distinction between downlink and uplink interference.

In this paper, we consider the case where *downlink cochannel interference occurs between adjacent femtocells*. Acknowledging a degree of loss of generality, we have limited the number of femtocells to two primarily for two reasons. First, practical building structures very often result in a dominant interferer case especially when FBS penetration remains moderate. Secondly, analyzing a system comprising two femtocells and two users permits the derivation of compact closed form expressions for SINR and the performance metrics. Furthermore, we assume that the transmission power in FBSs is constant and handover is not enabled.

3.2. Employed Assumptions. We have adopted the following assumptions regarding the general framework.

(A1) We focus on a two-cell scenario where adjacent FBSs create downlink cochannel interference to the UE of the reference cell. Transmission power in the FBSs is constant and handover between cells is not possible, that is, CSG configuration is applied but *the UE can form a control connection to both serving and interfering FBS units*.

(A2) There are M transmit antennas in both FBSs and a single receive antenna in a UE. The terminal can estimate signals from the different antennas of both the serving and the interfering FBSs. Channel estimation is assumed to be perfect. The terminal may send a feedback message to both femtocellular transceivers including information for the antenna weight selection. *The impact of delay of feedback is ignored.*

(A3) Channels related to different antennas of the same FBS are i.i.d. complex zero-mean Gaussian, while the mean transmission power is different for separate FBSs. Fast fading from different FBSs is uncorrelated.

Let us briefly discuss the validity of the aforementioned assumptions. The interference scenario of (A1) is valid for instance, for the HSDPA case since the first home femtocellular deployments employ HSDPA. Moreover, due to constraints in spectrum availability, it is not attractive for operators to dedicate more than one carrier for femtocellular operations. Usage of fixed transmission power and CSG are expected in many deployments while control connection to adjacent BSs is currently possible only with macrocell systems. Yet, this extension to the current femtocell capabilities is the main research question: how much benefit can be accrued by establishing a control channel connection to the interfering adjacent FBS?

We note that our discussion focuses on the benefits from transmit beamforming control over adjacent femtocells when the downlink transmission power is fixed. Yet, it is known from [15] that the adjustable transmission power in femtocells is a good option although it may lead to either undesired power competition between households or coverage problems if FBS transmission power is allowed to decrease excessively. Thus, self-organizing femtocells with a feasible combination of power control and interference mitigation capabilities are a good topic for future work.

In order to keep the discussion on a generic level, we have adopted in (A2) the M transmit antenna assumption although a two-antenna approach is currently more feasible since transmit beamforming in HSDPA is defined for two antennas. Yet, in LTE there will be a support for four-antenna transmit beamforming methods [16]. Legacy HSDPA terminals are equipped with one receive antenna and they can estimate channels of two different BS antennas from primary common pilot channels (P-CPICHs) and define the beamforming feedback that is then sent to the BS through a dedicated feedback channel. For handover purposes, the HSDPA terminal is also able to estimate P-CPICH signals from adjacent BSs and thus, it is able to define related beamforming feedback for adjacent BSs. In Wideband Code Division Multiple Access (WCDMA), soft handover terminal defines the beamforming feedback that best fits with the transmission from BSs in the so-called active

set [17]. In HSDPA the additional cost from the proposed method would be to introduce dedicated physical control channel (DPCCH) between user and interfering FBS. The actual feedback information would contain 1 bit per time slot in DPCCH time slot like in current HSDPA two-antenna transmit beamforming. The feedback delay can be ignored because user mobility in femtocell system is low.

The channel statistics may vary depending on the building structures but due to rich scattering the Rayleigh fading assumption of (A3) is a good approximation although it fails when there is a line-of-sight between transmitter and receiver. *Thus, the analysis is valid for the Rayleigh fading case.* The mean transmission power from different FBSs is not the same due to locations in separate apartments but antenna correlations of the same FBS may occur in practice. Yet, correlation is usually small and can be ignored when rich scattering around the FBS takes place.

4. Transmit Beamforming and Interference Mitigation Methods

4.1. Preliminaries. The work possesses two goals: first, we consider an extension for the practical two-antenna transmit beamforming method of HSDPA. This method is also referred to as a closed-loop mode 1 transmit diversity [17] and we use it as a tool in interference mitigation. In current HSDPA implementations, the mode 1 is defined only for two-antenna system but we also analyze M antenna case in order to demonstrate the gains that achievable when increasing the number of antennas in beamforming. We note that our results for the two-antenna case illustrate the performance benefit that can be obtained by present HSDPA beamforming method with only minor adjustments to the 3GPP specifications. Practical transmit beamforming methods similar to one used in HSDPA have been previously studied in, for example, [18–20] while more general research approaches can be found from, for example, [21–26]. Second, we focus on the usage of transmit antenna selection as a part of the interference mitigation method because it provides a lower bound for the reachable gain from proposed approach and also allows simple closed-form analysis where the impact of different parameters can be easily observed. Antenna selection is also quite practical due to small signalling overhead.

4.2. Transmit Beamforming

4.2.1. Mode 1. We start by recalling the transmit beamforming of HSDPA. As depicted in Figure 1 the receiver encodes channel state information (CSI) into the feedback message that is transmitted using the feedback indicator (FBI) field in the uplink channel. Similarly, transmit power control (TPC) commands are passed in the TPC field. Note that the transmit power control that compensates fast fading is used in downlink only for services with strict latency requirements like circuit-switched voice, while data services mostly employ High-Speed Downlink Shared Channel (HS-DSCH) where TPC is not present.

Assuming an interference free case, the received signal at the terminal is of the form

$$r = (\mathbf{h} \cdot \mathbf{w})s + n = \left(\sum_{m=1}^{M} w_m h_m \right) s + n, \tag{1}$$

where s is the transmitted symbol, $\mathbf{h} = (h_1, \ldots, h_M)$ consists of complex zero-mean Gaussian channel coefficients, n refers to additive white Gaussian noise, and vector $\mathbf{w} \in \mathbf{W}$ refers to the codebook of complex transmit beamforming weights such that $\|\mathbf{w}\| = 1$ and $\mathbf{w} \cdot \mathbf{h} = w_1 h_1 + \ldots w_M h_M$. Given received signal (1) and quantization set $\mathbf{W}$, the weight $\hat{\mathbf{w}}$ that maximizes SNR in reception can be found after evaluating (1) for all weight vectors. Thus, for a given channel coefficient vector $\mathbf{h}$, the applied weight $\hat{\mathbf{w}}$ is found after solving the finite dimensional optimization problem

$$\text{Find } \hat{\mathbf{w}} \in \mathbf{W} : \left| \mathbf{h} \cdot \hat{\mathbf{w}} \right| = \underset{\mathbf{w} \in \mathbf{W}}{\operatorname{argmax}} |\mathbf{h} \cdot \mathbf{w}|. \tag{2}$$

In two-antenna HSDPA, transmit beamforming $\mathbf{h} = (h_1, h_2)$ is obtained after estimating the P-CPICH signals. The antenna phasing at the BS is done by interpolation over two consecutive one-bit feedback messages after intermediate 90 degree rotation of the constellation. In low mobility environment where channel fluctuations during consecutive feedback messages are negligible, this leads to QPSK phasing and related phasing weights. Since amplitude weights are not used, $\mathbf{W}$ basically contains vectors $(1, e^{jn\pi/2})/\sqrt{2}$, $n = 0, 1, 2, 3$. When using the extended mode 1 for M antennas, the beamforming weights are selected from the set of vectors $(1, e^{jn_2\pi/2}, \ldots, e^{jn_M\pi/2})/\sqrt{M}$, $n_m \in \{0, 1, 2, 3\}$. For more detailed discussion on mode 1 and its extension, see [20].

4.2.2. Transmit Antenna Selection. In antenna selection method, $\mathbf{W}$ consists of M vectors of the form, $\mathbf{w} = (0, \ldots, 0, 1, 0, \ldots, 0)$, where the non-zero component indicates the best channel in terms of the received power.

We note that feedback overhead during each update is $2(M - 1)$ bits for extended mode 1 with QPSK phasing and $2\lceil \log_2(M) \rceil$ bits for antenna selection. The actual feedback capacity need depends on the update rate which is decided in system design based on expected fading rate due to terminal mobility. In HSDPA, the update rate is 1.5 kbps.

4.3. Interference Mitigation. Let us first consider the model for the instantaneous Signal to Interference and Noise Ratio (SINR) without transmit beamforming. Assuming that there are K femtocellular BSs that each apply the transmission power P_{Tx} and suppose that the total instantaneous path losses between BSs and mobile receiver are denoted by L_k, the SINR at the receiver is of the form

$$\Upsilon = \frac{P_{\text{Tx}}/L_1}{P_N + \sum_{k=2}^{K} P_{\text{Tx}}/L_k} = \frac{P_{\text{Tx}}/L_1}{P_I + P_{\text{Tx}}/L_2}, \tag{3}$$

where index $k = 1$ refers to the BS that receiver is connected and P_N is the Additional White Gaussian Noise (AWGN) term. The second form on the right we have introduced in order to separate the strongest interference source that is

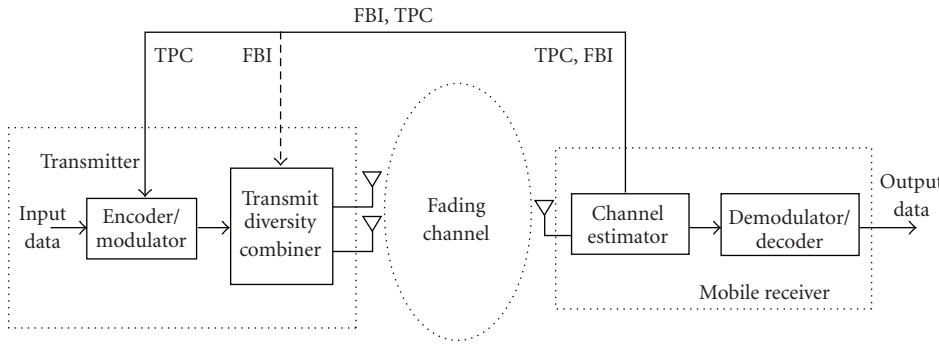

Figure 1: General system structure for UTRA FDD downlink with mode 1.

assumed to be BS with $k = 2$, and noise and interference from other interfering base stations (P_I). Now we can write

$$\Upsilon = \frac{\gamma_{1\to 1}}{1+\gamma_{2\to 1}}, \quad \gamma_{1\to 1} = \frac{P_{\mathrm{Tx}}}{P_I L_1}, \gamma_{2\to 1} = \frac{P_{\mathrm{Tx}}}{P_I L_2}, \tag{4}$$

where $\gamma_{1\to 1}$ is the SINR at the receiver excluding the dominant interference and $\gamma_{2\to 1}$ is the SINR of the dominant interfering signal. If single interferer dominates, then these variables can be written in the form

$$\gamma_{m\to 1} = \overline{\gamma}_{m\to 1}|h|^2, \qquad \overline{\gamma}_{m\to 1} = E\left\{\frac{P_{\mathrm{Tx}}}{(P_I L_m)}\right\}, \tag{5}$$

where $\overline{\gamma}_{m\to 1}$ is the mean received power and $|h|^2$ is the instantaneous channel power that is normalized, $E\{|h|^2\} = 1$.

In HSDPA, transmissions from different BSs are separated by scrambling codes and after descrambling the desired message, the interference P_I is seen as an increase in the noise level. Thus, the impact of P_I in (4) is seen as a noise level increase for both $\gamma_{1\to 1}$ and $\gamma_{2\to 1}$. We note that in reception only, $\gamma_{1\to 1}$ includes the spreading gain if SINR is measured after despreading of the signal. We also note that in HSDPA downlink transmission is carried out over the whole bandwidth and users are separated in each cell by spreading codes. The wideband interference from adjacent cells is white noise-like and by applying wideband transmit beamforming weights selected by an interfered user the noise level can be decreased.

In the following, we assume a scenario consisting of one desired user and a dominant interferer. This assumption simplifies the analysis and can be generalized to more interferers in simulations. The signal-to-noise ratio (SNR) received by kth user from lth femto transmitter is denoted by

$$\gamma_{l\to k} = \overline{\gamma}_{l\to k}\left|\mathbf{h}_{l\to k}\cdot\widehat{\mathbf{w}}_{l\to l}\right|^2, \tag{6}$$

where $\overline{\gamma}_{l\to k}$ is the mean SNR in the link. We note that in conventional transmit beamforming, the weight is selected according to (2) and it maximizes SNR when $k = l$, that is, when transmission is directed to the dedicated femto user. Since vector channels $\mathbf{h}_{l\to l}$ and $\mathbf{h}_{l\to k}$ are uncorrelated, the interference $\mathbf{h}_{l\to k}\cdot\widehat{\mathbf{w}}_{l\to l}$ is zero-mean Gaussian.

When transmit beamforming is applied and there are two FBS and two terminals, the signal to interference and noise ratios (SINRs) in first and second UE are given by

$$\begin{aligned}\Upsilon_1 &= \frac{\gamma_{1\to 1}}{1+\gamma_{2\to 1}} = \frac{\overline{\gamma}_{1\to 1}\left|\mathbf{h}_{1\to 1}\cdot\widehat{\mathbf{w}}_{1\to 1}\right|^2}{1+\overline{\gamma}_{2\to 1}\left|\mathbf{h}_{2\to 1}\cdot\widehat{\mathbf{w}}_{2\to 2}\right|^2},\\ \Upsilon_2 &= \frac{\gamma_{2\to 2}}{1+\gamma_{1\to 2}} = \frac{\overline{\gamma}_{2\to 2}\left|\mathbf{h}_{2\to 2}\cdot\widehat{\mathbf{w}}_{2\to 2}\right|^2}{1+\overline{\gamma}_{1\to 2}\left|\mathbf{h}_{1\to 2}\cdot\widehat{\mathbf{w}}_{1\to 1}\right|^2}.\end{aligned} \tag{7}$$

We note that in case of multiple users, the transmit beamforming weights in own cell are applied separately on each users subchannels. Due to (A1), handover between FBSs is not allowed and either of the FBSs may dominate. To track this we denote the mean SNR ratios by

$$\nu_1 = \frac{\overline{\gamma}_{1\to 1}}{\overline{\gamma}_{2\to 1}}, \qquad \nu_2 = \frac{\overline{\gamma}_{2\to 2}}{\overline{\gamma}_{1\to 2}}. \tag{8}$$

If femtocells are sufficiently separated, then both ν_1 and ν_2 are large and the interference is negligible. On the other hand, extreme cases exist where both ν_1 and ν_2 are small; see [27]. However, such situations are rare and in most of the cases at least one of the ratios is large.

Let us adopt the most common interference situation where either of the two links possesses a good channel. For simplicity we assume that the user in the first (reference) femtocell suffers from interference originating from the second femtocell, but the user in the second femtocell possesses a good channel, that is, $\nu_2 \gg 1$. In the applied interference mitigation method, we allow the user terminal in first femtocell to establish a control channel connection with the interfering FBS according to (A1) and (A2). Then the interfered terminal can request second FBS to replace $\widehat{\mathbf{w}}_{2\to 2}$ by the weight $\check{\mathbf{w}}_{2\to 1}$ that is selected using the criteria

$$\text{Find } \check{\mathbf{w}} \in \mathbf{W} : |\mathbf{h}_{2\to 1}\cdot\check{\mathbf{w}}| = \underset{\mathbf{w}\in\mathbf{W}}{\operatorname{argmin}}\,|\mathbf{h}_{2\to 1}\cdot\mathbf{w}|. \tag{9}$$

This approach will minimize the interference term in Υ_1 of (7) while the user terminals in second femtocell will loose gain from transmit beamforming because $\check{\mathbf{w}}_{2\to 1}$ is selected independently from the second cell user channels. Given that $\nu_2 \gg 1$, it is expected that loosing beamforming gain is not critical for the user of the second femtocell. In practice

an FBS may probe the interference situation in its cell by requesting reports from users that it is serving. If received signal strengths are well sufficient for the served terminals, then it may apply available transmit beamforming methods to decrease the interference level in adjacent cell provided that this operation is not violating connections of its own users.

The SINR formulae of (7) are now given by

$$\Upsilon_{(1)} = \frac{\hat{\gamma}_{1\to 1}}{1+\check{\gamma}_{2\to 1}} = \frac{\overline{\gamma}_{1\to 1}\left|\mathbf{h}_{1\to 1}\cdot\hat{\mathbf{w}}_{1\to 1}\right|^2}{1+\overline{\gamma}_{2\to 1}\left|\mathbf{h}_{2\to 1}\cdot\check{\mathbf{w}}_{2\to 1}\right|^2},$$
$$\Upsilon_{(2)} = \frac{\widetilde{\gamma}_{2\to 2}}{1+\widetilde{\gamma}_{1\to 2}} = \frac{\overline{\gamma}_{2\to 2}\left|\mathbf{h}_{2\to 2}\cdot\check{\mathbf{w}}_{2\to 1}\right|^2}{1+\overline{\gamma}_{1\to 2}\left|\mathbf{h}_{1\to 2}\cdot\hat{\mathbf{w}}_{1\to 1}\right|^2}. \quad (10)$$

Here weights $\hat{\mathbf{w}}_{1\to 1}$ and $\check{\mathbf{w}}_{2\to 1}$ are selected according to (2) and (9), leading to SNRs $\hat{\gamma}_{1\to 1}$ and $\check{\gamma}_{2\to 1}$ of dedicated and suppressed signals. Notations $\widetilde{\gamma}_{2\to 2}$ and $\widetilde{\gamma}_{1\to 2}$ refer to signal SNRs in cases where transmit beamforming weights are selected independently from the channels. Finally, SINR subscripts are in parentheses to emphasize the fact that the first user is preferred when defining beamforming weights.

An approach similar to (10) was previously used in the case of a single cell multiuser scheduling and two antennas [28, 29]. There a BS applies orthogonal weight vectors to suppress its own cell interference when simultaneous transmission to two users is executed. When the number of users in scheduling queue is large, the BS scheduler may find a user pair with roughly orthogonal channels and the method provides gain in terms of cell throughput. The method of [28, 29] is designed to enable simultaneous transmission to two users from a single BS so that interference between transmissions is as small as possible. The proposed method for femtocells is different because interference comes from different FBS than the desired signal and an additional control channel is needed between user terminal and interfering FBS.

5. Performance Analysis

Given the proposed method defined by (10), we now proceed with the system performance analysis employing both the cumulative distribution function (CDF) of SINR as well as outage and average rates. In the performance figures, closed form results have been used for antenna selection while mode 1 was studied using only numerical techniques due to the complexity of the detailed mathematical analysis involved.

5.1. Cumulative Distribution Function for SINR. The derivation of the CDF for SINR has been carried out in Appendix A. The resulting formulae are (A.6), (A.7), and (A.8).

Given the CDF value or SINR, equations (A.6)–(A.8) can be used to investigate the impact of different parameters such as mean SNRs and number of antennas. For example, while designing the decision threshold for usage of proposed method, the performance degradation can be calculated from (A.7), (A.8) while expected gain is obtained from (A.6).

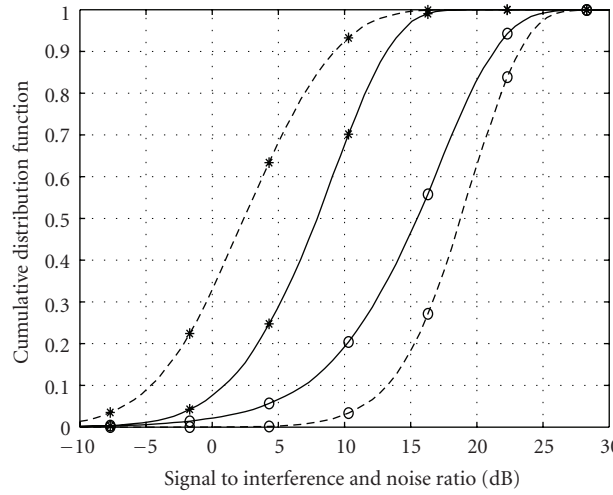

Figure 2: Cumulative distribution functions for Υ_1 (dashed curve, "*"), Υ_2 (dashed curve, "o"), $\Upsilon_{(1)}$ (solid curve, "*"), and $\Upsilon_{(2)}$ (solid curve, "o") when mode 1 with two antennas is employed. The mean SNR values are equal to $\overline{\gamma}_{1\to 1} = 10$ dB, $\overline{\gamma}_{2\to 2} = 20$ dB, $\overline{\gamma}_{2\to 1} = 10$ dB, and $\overline{\gamma}_{1\to 2} = 0$ dB.

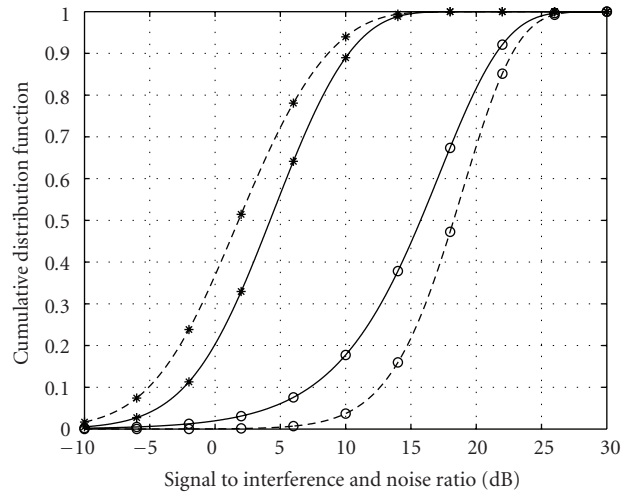

Figure 3: Cumulative distribution function for Υ_1 (dashed curve, "*"), Υ_2 (dashed curve, "o"), $\Upsilon_{(1)}$ (solid curve, "*"), and $\Upsilon_{(2)}$ (solid curve, "o") when antenna selection over two antennas is applied. Mean SNRs are $\overline{\gamma}_{1\to 1} = 10$ dB, $\overline{\gamma}_{2\to 2} = 20$ dB, $\overline{\gamma}_{2\to 1} = 10$ dB, and $\overline{\gamma}_{1\to 2} = 0$ dB.

Suppose we consider the numerical example where the network supports a dedicated signal in first femtocell that possesses a relatively good signal strength (e.g., $\overline{\gamma}_{1\to 1} = 10$ dB) but an interfering signal originating from the adjacent femtocell is also strong (e.g., $\overline{\gamma}_{2\to 1} = 10$ dB). Simultaneously, a second signal being served by the FBS also possesses a good signal strength ($\overline{\gamma}_{2\to 2} = 20$ dB) while the strength of a interfering signal is weak ($\overline{\gamma}_{1\to 2} = 0$ dB).

The resulting SINR performance based on the aforementioned scenario is given for the case of two antennas in Figures 2 and 3 as well as for the case of four antennas in

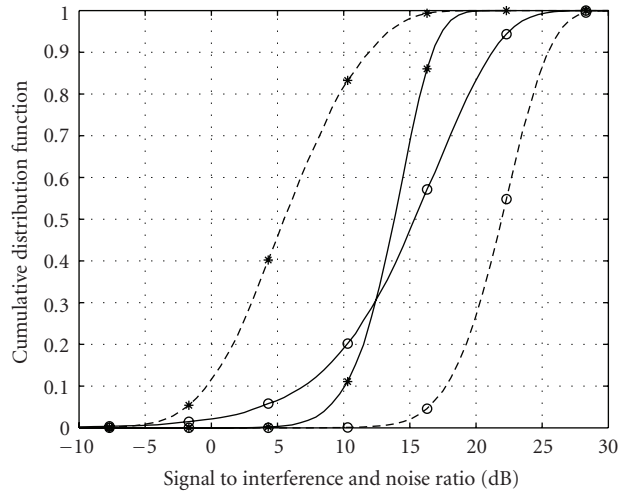

Figure 4: Cumulative distribution function for Υ_1 (dashed curve, "*"), Υ_2 (dashed curve, "o"), $\Upsilon_{(1)}$ (solid curve, "*"), and $\Upsilon_{(2)}$ (solid curve, "o") when mode 1 with four antennas is applied. The mean SNR values are $\overline{\gamma}_{1\to 1} = 10\,\text{dB}$, $\overline{\gamma}_{2\to 2} = 20\,\text{dB}$, $\overline{\gamma}_{2\to 1} = 10\,\text{dB}$, and $\overline{\gamma}_{1\to 2} = 0\,\text{dB}$.

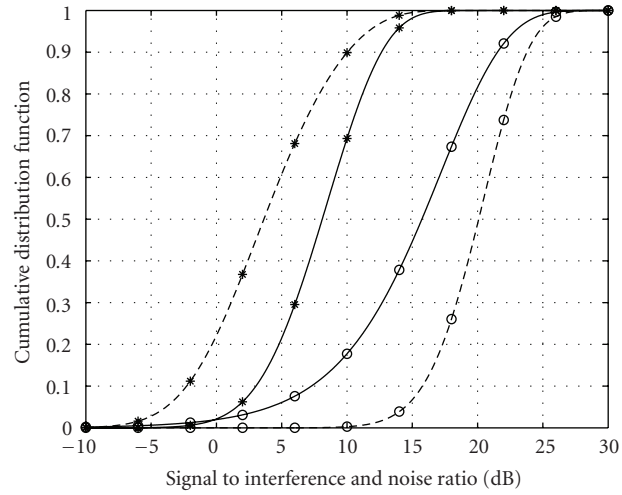

Figure 5: Cumulative distribution function for Υ_1 (dashed curve, "*"), Υ_2 (dashed curve, "o"), $\Upsilon_{(1)}$ (solid curve, "*"), and $\Upsilon_{(2)}$ (solid curve, "o") when antenna selection over four antennas is applied. The mean SNR values are $\overline{\gamma}_{1\to 1} = 10\,\text{dB}$, $\overline{\gamma}_{2\to 2} = 20\,\text{dB}$, $\overline{\gamma}_{2\to 1} = 10\,\text{dB}$, and $\overline{\gamma}_{1\to 2} = 0\,\text{dB}$.

Figures 4 and 5. The dashed curves in these figures illustrate the SINR performance when cells operate separately while the solid curves denote the situation when proposed interference mitigation is applied. We observe in both Figures 2 and 3 that mode 1 provides better performance relative to antenna selection at the expense of a slightly greater amount of transmission feedback overhead. Figure 2 also shows that even with two antennas the proposed method improves the SINR performance of the transmission links by more than 5 dB (up to the 70th percentile of the CDF) in the first cell while SINR simultaneously remains at an acceptable level in second cell despite having it use its antenna resources to mitigate interference in the first cell. Furthermore, from Figure 4 it is observed that the four-antenna extension of mode 1 yields up to a 10 dB increase in the SINR at the 10th percentile of the CDF in first cell with a corresponding decrease in the SINR in the second cell. Consequently, mode 1 and its extension can be effectively used to share radio resources in a more fair manner between adjacent femtocells, although transmission powers in FBSs are fixed and the direct communications between FBSs is nonexistent. Finally, we observe that the antenna selection method is less effective when performing interference mitigation. For instance, a system possessing four transmit antennas provides approximately the same performance as a system employing two-antenna mode 1.

5.2. Outage Rate. It is also worthwhile to investigate the system performance in terms of outage rate. Suppose we define the outage rate by the expression:

$$R^{\text{out}}(P^{\text{out}}) = A \cdot \log_2\left(1 + B \cdot \gamma(P^{\text{out}})\right), \tag{11}$$

where $\gamma(P^{\text{out}})$ is the SINR needed to achieve a given outage probability P^{out}, and the parameters A and B are the bandwidth and SNR efficiency factors used to fit the rate of the system with the set of adaptive modulation and coding curves obtained via system simulations. For example, it has been shown that values $A = 0.83$ and $B = 1/1.25$ provide a good fit with the set of LTE adaptive modulation and coding curves [30]. In this paper, we shall set the values $A = B = 1$ in order to provide the upper bound for the system transmission rate.

With respect to the value of $\gamma(P^{\text{out}})$, this can be obtained by computing the solution for the following equation:

$$P^{\text{out}} = P\left(\log_2(1+\gamma) < R_0\right) = \int_0^{\gamma_{R_0}} f_\Upsilon(\gamma)\,d\gamma = F_\Upsilon(\gamma_{R_0}). \tag{12}$$

In this case, $\gamma_{R_0} = 2^{R_0} - 1$ is the SINR related to the limit rate R_0, and in the case of the antenna selection formula for F_Υ, it is given by (A.6), (A.7), or (A.8) depending on the employed approach. We note that for a given P^{out} the solution of (12) can be computed numerically.

In Figures 6 and 7, the outage rates R_1^{out} and $R_{(1)}^{\text{out}}$ are defined as functions of $\overline{\gamma}_{2\to 1}$ when $P^{\text{out}} = 0.1$ and the SNR value of the serving FBS is 10 dB. Comparing the curves in Figure 6 shows that the strength of the interference signal originating from the adjacent cell can be adequately attenuated by the proposed approach, especially when mode 1 is the employed transmit beamforming method. Based on the results, we observe that mode 1 is capable of significantly improving the outage rates. This is particularly true of the four-antenna mode 1 configuration, which provides an efficient tool for removing this form of interference. When comparing a system that employs this method with another system that does not use transmit beamforming, the gain is extremely large. Furthermore, Figure 7 indicates that antenna selection is less efficient in interference mitigation

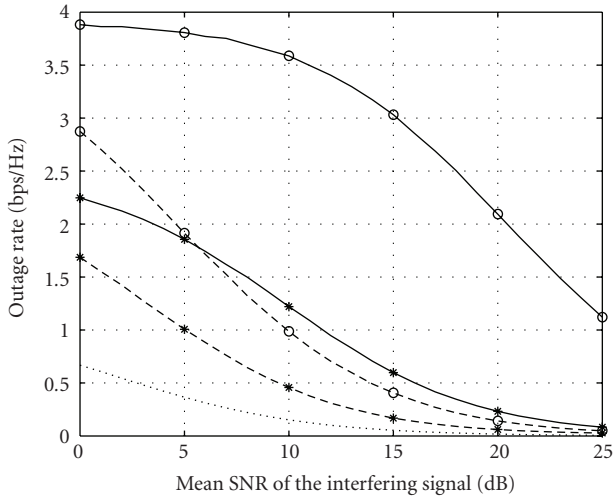

Figure 6: The outage rate without transmit beamforming (dotted curve), R_1^{out} (dashed curves), and $R_{(1)}^{\text{out}}$ (solid curves) as a function of $\overline{\gamma}_{2\to 1}$ when mode 1 over two ("*" markers) and four ("o" markers) antennas is used. The outage probability is 0.1 and mean SNR value of the serving cell signal ($\overline{\gamma}_{1\to 1}$) is 10 dB.

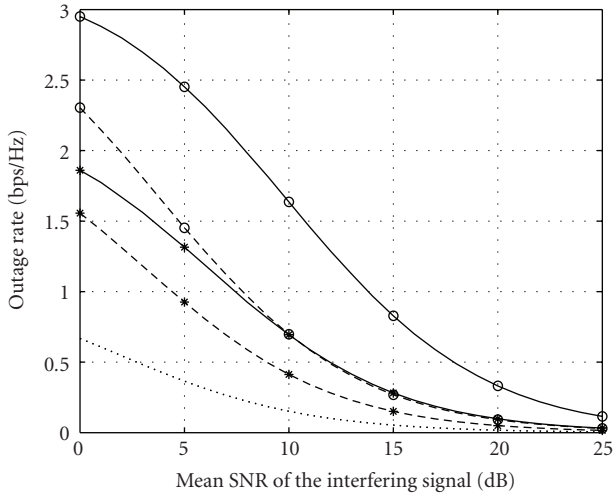

Figure 7: The outage rate without transmit beamforming (dotted curve), R_1^{out} (dashed curves), and $R_{(1)}^{\text{out}}$ (solid curves) as a function of $\overline{\gamma}_{2\to 1}$ when antenna selection over two ("*" markers) and four ("o" markers) antennas is used. The outage probability is 0.1 and mean SNR value of the serving cell signal ($\overline{\gamma}_{1\to 1}$) is 10 dB.

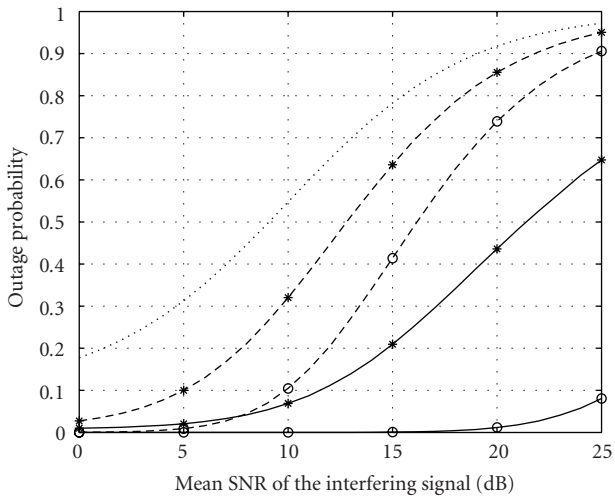

Figure 8: The outage probability without transmit beamforming (dotted curve), with two-antenna mode 1 ("*" markers), and with four-antenna mode 1 ("o" markers) when the interference mitigation is on (solid curves) and off (dashed curves). The outage rate is set to 1.0 bps/Hz and mean SNR value of the serving cell signal ($\overline{\gamma}_{1\to 1}$) is 10 dB.

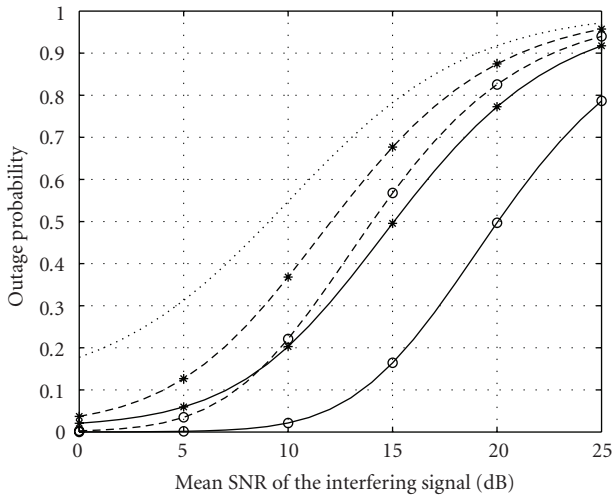

Figure 9: The outage probability without transmit beamforming (dotted curve), with two-antenna selection ("*" markers), and with four-antenna selection ("o" markers) when interference mitigation is on (solid curves) and off (dashed curves). The outage rate is set to 1.0 bps/Hz and mean SNR value of the serving cell signal ($\overline{\gamma}_{1\to 1}$) is 10 dB.

even though the four-antenna selection provides a noticeable link performance improvement.

Let us next observe the outage probability performance as a function of $\overline{\gamma}_{2\to 1}$ when the target rate requirement is fixed. We see in Figures 8 and 9 for a target rate set to 1.0 bits/s/Hz and the SNR value from the serving FBS equal to 10 dB that employing the proposed method significantly decreases the outage probability, especially when transmit beamforming is not applied. Employing the mode 1 method with four antennas allows the system to maintain an outage probability that is below 10% even when the interfering signal is stronger than the signal supported by the FBS by 15 dB.

5.3. Average Rate. Another metric for assessing the performance enhancements offered by the proposed methods is the average rate, which can be computed from the following formula:

$$R^{\text{av}}\left(\overline{\gamma}_{k\to k} \mid \overline{\gamma}_{l\to k}\right) = \int_0^\infty f_Y(\gamma)\log_2(1+\gamma)\,d\gamma \tag{13}$$

which is a function of the SNR value of the serving cell and conditioned upon the SNR value of the interfering signal. Using integration by parts, we obtain the following:

$$R^{\mathrm{av}}\left(\overline{\gamma}_{k\to k} \mid \overline{\gamma}_{l\to k}\right) = \log_2(e)\int_0^{\infty}\frac{1-F_{\Upsilon}(\gamma)}{1+\gamma}d\gamma. \tag{14}$$

If the proposed interference mitigation technique is employed, we then have according to (A.6) the following expression:

$$\int_0^{\infty}\frac{1-F_{\Upsilon_{(1)}}(\gamma)}{1+\gamma}d\gamma = \sum_{m=1}^{M}\binom{M}{m}\int_0^{\infty}\frac{(-1)^{m-1}e^{-m\gamma/\overline{\gamma}_{1\to 1}}d\gamma}{(1+\gamma)\left(1+(m/\nu_1 M)\gamma\right)}. \tag{15}$$

In order to compute the integral on the right side of this equation, we apply the following decomposition:

$$\frac{1}{(1+\gamma)\left(1+(m/\nu_1 M)\gamma\right)} = \frac{1}{1-m/\nu_1 M}\left(\frac{1}{1+\gamma}-\frac{m/\nu_1 M}{1+(m/\nu_1 M)\gamma}\right). \tag{16}$$

Thus, after combining the last two equations, we obtain a sum of two integrals in which we substitute $t = 1+\gamma$ and $t = 1+(m/\nu_1 M)\gamma$. Consequently, the resulting integrals yield expressions that are in terms of an exponential integral function ([31, equation (5.1.4)])

$$\begin{aligned}\int_0^{\infty}\frac{e^{-m\gamma/\overline{\gamma}_{1\to 1}}d\gamma}{1+\gamma} &= e^{m/\overline{\gamma}_{1\to 1}}E_1\left(\frac{m}{\overline{\gamma}_{1\to 1}}\right),\\ \frac{m}{\nu_1 M}\int_0^{\infty}\frac{e^{-m\gamma/\overline{\gamma}_{1\to 1}}d\gamma}{1+(m/\nu_1 M)\gamma} &= e^{M/\overline{\gamma}_{2\to 1}}E_1\left(\frac{M}{\overline{\gamma}_{2\to 1}}\right).\end{aligned} \tag{17}$$

Thus, the average rate in this case is given by

$$R^{\mathrm{av}}_{(1)}\left(\overline{\gamma}_{1\to 1} \mid \overline{\gamma}_{2\to 1}\right) = \log_2(e)\sum_{m=1}^{M}\binom{M}{m}(-1)^{m-1}\cdot A_m, \tag{18}$$

where

$$A_m = \frac{1}{1-m/\nu_1 M}\left(e^{m/\overline{\gamma}_{1\to 1}}E_1\left(\frac{m}{\overline{\gamma}_{1\to 1}}\right)-e^{M/\overline{\gamma}_{2\to 1}}E_1\left(\frac{M}{\overline{\gamma}_{2\to 1}}\right)\right). \tag{19}$$

It was assumed that $\overline{\gamma}_{1\to 1}\neq(m/M)\overline{\gamma}_{2\to 1}$. Furthermore, based on the exponential integral functions employed in this derivation, we observe the following:

$$A_m = e^{m/\overline{\gamma}_{1\to 1}}E_2\left(\frac{m}{\overline{\gamma}_{1\to 1}}\right),\quad \overline{\gamma}_{1\to 1} = \frac{m}{M}\overline{\gamma}_{2\to 1}. \tag{20}$$

For more details regarding this derivation, please refer to Appendix B of this paper. Note that the average rate $R^{\mathrm{av}}_{(2)}$ for the second user is obtained from (18) after setting $M = 1$ and replacing ν_1 by ν_2, $\overline{\gamma}_{1\to 1}$ by $\overline{\gamma}_{2\to 2}$ and $\overline{\gamma}_{2\to 1}$ by $\overline{\gamma}_{1\to 2}$.

If the links in the adjacent cells are operated independently, we can then use the CDF (A.8) from the calculation of Appendix A. Consequently, the resulting transmission rate (18) can now be expressed as

$$A_m = \begin{cases}\dfrac{1}{1-m/\nu_k}\left(e^{m/\overline{\gamma}_{k\to k}}E_1\left(\dfrac{m}{\overline{\gamma}_{k\to k}}\right)-e^{1/\overline{\gamma}_{l\to k}}E_1\left(\dfrac{1}{\overline{\gamma}_{l\to k}}\right)\right),\\ e^{1/\overline{\gamma}_{l\to k}}E_1\left(\dfrac{1}{\overline{\gamma}_{l\to k}}\right),\quad \overline{\gamma}_{l\to k}=\dfrac{\overline{\gamma}_{k\to k}}{m}.\end{cases} \tag{21}$$

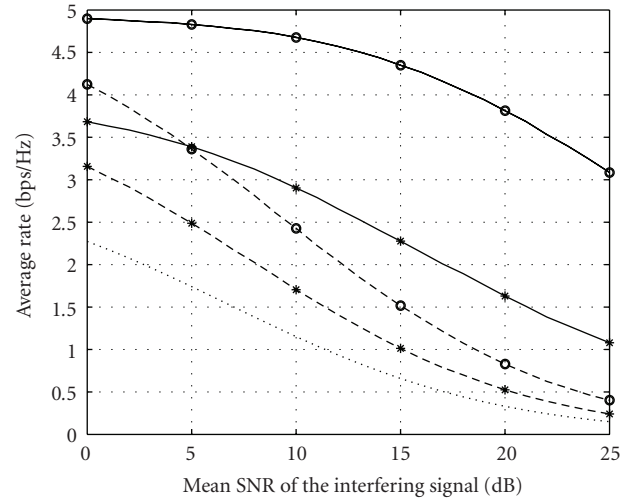

Figure 10: The average rate without transmit beamforming (dotted curve), with two-antenna mode 1 ("*"markers), and with four-antenna mode 1 ("o" markers) when interference mitigation is on (solid curves) and off (dashed curves). The mean SNR value of the serving cell signal ($\overline{\gamma}_{1\to 1}$) is 10 dB.

The resulting average rates produced by systems employing the proposed method are illustrated in Figures 10 and 11, where strength of the desired signal is set to 10 dB and the SNR value of the interfering signal from adjacent cell is increased to 25 dB. The observed results confirm the previously stated trends, namely, that mode 1 works better than antenna selection but both methods will enhance the system immunity with respect to cochannel interference.

6. Conclusions

When employing closed subscriber group configurations in femtocell deployment, where general handovers are not permitted between femto base stations, the signal strength of the interference can become unacceptably high due to the lack of coordination between base stations. Consequently, we proposed in this paper a practical interference mitigation method that can be used to mitigate the downlink cochannel interference from uncoordinated adjacent femto base stations.

In the proposed approach, the user equipment is allowed to create a control connection to the interfering femto-base station. Currently, a two-antenna transmit beamforming configuration is used in the HSDPA framework and usage of up to four antennas is expected in the LTE standard. Thus, the proposed method provides a simple yet practical way to

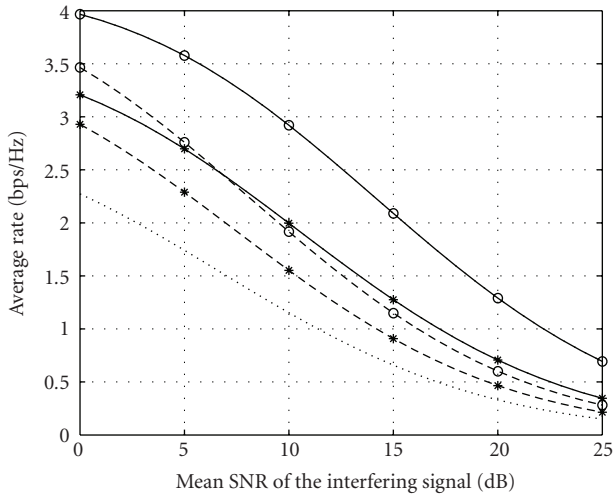

FIGURE 11: The average rate without transmit beamforming (dotted curve), with two-antenna selection ("*" markers), and with four-antenna selection ("o" markers) when interference mitigation is on (solid curves) and off (dashed curves). The mean SNR values of the serving cell signal ($\overline{\gamma}_{1\to 1}$) are 10 dB.

employ multiple antennas in a femtocell architecture while imposing minimal modifications to existing standards.

The level of interference mitigation obtained by systems based on two practical transmit beamforming methods was studied. Specifically, the existing HSDPA closed-loop transmit diversity mode 1 and its extension to four antennas, as well as the classical transmit antenna selection approach, were studied in this work. The results show that the former method is more relevant in practice since the two-antenna version is already employed in the 3GPP standard. However, one of the positive attributes of antenna selection is that it provides a suitable performance benchmark and it also allows for the calculation of simple closed-form expressions for various performance measures. The latter property can be employed to identify main gain mechanisms of the proposed approach from a theoretical perspective.

The performance analysis conducted in this work was based on both mathematical derivations and simulations. Measures for the performance were the cumulative distribution function for SINR, the outage rate, and the average rate. Performance results for all measures showed the same trend, namely, the proposed method is capable of achieving a substantially high mitigation of the interference originating from adjacent femtocells. The drawback is that if the transmit antenna resources are used to suppress the interference in adjacent cells, then the beamforming gain in target cell is lost. Nevertheless, in practice this is only a problem if both of the femtocells under investigation are suffering from heavy interference.

Results indicate that in uncoordinated closed femtocell deployments additional control channels can be used to improve the system performance. Thus, different control plane design principles for future macrocell and femtocell systems might provide great benefits. Yet, more research on this area is needed.

Appendices

A. Derivation of Analytical Performance Formulae

Suppose we define a function of random variables Z as follows:

$$Z = \frac{X}{1+Y}, \tag{A.1}$$

where X and Y are independent random variables. It follows that the CDF of Z, $F_Z(z)$, is then defined by [32]

$$F_Z(z) = \int_1^\infty F_X(zt) f_Y(t-1)dt, \tag{A.2}$$

where $f_Y(y)$ is the probability distribution function (PDF) of Y, and $F_X(x)$ is the CDF of X.

Suppose now we consider the distribution of $\Upsilon_{(1)}$ when antenna selection is used as the transmit beamforming method. According to (2), (9), and (A3), variables $\hat{\gamma}_{1\to 1}$ and $\check{\gamma}_{2\to 1}$ are then defined as the maximum and minimum values over M independent exponentially distributed variables. Consequently, we obtain the following expressions:

$$\begin{aligned} F_{\hat{\gamma}_{1\to 1}}(\gamma) &= \left(1 - e^{-\gamma/\overline{\gamma}_{1\to 1}}\right)^M, \\ F_{\check{\gamma}_{2\to 1}}(\gamma) &= \left(e^{-\gamma/\overline{\gamma}_{2\to 1}}\right)^M, \quad \gamma > 0 \end{aligned} \tag{A.3}$$

which after differentiation we find that the corresponding PDFs are of the following form:

$$\begin{aligned} f_{\hat{\gamma}_{1\to 1}}(\gamma) &= \frac{Me^{-\gamma/\overline{\gamma}_{1\to 1}}}{\overline{\gamma}_{1\to 1}}\left(1 - e^{-\gamma/\overline{\gamma}_{1\to 1}}\right)^{M-1}, \\ f_{\check{\gamma}_{2\to 1}}(\gamma) &= \frac{Me^{-M\gamma/\overline{\gamma}_{2\to 1}}}{\overline{\gamma}_{2\to 1}}, \quad \gamma > 0. \end{aligned} \tag{A.4}$$

Thus, in order to compute the CDF of $\Upsilon_{(1)}$, we recall the expression for $F_{\hat{\gamma}_{1\to 1}}$ as

$$F_{\hat{\gamma}_{1\to 1}}(\gamma) = \sum_{m=0}^{M} \binom{M}{m} (-1)^m e^{-m\gamma/\overline{\gamma}_{1\to 1}}, \tag{A.5}$$

where binomial series expansion has been applied. After combining (A.2) and (A.5) together, we then determine that

$$\begin{aligned} &F_{\Upsilon_{(1)}}(\gamma) \\ &\quad = \sum_{m=0}^{M} \binom{M}{m} (-1)^m \frac{Me^{M/\overline{\gamma}_{2\to 1}}}{\overline{\gamma}_{2\to 1}} \int_1^\infty e^{-tM/\overline{\gamma}_{2\to 1} - tm\gamma/\overline{\gamma}_{1\to 1}} dt \\ &\quad = \sum_{m=0}^{M} \binom{M}{m} \frac{(-1)^m \cdot \nu_1 \cdot M}{\nu_1 \cdot M + m\gamma} e^{-m\gamma/\overline{\gamma}_{1\to 1}}. \end{aligned} \tag{A.6}$$

We can then obtain $F_{\Upsilon_{(2)}}$ from (A.6) by replacing ν_1 with ν_2, $\overline{\gamma}_{1\to 1}$ with $\overline{\gamma}_{2\to 2}$, and setting $M = 1$, thus yielding

$$F_{\Upsilon_{(2)}}(\gamma) = 1 - \frac{\nu_2}{\nu_2 + \gamma} e^{-\gamma/\overline{\gamma}_{2\to 2}}. \tag{A.7}$$

Moreover, if antenna selection is performed independently across separate cells, we can then employ (A.6) in a similar approach in order to obtain the following result:

$$F_{\Upsilon_k}(\gamma) = \sum_{m=0}^{M} \binom{M}{m} \frac{(-1)^m \cdot \nu_k}{\nu_k + m\gamma} e^{-m\gamma/\overline{\gamma}_{k\to k}}. \tag{A.8}$$

B. Calculation of the Formula (20)

Using the notations $z = m/\overline{\gamma}_{1\to 1}$ and $\omega = M/\overline{\gamma}_{2\to 1}$, we can write

$$A_m = -\omega \cdot \frac{e^z E_1(z) - e^\omega E_1(\omega)}{z - \omega} =: g(z, \omega). \tag{B.1}$$

To deduce the expression for A_m in case $\omega = z$, we calculate the limit

$$\lim_{\omega \to z} g(z, \omega) = -z \frac{d}{dz}(e^z E_1(z)) = -z e^z E_1(z) + 1, \tag{B.2}$$

where formula (5.1.27) of [31] is used to obtain the second equality. After applying the formula $E_2(z) = e^{-z} - zE_1(z)$ ([31, equation (5.1.14)]), we find the desired result.

Acknowledgment

This work was prepared in CELTIC HOMESNET and MOTIVE frameworks and supported in part by Finnish Funding Agency for Technology and Innovation (Tekes), Nokia Siemens Networks (NSN), European Communications Engineering (ECE) and Academy of Finland (Grant 129446).

References

[1] H. Claussen, L. T. W. Ho, and L. G. Samuel, "An overview of the femtocell concept," *Bell Labs Technical Journal*, vol. 13, no. 1, pp. 221–246, 2008.

[2] S. Carlaw and C. Wheelock, "Femtocell market challenges and opportunities," ABI research, Research report, 2007.

[3] 3GPP, "3G home NodeB study item technical report," 3GPP Technical Report TR 25.820, September 2008, Ver. 8.2.0.

[4] 3GPP, "Service requirements for Home NodeBs and Home eNodeBs," 3GPP Technical Specification TS 22.220, November 2008, Ver. 1.0.0.

[5] 3GPP, "UTRAN architecture for 3G Home Node B," 3GPP Technical Specification TS 25.467, July 2009, Ver. 8.2.0.

[6] V. Chandrasekhar, J. G. Andrews, and A. Gatherer, "Femtocell networks: a survey," *IEEE Communications Magazine*, vol. 46, no. 9, pp. 59–67, 2008.

[7] D. N. Knisely, T. Yoshizawa, and F. Favichia, "Standardization of femtocells in 3GPP," *IEEE Communications Magazine*, vol. 47, no. 9, pp. 68–75, 2009.

[8] D. N. Knisely and F. Favichia, "Standardization of femtocells in 3GPP2," *IEEE Communications Magazine*, vol. 47, no. 9, pp. 76–82, 2009.

[9] G. Vannucci and R. S. Roman, "Measurement results on indoor radio frequency reuse at 900 MHz and 18 GHz," in *Proceedings of the 3rd IEEE International Conference on Personal, Indoor, and Mobile Radio Communications*, pp. 308–314, October 1992.

[10] C. R. Anderson, T. S. Rappaport, K. Bae, et al., "In-building wideband multipath characteristics at 2.5 and 60 GHz," in *Proceedings of the IEEE Vehicular Technology Conference*, vol. 1, pp. 97–101, September 2002.

[11] S. F. Hasan, N. H. Siddique, and S. Chakraborty, "Femtocell versus WiFi—a survey and comparison of architecture and performance," in *Proceedings of the 1st International Conference on Wireless Communication, Vehicular Technology, Information Theory and Aerospace Electronic Systems Technology*, pp. 916–920, May 2009.

[12] V. Chandrasekhar and J. G. Andrews, "Uplink capacity and interference avoidance for two-tier cellular networks," in *Proceedings of the 50th Annual IEEE Global Telecommunications Conference (GLOBECOM '07)*, pp. 3322–3326, November 2007.

[13] M. Z. Chowdhury, W. Ryu, E. Rhee, and Y. M. Jang, "Handover between macrocell and femtocell for UMTS based networks," in *Proceedings of the 11th International Conference on Advanced Communication Technology (ICACT '09)*, vol. 1, pp. 237–241, February 2009.

[14] Y. Bai, J. Zhou, and L. Chen, "Hybrid spectrum sharing for coexistence of macrocell and femtocell," in *Proceedings of the IEEE International Conference on Communications Technology and Applications (IEEE ICCTA '09)*, pp. 162–166, October 2009.

[15] H. Claussen, L. T. W. Ho, and L. G. Samuel, "Self-optimization of coverage for femtocell deployments," in *Proceedings of the 7th Annual Wireless Telecommunications Symposium (WTS '08)*, pp. 278–285, 2008.

[16] 3GPP, "Physical Channels and Modulation," 3GPP Technical Specification TS 36.211, May 2009, Ver. 8.7.0.

[17] 3GPP, "Physical layer procedures (FDD)," 3GPP Technical Specification TS 25.214, May 2009, Ver. 8.6.0.

[18] J. Hämäläinen and R. Wichman, "Closed-loop transmit diversity for FDD WCDMA systems," in *Proceedings of the 34th Asilomar Conference on Signals, Systems and Computers*, pp. 111–115, October 2000.

[19] J. Hämäläinen and R. Wichman, "Asymptotic bit error probabilities of some closed-loop transmit diversity schemes," in *Proceedings of the IEEE Global Telecommunications Conference (GLOBECOM '02)*, pp. 360–364, November 2002.

[20] J. Hämäläinen, R. Wichman, A. A. Dowhuszko, and G. Corral-Briones, "Capacity of generalized UTRA FDD closed-loop transmit diversity modes," *Wireless Personal Communications*. In press.

[21] A. Narula, M. Lopez, M. Trott, and G. Wornell, "Efficient use of side information in multipleantenna data transmission over fading channels," *IEEE Journal on Selected Areas in Communications*, vol. 16, no. 8, pp. 1423–1436, 1998.

[22] K. K. Mukkavilli, A. Sabharwal, E. Erkip, and B. Aazhang, "On beamforming with finite rate feedback in multiple-antenna systems," *IEEE Transactions on Information Theory*, vol. 49, no. 10, pp. 2562–2579, 2003.

[23] D. Love, R. Heath, and T. Strohmer, "Grassmannian beamforming for multipleinput multipleoutput wireless systems," *IEEE Transactions on Information Theory*, vol. 49, no. 10, pp. 2735–2747, 2003.

[24] S. Zhou, Z. Wang, and G. B. Giannakis, "Quantifying the power loss when transmit beamforming relies on finite-rate feedback," *IEEE Transactions on Wireless Communications*, vol. 4, no. 4, pp. 1948–1957, 2005.

[25] C. K. Au Yeung and D. J. Love, "On the performance of random vector quantization limited feedback beamforming in

a MISO system," *IEEE Transactions on Wireless Communications*, vol. 6, no. 2, pp. 458–462, 2007.

[26] W. Santipach and M. L. Honig, "Capacity of a multiple-antenna fading channel with a quantized precoding matrix," *IEEE Transactions on Information Theory*, vol. 55, no. 3, pp. 1218–1234, 2009.

[27] M. Husso, J. Hämäläinen, R. Jäntti, and A. M. Wyglinski, "Adaptive antennas and dynamic spectrum management for femtocellular networks: a case study," in *Proceedings of the 3rd IEEE Symposium on New Frontiers in Dynamic Spectrum Access Networks (DySPAN '08)*, pp. 699–703, October 2008.

[28] A. A. Dowhuszko, G. Corral-Briones, J. Hämäläinen, and R. Wichman, "Achievable sum-rate analysis of practical multiuser scheduling schemes with limited feedback," in *Proceedings of the IEEE International Conference on Communications*, pp. 4381–4386, 2007.

[29] A. A. Dowhuszko, G. Corral-Briones, J. Hmlinen, and R. Wichman, "On throughput-fairness tradeoff in virtual MIMO systems with limited feedback," *EURASIP Journal on Wireless Communications and Networking*, vol. 2009, 2009.

[30] P. Mogensen, W. Na, I. Z. Kováes, et al., "LTE capacity compared to the shannon bound," in *Proceedings of the IEEE 65th Vehicular Technology Conference (VTC '07)*, pp. 1234–1238, April 2007.

[31] M. Abramowitz and I. Stegun, Eds., *Handbook of Mathematical Functions*, National Bureau of Standards, Washington, DC, USA, 1972.

[32] A. Papoulis, *Probability, Random Variables, and Stochastic Processes*, McGraw–Hill, New York, NY, USA, 3rd edition, 1991.

Hindawi Publishing Corporation
EURASIP Journal on Wireless Communications and Networking
Volume 2010, Article ID 285714, 14 pages
doi:10.1155/2010/285714

Research Article

Joint Power Control, Base Station Assignment, and Channel Assignment in Cognitive Femtocell Networks

John Paul M. Torregoza,[1] Rentsen Enkhbat,[2] and Won-Joo Hwang[3]

[1] *Graduate School of Natural Sciences, Department of Computer Science, Inje University, Obang-dong, Gimhae, Gyeongnam 621-749, South Korea*
[2] *Department of Applied Mathematics, National University of Mongolia, Baga toiruu, Sukhbaatar district, Ulaanbaatar, 210646, Mongolia*
[3] *Graduate School of Engineering, Department of Information and Communications Engineering, Inje University, Obang-dong, Gimhae, Gyeongnam 621-749, South Korea*

Correspondence should be addressed to Won-Joo Hwang, ichwang@inje.ac.kr

Received 1 September 2009; Revised 15 December 2009; Accepted 29 January 2010

Academic Editor: Ismail Guvenc

Cognitive radio and femtocells are recent technology breakthroughs that aim to achieve throughput improvement by means of spectrum management and interference mitigation, respectively. However, these technologies are limited by the former's susceptibility to interference and the latter's dependence on bandwidth availability. In this paper, we overcome these limitations by integrating cognitive radio and femtocell technology and exploring its feasibility and throughput improvement. To realize this, we propose an integrated architecture and formulate a multiobjective optimization problem with mixed integer variables for the joint power control, base station assignment, and channel assignment scheme. In order to find a pareto optimal solution, a weighted sum approach was used. Based on numerical results, the optimization framework is found to be both stable and converging. Simulation studies further show that the proposed architecture and optimization framework improve the aggregate throughput as the client population rises, hence confirming the successful and beneficial integration of these technologies.

1. Introduction

Regulatory bodies throughout the world have found that communication bandwidth is becoming scarce, with two of the major causes being inefficient use of the spectrum and ineffective interference mitigation [1]. Studies have found that the majority of the spectrum bands, particularly the licensed bands, are inefficiently utilized. For example, cellular and ISM bands are overloaded in most parts of the world while UHF TV and amateur radio bands are underutilized in some locations at some specific time instances [2, 3]. In accordance with this, increasing interference levels in the overloaded spectrum render interference mitigation schemes ineffective. In the ISM band, for instance, Bluetooth transmissions suffer from significant packet loss in the presence of WLAN interference [4]. In this work, we make use of cognitive radio and femtocell technology to resolve inefficient spectrum utilization and high levels of interference, respectively.

Cognitive radio (CR) was proposed in an endeavor to allow opportunistic use of unutilized licensed resources, also called spectrum holes, by sensing the communication environment [5]. The sensed information is used to change the communication parameters of cognitive radio users, called *secondary users*, using software-defined radios without producing significant interference to licensed users, called *primary users*. Cognitive radios also exhibit autoconfiguration and intelligent sensing characteristics [6, 7]. On the other hand, femtocells are short-range, low-power base stations installed by customers to limit interference, thereby increasing network capacity, in a small area. The installed device, called a *Femtocell Base Station* (*FBS*), communicates with the main base station, called a *Macrocell Base Station* (*MBS*), either by dedicated channels or wired

communication. The noise mitigation characteristic of the femtocell architecture is a result of "microization", a recent network concept in which a large area network is divided into smaller networks, thereby reducing the per base station load [8].

However, the aforementioned benefits derived from cognitive radios and femtocells may be nonexistent, if not minimal, when implemented separately, due to their respective limitations. In the case of cognitive radio, the spectrum management mechanism of this technology is limited by the user density as well as the communication behavior of primary clients [7]. Contention for spectrum holes also exists due to the large number of secondary clients searching for spectrum holes. In addition, if the utilization of licensed bands is high, the amount of usable bandwidth decreases exponentially as the number of secondary users increases. In contrast, femtocell performance is dependent on the available bandwidth, since the FBSs operate under the same spectrum as MBSs [9]. Upon these considerations, interference mitigation and interference control schemes need to be studied in order to improve cognitive radio performance. In a similar manner, spectrum management schemes should be considered for femtocell implementations. Based on this argument, the integration of cognitive radio and femtocell is expected to be mutually beneficial for these technologies. In addition, we introduce a compensation concept to address the backhaul communication issue for open access femtocells given in [8].

The main contributions of this paper can be summarized as follows.

(i) We propose a system architecture for a cognitive femtocell network architecture that incorporates cognitive radio and femtocells (Section 2).

(ii) We propose a joint power control, base station assignment, and channel assignment scheme for cognitive femtocell networks. In this scheme, the power of each node, as well as the selection of the base station to which a node connects, is controlled so as to maximize the aggregate throughput. In addition, we also propose a compensation scheme to compensate femtocell owners for usage of their resources. We also formulated a mixed integer multiobjective optimization model for the proposed schemes and found the global solution using the branch and bound method (Section 3).

(iii) Finally, we provided numerical and simulation results to show that the proposed joint power control, base station assignment, and channel assignment scheme for cognitive femtocell networks achieves better performance than conventional architectures (Section 4).

2. Problem Definition and System Architecture

We begin by discussing the benefits derived from cognitive radio and how the femtocell architecture gains from the use of CRs. To help with the discussion, graphical representations

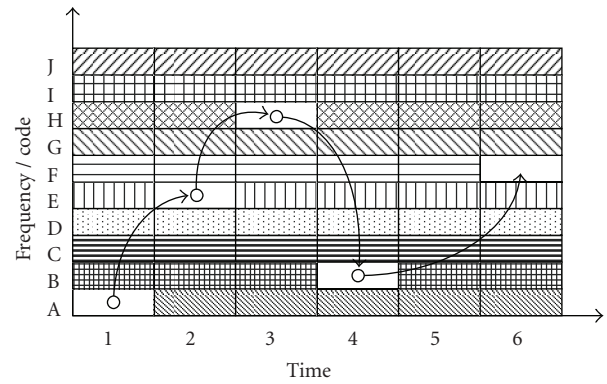

Figure 1: Cognitive Radio Operation. The arrows show the movement of secondary clients from one spectrum hole to another. A spectrum hole is used to describe unused spectrum resource. The vertical axis represents the unit of spectrum resource. For WiMAX and LTE, spectrum resource is classified by frequency while for W-CDMA(UMTS), the spectrum is classified by code.

are presented in Figures 1 and 2. Figure 1 presents a pictorial representation of spectrum mobility, where secondary users transfer to available spectrum, called *spectrum holes*, when the primary users need to use the spectrum currently used by these secondary users. A spectrum hole is a term describing spectrum resources that are unused. Also, for overlay implementations, a spectrum hole is also used to denote a unit of spectrum resource whose Signal to Interference and Noise Ratio (SINR) is below a predefined threshold. Note that *primary users* are those users that own the spectrum/resource while *secondary users* are those users that are opportunistically using the spectrum/resource owned by primary users. In this paper, the MBS is the primary user and each FBS is a secondary users. In Figure 1, there are 10 units of available spectrum resources (A to J) for a particular cell. These units of spectrum resource can be described by frequency bandwidth (WiMAX, LTE) or code assignment (W-CDMA). At time instance 1, an FBS is using resource A. Upon time instance 2, resource A is needed by the MBS, and the FBS needs to find a new spectrum, designated in figure as resource E. A similar event happens in time instance 3 where the FBS releases resource E to continue transmission using resource H. Suppose there are several spectrum holes available, as in time instance 4. In this case, the FBS chooses the spectrum hole that would provide higher throughput, which in Figure 1 is resource B. Furthermore, there is a possibility that no unused resource is available. In this case, as in time instance 5, the FBS may adjust its power and continue using resource B under the condition that it does not add significant interference to the MBS. The FBS continues to transmit in low-power until it finds a new spectrum hole. However, note that if the FBS contributes a significant amount of interference to the macrocell network despite low-power transmission, then the femtocell should defer its transmission until it finds a new spectrum hole. In addition, in a case where several FBSs and a single spectrum hole exist, the FBSs would contend to use the resource. As can be seen in the scenario from Figure 1, the use of

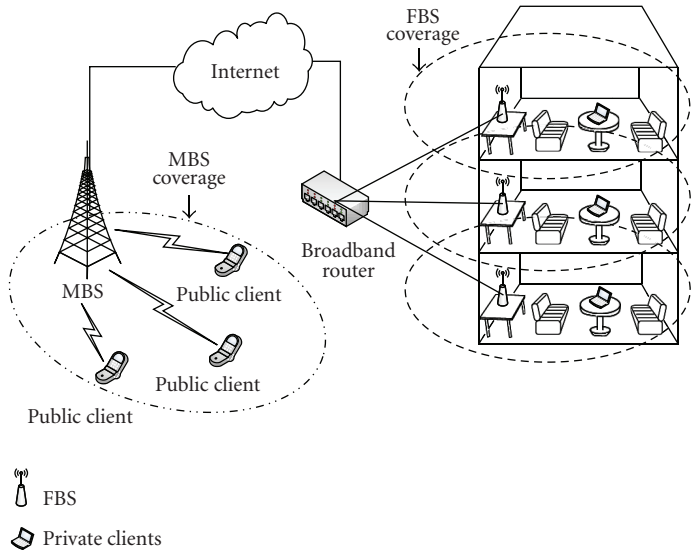

Figure 2: Femtocell Operation. The femtocell architecture consists of several private base stations called FBSs, which service *private clients* who own these FBSs. A main base station called MBS also exists to provide service to nonfemtocell owners, called *public clients.*

cognitive radio exploits sensing the environment to maintain a predetermined threshold of SINR level.

A common femtocell architecture is illustrated in Figure 2. The FBS in this figure communicates with the MBS through the Internet while other means, such as dedicated wireless channels, can be used for connectivity. Coverage enhancement and interference mitigation are two advantages derived from using the femtocell architecture. System coverage is extended since unreachable users can connect to the MBS through the FBSs. On the other hand, FBS installations can also reduce interference in highly dense areas, since private clients do not have to compete for the macrocell network resources [8]. However, different installations of FBSs may interfere with each other, since these base stations usually reuse the same set of frequencies. In a worst-case scenario, such as the apartment setup in Figure 2, massive contention may occur. From this, we can see that the performance of femtocell architectures is limited by the available frequency spectrum [8]. The femtocell architecture benefits from using cognitive radio in that it gains the capability of sensing its environment and can thereupon adapt its configuration based on the sensed information.

With the knowledge of the benefits and limitations of cognitive radio and femtocell technologies, it is straightforward that merging these technologies provides a potential direction to achieve maximum performance. Figure 3 illustrates the architecture proposed in this paper. The system is composed of three major entities: (1) MBS, (2) FBSs, and (3) private and public clients.

The MBS is the central entity of the whole system. As previously mentioned, this base station serves as the primary user of the licensed spectrum and is operated by the service providers. The FBSs are equipped with cognitive radio with spectrum sensing, spectrum management, spectrum sharing,

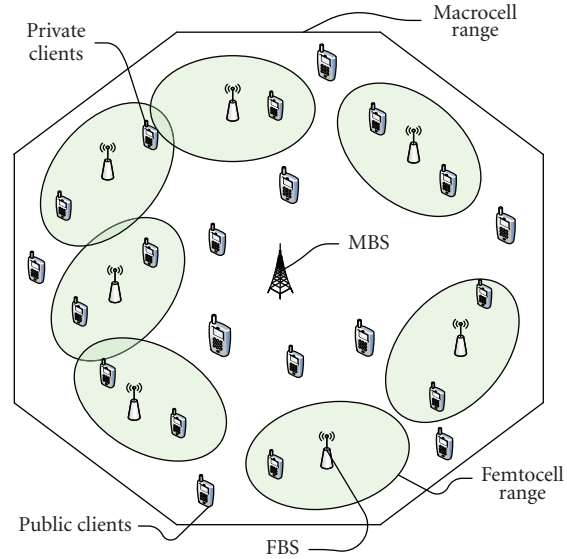

Figure 3: Cognitive femtocell network architecture. The architecture is composed of a single MBS with several FBSs Each FBS controls its power to reduce interference caused to neighbour FBSs and also to the MBS.

and spectrum mobility functionalities, as defined in [7]. With this feature, each FBS has the ability to sense its environment and change to different channels based on the sensed information. Each FBS connects to the MBS via TDMA slotted communication. Each FBS is given time slots used to forward data to the macrocell network.

In addition, we consider an open access femtocell architecture [8]. In this architecture, femtocells allow connection of public clients in order for these clients to connect to

the macrocell network. To support an open access femtocell architecture, a compensation scheme is needed, since the use of an open access femtocell architecture would decrease the effective throughput of private clients. Public clients normally associate with the MBS. In our open access scheme, these public clients may connect to other FBSs under the condition that the FBSs to which these clients connect must be compensated by the MBS. In this paper, these FBSs that accommodate public clients are compensated by being provided additional time slots in backhaul communication. Details of this compensation scheme are given in Section 3. Furthermore, the FBSs may also adjust their power to control their transmission range communication if the MBS requests coverage enhancement and for interference mitigation purposes.

In this paper, we assume that the MBS and FBS use OFDMA-based WiMAX and that resources are assigned based on a frequency-time basis. In addition, each base station is equipped with a single radio and can operate at a single frequency for each time instance. Also, for analysis purposes, its assumed that the cell is on a high-density area and that all clients need to transmit some data.

The problem this paper aims to resolve is the maximization of throughput performance by controlling the BS assignment of public clients, the channel allocation for each BS, and the transmission power. In controlling the power and channel allocation, the interference between clients and BSs is reduced. The BS assignment allows public clients to connect to FBSs subject to compensation from the MBS.

3. Joint Power Control, Base Station Assignment, and Channel Assignment Model

In this paper's model, two objectives are considered. The first objective is to maximize the achievable throughput in the network while the second deals with what we call femtocell compensation. The goal of the whole formulation is to maximize the achievable throughput of the system while minimizing the need for femtocell compensation. In the following subsections, the formulation for uplink and downlink scenarios, as well as the branch and bound method used to solve the scheme, is detailed.

3.1. Uplink Optimization Model. Suppose that a cell consists of 1 MBS, M FBSs, and N client nodes. Also, assume that the cell is provided with J available frequencies. It can be shown that the transmission power of any node i can be expressed in terms of the measured power at any node k, as given by (1). Note that, given that $h^j_{i,i} = 1$, it can be shown that $p_i = \hat{p}^j_{i,i}$. From the Shannon Formula [10], $v^j_{i,k}$ can be formulated as (2). It can be shown that the aggregate uplink achievable throughput can be formulated using (2), as in (3), where $a_i, b_{i,k}$, and $c_{i,k}$ are binary elements of coverage matrices $(\mathbf{A}, \mathbf{B}, \mathbf{C})$, as defined in Table 1. This aggregate uplink achievable throughput $\mathbb{T}^U(\mathbf{A}, \mathbf{C}, \mathbf{F}^U, \mathbf{P})$ is the equation for the first objective of the uplink optimization formulation

$$p_i = \frac{\hat{p}^j_{i,k}}{h^j_{i+M,k}}, \tag{1}$$

$$v^j_{i,k} = \log_2\left(1 + \frac{p_i h^j_{i+M,k}}{\sum_{u\neq i,\, u\in[1,N]} \hat{p}^j_{u,i} h^j_{u+M,k}/h^j_{u+M,i+M} + \mathbb{I}_{\text{noise}}}\right), \tag{2}$$

$$\mathbb{T}^U\left(\mathbf{A}, \mathbf{C}, \mathbf{F}^U, \mathbf{P}\right) : \sum_{j=1}^{J}\sum_{i=1}^{N} a_i f^U_{i,j} v^j_{i,0} + \sum_{j=1}^{J}\sum_{k=1}^{M}\sum_{i=1}^{N} (b_{i,k}+c_{i,k}) f^U_{i,j} v^j_{i,k}. \tag{3}$$

As can be seen from (3), the first objective function for throughout maximization is a joint scheme for incorporating power control, BS assignment, and channel assignment. In this objective function, the power control scheme controls the transmission powers $(\mathbf{P})$ of client nodes in order to minimize the contributed interference. In addition, we define BS assignment $(\mathbf{A}, \mathbf{B}, \mathbf{C})$ as a representation of the BS to which these clients connect, that is, if they are connected to any FBSs or the MBS. The association of public clients to the FBSs is subject to the MBS load and interference conditions. Finally, the channel assignment $(\mathbf{F}^U)$ is chosen from the J available channels for each node. These parameters are computed for each time frame.

Due to the use of an open access femtocell architecture, it is necessary to introduce a scheme to control the backhaul, that is, the communication between MBS and FBSs. For this paper, we assume that a TDMA scheme is used for backhaul communication between MBS and FBSs. Here a fixed time frame τ is initially divided into M slots. Each of the M FBSs gets a dedicated β_{rate}/M data rate for each time slot. In the event that a public client connects to a FBS, the FBS is compensated by getting additional slots in the backhaul. Since our architecture allows public clients to use the FBS, it would incur costs for private clients who own the FBS. These costs shouldered by the private users should be compensated by the service providers of the macrocell network. In order to quantify the amount of backhaul bandwidth used by public clients, the achievable uplink throughput value of the public client and aggregate uplink throughput value at the FBS are compared, as seen in (4). $\mathbb{C}^U(\mathbf{C}, \mathbf{F}^U, \mathbf{P})$ quantifies the bandwidth lost by the private clients and used by the public clients. The compensation mechanism in (4) provides the FBS with a means to increase backhaul traffic rate as compensation for the decreased data transmission rate in the uplink towards the FBS:

$$\mathbb{C}^U\left(\mathbf{C}, \mathbf{F}^U, \mathbf{P}\right) = \sum_{k=1}^{M} \frac{\beta_{\text{rate}} \dfrac{\sum_{j=1}^{J}\sum_{i=1}^{N} (c_{i,k}) f^U_{i,j} v^j_{i,k}}{\sum_{j=1}^{J}\sum_{i=1}^{N} (b_{i,k}+c_{i,k}) f^U_{i,j} v^j_{i,k}}}{M + \dfrac{\sum_{j=1}^{J}\sum_{i=k}^{K} (c_{i,k}) f^U_{i,j} v^j_{i,k}}{\sum_{j=1}^{J}\sum_{i=1}^{N} (b_{i,k}+c_{i,k}) f^U_{i,j} v^j_{i,k}}}. \tag{4}$$

Table 1: Notation summary.

Symbol	Description
M	Total number of FBS
N	Total number of clients
$\mathbb{I}_{\text{noise}}$	Hardware noise and environmental noise
τ	Time frame
β_{rate}	Maximum backhaul link capacity
$\gamma_{\text{th}}^{\text{PU}}$	Constant parameter for the SINR threshold of MBS
$\gamma_{\text{th}}^{\text{SU}}$	Constant parameter for the SINR threshold of the FBS
P_{MAX}	Constant parameter for the maximum transmission power of clients
$Q_{\text{MAX}}^{\text{MBS}}$	Constant parameter for the maximum transmission power of MBS
$Q_{\text{MAX}}^{\text{FBS}}$	Constant parameter for the maximum transmission power of FBS
w	Weight parameter for the weighted sum approach
$\mathbf{P} = \{p_i \mid i = \overline{1,N}\}$	Transmission power vector of clients
$\mathbf{Q} = \{q_k \mid k = \overline{0,M}\}$	Transmission power vector of BS
$\hat{\mathbf{P}} = \{\hat{p}_{i,k}^j \mid i,k = \overline{1,N}, j = \overline{1,J}\}$	Measured power of client k at client i using channel j
$\mathbf{Q} = \{\hat{q}_{i,k}^j \mid i,k = \overline{0,M}, j = \overline{1,J}\}$	Measured power of BS k at BS i
$v_{i,k}^j$	Uplink achievable throughput from client i to BS k using frequency j
$\delta_{k,i}^j$	Downlink achievable throughput from BS k to client i using frequency j
$\mathbf{H} = \{h_{i,k}^j \mid h_{i,i}^j = 1, h_{i,k}^j = h_{k,i}^j,$ $i = \overline{0,N+M+1}, k = \overline{0,N+M+1}, j = \overline{1,J}\}$	Transmission gain matrix between network elements. Note that index 0 represents the MBS, indices 1 to M represent FBSs, and indices $M+1$ to $M+N$ represent clients
$\mathbf{A} = \{a_i \mid i = \overline{1,N}\}$	Coverage scheme variable for set of public users associated with MBS
$\mathbf{B} = \{b_{i,k} \mid i = \overline{1,N}, k = \overline{1,M}\}$	Coverage scheme constant for set of private users i associated with an FBS k
$\mathbf{C} = \{c_{i,k} \mid i = \overline{1,N}, k = \overline{1,M}\}$	Coverage scheme variable for set of public users i associated with FBS k
$\mathbf{F}^U = \{f_{i,j}^U \mid i = \overline{1,N}, j = \overline{1,J}\}$	Uplink channel assignment variable for client i using frequency j
$\mathbf{F}^D = \{f_{k,j}^D \mid k = \overline{0,N}, j = \overline{1,J}\}$	Downlink channel assignment variable for BS k using frequency j
$\mathbb{T}^U(\mathbf{A}, \mathbf{C}, \mathbf{F}^U, \mathbf{P})$	Uplink throughput objective function
$\mathbb{T}_i^U(a_i, \mathbf{C}_i, \mathbf{F}_i^U, p_i)$	Distributed uplink throughput objective function at each client i
$\mathbb{T}^D(\mathbf{A}, \mathbf{C}, \mathbf{F}^D, \mathbf{Q})$	Downlink throughput objective function
$\mathbb{T}_0^D(\mathbf{F}_0^D, q_i)$	Distributed downlink throughput for the MBS
$\mathbb{T}_k^D(\mathbf{F}_k^D, q_i)$	Distributed downlink throughput at each FBS
$\mathbb{C}^U(\mathbf{C}, \mathbf{F}^U, \mathbf{P})$	Uplink compensation objective function
$\mathbb{C}^D(\mathbf{C}, \mathbf{F}^D, \mathbf{Q})$	Downlink compensation objective function
$\mathbb{C}_i^U(\mathbf{C}_i, \mathbf{F}_i^U, p_i)$	Distributed compensation objective function at each client i
$\mathbb{C}_k^D(\mathbf{F}_k^D, q_k)$	Distributed downlink compensation objective function at each BS k
$W^U(\mathbf{A}, \mathbf{C}, \mathbf{F}^U, \mathbf{P})$	Weighted sum problem for uplink model
$W_i^U(a_i, \mathbf{C}_i, \mathbf{F}_i^U, p_i)$	Distributed uplink weighted sum problem
$W^D(\mathbf{A}, \mathbf{C}, \mathbf{F}^D, \mathbf{Q})$	Weighted sum problem for downlink model
$W_0^D(\mathbf{F}_0^D, q_0)$	Distributed downlink weighted sum problem at the MBS
$W_k^D(\mathbf{F}_k^D, q_k)$	Distributed downlink weighted sum problem at each FBS
$v_{e-i,k}^j$	Distributed achievable throughput from client i to BS k using frequency j at each client e
$\delta_{e-k,i}^j$	Downlink achievable throughput from BS k to client i using frequency j at each BS e

We illustrate this using Figure 2. Suppose a private client at the first floor of the apartment is connected to the FBS that he/she owns. Assume the backhaul link has a link capacity of 1 Mpbs. In the figure, there are a total of 3 FBSs in the network; then each of these FBSs experiences an effective rate of 0.33 Mbps in the backhaul. Now suppose that a public client connects to the FBS at the first floor and the ratio of the achievable uplink throughput of the public client and aggregate uplink throughput at that FBS is 0.15, that is, 15% of the bandwidth are used by the public clients. In this scenario, the backhaul capacity is divided into 3.15. The first floor FBS that connects the public client gets a 0.37 Mbps

effective backhaul rate while the other 2 FBSs in the second and third floors receive 0.317 Mbps:

$$\max_{(\mathbf{A},\mathbf{C},\mathbf{F}^U,\mathbf{P})} \mathbb{T}^U\left(\mathbf{A},\mathbf{C},\mathbf{F}^U,\mathbf{P}\right), \tag{5a}$$

$$\min_{(\mathbf{C},\mathbf{F}^U,\mathbf{P})} \mathbb{C}^U\left(\mathbf{C},\mathbf{F}^U,\mathbf{P}\right), \tag{5b}$$

$$\text{such that } a_i + \sum_{k=1}^{M}\left(b_{i,k}+c_{i,k}\right) = 1, \tag{5c}$$

$$\frac{a_i p_i h_{i+M,0}^j}{\sum_{u\neq i,\, u\in[1,N]} \widehat{p}_{u,i}^j h_{u+M,0}^j / h_{u+M,i+M}^j + \mathbb{I}_{\text{noise}}} \geq \gamma_{\text{th}}^{\text{PU}}, \tag{5d}$$

$$\frac{\left(b_{i,k}+c_{i,k}\right) p_i h_{i+M,k}^j}{\sum_{u\neq i,\, u\in[1,N]} \widehat{p}_{u,i}^j h_{u+M,k}^j / h_{u+M,i+M}^j + \mathbb{I}_{\text{noise}}} \geq \gamma_{\text{th}}^{\text{SU}}, \tag{5e}$$

$$\sum_{j=1}^{J} f_{i,j}^U \leq 1, \quad i = 1,2,\ldots,N, \tag{5f}$$

$$0 \leq p_i \leq P_{\text{MAX}}, \quad i = 1,2,\ldots,K,$$

$$a_i, c_{i,k}, f_{i,j}^U \in \{0,1\}, \tag{5g}$$

$$i = 1,2,\ldots,K,\ k = 1,2,\ldots,M.$$

The multiobjective problem is formulated in (5a) to (5g). The first objective (5a) maximizes the aggregate uplink throughput given by (3). The second objective (5b) minimizes the compensation objective given by (4). Note that the compensation objective $\mathbb{C}^U(\mathbf{C},\mathbf{F}^U,\mathbf{P})$ is minimized, since the ideal case is for public users to connect using the MBS. Also, an increase in the compensation for a certain FBS would result in a decrease in the backhaul rate for other FBSs. There are five major constraints for the formulation in (5a) to (5g). The first constraint (5c) assures that sets **A**, **B**, or **C** are disjoint. Moreover, this implies that each client associates with only one base station. The next two constraints, given by (5d) and (5e), denote the SINR constraints for each base station. The constraint in (5f) states that a client or FBS is assigned only one frequency. Finally, (5g) describes the limit in transmission power for each client in the uplink.

The multiobjective problem is solved jointly using a weighted-sum approach with the objective function given by (6a) to (6g). In order to incorporate the two objectives, a weight parameter w is introduced. The value of the parameter is limited by (6g). The optimal value of the weight is determined by finding the pareto optimal solution for the two objective functions, $\mathbb{T}^U(\mathbf{A},\mathbf{C},\mathbf{F}^U,\mathbf{P})$ and $\mathbb{C}^U(\mathbf{C},\mathbf{F}^U,\mathbf{P})$:

$$W^U\left(\mathbf{A},\mathbf{C},\mathbf{F}^U,\mathbf{P}\right):$$

$$\max_{(\mathbf{A},\mathbf{C},\mathbf{F}^U,\mathbf{P})} w\mathbb{T}^U\left(\mathbf{A},\mathbf{C},\mathbf{F}^U,\mathbf{P}\right) - (1-w)\mathbb{C}^U\left(\mathbf{C},\mathbf{F}^U,\mathbf{P}\right) \tag{6a}$$

$$\text{such that } a_i + \sum_{k=1}^{M}\left(b_{i,k}+c_{i,k}\right) = 1, \tag{6b}$$

$$\frac{a_i p_i h_{i+M,0}^j}{\sum_{u\neq i,\, u\in[1,N]} \widehat{p}_{u,i}^j h_{u+M,0}^j / h_{u+M,i+M}^j + \mathbb{I}_{\text{noise}}} \geq \gamma_{\text{th}}^{\text{PU}}, \tag{6c}$$

$$\frac{\left(b_{i,k}+c_{i,k}\right) p_i h_{i+M,k}^j}{\sum_{u\neq i,\, u\in[1,N]} \widehat{p}_{u,i}^j h_{u+M,k}^j / h_{u+M,i+M}^j + \mathbb{I}_{\text{noise}}} \geq \gamma_{\text{th}}^{\text{SU}}, \tag{6d}$$

$$\sum_{j=1}^{J} f_{i,j}^U \leq 1, \quad i = 1,2,\ldots,N, \tag{6e}$$

$$0 \leq p_i \leq P_{\text{MAX}}, \quad i = 1,2,\ldots,K, \tag{6f}$$

$$0 < w < 1,$$

$$a_i, c_{i,k}, f_{i,j}^U \in \{0,1\}, \tag{6g}$$

$$i = 1,2,\ldots,N,\ k = 0,1,2,\ldots,M.$$

3.2. Downlink Optimization Model. It has been shown [11] that the uplink and downlink models for general wireless networks can be formulated through duality by changing constraints under the assumption that the transmission gain matrix is symmetric, that is, $h_{i,k}^j = h_{k,i}^j$. Based on this principle, we can formulate the downlink model as follows. The downlink achievable throughput is defined as in (7). For the downlink transmission, the aggregate throughput and compensation objective functions can be derived, as given in (8) and (9), respectively,

$$\delta_{k,i}^j = \log\left(1 + \frac{q_k h_{k,i+M}^j}{\sum_{u\neq k,\, u\in[0,M]} \widehat{q}_{u,k}^j h_{u,i+M}^j / h_{u,k}^j + \mathbb{I}_{\text{noise}}}\right), \tag{7}$$

$$\mathbb{T}^D(\mathbf{A},\mathbf{C},\mathbf{F}^D,\mathbf{Q}) : \sum_{j=1}^{J}\sum_{i=1}^{N} a_i f_{i,j}^D \delta_{0,i}^j + \sum_{j=1}^{J}\sum_{k=1}^{M}\sum_{i=1}^{N}\left(b_{i,k}+c_{i,k}\right) f_{i,j}^D \delta_{k,i}^j, \tag{8}$$

$$\mathbb{C}^D\left(\mathbf{C},\mathbf{F}^D,\mathbf{Q}\right) = \sum_{k=1}^{M} \frac{\beta_{\text{rate}} \dfrac{\sum_{j=1}^{J}\sum_{i=1}^{N}\left(c_{i,k}\right) f_{i,j}^D \delta_{k,i}^j}{\sum_{j=1}^{J}\sum_{i=1}^{N}\left(b_{it}+c_{it}\right) f_{i,j}^D \delta_{k,i}^j}}{M + \dfrac{\sum_{j=1}^{J}\sum_{i=1}^{N}\left(c_{i,k}\right) f_{i,j}^D \delta_{k,i}^j}{\sum_{j=1}^{J}\sum_{i=1}^{N}\left(b_{i,k}+c_{i,k}\right) f_{i,j}^D \delta_{k,i}^j}}. \tag{9}$$

In a similar manner, the downlink optimization model can be formulated as in (10a) to (10h). It can be observed that the duality formulation differs only in the transmission power vector Q and the transmission gain matrix. However, considering the assumption that the transmission gain matrix is symmetric, then the formulation is similar to the

(1) BEGIN
(2) Initialize. $CURR = \infty$, $LB(S_0) = G(S_0)$, $LIVESET = S_0$, $count = 0$
(3) Get Problem from $LIVESET$; $S_{\text{PARENT}} = LIVESET(count)$
(4) **while** $LIVESET \neq \phi$ **do**
(5) Branch out sets from S_A and S_B from S_{PARENT} such that $S_A \cup S_B = S_{\text{PARENT}}$
(6) Prune S_{PARENT}; $count = count - 1$
(7) Compute $LB(S_A) = G(S_A)$, $LB(S_B) = G(S_B)$
(8) **if** $LB(S_A) > LB(S_B)$ **then**
(9) Append S_A to $LIVESET$; $count = count + 1$
(10) Append S_B to $LIVESET$; $count = count + 1$
(11) **else**
(12) Append S_B to $LIVESET$; $count = count + 1$
(13) Append S_A to $LIVESET$; $count = count + 1$
(14) **end if**
(15) Get Problem from $LIVESET$; $S_{\text{PARENT}} = LIVESET(count)$
(16) **if** $LB(S_{\text{PARENT}}) = F(\widetilde{A}, \widetilde{C}, \widetilde{F}, \widetilde{P})$ for a feasible solution $(\widetilde{A}, \widetilde{C}, \widetilde{F}, \widetilde{P})$ **then**
(17) **if** $F(\widetilde{X}) < CURR$ **then**
(18) $CURR = F(\widetilde{A}, \widetilde{C}, \widetilde{F}, \widetilde{P})$; $(\widetilde{A}^*, \widetilde{C}^*, \widetilde{F}^*, \widetilde{P}^*) = (\widetilde{A}, \widetilde{C}, \widetilde{F}, \widetilde{P})$
(19) **end if**
(20) **end if**
(21) **if** $LB(S_{\text{PARENT}}) \geq CURR$ **then**
(22) Prune S_{PARENT} from $LIVESET$; $count = count - 1$
(23) Get Problem from $LIVESET$; $S_{\text{PARENT}} = LIVESET(count)$
(24) **end if**
(25) **end while**
(26) END.

Algorithm 1: Branch and bound method.

uplink model:

$$W^D\left(\mathbf{A}, \mathbf{C}, \mathbf{F}^D, \mathbf{Q}\right): \max_{(\mathbf{A},\mathbf{C},\mathbf{F}^D,\mathbf{Q})} w\mathbb{T}^D\left(\mathbf{A}, \mathbf{C}, \mathbf{F}^D, \mathbf{Q}\right) - (1-w)\mathbb{C}^D\left(\mathbf{C}, \mathbf{F}^D, \mathbf{Q}\right) \tag{10a}$$

$$\text{such that } a_i + \sum_{k=1}^{M}\left(b_{i,k} + c_{i,k}\right) = 1, \tag{10b}$$

$$\frac{a_i q_0 h^j_{0,i+M}}{\sum_{u\neq 0,\, u\in[0,M]} \hat{q}^j_{u,0} h^j_{u,i+M}/h^j_{u,0} + \mathbb{I}_{\text{noise}}} \geq \gamma^{\text{PU}}_{\text{th}}, \tag{10c}$$

$$\frac{(b_{i,k} + c_{i,k}) q_k h^j_{k,i+M}}{\sum_{u\neq k,\, u\in[0,M]} \hat{q}^j_{u,k} h^j_{u,i+M}/h^j_{u,k} + \mathbb{I}_{noise}} \geq \gamma^{\text{SU}}_{\text{th}}, \tag{10d}$$

$$\sum_{j=1}^{J} f^D_{i,j} \leq 1, \quad i = 1, 2, \ldots, N, \tag{10e}$$

$$0 \leq q_0 \leq Q^{\text{MBS}}_{\text{MAX}}, \tag{10f}$$

$$0 \leq q_k \leq Q^{\text{FBS}}_{\text{MAX}}, \quad k = 1, 2, \ldots, K, \tag{10g}$$

$$0 < w < 1,$$

$$a_i, c_{i,k}, f^D_{i,j} \in \{0, 1\}, \tag{10h}$$

$$i = 1, 2, \ldots, N,\ k = 0, 1, 2, \ldots, M.$$

3.3. Joint Power Control, Base Station Assignment, and Channel Assignment Scheme using Branch and Bound Method. It can be shown that the uplink and downlink joint power control, base station assignment, and channel assignment scheme formulation problems in (6a) to (6g) and (10a) to (10h) are nonconvex problems due to the mixed integer problem and high-order objectives. These types of problems are well-known NP-Hard problems. However, for a fixed number of variables, the branch and bound method is capable of solving a mixed integer problem in predetermined time. The branch and bound method used in this paper is given by Algorithm 1. The notation for parameters used in the method are provided in Table 2. The method begins by initializing the parameters needed for the method (line 2). The *CURR* parameter represents the upper bound of the solution. The branch and bound method starts from an initial set S_0, which is listed in the set list *LIVESET*. In this case, S_0 is the set of possible solutions for the uplink and downlink problems without the constraint $a_i, c_{i,k}, f^U_{i,j} \in \{0, 1\}$, that is, the integer variables are relaxed and considered to be continuous variables. The lower bound for set S_0 can be found by solving the problem using convex problem methods. In this paper, we used the conditional gradient method [12], represented by the function $G(S)$, where S is the current set analyzed. Then, while *LIVESET* is not empty, the method performs (line 5) to (line 25).

We take a set S_{PARENT} from *LIVESET* and branch out to two sets, S_A and S_B, where $S_A \bigcup S_B = S_{\text{PARENT}}$ (line 5). S_{PARENT} is then pruned from *LIVESET*, since it has already

Table 2: Branch and bound method notation summary.

Symbol	Meaning
CURR	Current upper bound
$LB(S)$	Lower bound of the problem on set S
$G(S)$	Conditional gradient method over set S
LIVESET	Set of unanalyzed sets
S_A, S_B	Offspring set of each iteration
S_{PARENT}	Current iteration's parent set

produced all its offspring (line 6). After pruning S_{PARENT}, the method decides the order in which S_A and S_B should be inserted into *LIVESET* (line 7–line 14). To determine the order, the value of the lower bound for each of S_A and S_B is computed. The set whose lower bound is lower is analyzed first. These series of steps are important, because if a solution is found traversing the set a lesser lower bound, then the likelihood of finding a better solution from the other set would be decreased. The set with a lesser lower bound is chosen as S_{PARENT} (line 15). A check procedure is conducted if the $LB(S_{\text{PARENT}})$ is a feasible solution for the unrelaxed problems in (6a) to (6g) and (10a) to (10h). If this is true, then the upper bound *CURR* is adjusted to $LB(S_{\text{PARENT}})$ and the current solution is $(\widetilde{A}, \widetilde{C}, \widetilde{F}, \widetilde{P})$ (line 16–line 21). Another check is conducted if the lower bound of S_{PARENT} is greater than the upper bound *CURR*, and then no better solution can be found inside the set S_{PARENT}. S_{PARENT} is then pruned from *LIVESET* and the next parent is taken from *LIVESET* (line 21–24). If both conditions in line 16 and line 21 are not met, then the method branches out and prunes the current S_{PARENT}. The process repeats until *LIVESET* is empty.

The method presented in Algorithm 1 is a First-In Last-Out search technique applied to the branch and bound method. As mentioned previously, analyzing sets whose lower bounds are lesser than other sets reduces the probability of the need to analyze the other sets. As such, the computation time can be proven to be between $\mathbb{O}(N)$ and $\mathbb{O}(2^{N-1})$.

3.4. Distributed Implementation of the Joint Power Control, Base Station Assignment, and Channel Assignment Scheme. To implement the Joint power control, base station assignment and channel assignment scheme in a distributed way, we first look at the separability of the objective functions in (6a) to (6g) and (10a) to (10h) and, as well as the separability of the constraint set:

$$\mathbb{T}_i^U\left(a_i, \mathbf{C}_i, \mathbf{F}_i^U, p_i\right) : \sum_{j=1}^{J} a_i f_{i,j}^U v_{i,0}^j + \sum_{j=1}^{J}\sum_{k=1}^{M} (b_{i,k} + c_{i,k}) f_{i,j}^U v_{i,k}^j, \tag{11}$$

$$v_{-ei,k}^j = \log_2\left(1 + \frac{\widehat{p}_{i,e}^j h_{i+M,k}^j / h_{i+M,e+M}^j}{\sum_{u\neq eu\in[1,N]} \widehat{p}_{u,i}^j h_{u+M,k}^j / h_{u+M,i+M}^j + \mathbb{I}_{\text{noise}}}\right), \tag{12}$$

$$\mathbb{C}_i^U\left(\mathbf{C}_i, \mathbf{F}_i^U, p_i\right) = \sum_{k=1}^{M} \frac{\beta_{\text{rate}}\varphi}{M+\varphi}, \tag{13}$$

where

$$\varphi = \frac{\sum_{j=1}^{J}\sum_{e=1}^{N} (c_{i,k}) f_{i,j}^U v_{-ei,k}^j}{\sum_{j=1}^{J}\sum_{e=1}^{N} (b_{ek} + c_{ek}) f_e^j v_{-ie,k}^j}. \tag{14}$$

For the objective function, the throughput objective for the uplink joint power control, base station assignment, and channel assignment scheme (3) is observed to be separable to (11) for each client i. For the compensation mechanism in (4), the nonseparability lies in the sum of achievable throughputs at a BS given by $\sum_{j=1}^{J}\sum_{t=1}^{M}\sum_{i=1}^{K}(b_{i,k}+c_{i,k}) f_{i,j}^U v_{i,k}^j$. To resolve this, the measure power of neighbor nodes and (1) is used to modify (4). Let $v_{ei,k}^j$ (12) be the uplink achievable throughput between client i and BS k as seen from BS e using channel j. Using (12), the compensation mechanism in (4) can be separable as in (13). Finally, it is easily seen that the constraint sets for the uplink joint power control, base station assignment, and channel assignment scheme are separable

$$\begin{aligned}
&W_i^U\left(a_i, \mathbf{C}_i, \mathbf{F}_i^U, p_i\right) :\\
&\max_{(a_i, C_i, F_i^U, p_i)} w\mathbb{T}_i^U\left(a_i, C_i, F_i^U, p_i\right) - (1-w)\mathbb{C}_i^U\left(C_i, F_i^U, p_i\right)\\
&\text{such that } a_i + \sum_{k=1}^{M}(b_{i,k} + c_{i,k}) = 1,\\
&\frac{a_i p_i h_{i+M,0}^j}{\sum_{u\neq i, u\in[1,N]} \widehat{p}_{u,i}^j h_{u+M,k}^j / h_{u+M,i+M}^j + \mathbb{I}_{\text{noise}}} \geq \gamma_{\text{th}}^{\text{PU}},\\
&\frac{(b_{i,k}+c_{i,k}) p_i h_{i+M,k}^j}{\sum_{u\neq i, u\in[1,N]} \widehat{p}_{u,i}^j h_{u+M,k}^j / h_{u+M,i+M}^j + \mathbb{I}_{\text{noise}}} \geq \gamma_{\text{th}}^{\text{SU}},\\
&\sum_{j=1}^{J} f_{i,j}^U \leq 1,\\
&0 \leq p_i \leq P_{\text{MAX}},\\
&0 < w < 1,\\
&a_i, c_{i,k}, f_{i,j}^U \in \{0, 1\}.
\end{aligned} \tag{15}$$

From (11) to (13), the uplink joint power control, base station assignment, and channel assignment scheme in (6a) to (6g) can be reformulated as (15) for each client.

We consider the problem of maximizing the total utility functions over separable sets. It can be shown that the objective function in (15) is nonconvex. The optimal solutions in (15) with separable functions are characterized in Lemma 1. Let

$$\begin{aligned}
&\Phi_i^U\left(\mathbf{A}, \mathbf{C}, \mathbf{F}^U, \mathbf{P}\right)\\
&\quad = w\mathbb{T}_i^U\left(a_i, \mathbf{C}_i, \mathbf{F}_i^U, p_i\right) - (1-w)\mathbb{C}_i^U\left(\mathbf{C}_i, \mathbf{F}_i^U, p_i\right),\\
&\Phi^U\left(\mathbf{A}, \mathbf{C}, \mathbf{F}^U, \mathbf{P}\right) = \sum_{i=1}^{N} \Phi_i^U.
\end{aligned} \tag{16}$$

Lemma 1. *Assume that* $(a_i^*, \mathbf{C}_i^*, \mathbf{F}_i^U *, p_i^*)$, $i = \overrightarrow{1,N}$, *is the solution for* (15) *at each i. Then* $\mathbf{A}^* = (a_1^*, a_2^*, \ldots, a_N^*)$, $\mathbf{C}^* = (\mathbf{C}_1^*, \mathbf{C}_2^*, \ldots, \mathbf{C}_N^*)$, $F^{U*} = (\mathbf{F}_1^{U*}, \mathbf{F}_2^{U*}, \ldots, \mathbf{F}_N^{U*})$, $\mathbf{P}^* = (p_1^*, p^*, \ldots, p_N^*)$.

Proof. The proof is an obvious consequence of the following inequalities:

$$\begin{aligned}
&\Phi^U\left(\mathbf{A}, \mathbf{C}, \mathbf{F}^U, \mathbf{P}\right) \\
&= \sum_{i=1}^{N} \Phi_i^U\left(\mathbf{A}, \mathbf{C}, \mathbf{F}^U, \mathbf{P}\right) \le \sum_{i=1}^{N} W_i^U\left(a_i, \mathbf{C}_i, \mathbf{F}_i^U, p_i\right) \\
&= \sum_{i=1}^{N} \Phi_i^U\left(a_i^*, \mathbf{C}_i^*, \mathbf{F}_i^{U*}, p_i^*\right) = \Phi^U\left(a_i^*, \mathbf{C}_i^*, \mathbf{F}_i^{U*}, p_i^*\right).
\end{aligned} \tag{17}$$

□

The distributed implementation for the downlink joint power control, base station assignment, and channel assignment scheme can be formulated in a similar way as the uplink scheme. In the downlink, we consider the distributed computation by having each BS controls its power, base station assignment, and channel assignment. It is assumed that the uplink solutions for $\mathbf{A}$ and $\mathbf{C}$ are used by the downlink. In this way, the downlink implementation only solves the optimal value for $\mathbf{F}^D$ and $\mathbf{P}$. The throughput can be formulated for MBS and FBSs as (18) and (19), respectively. Let $\delta_{e\leftarrow k,i}^j$ (20) be the uplink achievable throughput between client i and BS k as seen from BS e using channel j:

$$\mathbb{T}_0^D\left(\mathbf{F}_0^D, q_0\right) : \sum_{j=1}^{J} \sum_{i=1}^{N} a_i f_{i,j}^D \delta_{0,i}^j, \tag{18}$$

$$\mathbb{T}_k^D\left(\mathbf{F}_k^D, q_k\right) : \sum_{j=1}^{J} \sum_{i=1}^{N} \left(b_{i,k} + c_{i,k}\right) f_{i,j}^D \delta_{k,i}^j, \tag{19}$$

$$\delta_{ek,i}^j = \log_2\left(1 + \frac{\hat{q}_{i,e}^j h_{k,i+M}^j / h_{i,e}^j}{\sum_{u \ne e,\, u \in [0,M]} \hat{q}_{u,e}^j h_{u,i+M}^j / h_{u,e}^j + \mathbb{I}_{\text{noise}}}\right). \tag{20}$$

From (18) to (20), the compensation mechanism for distributed implementation at each FBS is given as (21). Note that there is no compensation scheme at the MBS:

$$\mathbb{C}_k^D\left(\mathbf{F}_k^D, q_k\right) = \frac{\beta_{\text{rate}} \psi}{M + \psi}, \tag{21}$$

where

$$\psi = \frac{\sum_{j=1}^{J} \sum_{i=1}^{N} \left(c_{i,k}\right) f_{i,j}^D \delta_{e\leftarrow i,k}^j}{\sum_{j=1}^{J} \sum_{i=1}^{N} \left(b_{it} + c_{it}\right) f_{i,j}^D \delta_{e\leftarrow i,k}^j}. \tag{22}$$

The distributed downlink joint power control, base station assignment and channel assignment scheme for MBS and FBS is given by (23) and (24), respectively. It should be pointed out that in (24), the constraint regarding the SINR threshold for the MBS is still included. This is because the FBSs, which are considered secondary users, should use the spectrum with the condition that the SINR of the MBS is not exceeded:

$$\begin{aligned}
&W_0^D\left(\mathbf{F}_0^D, q_0\right) : \\
&\max_{\left(\mathbf{F}_0^D, q_k\right)} \mathbb{T}_0^D\left(a_i, \mathbf{C}_i, \mathbf{F}_0^D, q_i\right) \\
&\text{such that } \frac{a_i q_0 h_{0,i+M}^j}{\sum_{u \ne 0,\, u \in [0,M]} \hat{q}_{u,0}^j h_{0,i+M}^j / h_{u,0}^j + \mathbb{I}_{\text{noise}}} \ge \gamma_{\text{th}}^{\text{PU}}, \\
&\sum_{j=1}^{J} f_{i,j}^D \le 1, \\
&0 \le q_0 \le Q_{\text{MAX}}^{\text{MBS}}, \\
&f_{i,j}^D \in \{0, 1\},
\end{aligned} \tag{23}$$

$$\begin{aligned}
&W_k^D\left(\mathbf{F}_k^D, q_k\right) : \\
&\max_{\left(\mathbf{F}_k^D, q_k\right)} w\mathbb{T}_k^D\left(\mathbf{F}_k^D, q_k\right) - (1 - w)\mathbb{C}_k^D\left(\mathbf{F}_k^D, q_k\right) \\
&\text{such that } \frac{a_i\left(\hat{q}_{0,k}^j h_{0,i+M}^j / h_{0,k}^j\right)}{\sum_{u \ne 0,\, u \in [0,M]} \hat{q}_{u,0}^j h_{0,i+M}^j / h_{u,0}^j + \mathbb{I}_{\text{noise}}} \ge \gamma_{\text{th}}^{\text{PU}}, \\
&\frac{\left(b_{i,k} + c_{i,k}\right) q_k h_{k,i+M}^j}{\sum_{u \ne k,\, u \in [0,M]} \hat{q}_{u,k}^j h_{u,i+M}^j / h_{u,k}^j + \mathbb{I}_{\text{noise}}} \ge \gamma_{\text{th}}^{\text{SU}}, \\
&\sum_{j=1}^{J} f_{i,j}^D \le 1, \\
&0 \le q_k \le Q_{\text{MAX}}^{\text{FBS}}, \\
&0 < w < 1, \\
&f_{i,j}^D \in \{0, 1\}.
\end{aligned} \tag{24}$$

With the formulation for distributed implementation, the overall optimization problem can be solved by each element in the network. Each element computes the solution to the problem by running Algorithm 1 for each of their distributed problems given in (15), (23), and (24).

4. Simulation Studies and Numerical Results

A numerical simulation was conducted to explore the consequences of the formulation and to show that the branch and bound method converges to the optimal solution. The numerical analysis is conducted using MATLAB. The numerical analysis scenario consists of one MBS, three FBSs (FBS_A, FBS_B, and FBS_C), one private client for each FBS (MC_1, MC_2, and MC_3, resp.), and randomly distributed public clients. The SINR threshold for the MBS is set at 0.8 while the SINR threshold for the FBSs is set to 0.3. These high SINR threshold values simulate high-density traffic in the area and assure that the FBSs will have to search for

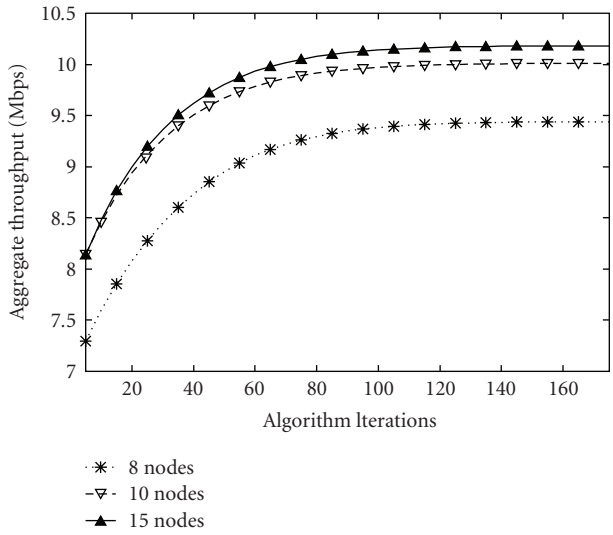

Figure 4: Convergence of the branch and bound method for the joint power control, base station assignment, and channel assignment scheme. The number of nodes is varied from 8,10 and 15 clients. The clients are randomly distributed in each of the 8-client, 10-client, and 15-client configurations except for 3 private clients.

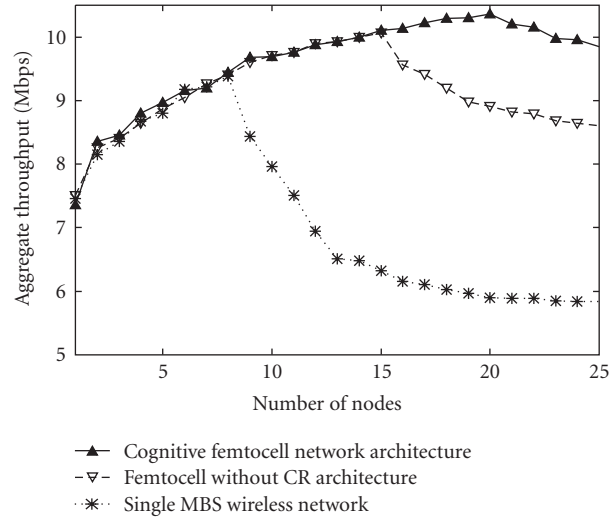

Figure 5: Network achievable throughput. The achievable throughput for our joint power control, base station assignment, and channel assignment scheme is compared with the throughput of Li et al. and a single MBS WiMAX network as the number of nodes is varied.

available spectrum holes. The MBS power $Q_{\text{MAX}}^{\text{MBS}}$ is limited to 1 W while the FBS's power threshold $Q_{\text{MAX}}^{\text{FBS}}$ is at 0.5 W.

The convergence of the conditional gradient method for power optimization can be seen from Figure 4 for 8-node, 10-node, and 15-node configurations. As can be seen in this figure, the solution converges to the optimal solution for a given number of nodes after about 150 iterations. Each iteration involves the splitting of a parent set, as seen in Algorithm 1.

The performance of the architecture is also compared to that of a femtocell network without CR and a traditional single MBS wireless network, respectively. This performance comparison shows the benefits of the cognitive femtocell network architecture in terms of throughput improvement when compared with current architectures. It can be seen from Figure 5 that, as the number of nodes increases, the proposed cognitive femtocell network architecture outperforms both of the traditional networks. The improvement originates from the femtocell owners allowing public clients to utilize their private resources. For less than 8 nodes, the cognitive femtocell behaves in a manner similar to that of a traditional femtocell. In addition, in cases of congestion, the FBS searches for new spectrum holes, which further increases performance. As expected, the performance of the single MBS wireless network degrades as the number of clients increases. In addition, we observe that as the number of clients increases, the macrocell cannot meet the SINR threshold requirement. Thus, some clients are not allowed to transmit. Traditional femtocell networks behave similarly to the cognitive femtocell network architecture. However, when congestion occurs (in this case at $N = 15$), the performance of the traditional femtocell degrades. Upon congestion at $N = 15$, the cognitive femtocell searches for spectrum holes.

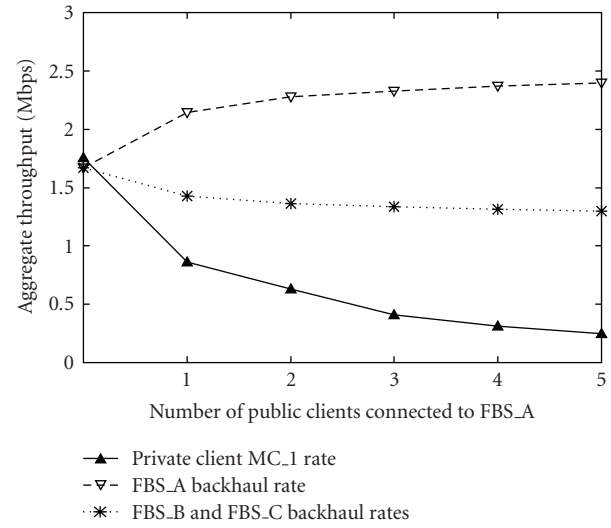

Figure 6: Private mode achievable rate versus backhaul rate. This figure shows the effects of allowing public clients to connect to an FBS. It can be seen that the achievable throughput of the private client which owns the FBS decreases as the number of public clients connecting to the FBS increases. It can also be observed that, using our compensation mechanism, the backhaul rate of the affected FBS is increased to compensate for the service to public clients.

However, at $N = 20$, there are no spectrum holes to be found and the transmission would either operate at a lower data rate (low-power) or be deferred. This results in a slow degradation of throughput performance.

In Figure 6, the effects of an open access femtocell architecture and our proposed compensation mechanism

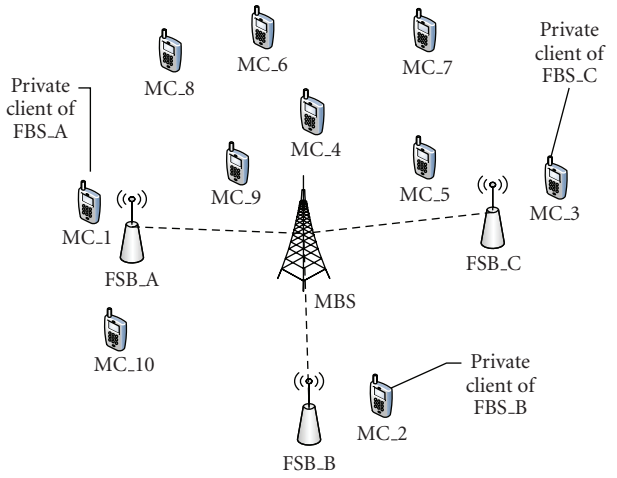

Figure 7: Simulation Scenario. In this scenario, there is 1 MBS, 3 FBSs, and 10 clients. Out of these 10 clients, 3 are private clients to an FBS. The dotted line between FBSs and MBS represents the backhaul line between them.

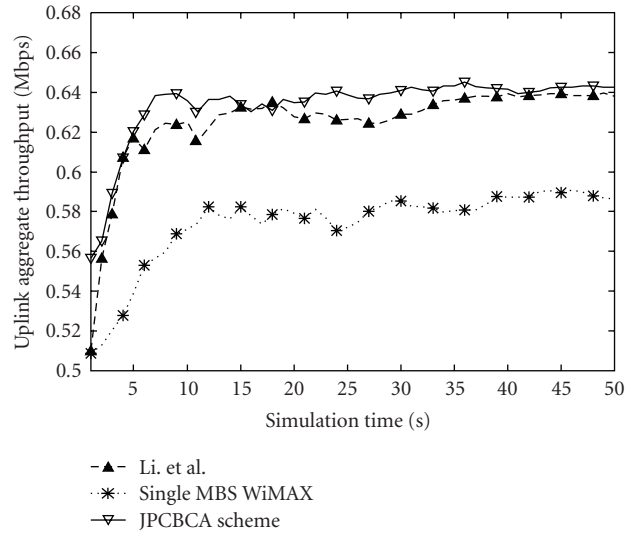

Figure 8: Uplink aggregate throughput. This figure shows that our Joint Power Control, Base Station Assignment, and Channel Assignment (JPCBCA) Scheme can achieve higher throughput as compared to the single MBS WiMAX network and the work by Li et al.

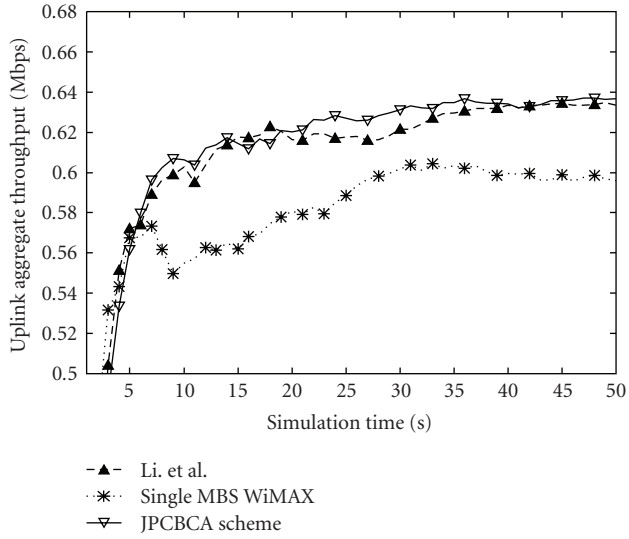

Figure 9: Downlink aggregate throughput. Similar to uplink, the throughput for the joint power control, base station assignment, and channel assignment scheme at the downlink can be seen to be better than the single MBS WiMAX network and the work by Li et al. This is due to the contention for the single MBS WiMAX network. However, for the work by Li et al., power consumption is less than that of the proposed scheme, since reduced power consumption is considered a priority in their formulation.

are investigated. We vary the public clients connected to FBS_A while FBS_B and FBS_C only service their respective private clients. As the number of public clients connecting to FBS_A is increased, the spectrum resource of FBS_A is divided between the connected public and private clients. This results in a decrease in the achievable rate for the private client MC_1, as shown in the figure. On the backhaul side, FBS_A is given additional slots for each public client that it serves, resulting in an increase in the backhaul rate. However, this also results in a decrease in the backhaul rate for the other FBSs, FBS_B and FBS_C.

The scenario for the simulation study is presented in Figure 7. There are 3 FBSs namely, FBS_A, FBS_B, and FBS_C, which are installed by private clients MC_1, MC_2, and MC_3, respectively. The public clients MC_4 to MS_10 connect to the MBS but may connect to any FBS subject to compensation. The network works under the a WiMAX environment with 2 channels available for allocation for a given time instance. The limitation of the 2 channels is necessary to assure contention for the resources for the given number of clients and base stations. Also, the MBS is capable of transmitting up to 19 Mbps while the FBSs are limited to 9 Mpbs. The joint power control, base station assignment, and channel assignment scheme is compared with the work of Li et al. [13] and a single MBS WiMAX network. The work of Li is a cognitive interference management scheme for a cognitive femtocell network architecture that chooses its transmission schedule by optimizing the channel assignment and power control.

The uplink and downlink aggregate throughput is plotted in Figures 8 and 9. It can be seen that our joint power control, base station assignment, and channel assignment scheme achieves higher throughput than the other schemes. In Li's work, the lower throughput results from connecting to the nearest BS so as to reduce power. For instance, in Figure 7, the public client MC_5 connects to FBS_C. Since FBS_C has a lower transmission rate than the MBS, the aggregate throughput decreases to a value lower than that of our scheme. The single MBS WiMAX network achieves lower throughput reading due to the contention of nodes for 2 channels.

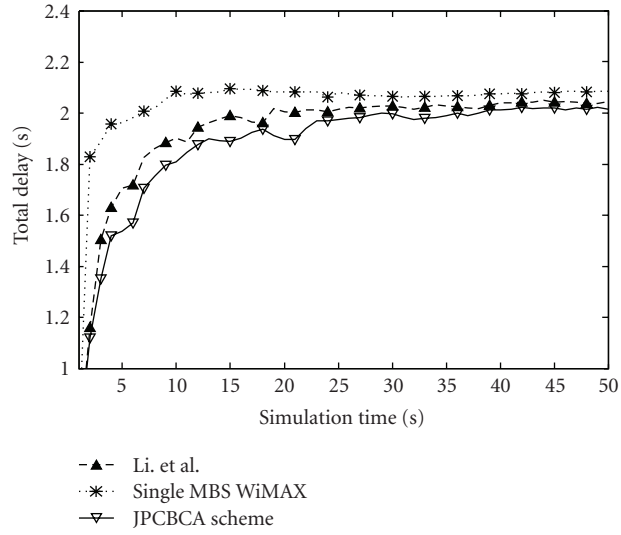

Figure 10: Delay comparison. The proposed joint power control, base station assignment, and channel assignment scheme has an average total delay of 1.8 sec. as compared to 1.9 sec. in Li et al. and 2.1 sec. in single MBS WiMAX.

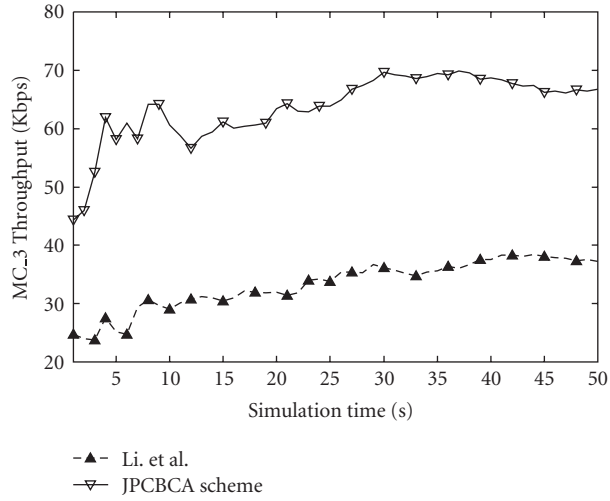

Figure 11: Private Client Throughput Comparison. This figure shows the aggregate throughput for MC_3. The throughput is higher for the joint power control, base station assignment, and channel assignment scheme since MC_5 is connected to the MBS. The client MC_5 is connected to in our scheme since the MBS is not yet in the threshold. In the event that MBS reaches its threshold, then MC_5 connects to FBS_3 in our scheme and the throughput value is the same as in Li's.

The total delay experienced by transmissions is also observed to be less for our joint power control, base station assignment, and channel assignment scheme. Figure 10 shows the improvement in the delay experienced by transmissions. The single MBS WiMAX experiences higher delay readings due to relatively more clients competing for the two channel resources as compared to Li et al. and our scheme. However, due to MC_5 connecting to FBS_C instead of the MBS, the scheme by Li results in a slightly higher delay than our Joint power control, base station assignment, and channel assignment scheme. It can also be seen in Figure 11 that the aggregate throughput of MC_3 for Li et al. is lower than that of our scheme due to the connection of MC_5 to FBS_C. This results from the difference between our scheme and Li's scheme. Since Y. Li's scheme is much more concerned with power consumption, their scheme attempts to connect to the nearest BS, either MBS or FBS. In the simulation scenario, Li's scheme would have MC_5 connected to FBS_C. This connection drastically decreases the achievable rate for MC_3. This situation is unfair to the private client MC_3, since it owns FBS_C. Although compensated through the backhaul rate, the loss of MC_3 in terms of achievable rate is higher than the gain obtained by the network as a whole.

5. Discussion of Related Works

The depletion of wireless spectrum resources is well documented in the literature. In a work by Staple and Werbach [1], the authors discussed the current status of the frequency spectrum. In addition, they also reported on current efforts to solve the problem of spectrum scarcity. One of the most recent efforts involves the use of software-defined radios with sensing capabilities, called cognitive radio. Mitola and Maguire [5] published a paper on cognitive radio in 1999, but it has only recently won attention by researchers as a viable solution to improving spectrum efficiency. A number of studies have been conducted to quantify the benefits of using cognitive radios. Srinivasa and Jafar [14] carried out a theoretical study on the throughput potential of cognitive radios using different cognitive perspectives. Several studies [15, 16] have also proposed architectures and applications for cognitive radios. The focus of these works was primarily on to how to handle base station hand-offs and decision mechanisms. In addition, research on spectrum management [6, 17, 18], power control [19], and node coordination [18] has been reported. In most of these works, the formulations are conducted for the spectrum configuration only. Fully-cognitive radios have generally not been addressed in recent works. Also, the coexistence of several cognitive radios has received little attention as compared to the minimization of interference to primary clients. Although several studies have concentrated on the interference contributions [20, 21], most either focus on cognitive radios or on primary client interference. These two concerns are addressed in our paper along with throughput improvement and coverage. Femtocell architecture [8, 22, 23] has been used to mitigate the noise in cognitive radio communications. Research on femtocells has shown that they are limited by the amount of usable bandwidth in a small area [8, 22]. However, most studies assume that adjacent FBSs would not interfere with each other. This assumption is valid for a moderately dense network. On the other hand, for a dense network, interference is unavoidable. This paper merges the cognitive capabilities with a femtocell architecture to mitigate this

drawback. The assumption of noninterfering base stations can now be validated even for the case of dense networks.

6. Conclusion

This paper focused on the congestion problem in radio frequency transmission. With continuing improvements of wireless technology, the scarcity of spectrum resources has exponentially increased. Nevertheless, most of the radio frequency spectrum bands are not efficiently utilized, especially the licensed bands.

To resolve this problem, recent studies have developed the use of cognitive radio based on Mitola's 1999 proposal. Using cognitive radio, the wasted bandwidth in licensed bands can be used by unlicensed bands as long as the primary licensed users do not utilize them. However, the benefits of using cognitive radios are dependent on the transmission behavior of the primary clients. If no spectrum holes are available, the cognitive clients cannot transmit. To overcome this problem, the use of femtocell a architecture is a good alternative. Femtocells are consumer-installed base stations that enable short-range communication indoors. The advantage of using femtocells is the capacity gain derived from minimizing the range at which they are transmitting.

In this paper, we proposed a cognitive femtocell network architecture that aims to efficiently utilize the radio frequency spectrum while meeting the service requirements of the clients. A joint power control, base station assignment, and channel assignment scheme is derived to efficiently maximize the overall throughput. Results show that significant improvements can be derived in using this architecture as the number of nodes in the network increases. This paper also demonstrated that using a compensation mechanism assures mutual benefits in sharing private clients between femtocell owners and the primary network.

Acknowledgments

This work was supported by the National Research Foundation of Korea's (NRF) grant funded by the Korean government (MEST) (no. 2009-0074938). They would also like to extend our gratitude to the anonymous reviewers and editor for their valuable comments and suggestions which improved the earlier versions of the paper.

References

[1] G. Staple and K. Werbach, "The end of spectrum scarcity," *IEEE Spectrum*, vol. 41, no. 3, pp. 48–52, 2004.

[2] D. Cabric, S. M. Mishra, and R. W. Brodersen, "Implementation issues in spectrum sensing for cognitive radios," in *Proceedings of the 38th Asilomar Conference on Signals, Systems and Computer*, vol. 1, pp. 772–776, Pacific Grove, Calif, USA, November 2004.

[3] T. A. Weiss and F. K. Jondral, "Spectrum pooling: an innovative strategy for the enhancement of spectrum efficiency," *IEEE Communications Magazine*, vol. 42, no. 3, pp. S8–S14, 2004.

[4] N. Golmie and F. Mouveaux, "Interference in the 2.4 GHz ISM band: impact on the bluetooth access control performance," in *IEEE International Conference on Communications (ICC '01)*, vol. 8, pp. 2540–2545, Helsinki, Finland, June 2001.

[5] J. Mitola III and G. Q. Maguire Jr., "Cognitive radio: making software radios more personal," *IEEE Personal Communications*, vol. 6, no. 4, pp. 13–18, 1999.

[6] I. F. Akyildiz, W.-Y. Lee, M. C. Vuran, and S. Mohanty, "A survey on spectrum management in cognitive radio networks," *IEEE Communications Magazine*, vol. 46, no. 4, pp. 40–48, 2008.

[7] I. F. Akyildiz, W.-Y. Lee, M. C. Vuran, and S. Mohanty, "NeXt generation/dynamic spectrum access/cognitive radio wireless networks: a survey," *Computer Networks*, vol. 50, no. 13, pp. 2127–2159, 2006.

[8] V. Chandrasekhar, J. G. Andrews, and A. Gatherer, "Femtocell networks: a survey," *IEEE Communications Magazine*, vol. 46, no. 9, pp. 59–67, 2008.

[9] V. Chandrasekhar and J. Andrews, "Uplink capacity and interference avoidance for two-tier femtocell networks," *IEEE Transactions on Wireless Communications*, vol. 8, no. 7, pp. 3498–3509, 2009.

[10] J. F. Kurose and K. W. Ross, *Computer Networking: A Top-Down Approach Featuring the Internet*, Pearson Education, 3rd edition, 2005.

[11] J. M. Park and S.-L. Kim, "Distributed throughput-maximization using the up- and downlink duality in wireless networks," in *Proceedings of the International Wireless Communications and Mobile Computing Conference (IWCMC '07)*, pp. 97–102, August 2007.

[12] D. P. Bertsekas, *Nonlinear Programming*, Athena Scientific, 2nd edition, 1999.

[13] Y. Li, M. Macuha, E. Sousa, T. Sato, and M. Nanri, "Cognitive interference management in 3G femtocells," in *Proceedings of the 20th Personnal, Indoor and Mobile Radio Communications Symposium (PIMRC '09)*, Tokyo, Japan, September 2009.

[14] S. Srinivasa and S. A. Jafar, "The throughput potential of cognitive radio: a theoretical perspective," in *Proceedings of the 40th Asilomar Conference on Signals, Systems and Computers*, pp. 221–225, October 2006.

[15] T. Ueda, K. Takeuchi, S. Kaneko, S. Nomura, and K. Sugiyama, "Packet switch and its impact on dynamic base station relocation in mesh networks using cognitive radio," *IEICE Transactions on Communications*, vol. E91-B, no. 1, pp. 102–109, 2008.

[16] F. Ge, Q. Chen, Y. Wang, C. W. Bostian, T. W. Rondeau, and B. Le, "Cognitive radio: from spectrum sharing to adaptive learning and reconfiguration," in *Proceedings of the IEEE Aerospace Conference*, pp. 1–10, March 2008.

[17] E. Adamopoulou, K. Demestichas, and M. Theologou, "Enhanced estimation of configuration capabilities in cognitive radio," *IEEE Communications Magazine*, vol. 46, no. 4, pp. 56–63, 2008.

[18] Z. Quan, S. Cui, and A. H. Sayed, "Optimal linear cooperation for spectrum sensing in cognitive radio networks," *IEEE Journal on Selected Topics in Signal Processing*, vol. 2, no. 1, pp. 28–40, 2008.

[19] Y. Chen, G. Yu, Z. Zhang, H.-H. Chen, and P. Qiu, "On cognitive radio networks with opportunistic power control strategies in fading channels," *IEEE Transactions on Wireless Communications*, vol. 7, no. 7, pp. 2752–2761, 2008.

[20] S. Geirhofer, L. Tong, and B. M. Sadler, "Cognitive medium access: constraining interference based on experimental models," *IEEE Journal on Selected Areas in Communications*, vol. 26, no. 1, pp. 95–105, 2008.

[21] J. O. Neel, R. Menon, A. B. MacKenzie, J. H. Reed, and R. P. Gilles, "Interference reducing networks," in *Proceedings of the 2nd International Conference on Cognitive Radio Oriented Wireless Networks and Communications (CrownCom '07)*, pp. 96–104, Orlando, Fla, USA, August 2007.

[22] H. Claussen, L. T. W. Ho, and L. G. Samuel, "Self-optimization of coverage for femtocell deployments," in *Proceedings of the 7th Annual Wireless Telecommunications Symposium (WTS '08)*, pp. 278–285, Ponoma, Calif, USA, April 2008.

[23] S. B. Kang, Y. M. Seo, Y. K. Lee, et al., "Soft QoS-based CAC scheme for WCDMA femtocell networks," in *Proceedings of the 10th International Conference on Advanced Communication Technology (ICACT '08)*, vol. 1, pp. 409–412, February 2008.

Hindawi Publishing Corporation
EURASIP Journal on Wireless Communications and Networking
Volume 2010, Article ID 391684, 10 pages
doi:10.1155/2010/391684

Research Article

A Bayesian Game-Theoretic Approach for Distributed Resource Allocation in Fading Multiple Access Channels

Gaoning He,[1] Mérouane Debbah,[2] and Eitan Altman[3]

[1] *Motorola Labs, Parc Les Algorithmes, 91193 Gif sur Yvette, France*
[2] *Alcatel-Lucent Chair on Flexible Radio, 3 Rue Joliot-Curie, 91192 Gif sur Yvette, France*
[3] *INRIA, 2004 Route des Lucioles, 06902 Sophia Antipolis, France*

Correspondence should be addressed to Gaoning He, gaoning.he@gmail.com

Received 31 August 2009; Revised 7 January 2010; Accepted 13 March 2010

Academic Editor: Ozgur Oyman

A Bayesian game-theoretic model is developed to design and analyze the resource allocation problem in K-user fading multiple access channels (MACs), where the users are assumed to selfishly maximize their average achievable rates with incomplete information about the fading channel gains. In such a game-theoretic study, the central question is whether a Bayesian equilibrium exists, and if so, whether the network operates efficiently at the equilibrium point. We prove that there exists exactly one Bayesian equilibrium in our game. Furthermore, we study the network sum-rate maximization problem by assuming that the users coordinate according to a symmetric strategy profile. This result also serves as an upper bound for the Bayesian equilibrium. Finally, simulation results are provided to show the network efficiency at the unique Bayesian equilibrium and to compare it with other strategies.

1. Introduction

The fading multiple access channel (MAC) is a basic wireless channel model that allows several transmitters connected to the same receiver to transmit over it and share its capacity. The capacity region of the fading MAC and the optimal resource allocation algorithms have been characterized and well studied in many pioneering works with different information assumptions [1–4]. However, in order to achieve the full capacity region, it usually requires a central computing resource (a scheduler with comprehensive knowledge of the network information) to globally allocate the system resources. This process is centralized, since it involves feedback and overhead communication whose load scales linearly with the number of transmitters in the network. In addition, with the fast evolution of wireless techniques, this centralized network infrastructure begins to expose its weakness in many aspects, for example, slow reconfiguration against varying environment, increased computational complexity, and so forth. This is especially crucial for femtocell networks where it is quite difficult to centralize the information due to a limited capacity backhaul. Moreover, the high density of base stations would increase the cost of centralizing the information.

In recent years, increased research interest has been given to self-organizing wireless networks in which mobile devices allocate resources in a decentralized manner [5]. Tools from game theory [6] have been widely applied to study the resource allocation and power control problems in fading MAC [7], as well as many other types of channels, such as orthogonal frequency division multiplexing (OFDM) [8], multiple input and multiple output (MIMO) channels [9, 10], and interference channels [11]. Typically, the game-theoretic models used in these previous works assume that the knowledge, for example, channel state information (CSI), about other devices is available to all devices. However, this assumption is hardly met in practice. In practical wireless scenarios, mobile devices can have local information but can barely access to global information on the network status.

A static noncooperative game has been introduced in the context of the two-user fading MAC, known as "waterfilling game" [7]. By assuming that users compete with transmission rates as utility and transmit powers as moves, the authors show that there exists a unique Nash equilibrium

[12] which corresponds to the maximum sum-rate point of the capacity region. This claim is somewhat surprising, since the Nash equilibrium is in general inefficient compared to the Pareto optimality. However, their results rely on the fact that both transmitters have complete knowledge of the CSI, and in particular, perfect CSI of all transmitters in the network. As we previously pointed out, this assumption is rarely realistic in practice.

Thus, this power allocation game needs to be reconstructed with some realistic assumptions made about the knowledge level of mobile devices. Under this consideration, it is of great interest to investigate scenarios in which devices have "incomplete information" about their components, for example, a device is aware of its own channel gain, but unaware of the channel gains of other devices. In game theory, a strategic game with incomplete information is called a "Bayesian game." Over the last ten years, Bayesian game-theoretic tools have been used to design distributed resource allocation strategies only in a few contexts, for example, CDMA networks [13, 14], multicarrier interference networks [15]. The primary motivation of this paper is therefore to investigate how Bayesian games can be applied to study the resource allocation problems in the fading MAC. In some sense, this study can help to design a self-organizing femto-cell network where different frequency bands or subcarriers are used for the femto-cell coverage, for example, different femto-cells operate on different frequency bands to avoid interference.

In this paper, we introduce a Bayesian game-theoretic model to design and analyze the resource allocation problem in a fading MAC, where users are assumed to selfishly maximize their ergodic capacity with incomplete information about the fading channel gains. In such a game-theoretic study, the central question is whether a Bayesian equilibrium exists, and if so, whether the network operates efficiently at the equilibrium point. We prove that there exists exactly one Bayesian equilibrium in our game. Furthermore, we study the network sum-rate maximization problem by assuming that all users coordinate to an optimization-based symmetric strategy. This centralized strategy is important when the fading processes for all users are relatively stationary and the global system structure is fixed for a long period of time. This result also serves as an upper bound for the unique Bayesian equilibrium.

The paper is organized in the following form: In Section 2, we introduce the system model and state important assumptions. In Section 3, the K-user MAC is formulated as a static Bayesian game. In Section 4, we characterize the Bayesian equilibrium set. In Section 5, we give a special discussion on the optimal symmetric strategy. Some numerical results are provided to show the efficiency of the Bayesian equilibrium in Section 6. Finally, we close with some concluding remarks in Section 7.

2. System Model and Assumptions

2.1. System Model. We consider the uplink of a single-cell network where K users are simultaneously sending information to one base station. This corresponds to a fading MAC, in which the users are the transmitters and the base station is the receiver. The signal received at the base station can be mathematically expressed as

$$y(t) = \sum_{k=1}^{K} \sqrt{g_k(t)}\, x_k(t) + z(t), \tag{1}$$

where $x_k(t)$ and $g_k(t)$ are the input signal and fading channel gain of user k, and $z(t)$ is a zero-mean white Gaussian noise with variance σ^2. The input signal $x_k(t)$ can be further written as

$$x_k(t) = \sqrt{p_k(t)}\, s_k(t), \tag{2}$$

where $p_k(t)$ and $s_k(t)$ are the transmitted power and data of user k at time t.

In this study, we consider the wireless transmission in fast fading environments, that is, the coherence time of the channel is small relative to the delay constraint of the application. When the receiver can perfectly track the channel but the transmitters have no such information, the codewords cannot be chosen as a function of the state of the channel but the decoding can make use of such information. When the fading process is assumed to be stationary and ergodic within the considered interval of signal transmission, the channel capacity in a fast fading channel corresponds to the notion of ergodic capacity, that is,

$$\mathbb{E}_{\mathbf{g}}\left[\log\left(1 + \frac{g_k p_k}{\sigma^2 + \sum_{j=1, j\neq k}^{K} g_j\, p_j}\right)\right], \tag{3}$$

where $\mathbf{g} = \{g_1, \ldots, g_K\}$ is a vector of channel gain variables. Note that in (3) we assume that the receiver applies a single-user decoding and there is not sophisticated successive decoding to be used. An intuitive understanding of this result can be obtained by viewing capacities in terms of time averages of mutual information [16]. Although the study of multiuser decoding is important, which may involve Stackelberg games, fairness concepts, and generalized Nash games, it is not provided in this study. The interested readers are referred to [17] for this topic.

2.2. Assumption of Finite Channel States. Before introducing our game model, we need to clarify a prior assumption for this section.

Assumption 1. We assume that each user's channel gain g_k is i.i.d. from two discrete values: g_- and g_+ with probability ρ_- and ρ_+, respectively. Without loss of generality, we assume $g_- < g_+$.

On the one hand, our assumption is closely related to the way how feedback information is signalled to the transmitters. In order to get the channel information g_k at the transmitter side, the base station is required to feedback an estimate of g_k to user k *at a given precision*. Since in digital communications, any information is represented by a finite

number of bits (e.g., x bits), channels gains are mapped into a set that contains a finite number of states (2^x states).

On the other hand, this is a necessary assumption for analytical tractability, since in principle the functional strategic form of a player can be quite complex with both actions and states being continuous (or infinite). To avoid this problem, in [15] the authors successfully modelled a multicarrier Gaussian interference channel as a Bayesian game with discrete (or finite) actions and continuous states. Inspired from [15], we also model the fading MAC as a Bayesian game under the assumption of continuous actions and discrete states.

3. Game Formulation

We model the K-user fading MAC as a Bayesian game, in which users do not have complete information. In a K-user MAC, to have "complete information" means that, at each time t, the channel gain realizations $g_1(t),\ldots,g_K(t)$ are known at all the transmitters, denoted by $\mathrm{Tx}_1,\ldots,\mathrm{Tx}_K$. Any other condition corresponds to a situation of incomplete information. In this paper, the "incomplete information" particularly refers to a situation where each Tx_k only knows its own channel gain realization $g_k(t)$, but does not know the channel gains of other transmitters $\mathrm{g}_{-k}(t) = \{g_1(t),\ldots,g_{k-1}(t),g_{k+1}(t),\ldots,g_K(t)\}$. We will denote by g_k the channel gain variable of user k, whose distribution is assumed to be stationary and ergodic in this section.

In such a communication system, the natural object of each user is to maximize its ergodic capacity subject to an average power constraint, that is,

$$\begin{aligned} \max_{p_k} \quad & \mathbb{E}_{\mathbf{g}}\left[\log\left(1+\frac{g_k p_k(g_k)}{\sigma^2+\sum_{j\neq k} g_j p_j\left(g_j\right)}\right)\right] \\ \text{s.t.} \quad & \mathbb{E}_{g_k}\left[p_k(g_k)\right] \leq P_k^{\max} \\ & p_k(g_k) \geq 0, \end{aligned} \tag{4}$$

where $p_k(\cdot)$ and $P_k^{\max}$ are transmit power strategy and average power constraint of user k, respectively. Under the assumption that each user has incomplete information about the channel gains, user k's strategy $p_k(\cdot)$ is defined as a function of its own channel gain g_k, that is, $p_k(g_n)$. Note that (4) implies that user k should know at least the statistics of other users' channels.

For a given set of power strategies $\mathbf{p}_{-k} = \{p_1,\ldots, p_{k-1}, p_{k+1},\ldots, p_K\}$, the single-user maximization problem (4) is a convex optimization problem [18]. Via Lagrangian duality, the solution is given by the following equation:

$$\mathbb{E}_{\mathbf{g}_{-k}}\left[\frac{g_k}{\sigma^2+g_k p_k(g_k)+\sum_{j\neq k} g_j p_j\left(g_j\right)}\right] = \lambda_k, \tag{5}$$

where the dual variable λ_k is chosen such that the power constraint in (4) is satisfied with equality. However, the solution of (5) depends on $\mathbf{p}_{-k}(\cdot)$ which user k does not know, and the same holds for all other users. Thus, in order to obtain the optimal power allocation, each user must adjust its power level based on the guess of all other users' strategies. Now, given the following game model, each user is able to adjust its strategy according to the belief it has about the strategy of the other user.

The K-player MAC Bayesian game can be completely characterized as

$$\mathcal{G}_{\mathrm{MAC}} \triangleq \langle \mathcal{K}, \mathcal{T}, \mathcal{P}, \mathcal{Q}, \mathcal{U}\rangle. \tag{6}$$

(i) Player set: $\mathcal{K} = \{1,\ldots,K\}$.

(ii) Type set: $\mathcal{T} = \mathcal{T}_1 \times \cdots \times \mathcal{T}_K$ ("$\times$" stands for the Cartesian product) where $\mathcal{T}_k = \{g_-, g_+\}$. A player's type is defined as its channel gain, that is, $g_k \in \mathcal{T}_k$.

(iii) Action set: $\mathcal{P} = \mathcal{P}_1 \times \cdots \times \mathcal{P}_K$ where $\mathcal{P}_k = [0, P_k^{\max}]$. A player's action is defined as its transmit power, that is, $p_k \in \mathcal{P}_k$.

(iv) Probability set: $\mathcal{Q} = \mathcal{Q}_1 \times \cdots \times \mathcal{Q}_K$ where $\mathcal{Q}_k = \{\rho_-, \rho_+\}$, we have $\rho_+ = \Pr(g_k = g_+)$ and $\rho_- = \Pr(g_k = g_-)$.

(v) Payoff function set: $\mathcal{U} = \{u_1,\ldots,u_K\}$ where u_k is chosen as player k's achievable rate

$$u_k(p_1,\ldots,p_K) = \log\left(1+\frac{g_k p_k(g_k)}{\sigma^2+\sum_{j=1,j\neq k}^{K} g_j p_j\left(g_j\right)}\right). \tag{7}$$

In games of incomplete information, a player's type represents any kind of private information that is relevant to its decision making. In our context, the fading channel gain g_k is naturally considered as the type of user k, since its decision (in terms of power) can only rely on g_k. Note that this is a *continuous game* (a continuous game extends the notion of a discrete game (where players choose from a finite set of pure strategies), it allows players to choose a strategy from a continuous pure strategy set) with discrete states, since each player's action p_k can take any value satisfying the constraint $p_k \in [0, P_k^{\max}]$ and the channel state g_k is finite $g_k \in \{g_-, g_+\}$.

4. Bayesian Equilibrium

4.1. Definition of Bayesian Equilibrium. What we can expect from the outcome of a Bayesian game if every selfish and rational (rational player means a player chooses the best response given its information) participant starts to play the game? Generally speaking, the process of such players' behaviors usually results in a Bayesian equilibrium, which represents a common solution concept for Bayesian games. In many cases, it represents a "stable" result of learning and evolution of all participants. Therefore, it is important to characterize such an equilibrium point, since it concerns the performance prediction of a distributed system.

Now, let $\{\widehat{p}_k(\cdot), \mathbf{p}_{-k}(\cdot)\}$ denote the strategy profile where all players play $p(\cdot)$ except player k who plays $\widehat{p}_k(\cdot)$, we can then describe player k's payoff as

$$u_k(\widehat{p}_k, \mathbf{p}_{-k}) = u_k(p_1, \ldots, p_{k-1}, \widehat{p}_k, p_{k+1}, \ldots, p_K). \quad (8)$$

Definition 2 (Bayesian equilibrium). The strategy profile $p^\star(\cdot) = \{p_k^\star(\cdot)\}_{k\in\mathcal{K}}$ is a (pure strategy) Bayesian equilibrium, if for all $k \in \mathcal{K}$, and for all $p_k(\cdot) \in \mathcal{P}_k$ and $\mathbf{p}_{-k}(\cdot) \in \mathcal{P}_{-k}$

$$\overline{u}_k\left(p_k^\star, \mathbf{p}_{-k}^\star\right) \geq \overline{u}_k\left(p_k, \mathbf{p}_{-k}^\star\right), \quad (9)$$

where we define $\overline{u}_n \triangleq \mathbb{E}_{\mathbf{g}}[u_k]$.

From this definition, it is clear that at the Bayesian equilibrium no player can benefit from changing its strategy while the other players keep theirs unchanged. Note that in a strategic-form game with complete information each player chooses a concrete action, whereas in a Bayesian game each player k faces the problem of choosing a set or collection of actions (power strategy $p_k(\cdot)$), one for each type (channel gain g_k) it may encounter. It is also worth to mention that the action set of each player is independent of the type set, that is, the actions available to user k are the same for all types.

4.2. Characterization of the Bayesian Equilibrium Set. It is well known that, in general, an equilibrium point does not necessarily exist [6]. Therefore, our primary interest in this paper is to investigate the *existence* and *uniqueness* of a Bayesian equilibrium in $\mathcal{G}_{\text{MAC}}$. We now state our main result.

Theorem 3. *There exists a unique Bayesian equilibrium in the K-user* MAC *game $\mathcal{G}_{\text{MAC}}$.*

Proof. It is easy to prove the existence part, since the strategy space p_k is convex, compact, and nonempty for each k; the payoff function u_k is continuous in both p_k and $\mathbf{p}_{-k}$; u_k is concave in p_k for any $\mathbf{p}_{-k}$ [6].

In order to prove the uniqueness part, we should rely on a sufficient condition given in [19]: a non-cooperative game has a unique equilibrium, if the nonnegative weighted sum of the payoff functions is *diagonally strictly concave*. We firstly give the definition.

Definition 4 (diagonally strictly concave). A weighted nonnegative sum function $f(\mathbf{x}, \mathbf{r}) = \sum_{i=1}^{n} r_i \varphi_i(\mathbf{x})$ is called diagonally strictly concave for any vector $\mathbf{x} \in \mathbb{R}^{n\times 1}$ and fixed vector $\mathbf{r} \in \mathbb{R}_{++}^{n\times 1}$, if for any two different vectors $\mathbf{x}^0, \mathbf{x}^1$, we have

$$\Omega(\mathbf{x}^0, \mathbf{x}^1, \mathbf{r}) \triangleq (\mathbf{x}^1 - \mathbf{x}^0)^{\mathrm{T}} \delta(\mathbf{x}^0, \mathbf{r}) + (\mathbf{x}^0 - \mathbf{x}^1)^{\mathrm{T}} \delta(\mathbf{x}^1, \mathbf{r}) > 0, \quad (10)$$

where $\delta(\mathbf{x}, \mathbf{r})$ is called pseudogradient of $f(\mathbf{x}, \mathbf{r})$, defined as

$$\delta(\mathbf{x}, \mathbf{r}) \triangleq \begin{bmatrix} r_1 \dfrac{\partial \varphi_1}{\partial x_1} \\ \vdots \\ r_n \dfrac{\partial \varphi_n}{\partial x_n} \end{bmatrix}. \quad (11)$$

We start with the following lemma.

Lemma 5. *The weighted nonnegative sum of the average payoffs $\overline{u}_k$ in $\mathcal{G}_{\text{MAC}}$ is diagonally strictly concave for $\mathbf{r} = c^+\mathbf{1}$, where c^+ is a positive scalar, $\mathbf{1}$ is a vector whose every entry is* 1.

Proof. Write the weighted nonnegative sum of the average payoffs as

$$f^u(\mathbf{p}, \mathbf{r}) \triangleq \sum_{k=1}^{K} r_k \overline{u}_k(\mathbf{p}), \quad (12)$$

where $\mathbf{p} = [p_1 \cdots p_K]^{\mathrm{T}}$ is the transmit power vector and $\mathbf{r} = [r_1 \cdots r_K]^{\mathrm{T}}$ is a nonnegative vector assigning weights $r_1, \ldots, r_K$ to the average payoffs $\overline{u}_1, \ldots, \overline{u}_K$, respectively. Similar to (11), we let $\delta^u(\mathbf{p}, \mathbf{r}) \triangleq [r_1(\partial \overline{u}_1/\partial p_1) \ldots r_K(\partial \overline{u}_K/\partial p_K)]^{\mathrm{T}}$ be the pseudogradient of $f^u(\mathbf{p}, \mathbf{r})$. Now, we define

$$p_k \triangleq p_k(g_-) \quad \forall k, \quad (13)$$

the transmit power of player k when its channel gain is g_-. Since we have shown from the Lagrangian that, at the equilibrium, the power constraint is satisfied with equality, that is, $\mathbb{E}_{g_k}[p_k(g_k)] = P_k^{\max}$, we can write $P_k^{\max} - \rho_- p_k(g_-) = \rho_+ p_k(g_+)$ for all k, as the transmit power when its channel gain is g_+. Therefore, it is easy to find that the average payoff $\overline{u}_k$ can be actually transformed into a weighted sum-log function as follows:

$$\overline{u}_k(p_k) = \sum_i \omega_i \log\left[1 + \frac{\alpha_k^i + \beta_k^i p_k}{\sigma^2 + \sum_{j\neq k}\left(\alpha_j^i + \beta_j^i p_j\right)}\right], \quad (14)$$

where i represents the index for different jointly probability events, ω_i represents the corresponding probability for event i that are related to the probabilities $\{\rho_-, \rho_+\}$, and α_k^i and β_n^i represent some positive and nonzero real numbers that are related to the channel gains $\{g_-, g_+\}$. Note that the following conditions hold for all i, k:

$$\omega_i > 0, \quad \alpha_k^i + \beta_k^i p_k \geq 0, \quad \alpha_k^i > 0, \quad \beta_k^i \neq 0, \quad \sigma^2 > 0. \quad (15)$$

Now, we can write the pseudogradient δ^u as

$$\begin{aligned} \delta^u(\mathbf{p}, \mathbf{r}) &= \begin{bmatrix} c^+ \dfrac{\partial \overline{u}_1}{\partial p_1} \\ \vdots \\ c^+ \dfrac{\partial \overline{u}_K}{\partial p_K} \end{bmatrix} \\ &= \begin{bmatrix} c^+ \sum\limits_i \omega_i \beta_1^i \phi_i^{-1}(\mathbf{p}) \\ \vdots \\ c^+ \sum\limits_i \omega_i \beta_K^i \phi_i^{-1}(\mathbf{p}) \end{bmatrix} \\ &= c^+ \sum_i \begin{bmatrix} \omega_i \beta_1^i \phi_i^{-1}(\mathbf{p}) \\ \vdots \\ \omega_i \beta_K^i \phi_i^{-1}(\mathbf{p}) \end{bmatrix}, \end{aligned} \quad (16)$$

where the function $\phi_i(\mathbf{x})$ is defined as

$$\phi_i(\mathbf{x}) \triangleq \sigma^2 + \sum_{k=1}^{K} \left(\alpha_k^i + \beta_k^i x_k\right). \tag{17}$$

To check the diagonally strictly concave condition (10), we let $\mathbf{p}^0, \mathbf{p}^1$ be two different vectors satisfying the power constraint, and define

$$\begin{aligned}
\Omega^u(\mathbf{p}^0, \mathbf{p}^1, \mathbf{r}) &\triangleq (\mathbf{p}^1 - \mathbf{p}^0)^{\mathrm{T}} \delta^u(\mathbf{p}^0, \mathbf{r}) + (\mathbf{p}^0 - \mathbf{p}^1)^{\mathrm{T}} \delta^u(\mathbf{p}^1, \mathbf{r}) \\
&= (\mathbf{p}^1 - \mathbf{p}^0)^{\mathrm{T}} [\delta^u(\mathbf{p}^0, \mathbf{r}) - \delta^u(\mathbf{p}^1, \mathbf{r})] \\
&= [\Delta p_1 \ \cdots \ \Delta p_K] \\
&\quad \times \begin{bmatrix} c^+ \sum_i \omega_i \beta_1^i (\phi_i^{-1}(\mathbf{p}^0) - \phi_i^{-1}(\mathbf{p}^1)) \\ \vdots \\ c^+ \sum_i \omega_i \beta_K^i (\phi_i^{-1}(\mathbf{p}^0) - \phi_i^{-1}(\mathbf{p}^1)) \end{bmatrix} \\
&= c^+ \sum_i \omega_i [\phi_i^{-1}(\mathbf{p}^0) - \phi_i^{-1}(\mathbf{p}^1)] \zeta_i \\
&= c^+ \sum_i \omega_i \phi_i^{-1}(\mathbf{p}^0) \phi_i^{-1}(\mathbf{p}^1) \zeta_i^2,
\end{aligned} \tag{18}$$

where Δp_k and ζ_i are defined as

$$\begin{aligned}
\Delta p_k &\triangleq p_k^1 - p_k^0, \\
\zeta_i &\triangleq \sum_{k=1}^{K} \beta_k^i \Delta p_k,
\end{aligned} \tag{19}$$

Since $\mathbf{p}^0$, $\mathbf{p}^1$ are assumed to be two different vectors, we must have $\Delta\mathbf{p} = [\Delta p_1 \cdots \Delta p_K]^{\mathrm{T}} \neq \mathbf{0}$. Now, we can draw a conclusion from the equation above: $\Omega^u(\mathbf{p}^0, \mathbf{p}^1, \mathbf{r}) > 0$. This is because: (1) the first part $\omega_i \phi_i^{-1}(\mathbf{p}^0) \phi_i^{-1}(\mathbf{p}^1) > 0$ for all i, since $\omega_i > 0, \sigma^2 > 0$ and $\alpha_k^i + \beta_k^i p_k \geq 0$ for all i, k; (2) the second part $\zeta_i^2 \geq 0$ for all i, and there exists at least one nonzero term ζ_i^2, due to $\Delta\mathbf{p} \neq 0$ and $r_k \neq 0$, $\beta_k^i \neq 0$ for all i, k. Therefore, the summation of all the products of the first and the second terms must be positive. From Definition 4, the sum-payoff function $f^u(\mathbf{p}, \mathbf{r})$ satisfies the condition of diagonally strictly concave. This completes the proof of this lemma. □

Since our sum-payoff function $f^u(\mathbf{p}, \mathbf{r})$ given in (12) is diagonally strictly concave, the uniqueness of Bayesian equilibrium in our game $\mathcal{G}_{\mathrm{MAC}}$ follows directly from [19, Theorem 2]. □

5. Optimal Symmetric Strategies

The Bayesian game-theoretic approach provides us a better understanding of the wireless resource competition existing in the fading MAC when every mobile device acts as a selfish and rational decision maker (this means a device always chooses the best response given its information). The advantage of this model is that it mathematically captures the behavior of selfish wireless entities in strategic situations, which can automatically lead to the convergence of system performance. The introduced Bayesian game-theoretic framework fits very well the concept of self-organizing networks, where the intelligence and decision making is distributed. Such a scheme has apparent benefits in terms of operational complexity and feedback load.

However, from the global system performance perspective, it is usually inefficient to give complete "freedom" to mobile devices and let them take decisions without any policy control over the network. It is very interesting to note that a similar situation happens in the market economy, where consumers can be modeled as players to complete for the market resources. In the famous literature *The Wealth of Nations*, Adam Smith (a Scottish moral philosopher, pioneer of political economy, and father of modern economics) expounded how rational self-interest and competition can lead to economic prosperity and well-being through macroeconomic adjustments. For example, all states today have some form of macroeconomic control over the market that removes the free and unrestricted direction of resources from consumers and prices such as tariffs and corporate subsidies.

In particular, wireless service providers would like to design an appropriate policy to efficiently manage the system resource so that the global network performance can be optimized or enhanced to a certain theoretical limit, for example, Shannon capacity or capacity region [20]. Apparently, a centralized scheduler with comprehensive knowledge of the network status can globally optimize the resource utility. However, this approach usually involves sophisticated optimization techniques and a feedback load that grows with the number of wireless devices in the network. Thus, the optimization-based centralized decision has to be frequently updated as long as the wireless environment varies, or the system structure changes, for example, a user joins or exits the network.

In this section, we consider that the channel statistics (fading processes) for all wireless devices are jointly stationary for a relatively long period of signal transmission, and the global system structure remains unchanged. In addition, we neglect the problem of computational complexity at the scheduler and the impact of feedback load to the useful data transmission rate. In this case, the network service provider would strictly prefer to use a centralized approach, that is, a scheduler assigns some globally optimal strategies to the wireless devices, guiding them how to react under all kinds of different situations. Based on the Bayesian game settings, we provide a special discussion on the optimal symmetric strategy design. Note that this result can be treated as a theoretical upperbound for the performance measurement of Bayesian equilibrium.

We now introduce a necessary assumption.

Assumption 6. Mobile devices are designed to use the same power strategies, that is, they send the same power if their observations on the channel states are symmetric. In addition, we assume that the mobile devices have the same average power constraint, that is, $P_1^{\max} = \cdots = P_K^{\max} \triangleq P^{\max}$.

5.1. Two Channel States. For simplicity of our presentation, We first consider the scenario of two users with two channel states. In fact, the analysis of multiuser MAC can be extended in a similar way. According to Assumption 6, we define

$$\begin{aligned} p_- &\triangleq p_1(g_-) = p_2(g_-), \\ p_+ &\triangleq p_1(g_+) = p_2(g_+), \end{aligned} \tag{20}$$

and we have $\rho_- p_- + \rho_+ p_+ = P^{\max}$. Write user 1's average payoff as (Without loss of generality, we consider user 1 in the following context, since the problem is symmetric for user 2)

$$\begin{aligned} \overline{u}_1 &= \mathbb{E}_{g_1,g_2}\left[\log_2\left(1+\frac{g_1 p_1(g_1)}{\sigma^2+g_2 p_2(g_2)}\right)\right] \\ &= \rho_-^2 \log_2\left(1+\frac{g_- p_-}{\sigma^2+g_- p_-}\right) \\ &\quad + \rho_-\rho_+ \log_2\left(1+\frac{g_- p_-}{\sigma^2+g_+(P^{\max}-\rho_- p_-)/\rho_+}\right) \\ &\quad + \rho_-\rho_+ \log_2\left(1+\frac{g_+(P^{\max}-\rho_- p_-)/\rho_+}{\sigma^2+g_- p_-}\right) \\ &\quad + \rho_+^2 \log_2\left(1+\frac{g_+(P^{\max}-\rho_- p_-)/\rho_+}{\sigma^2+g_+(P^{\max}-\rho_- p_-)/\rho_+}\right). \end{aligned} \tag{21}$$

Now, $\overline{u}_1$ is transformed into a function of p_-, write it as $\overline{u}_1(p_-)$. To maximize the average achievable rate, user 1 needs to solve the following optimization problem, as mentioned in (4)

$$\begin{aligned} &\max_{p_-} \quad \overline{u}_1(p_-) \\ &\text{s.t.} \quad 0 \le p_- \le \frac{P^{\max}}{\rho_-}. \end{aligned} \tag{22}$$

Under Assumption 6, it can be shown that (due to the symmetric property) this single-user maximization problem is equivalent to the multiuser sum average rate maximization problem, that is, $\max(\overline{u}_1 + \overline{u}_2)$, which is our object in this section.

But unfortunately, $\overline{u}_1$ may not be a convex function [18], so the single-user problem may not be a convex optimization problem. It can be further verified that $\overline{u}_1$ is convex under some special conditions, depending on all the parameters $g_-, g_+, \rho_-, \rho_+, P^{\max}$, and σ^2. Here, we will not discuss all the convex cases, but only focus on the high SNR regime (meaning that the noise can be omitted compared to the signal strength). In this case, we have

$$\begin{aligned} \lim_{\sigma^2\to 0} u_1 = \rho_-\rho_+ \Bigg[&\log_2\left(1+\frac{g_- p_-}{g_+(P^{\max}-\rho_- p_-)/\rho_+}\right) \\ &+\log_2\left(1+\frac{g_+(P^{\max}-\rho_- p_-)/\rho_+}{g_- p_-}\right)\Bigg] \\ &+ \rho_-^2 + \rho_+^2. \end{aligned} \tag{23}$$

This function is strict convex. To be more precise, it is decreasing on $[0, g_+P^{\max}/(g_-\rho_+ + g_+\rho_-))$ and increasing on $(g_+P^{\max}/(g_-\rho_+ + g_+\rho_-), P^{\max}/\rho_-]$, and the solution is given by

$$\{p_-^\star, p_+^\star\} = \begin{cases} \left\{0, \dfrac{P^{\max}}{\rho_+}\right\}, & \dfrac{g_+}{\rho_+} \ge \dfrac{g_-}{\rho_-}, \\ \left\{\dfrac{P^{\max}}{\rho_-}, 0\right\}, & \dfrac{g_+}{\rho_+} < \dfrac{g_-}{\rho_-}. \end{cases} \tag{24}$$

Note that in this setting the choice of the optimal symmetric strategy is to concentrate the full available power on a single channel state. The selection of the channel state on which to transmit depends not only on the channel conditions but also on the probability of the channel states. This result implies that, in the high SNR regime, the optimal symmetric power strategy is to transmit information in an "opportunistic" way. For a better understanding of the "opportunistic" transmission, the interested reads are referred to [2].

5.2. Multiple Channel States. In this subsection, we discuss the extension to arbitrary L ($L \ge 2$) channel states. Note that the result of this subsection can also be applied to the case of two channel states.

Assumption 7. Each user's channel gain g_k has L positive states, which are $a_1, \ldots, a_L$ with probability $\rho_1, \ldots, \rho_L$, respectively (Without loss of generality, $a_1 < \cdots < a_L$), and we have $\sum_{\ell=1}^{L} \rho_\ell = 1$.

Based on Assumption 6, we define $p_\ell \triangleq p_1(a_\ell) = p_2(a_\ell), \ell = 1, \ldots, L$, as the transmit power when a user's channel gain is a_ℓ. As previously mentioned, our object in this part is to maximize the sum ergodic capacity of the system, that is, $\max \sum_k \overline{u}_k$. Under the symmetric assumption, this sum-ergodic-capacity maximization problem is equivalent to the following single-user maximization problem

$$\begin{aligned} &\max_{\mathbf{p}} \quad \sum_i \sum_j \rho_i \rho_j \log_2\left(1+\frac{g_i p_i}{\sigma^2+g_j p_j}\right) \\ &\text{s.t.} \quad \sum_i \rho_i p_i \le P^{\max} \\ &\qquad p_i \ge 0, \quad i = 1, \ldots, L, \end{aligned} \tag{25}$$

where $\mathbf{p}$ is now defined as $\mathbf{p} = \{p_1, \ldots, p_L\}$. This optimization problem is difficult, since the objective function is again nonconvex in $\mathbf{p}$. However, we can consider a relaxation of the optimization by introducing a lower bound [21]

$$\alpha \log z + \beta \le \log(1+z), \tag{26}$$

where α and β are chosen specified as

$$\begin{aligned} \alpha &= \frac{z_0}{1+z_0}, \\ \beta &= \log(1+z_0) - \frac{z_0}{1+z_0}\log z_0, \end{aligned} \tag{27}$$

we say that the lower bound (26) is tight with equality at a chosen value z_0.

Let us consider the lower bound (denoted as ξ) by using the relaxation (26) to the objective function in (25)

$$\xi(\mathbf{p}) \triangleq \sum_i \sum_j \rho_i \rho_j \left[\alpha_{i,j} \log_2 \left(\frac{g_i p_i}{\sigma^2 + g_j p_j} \right) + \beta_{i,j} \right] \tag{28}$$

which is still nonconvex, and so it is not concave in $\mathbf{p}$. However, with a logarithmic change of the following variables and constants: $\widetilde{p}_i = \log_2 p_i$, $\widetilde{\mathbf{p}}_i = \log_2 \mathbf{p}_i$ and $\widetilde{g}_i = \log_2 g_i$, we can turn the geometric programming [18] associated with the objective function (28) into the following problem:

$$\begin{aligned} \max_{\widetilde{\mathbf{p}}} \quad & \xi(\widetilde{\mathbf{p}}) \\ \text{s.t.} \quad & \sum_i \rho_i 2^{\widetilde{p}_i} \le P^{\max}, \end{aligned} \tag{29}$$

where $\xi(\widetilde{\mathbf{p}})$ is defined as

$$\begin{aligned} \xi(\widetilde{\mathbf{p}}) = & \sum_i \sum_j \rho_i \rho_j \alpha_{i,j} (\widetilde{g}_i + \widetilde{p}_i) \\ & - \sum_i \sum_j \rho_i \rho_j \alpha_{i,j} \log_2 \left(\sigma^2 + 2^{(\widetilde{g}_j + \widetilde{p}_j)} \right) \\ & + \sum_i \sum_j \rho_i \rho_j \beta_{i,j}. \end{aligned} \tag{30}$$

Now, it is easy to verify that the lower bound ξ is concave in the transformed set $\widetilde{\mathbf{p}}$, since the log-sum-exp function is convex. The constraints of the optimization problem are such that Slater's condition is satisfied [18]. So, the Karush-Kuhn-Tucker (KKT) condition of the optimization is sufficient and necessary for the optimality. Given the following Lagrangian dual function (denoted by $\mathcal{L}$):

$$\begin{aligned} \mathcal{L}(\widetilde{\mathbf{p}}, \nu) = & \sum_i \sum_j \rho_i \rho_j \alpha_{i,j} (\widetilde{a}_i + \widetilde{p}_i) \\ & - \sum_i \sum_j \rho_i \rho_j \alpha_{i,j} \log_2 \left(\sigma^2 + 2^{(\widetilde{a}_j + \widetilde{p}_j)} \right) \\ & + \sum_i \sum_j \rho_i \rho_j \beta_{i,j} - \nu \left(\sum_i 2^{(\widetilde{a}_i + \widetilde{p}_i)} - P^{\max} \right), \end{aligned} \tag{31}$$

the KKT conditions are

$$\begin{aligned} & \rho_\ell \sum_j \rho_j \alpha_{\ell,j} - \rho_\ell \left(\frac{2^{(\widetilde{a}_\ell + \widetilde{p}_\ell)}}{\sigma^2 + 2^{(\widetilde{a}_\ell + \widetilde{p}_\ell)}} \right) \\ & \quad \times \sum_i \rho_i \alpha_{i,\ell} - (\nu \ln 2) 2^{(\widetilde{a}_\ell + \widetilde{p}_\ell)} = 0, \quad \forall \ell, \end{aligned} \tag{32}$$

where $\widetilde{a}_\ell = \log_2 a_\ell$, and $\nu \ge 0$ is a dual variable associated with the power constraint in (29).

Define $x_\ell \triangleq 2^{(\widetilde{a}_\ell + \widetilde{p}_\ell)}, \ell = 1, \ldots, L$, the equivalent KKT conditions can be simply written as a quadratic equation

$$A_\ell x_\ell^2 + B_\ell x_\ell + C_\ell = 0, \quad \forall \ell, \tag{33}$$

where the parameters A_ℓ, B_ℓ, C_ℓ are expressed as

$$\begin{aligned} A_\ell &= \nu \ln 2, \quad \forall \ell \\ B_\ell &= \rho_\ell \sum_i \rho_i (\alpha_{i,\ell} - \alpha_{\ell,i}) + \sigma^2 \nu \ln 2, \quad \forall \ell \\ C_\ell &= -\rho_\ell \sigma^2 \sum_i \rho_i \alpha_{\ell,i}, \quad \forall \ell. \end{aligned} \tag{34}$$

Note that A_ℓ and B_ℓ are functions of ν, we can write them as $A_\ell(\nu)$ and $B_\ell(\nu)$. Since $x_\ell \ge 0$, the solution to the KKT conditions can only be one of the roots to the quadratic equation, that is,

$$p_\ell^\star = \frac{-B_\ell(\nu) + \sqrt{B_\ell^2(\nu) - 4A_\ell(\nu) C_\ell}}{2 a_\ell A_\ell(\nu)}, \quad \forall \ell, \tag{35}$$

where ν is chosen such that $\sum_\ell \rho_\ell p_\ell^\star = P^{\max}$. Thus, for some fixed value of α, β, we can directly apply (35) to maximize the lower bound ξ (28). Then, it is natural to improve the bound periodically. Based on the discussion above, we propose the following algorithm, namely Lower Bound Tightening (LBT) algorithm

The algorithm convergence can be easily proved, since the objective is monotonically increasing at each iteration. However, the global optimum is not always guaranteed, due to the nonconvex property.

6. Numerical Results

In this section, numerical results are presented to validate our theoretical claims. For Figures 1 and 2, the network parameters are chosen as $\rho_- = \rho_+ = 0.5$, $P^{\max} = 1$ and $\sigma^2 = 0.1$.

First, we show the existence and uniqueness of Bayesian equilibrium in the scenario of two-user fading MAC. In Figure 1(a), we assume the channel gains are $g_- = 1$, $g_+ = 3$; in Figure 1(b), we assume $g_- = 1, g_+ = 10$. On both X and Y axis, p_1 and p_2 represent the power allocated by user 1 and user 2 when the channel gain is g_-. The curves $r_1(p_2)$ and $r_2(p_1)$ represent the best-response functions of user 1 and user 2, respectively. As expected, the Bayesian equilibrium is unique in both cases, that is, (0.6,0.6) and (0.5,0.5).

Second, we investigate the efficiency of Bayesian equilibrium from the viewpoint of global average network performance. The X axis, SNR is defined as the ratio between the power constraint $P^{\max}$ and the noise variance σ^2. In Figure 2(a), again, we assume $g_- = 1$, $g_+ = 3$; in Figure 2(b), we assume $g_- = 1$, $g_+ = 10$. The curve "Pareto" represents the Nash equilibrium in the waterfilling game, in which users have complete information. This gives the upper bound for our Bayesian equilibrium, since it is also the Pareto optimal solution [7]. The curve "Uniform"

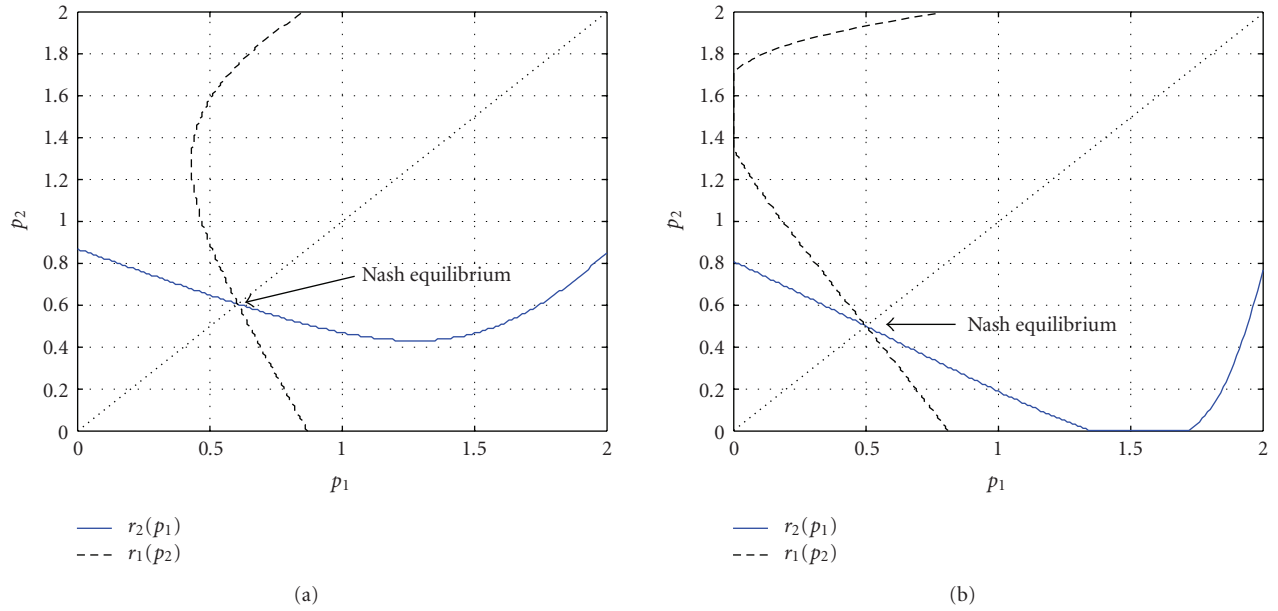

FIGURE 1: The uniqueness of Bayesian equilibrium. (a) $g_- = 1,\ g_+ = 3$, (b) $g_- = 1,\ g_+ = 10$.

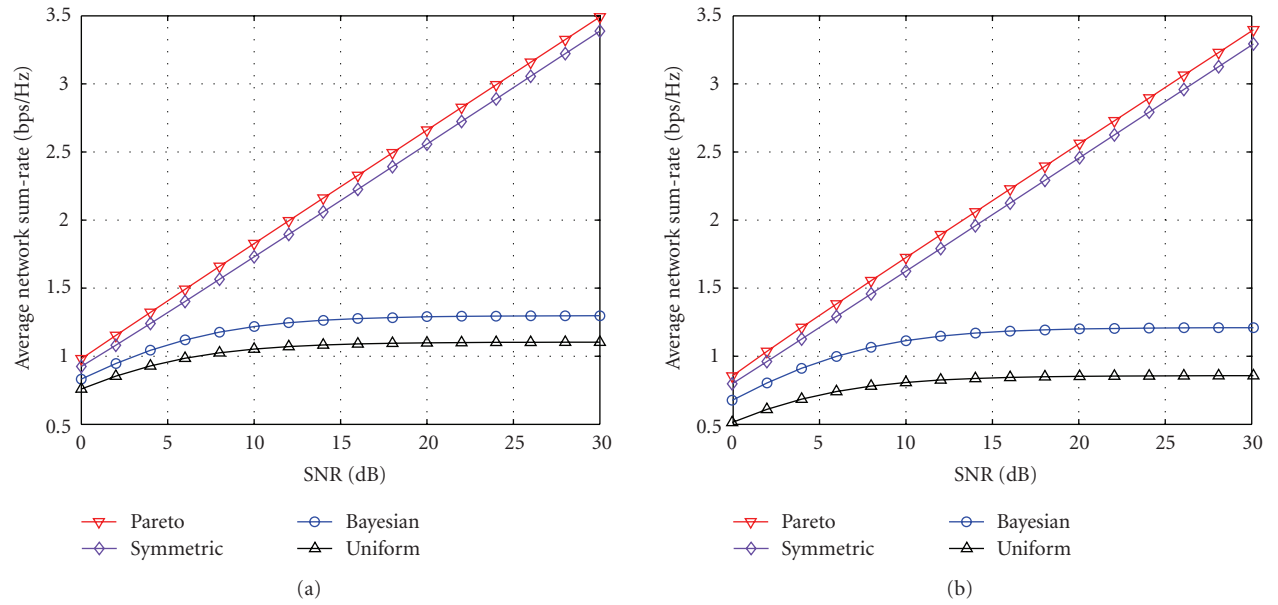

FIGURE 2: Average network sum-rate. (a) $g_- = 1,\ g_+ = 3$, (b) $g_- = 1,\ g_+ = 10$.

represents the time-domain uniform power allocation. Since this is the strategy when users have no information about the channel gains, it corresponds obviously to a lower bound. The curve "Symmetric" represents the optimal symmetric strategy presented in Section 5. This can be treated as a weaker upper bound (inferior to the Pareto optimality) for the Bayesian equilibrium. From the slopes of these curves, we can clearly observe the inefficiency of the Bayesian equilibrium, especially in the high SNR regime. This can be explained as follows: in our game $\mathcal{G}_{\text{MAC}}$, users with incomplete information improve the global network performance (comparing to the scenario in which the users have no information), however, it does not improve the performance slope.

Finally, we show the convergence behavior of the lower bound tightening (LBT) algorithm. In Figure 3, we choose the parameters as $L = 3,\ g_1 = 1,\ g_2 = 2,\ g_3 = 3$, and $\rho_1 = \rho_2 = \rho_3 = 1/3$. The sum capacity versus the SNR are plotted for five iterations. The upper bound is achieved by exhaustive search. As expected, one can easily observe the convergence behavior. In the low SNR regime, we can find that the algorithm converges to the local instead of the global maximum. However, we also find that the performance of the local optimum is improved while the SNR is increasing.

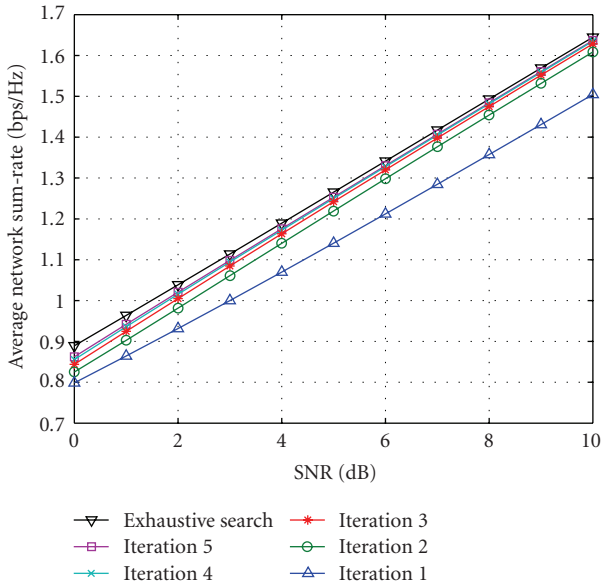

Figure 3: The convergence of the lower bound tightening (LBT) algorithm.

Initialize $t = 0$; $\nu = 0$; $\alpha_{i,j}^{(t)} = 1$, for $i = 1, \ldots, L$, $j = 1, \ldots, L$.
repeat
  repeat
    $\nu = \nu + \Delta\nu$
    for $i = 1$ to L **do**
      update A_i, B_i, C_i using (34)
      $p_i^{\star} = (-B_i + \sqrt{B_i^2 - 4A_iC_i})/2a_iA_i$
    end for
  until $\sum_i \rho_i p_i^{\star} = P^{\max}$
  for $i = 1$ to L and $j = 1$ to L **do**
    $z_{i,j}^{(t)} = a_i p_i^{\star}/(\sigma^2 + a_j p_j^{\star})$; $\alpha_{i,j}^{(t+1)} = z_{i,j}^{(t)}/(1 + z_{i,j}^{(t)})$
  end for
  $t = t + 1$
until converge

Algorithm 1: Lower Bound Tightening (LBT).

7. Conclusion

We presented a Bayesian game-theoretic framework for distributed resource allocation in fading MAC, where users are assumed to have only information about their own channel gains. By introducing the assumption of finite channel states, we successfully found a analytical way to characterize the Bayesian equilibrium set. First, we proved the existence and uniqueness. Second, the inefficiency was shown from numerical results. Furthermore, we analyzed the optimal symmetric power strategy based on the practical concerns of resource allocation design. Future extension is considered to improve the efficiency of Bayesian equilibrium through pricing or cooperative game-theoretic approaches.

References

[1] R. S. Cheng and S. Verdú, "Gaussian multiaccess channels with ISI. Capacity region and multiuser water-filling," *IEEE Transactions on Information Theory*, vol. 39, no. 3, pp. 773–785, 1993.

[2] R. Knopp and P. A. Humblet, "Information capacity and power control in single-cell multiuser communications," in *Proceedings of IEEE International Conference on Communications (ICC '95)*, vol. 1, pp. 331–335, Seattle, Wash, USA, June 1995.

[3] A. J. Goldsmith and P. P. Varaiya, "Capacity of fading channels with channel side information," *IEEE Transactions on Information Theory*, vol. 43, no. 6, pp. 1986–1992, 1997.

[4] D. N. C. Tse and S. V. Hanly, "Multiaccess fading channels—part I: polymatroid structure, optimal resource allocation and throughput capacities," *IEEE Transactions on Information Theory*, vol. 44, no. 7, pp. 2796–2815, 1998.

[5] M. Debbah, "Mobile flexible networks: the challenges ahead," in *Proceedings of the International Conference on Advanced Technologies for Communications (ATC '08)*, pp. 3–7, Hanoi, Vietnam, October 2008.

[6] D. Fudenberg and J. Tirole, *Game Theory*, MIT Press, Cambridge, Mass, USA, 1991.

[7] L. Lai and H. El Gamal, "The water-filling game in fading multiple-access channels," *IEEE Transactions on Information Theory*, vol. 54, no. 5, pp. 2110–2122, 2008.

[8] G. He, S. Beta, and M. Debbah, "Game-theoretic deployment design of small-cell OFDM networks," in *Proceedings of the 3rd ICST/ACM International Workshop on Game Theory in Communication Networks*, October 2009.

[9] S. Lasaulce, M. Debbah, and E. Altman, "Methodologies for analyzing equilibria in wireless games: a look at pure, mixed, and correlated equilibria," *IEEE Signal Processing Magazine*, vol. 26, no. 5, pp. 41–52, 2009.

[10] E.-V. Belmega, S. Lasaulce, and M. Debbah, "Power allocation games for mimo multiple access channels with coordination," *IEEE Transactions on Wireless Communications*, vol. 8, no. 6, pp. 3182–3192, 2009.

[11] E. Altman, M. Debbah, and A. Silva, "Game theoretic approach for routing in Dense ad-hoc networks," in *Proceedings of the Stochastic Networks Workshop*, Edinburg, UK, July 2007.

[12] J. F. Nash, "Equilibrium points in N-person games," *Proceedings of the National Academy of Sciences of the United States Of America*, vol. 36, no. 1, pp. 48–49, 1950.

[13] T. Heikkinen, "A minmax game of power control in a wireless network under incomplete information," Tech. Rep. 99-43, DIMACS, August 1999.

[14] C. A. St. Jean and B. Jabbari, "Bayesian game-theoretic modeling of transmit power determination in a self-organizing CDMA wireless network," in *Proceedings of the 60th IEEE Vehicular Technology Conference (VTC '04)*, vol. 5, pp. 3496–3500, 2004.

[15] S. Adlakha, R. Johari, and A. Goldsmith, "Competition in wireless systems via Bayesian interference games," http://arxiv.org/abs/0709.0516.

[16] R. Gallager, "An inequality on the capacity region of multiaccess fading channels," in *Communications and Cryptography: Two Sides of One Tapestry*, pp. 129–139, Kluwer Academic Publishers, Boston, Mass, USA, 1994.

[17] E. Altman, K. Avrachenkov, L. Cottatellucci, M. Debbah, G. He, and A. Suarez, "Operating point selection in multiple access rate regions," in *Proceedings of the 21st International Teletraffic Congress (ITC '09)*, Paris, France, June 2009.
[18] S. Boyd and L. Vandenberghe, *Convex Optimization*, Cambridge University Press, Cambridge, UK, 2004.
[19] J. B. Rosen, "Existence and uniqueness of equilibrium points for concave N-person games," *Econometrica*, vol. 33, pp. 520–534, 1965.
[20] T. M. Cover and J. A. Thomas, *Elements of Information Theory*, Wiley, New York, NY, USA, 1991.
[21] J. Papandriopoulos and J. S. Evans, "Low-complexity distributed algorithms for spectrum balancing in multi-user DSL networks," in *Proceedings of IEEE International Conference on Communications (ICC '06)*, vol. 7, pp. 3270–3275, June 2006.

Hindawi Publishing Corporation
EURASIP Journal on Wireless Communications and Networking
Volume 2010, Article ID 143413, 12 pages
doi:10.1155/2010/143413

Research Article

Dynamic Resource Partitioning for Downlink Femto-to-Macro-Cell Interference Avoidance

Zubin Bharucha,[1] Andreas Saul,[1] Gunther Auer,[1] and Harald Haas[2]

[1] *DOCOMO Communications Laboratories Europe GmbH, Landsberger Straße 312, 80687 Munich, Germany*
[2] *School of Engineering and Electronics, Institute for Digital Communications, Joint Research Institute for Signal and Image Processing, The University of Edinburgh, Edinburgh EH9 3JL, UK*

Correspondence should be addressed to Zubin Bharucha, bharucha@docomolab-euro.com

Received 31 December 2009; Accepted 26 April 2010

Academic Editor: Holger Claussen

Femto-cells consist of user-deployed Home Evolved NodeBs (HeNBs) that promise substantial gains in system spectral efficiency, coverage, and data rates due to an enhanced reuse of radio resources. However, reusing radio resources in an uncoordinated, random fashion introduces potentially destructive interference to the system, both, in the femto and macro layers. An especially critical scenario is a closed-access femto-cell, cochannel deployed with a macro-cell, which imposes strong downlink interference to nearby macro user equipments (UEs) that are not permitted to hand over to the femto-cell. In order to maintain reliable service of macro-cells, it is imperative to mitigate the destructive femto-cell to macro-cell interference. The contribution in this paper focuses on mitigating downlink femto-cell to macro-cell interference through dynamic resource partitioning, in the way that HeNBs are denied access to downlink resources that are assigned to macro UEs in their vicinity. By doing so, interference to the most vulnerable macro UEs is effectively controlled at the expense of a modest degradation in femto-cell capacity. The necessary signaling is conveyed through downlink high interference indicator (DL-HII) messages over the wired backbone. Extensive system level simulations demonstrate that by using resource partitioning, for a sacrifice of 4% of overall femto downlink capacity, macro UEs exposed to high HeNB interference experience a tenfold boost in capacity.

1. Introduction

There is a growing demand for increased user and system throughput in wireless networks. Naturally, such rapidly increasing demand is served by higher bandwidth allocation, but because bandwidth is scarce and expensive, a key to substantial throughput enhancement is to increase the spatial reuse of radio frequency resources. One powerful method of boosting wireless capacity is by shrinking the cell size. The reason for this is that smaller cell sizes enable a more efficient spatial reuse of spectrum [1]. Furthermore, the shorter transmission distances enhance link capacity due to higher channel gains [2].

Studies indicate that a significant proportion of data traffic originates indoors [3]. Poor signal reception caused by penetration losses through walls severely hampers the operation of indoor data services in state-of-the-art systems. Recently, the concept of 3rd generation (3G) and beyond 3G (B3G) femto-cells, in which HeNBs are placed indoors, has therefore attracted considerable interest. HeNBs are low-cost, low-power, short-range, plug-and-play base stations that are directly connected to the backbone network. HeNBs aim at extending broadband coverage to authorized UEs located indoors where it is most needed [3]. HeNBs therefore offload indoor users from the macro-cell, thus potentially enhancing the capacity both indoors by bypassing wall penetration losses, as well as outdoors by freeing up resources [4, 5]. Moreover, femto-cell deployment could potentially lead to an overall reduced energy consumption as penetration losses due to walls are circumvented [6].

In [7–9], the authors propose the *TDD underlay* concept. Owing to the asymmetric nature of traffic [10], one of the frequency division duplex (FDD) bands (the underloaded one) can be split in time such that the HeNB transmits and

receives information from its associated UE in a time division duplex (TDD) fashion. This proposal, while making efficient utilization of unused resources, still encounters a bottleneck, because typically, the link between the HeNB and its femto UEs is much stronger than that between the evolved NodeB (eNB) and the macro UE.

In this paper, both macro and femto-cells are assumed to operate in the same radio frequency spectrum in FDD mode, compliant with the specifications for B3G mobile communication systems [11]. Like in the original TDD underlay concept [7], the HeNB backhauls data through a dedicated broadband gateway (DSL/Ethernet/etc.) to the cellular operator network.

However, HeNBs are deployed without network planning, such that their deployment introduces additional interference [12]. Regarding hand-over between macro and femto-cells, two access control mechanisms, *open-access* and *closed-access*, are identified. In open-access femto-cells, macro UEs get *assimilated* into the femto-cell, which means that UEs that lie within the coverage area of a femto-cell are handed over to the corresponding HeNB. In closed-access systems the HeNB only grants access to a particular set of authorized UEs. It is these closed-access systems that cause (and receive) the most detrimental interference. This is because a "foreign" macro UE lying in the coverage area of a femto-cell is not allowed to communicate with the HeNB, but must communicate with the eNB that lies outdoors. Due to wall penetration losses, such macro UEs receive a highly attenuated signal from the eNB and, in addition, receive excessive interference originating from the HeNBs in whose coverage areas the macro UE lies. No matter the access control, it is crucial that the provision of base-coverage by the macro-cell network is not compromised by femto-cell deployment.

In [13], the feasibility of the coexistence of cochannel macro and femto-cells has been investigated. A power control method is defined in the downlink such that a constant femto-cell radius is maintained. In [14], the authors analyze the impact of femto-cell deployment on the macro-cell performance. In all of these papers, no active interference avoidance technique is discussed. In [15], the authors analyze the uplink capacity and interference avoidance for networks consisting of macro and femto-cells existing together in a code division multiple access (CDMA) network. In particular, the authors evaluate a network-wide area spectral efficiency metric, that is defined as the feasible combinations of the average number of macro-cell UEs and HeNBs per eNB that satisfy a target outage constraint. Interference avoidance in this case is done via a time-hopped CDMA physical layer and sectorization of antennas. In contrast to the above, the contribution in this paper comes in the form of a novel dynamic downlink interference avoidance technique that prioritizes macro UEs for a spectrum sharing orthogonal frequency division multiple access (OFDMA) system. The reason for this is twofold. First, the downlink is more critical in terms of femto-to-macro interference, because it is more likely that a macro UE suffers from downlink interference from a nearby HeNB than an eNB suffers from uplink interference from a femto UE, due to the asymmetry in cell-size, and the corresponding asymmetry in transmit powers, between macro and femto-cells. Second, priority should generally be given to the macro layer rather than the femto layer. To this end, if an HeNB is perceived to interfere severely with a macro UE, it must act so as to nullify this interference by smartly scheduling (partitioning) its resources. If no macro UE is affected, the femto-cell may use all resources (full frequency reuse).

For the B3G mobile communication system 3rd generation partnership project (3GPP) Long-Term Evolution (LTE) [11], high interference indicator (HII) messages are specified to deal with macro-to-macro interference in the uplink [16, 17], that are conveyed through the X2 interface via the wired backbone. In this work, it is demonstrated that the same framework can be applied for downlink interference coordination between macro and femto-cells, by signaling downlink high interference indicator (DL-HII) messages via an X2 connection to femto-cells.

In order to assess the impact of resource partitioning on macro and femto-cell performance, system level simulations are carried out. The performance of a closed-access system is compared against the performance of the same distribution of users using the aforementioned resource partitioning scheme. For comparison purposes, a benchmark system is simulated that closely reflects state-of-the-art cellular networks in which there are no HeNBs, and all femto UEs are served by eNBs.

2. System and Channel Model

The downlink of an OFDMA system is considered, where the system bandwidth B is divided into N resource blocks (RBs), $B = NB_{\mathrm{RB}}$. An RB represents one basic time-frequency unit with bandwidth B_{RB}. All eNBs transmit with a fixed power per RB, P_{m}, and all HeNBs transmit with a fixed power, P_{f}, per RB. Perfect synchronization in time and frequency is assumed.

Universal frequency reuse is considered, so that both macro and femto-cells utilize the entire system bandwidth B. Multiple receive antennas are assumed, and the M received signal streams are combined with maximum ratio combining (MRC). The gain from MRC is approximated by simulating M individual, uncorrelated receive streams and adding the achieved signal-to-interference-plus-noise ratio (SINR) [18]. The set of available RBs $\mathcal{N}$, with cardinality $|\mathcal{N}| = N$, is distributed by eNBs and HeNBs among their associated macro and femto UEs, respectively. Throughout this paper, u is used to identify any macro or femto UE, and v_u denotes the H/eNB that serves UE u. The received signal power observed by UE u at RB n is given by

$$Y_n^u = P_u \sum_m^M G_{m,n}^{u,v_u} + I_n^u + \eta, \tag{1}$$

where $G_{m,n}^{u,v_u}$ is the channel gain between UE u and its serving HeNB or eNB v_u, observed at receive antenna m and at RB n. Furthermore, η accounts for thermal noise per RB, which is constant across all RBs. The transmit power is set to $P_u = P_{\mathrm{m}}$, and $P_u = P_{\mathrm{f}}$ if UE u is served by an eNB or HeNB,

Table 1: Link to system mapping parameters.

Parameter	Value	Notes
α	0.6	Implementation losses
$\gamma_{\min}$ [dB]	−10	QPSK
$\gamma_{\max}$ [dB]	19.5	64QAM
$\overline{C}_{\max}$ [bps/Hz]	4.4	64QAM

respectively. The aggregate interference I_n^u is composed of macro and femto-cell interference

$$I_n^u = \sum_m^M \left\{ \sum_{i \in \mathcal{M}_{\text{int}}} G_{m,n}^{u,i} P_{\text{m}} + \sum_{i \in \mathcal{F}_{\text{int}}} G_{m,n}^{u,i} P_{\text{f}} \right\}, \tag{2}$$

where the first and second addends represent the macro and femto-cell interference, respectively. The set of interfering eNBs and HeNBs are denoted by $\mathcal{M}_{\text{int}}$ and $\mathcal{F}_{\text{int}}$. In case UE u is served by an eNB v_u, $\mathcal{M}_{\text{int}}$ comprises all eNBs except for v_u, that is, $v_u \notin \mathcal{M}_{\text{int}}$. In this case, $\mathcal{F}_{\text{int}}$ is the set of all HeNBs in the system. Likewise, if UE_u is served by an HeNB v_u, then $v_u \notin \mathcal{F}_{\text{int}}$. The SINR observed by UE u at RB n amounts to

$$\gamma_n^u = \frac{P_u \sum_m^M G_{m,n}^{u,v_u}}{I_n^u + \eta}. \tag{3}$$

Due to MRC at the receiver, the channel gains $G_{m,n}^{u,v_u}$ add constructively, so that the average SINR is increased by a factor of M, together with an M-fold diversity gain.

Link adaptation is implemented where the modulation and coding scheme used are selected based on the achieved SINR. In order to model link adaptation, the SINR is mapped to the capacity using the *attenuated and truncated Shannon bound* method [19]. Given a particular SINR γ_n^u, the spectral efficiency on RB n for UE u, $\overline{C}_n^u$, is determined by

$$\overline{C}_n^u = \begin{cases} 0 & \text{for } \gamma_n^u < \gamma_{\min}, \\ \alpha S(\gamma_n^u) & \text{for } \gamma_{\min} < \gamma_n^u < \gamma_{\max}, \\ \overline{C}_{\max} & \text{for } \gamma_n^u > \gamma_{\max}, \end{cases} \tag{4}$$

where $S(x) = \log_2(1+x)$ in [bit/s/Hz] is the Shannon bound, α is the attenuation factor representing implementation losses, and $\gamma_{\min}$ and $\gamma_{\max}$ are the minimum and maximum SINRs supported by the available modulation and coding schemes. These parameters are summarized in Table 1. The capacity C_u of UE_u is then calculated as the aggregate capacity on all the RBs allocated to it as

$$C_u = B_{\text{RB}} \sum_{i \in \mathcal{N}_u} \overline{C}_i^u, \tag{5}$$

where $\mathcal{N}_u$ is the set of RBs allocated to user u. The value for $\gamma_{\max}$ is taken from [20] based on a maximum modulation scheme of 64-QAM in the downlink.

2.1. Channel Model. The channel gain, $G_{m,n}^{u,v}$, between a transmitter v and a receiver u, observed at receive antenna m on RB n as defined in (1) is composed of distance-dependent path loss, log-normal shadowing, and channel variations due to frequency-selective fading:

$$G_{m,n}^{u,v} = \left| H_{m,n}^{u,v} \right|^2 10^{(-L(d)+X_\sigma)/10}, \tag{6}$$

where $H_{m,n}^{u,v}$ accounts for the channel transfer factor between transmitter v and receiver u observed at receive antenna m at RB n, $L(d)$ is the distance-dependent path loss (in dB), and X_σ is the log-normal shadowing value (in dB) with standard deviation σ [21]. Channel variations of $H_{m,n}^{u,v}$ on different receive antennas are mutually independent, while the path loss $L(d)$ is identical for all receive antennas m and RBs n. While the channel response generally exhibits time and frequency dispersions, channel fluctuations within an RB are neglected because the RB dimensions are significantly smaller than the coherence time and coherence frequency of the channel [22]. The delay profiles associated with applicable propagation scenarios of [21, 23] are used to generate the frequency-selective fading channel transfer factor $H_{m,n}^{u,v}$.

Table 2: Shadowing parameters.

	Macro-cell	Femto-cell
Standard Deviation, σ	8 dB	10 dB
Auto-correlation distance	50 m	3 m

2.2. Path Loss Models. Three path loss models are used depending on the type of link, as prescribed in [24]. For a purely outdoor link, that is, the link (useful or interfering) between an eNB and an outdoor macro UE, the path loss is calculated as

$$L\,[\text{dB}] = 15.3 + 37.6 \log_{10}(R), \tag{7}$$

where R (in m) is the distance between the transmitter and the receiver.

When considering the useful/interfering link between an eNB and a macro UE situated indoors or the interfering link between a femto UE (which is always situated indoors) and an eNB, the path loss includes the wall penetration loss and is calculated as

$$L\,[\text{dB}] = 15.3 + 37.6 \log_{10}(R) + L_{\text{W}}, \tag{8}$$

where L_{W} is the wall penetration loss (in dB).

Finally, when considering the useful/interfering link between an HeNB and a femto UE or the interfering link between a macro UE and an HeNB, the path loss is calculated as

$$L\,[\text{dB}] = 127 + 30 \log_{10}\left(\frac{R}{1000}\right). \tag{9}$$

This is a simplified model based on LTE-A evaluation methodology that avoids modelling any walls.

Log-normal shadowing is added to all links. Correlated shadowing maps are applied such that the correlation in

the shadowing values of two points is dependent on the distance between them. Table 2 shows the shadowing standard deviation σ and auto-correlation shadowing distances for the macro and femto-cells [24].

3. Femto-Cell Resource Partitioning

3.1. Downlink Interference Scenario for Closed-Access. As the eNB transmit power typically exceeds the HeNB transmit power by several orders of magnitude, $P_{\mathrm{f}} \ll P_{\mathrm{m}}$, in most cases, the interference seen by macro UE u will be dominated by eNB interference. Only if a macro-cell receiver, UE u, is located in close proximity to an HeNB i, UE u is exposed to high HeNB interference $G_n^{u,i}P_{\mathrm{f}}$, $i \in \mathcal{F}_{\mathrm{int}}$. In case UE u is located indoors, the situation is exacerbated by the poor channel gains, G_n^{u,v_u}, to the serving eNB v_u, caused by high wall penetration losses. This UE u is likely to experience poor SINR, (3). With full frequency reuse, femto-cells utilize all N RBs. Therefore, the received SINR is likely to be unacceptable over the entire set of RB allocated to UE u, that is, $\mathcal{N}_u$.

3.2. Avoiding Femto-to-Macro Interference. Suppose that macro UE u is located indoors within coverage of HeNB i, but served by an outdoor eNB v_u. An effective means of mitigating the destructive HeNB interference observed by UE u is to introduce the concept of resource partitioning, such that HeNB i is denied access to RBs, $\mathcal{N}_u$, that are assigned to UE u. In other words, the set of RBs allocated to UE u must be left idle by HeNB i. Doing so completely eliminates the interference originating from the interfering HeNB i, which, in this case, is the most dominant source of interference. This increases the SINR (3) achieved at the macro UE.

In order to implement femto-cell resource partitioning, a predefined interference threshold, I_{th}, is introduced. Each macro UE measures the average channel gains $\overline{G}^{u,v} = \mathrm{E}\{G_{m,n}^{u,v}\}$ of nearby HeNBs and performs the following threshold test:

$$10\log \mathrm{E}\left\{G_{m,n}^{u,v}\right\} = -L^{u,v}(d) + X_\sigma \geq I_{\mathrm{th}} - P_{\mathrm{f}} = G_{\mathrm{th}}. \quad (10)$$

In case the average channel gain between an HeNB and the vulnerable macro UEs exceeds G_{th}, the HeNB is instructed to perform resource partitioning by suppressing transmission on RBs that are reserved by the vulnerable macro UEs. Clearly, decreasing the value of I_{th} while keeping P_{f} fixed increases the size of the "exclusion region" and protects a larger number of macro UEs, as seen in Figure 2. Therefore, the lower the threshold I_{th}, the more resources are partitioned by HeNBs, so that the impact of resource partitioning on femto-cell performance increases as I_{th} decreases. The simulation results presented in Section 5 make use of two different values of I_{th} such that one translates to a large exclusion region and the other to a small one.

It is possible that more than one macro UE experiences heavy interference from more than one HeNB. Suppose that HeNB i causes strong interference to several UEs, as determined by the threshold test (10). Let the set of macro UEs exposed to strong interference from HeNB i be denoted by $\mathcal{U}_{\mathrm{aff}}^i$. The associated measurement and signaling procedures on how each UE in $\mathcal{U}_{\mathrm{aff}}^i$ identifies the interfering HeNB i are detailed in Section 3.3. As per the resource partitioning concept, HeNB i must partition resources such that it does not cause interference to the set of macro UEs $\mathcal{U}_{\mathrm{aff}}^i$. In other words, the resources that are prohibited for HeNB i are in the form

$$\overline{\mathcal{N}}_i = \bigcup_{u \in \mathcal{U}_{\mathrm{aff}}^i} \mathcal{N}_u \,. \quad (11)$$

We note that the affected macro UEs within $\mathcal{U}_{\mathrm{aff}}^i$ may be connected to different macro eNBs, as HeNB i may be within the coverage area of several macro-cells.

In general, every HeNB that causes high interference to nearby macro UEs must partition resources as explained by (11). However, due to the low HeNB transmit power, P_{f}, it is unlikely that *all* femto-cells cause high interference to many macro UEs. Hence, in most cases, only a small subset of the users served by an eNB are interfered by the same set of HeNBs, as illustrated in Figure 1. This implies that, in general, the number of RBs $|\overline{\mathcal{N}}_i| = \overline{N}_i$ that must not be used by an interfering HeNB is much smaller than the total number of RBs, $\overline{N}_i \ll N$, so that the overall degradation of femto-cell capacity is expected to be modest.

3.3. Practical Implementation in LTE Systems. In order to implement the resource partitioning concept, the interfering femto-cell needs to be identified and then be informed of the restricted resources $\overline{\mathcal{N}_i}$ it must not use according to (11). This involves integrating the proposed resource partitioning concept within the LTE network architecture. In abstract, femto-cell resource partitioning is integrated to the LTE network architecture by the following procedure.

(1) Macro UE u determines the cell-ID of surrounding HeNBs, by reading the corresponding broadcast channel (BCH), and stores them in a list containing neighboring cell-IDs.

(2) UE u identifies the heavily interfering HeNBs in its proximity using reference signal received power (RSRP) measurements.

(3) The cell-IDs of the corresponding HeNBs are reported to the serving eNB.

(4) The eNB prepares a DL-HII bitmap containing information about which RBs are transmitted with high power.

(5) The DL-HII bitmap is disseminated to neighboring H/eNBs over the X2 or S1 interfaces.

(6) If the receiving eNB is an HeNB, it will refrain from using the particular RBs marked in the DL-HII bitmap. In this way, detrimental downlink femto-cell interference at the vulnerable macro UEs is avoided.

The necessary UE measurements that identify which femto-cells are in close vicinity of a macro UE are similar to a handover procedure. In LTE, macro UEs read the broadcast channel (BCH) not only from their primary eNB, but also from one or several secondary eNBs. As the BCH

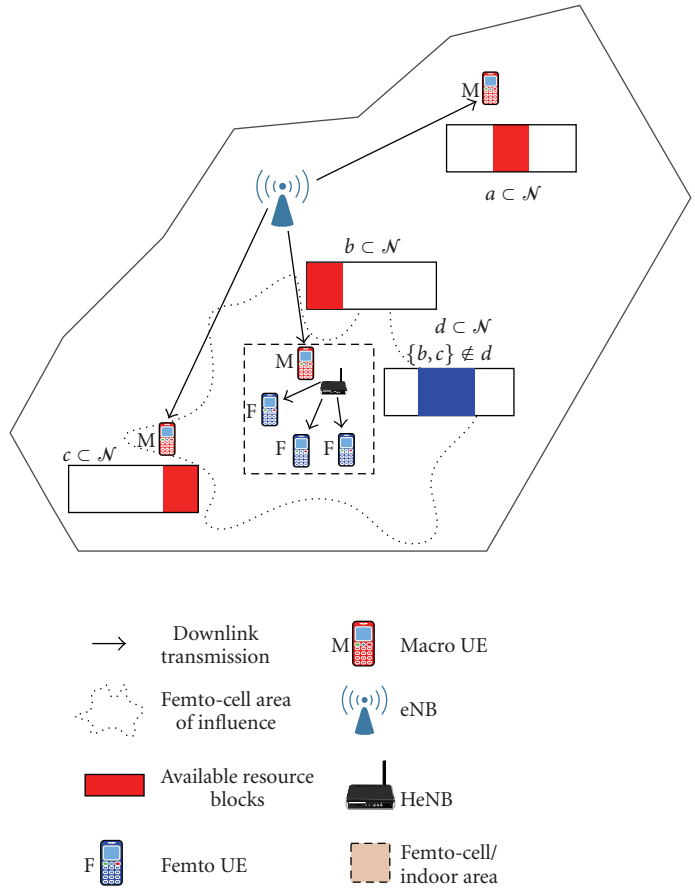

FIGURE 1: Resource partitioning in the vicinity of a femto-cell. The femto-cell is forbidden from using downlink resources allocated to nearby macro UEs, that is, b and c, but may continue using the set of resources a.

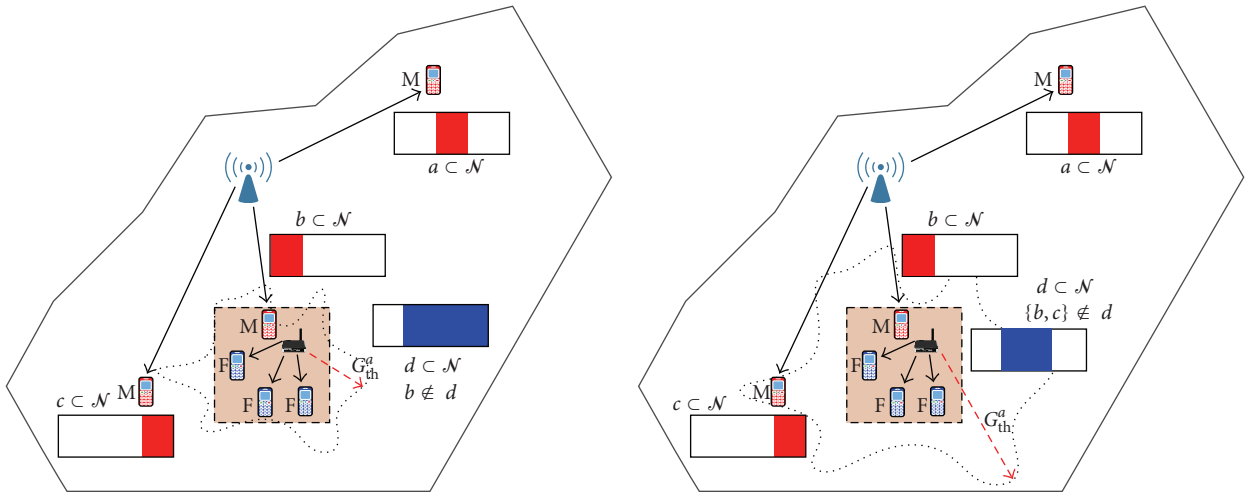

(a) High interference threshold

(b) Low interference threshold

FIGURE 2: Resource partitioning with two different thresholds ($G^a_{\text{th}} > G^b_{\text{th}}$). Using a lower threshold b leads to a larger number of partitioned resources.

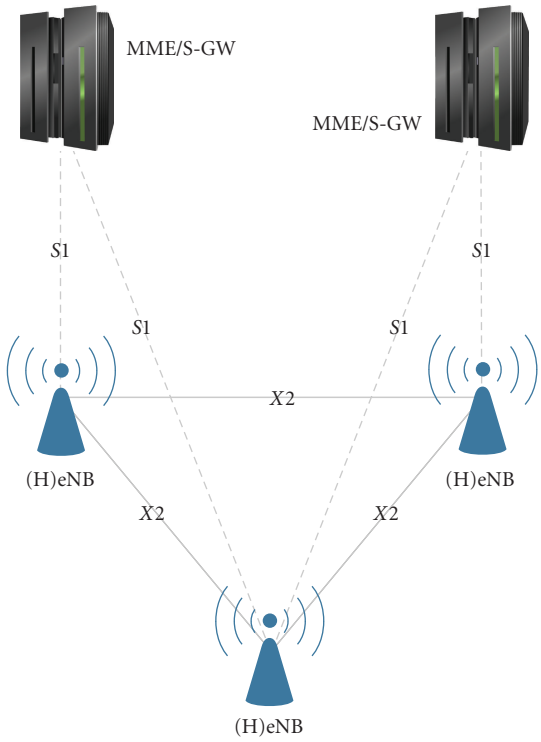

Figure 3: Overall LTE architecture showing S1 and X2 interfaces.

contains the cell-IDs, a UE can establish a list of neighboring eNBs. Knowledge of the cell-ID also enables UEs to read the cell-specific reference signals (also known as training symbols or pilots) of neighboring eNBs, that are needed to carry out RSRP measurements. These enable the estimation of the average channel gain between the UE and the surrounding eNBs, $\overline{G}^{u,v}$, in (10). RSRP for a specific cell is defined as the linear average over the power contributions (in W) of the Resource Elements (REs) which carry cell-specific reference signals within the considered measurement frequency bandwidth [11]. As HeNBs also broadcast their cell-ID in the BCH, as well as cell-specific reference signals, RSRP measurements allow the identification of HeNBs that are in close proximity of a macro UE. We note that this does not introduce any additional overhead because we utilize an existing signaling procedure between macro UEs and eNBs.

The eNB needs to inform the HeNB that causes interference of the restricted resources $\overline{\mathcal{N}_i}$ it must not use according to (11). This involves defining the transport of control information from eNBs to HeNBs using the LTE network architecture shown in Figure 3. The S1 interface connects the Serving Gateway (S-GW)/Mobility Management Entity (MME) with a pool of neighboring eNBs. The MME is a control node that processes the signaling between the UE and the core network (CN). Neighboring eNBs are interconnected via the X2 interface, that conveys control information related to handover and interference coordination. The X2 interface is therefore particularly suited for signaling related to femto-to-macro interference avoidance [16, 17].

In LTE, the network architecture is flat such that when a UE is handed over, to improve latency and efficiency, the handover procedure is exclusively controlled by the source and destination eNBs [25]. For intra-LTE handover, the default procedure is that the source eNB buffers the data and passes it to the destination eNB over the X2 interface. If no X2 connection exists between the source and destination eNBs, the handover is performed over the S1 interface. However, from the UE's viewpoint, there is no difference between the two types of handover [25]. In the case of closed-access femto-cells, where a handover is not possible between a source H/eNB and a destination HeNB, the proposed resource partitioning procedure requires that signaling information is conveyed from the source eNB to the destination HeNB.

In the LTE downlink, a bitmap known as the Relative Narrowband Transmit Power (RNTP) indicator is exchanged over the X2 interface between eNBs. The RNTP indicator is used by an eNB to signal to neighboring eNB on which RBs it intends to transmit with high power in the near future. Each bit of the RNTP indicator corresponds to one RB in the frequency domain and is used to inform the neighboring eNBs if the eNB in question is planning to exceed the transmit power for that RB or not [26]. The value of the threshold and the time period for which the indicator is valid are configurable parameters. This bitmap is intended to enable neighboring cells to estimate the amount of interference on each RB in future frames and therefore schedule their UEs accordingly. Furthermore, the source and destination cell IDs need is contained in the RNTP.

The DL-HII messages that indicate which resources a particular HeNB must not use may be conveyed by a bitmap that is equivalent to that of the RNTP indicator. Provided that HeNBs are also connected to the X2 interface, DL-HII messages emitted by eNBs may be configured to perform resource partitioning at certain HeNBs by using the format of the RNTP indicator. Suppose that macro UE u served by eNB v_u is trapped within the coverage area of a closed-access femto-cell, served by HeNB i. Then resource partitioning is implemented by sending a DL-HII message to HeNB i, where ones and zeros correspond to RBs where HeNB i may and may not transmit, respectively. The transmission format of the RNTP indicator is therefore perfectly suited for DL-HII messages.

In order to avoid that DL-HII messages are to be sent every subframe (i.e., at 1 ms intervals), the *lifetime* of DL-HII messages could be configured in a dedicated field within the DL-HII message format. Dependent on the underlying service the macro UE is using, the eNB estimates for how long the RBs utilized macro UE are to be reserved, and notes this estimate as the lifetime of the DL-HII message. Unless DL-HII message is updated before its lifetime expires, the HeNB may then reuse the restricted RBs after the lifetime of the DL-HII message has expired. This limits the signaling overhead due to DL-HII messages to a level comparable to that of a handover procedure, which is needed, for example, for macro-to-femto-cell handover in open access systems.

Historical UE information is propagated between eNBs during the X2 handover procedure [25]. Historical UE

information consists of the last few cells visited by the UE, together with the time for which the UE was camped at that eNB. The historical information is used to determine the occurrence of a handover ping-pong between cells. This is also a source of information that is useful in the context of resource partitioning. If a UE is camped to the last few eNBs for a short time interval, the resource partitioning procedure need not be carried out. This can be done to avoid unnecessary signaling.

4. System Level Simulation Setup

4.1. User Distribution and Sectorized eNBs. The simulation area comprises a two-tier, tessellated hexagonal cell distribution. In order to eliminate edge effects with regards to interference, additional two tiers are simulated. However, statistics are taken only from the central two tiers. The eNBs are placed at the junction of three hexagonal cells, such that each cell can be considered as a sector. In this way, each eNB serves three sectors, with each sector reusing all frequency resources. For each sector, the azimuth antenna pattern, $A(\theta)$, is described by [24]

$$A(\theta) = -\min\left[12\left(\frac{\theta}{\theta_{3\text{dB}}}\right)^2, A_m\right], \tag{12}$$

where the $\theta_{3\text{dB}} = 70^\circ$ is the angle from the central lobe at which the gain reduces to half the maximum value and $A_m = 20\,\text{dB}$ is the maximum possible attenuation due to sectorization.

We follow the simulation assumptions described in [24] where a 5×5 grid model is used to simulate femto-cell deployment. This setup models a single-floor building with 25 apartments that are arranged in a 5×5 grid. An HeNB may exist in an apartment with probability p_1. Furthermore, an HeNB may be active with probability p_2. Therefore, the probability p that an apartment contains an active HeNB is given by $p = p_1 p_2$. Every apartment that contains an active HeNB contains exactly one associated femto UE. These are dropped randomly and uniformly within the apartment with a specified minimum separation from the HeNB. In addition to this, macro UEs are also randomly and uniformly dropped within the tiered hexagonal system. As a result, it is possible that a macro UE lies within the confines of an apartment. Figure 4 shows one instance of a distribution of four apartment blocks and ten macro UEs per macro sector. It is observed that some macro UEs lie within apartment blocks. We assume a closed-access policy so that such macro UEs, despite their indoor location, are served by the eNB. In such a situation, these macro UEs suffer from severe interference originating from the nearby HeNBs. Macro UEs lying either inside an apartment block containing active HeNBs or very close to such an apartment block are the likely victims of high downlink femto-to-macro interference. The concept of resource partitioning addresses the mitigation of interference experienced by such macro UEs in the downlink. The macro UEs indicated by arrows in Figure 4 are the potential recipients of high interference originating from nearby femto-cells.

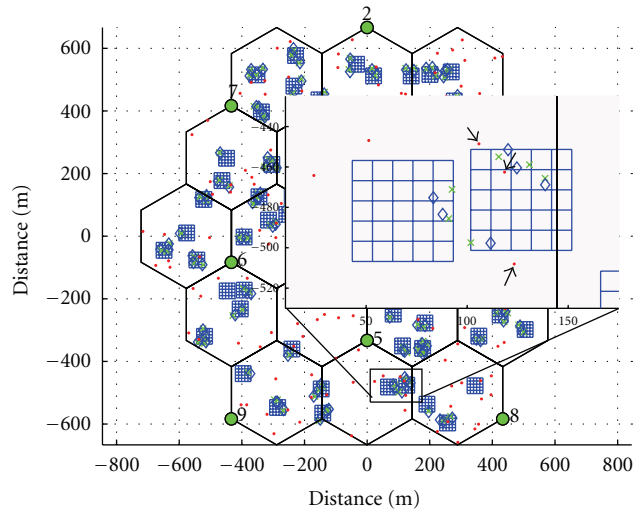

Figure 4: Four apartment blocks and ten macro UEs per macro sector. Macro UEs are denoted by red dots, femto UEs by blue diamonds, HeNBs by green crosses and eNBs by filled green circles, each denoted with a number. The close-up shows a few marked macro UEs undergoing potentially severe downlink interference from nearby active femto-cells.

In this particular case, if one or more HeNBs are indeed the cause of high interference, they will partition resources so as to enable the vulnerable macro UEs to attain a satisfactory downlink SINR.

4.2. Time Evolution. Since the resource allocation is random in nature, each run of the Monte Carlo simulation is iterated over a series of snapshots to obtain statistically accurate results. The duration of a snapshot is equivalent to the duration of one LTE subframe and the run is allowed to iterate over ten subframes (one LTE frame). At each iteration, the allocation of resources is randomized. It is assumed that the UEs are quasistatic for the duration of the run.

5. Results

The simulation is run for a full-buffer traffic model, that resembles the worst case scenario where all users in the system are active simultaneously. Furthermore, the users in the system are assumed to be static for the duration of the snapshot, so that the effects due to Doppler spread are neglected. Perfect synchronization in time and frequency is assumed, such that interference between neighboring RBs can be neglected as well. Relevant parameters used for the simulation are shown in Table 3.

Clearly, more than one macro UE can be affected by the same apartment block and more than one apartment block can affect the same macro UE (as demonstrated in Figure 4). The offending HeNBs must then perform resource partitioning using the method described in Sections 3.2 and 3.3. Due to the effects of shadowing, the corresponding exclusion region is not a circular area.

Table 3: Simulation parameters.

Parameter	Value
Avg. 5×5 apartment blocks per macro-cell sector	$\{4, 14\}$
Avg. macro UEs per macro-cell sector	10
Inter-site distance	500 m
Individual apartment dimensions	$10 \times 10\ \text{m}^2$
HeNB deployment probability, p_1	0.2
HeNB activation probability, p_2	0.5
Femto UEs per active femto-cell	1
Downlink FDD band	[2.62, 2.63] GHz
Tot. number of available RBs, N	50
RB bandwidth, B_{RB}	180 kHz
Thermal noise, η	-174 dBm/Hz
eNB transmit power per RB per sector, P_{m}	29 dBm
HeNB transmit power per RB, P_{f}	3 dBm
eNB antenna gain	14 dBi
Sectors per eNB	3
Min. distance between macro UE and eNB	35 m
Min. distance between femto UE and HeNB	0.2 m
Number of macro/femto UE Rx antennas	2 Rx
Wall penetration loss, L_{W}	20 dB
Interference threshold, I_{th}	$\{-72, -87\}$ dBm
Subframe time duration, t_{s}	1 ms

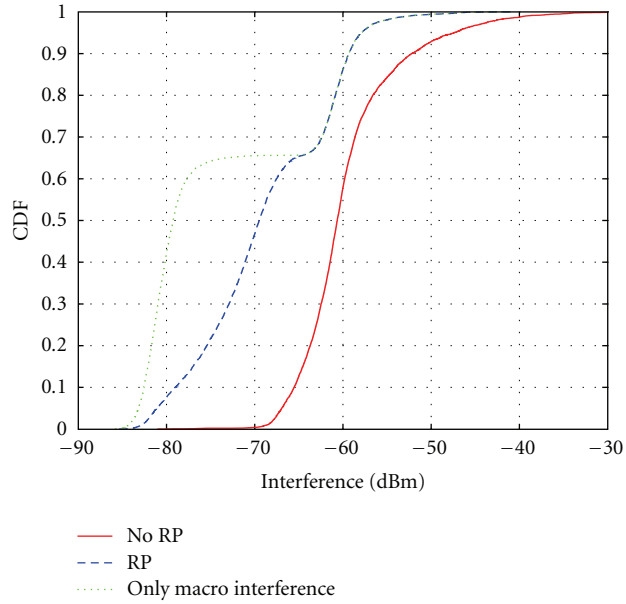

Figure 5: CDFs showing downlink interference for affected macro UEs in systems with and without resource partitioning, compared against a system with no femto interference.

For a meaningful performance assessment, the definition of "affected" macro and femto UEs is to be introduced. A macro UE is said to be "affected" if its average channel gain to at least one HeNB exceeds the predefined threshold I_{th}, as defined in (10). This section shows results for different classes of UEs: overall macro (all macro UEs in the system, regardless of their location), overall femto (all femto UEs, all lying strictly indoors associated with an active HeNB), affected macro (only macro UEs in the vicinity of active femto-cells as described above), and affected femto (only femto UEs served by offending HeNBs).

Figure 5 demonstrates the need for femto-to-macro interference coordination and the benefit of resource partitioning. The cumulative distribution function (CDF) of downlink interference for affected macro UEs with and without resource partitioning is shown in this figure. An interference threshold of $I_{\text{th}} = -72$ dBm is used, which translates to $G_{\text{th}} = -75$ dB. For comparison purposes, a third CDF is displayed showing the interference only from the macro layer, where HeNB transmit powers are reduced to zero, keeping the allocation of resources unchanged. This third case represents the "ideal" situation without interference from the femto layer. This "ideal" case therefore represents an upper bound for the performance of any femto-to-macro interference avoidance scheme. It is clear from the figure that resource partitioning reduces the interference by approximately 10 dB at the 50th percentile. Furthermore, it is seen that resource partitioning approaches the performance of the upper bound particularly in the high interference regime, where the offending HeNBs suppress transmission on the vulnerable RBs. The difference between the lower interference regimes of the curve with resource partitioning and the case without femto interference indicates the amount of additional interference caused by those HeNBs that do not perform resource partitioning, because they do not lie in the vicinity of any vulnerable macro UEs. It is clear from this figure that there is a significant benefit from resource partitioning. The following figures show the effect of resource partitioning on the macro and femto performance.

The capacities of combined macro and femto-cell depicted in Figures 6 through 9 are compared against a benchmark system that emulates a state-of-the-art cellular network. In this benchmark system, no HeNBs exist, and all UEs previously classified as femto UEs are served by the outdoor eNBs. *All* UEs in the benchmark system are therefore macro UE and must therefore share the available macro resources.

Figure 6 shows the overall downlink macro user capacity for 4 and 14 grids with 10 macro UEs per macro-cell sector with the interference thresholds $I_{\text{th}} = -72$ and -87 dBm. The two I_{th} thresholds are chosen because they represent two extreme cases: one in which the exclusion region causes approximately 13% of HeNBs to partition resources ($I_{\text{th}} = -72$ dBm) and the other (-87 dBm) where the exclusion region causes approximately 76% of HeNBs to partition resources. In this case, capacity statistics are collected from all macro UEs, regardless of whether they lie outdoors or indoors and regardless of whether they are vulnerable to heavy HeNB interference or not. It is observed that when resource partitioning is applied, a consistent gain is achieved over the benchmark, where, both macro and femto-cells fully utilise all available resources.

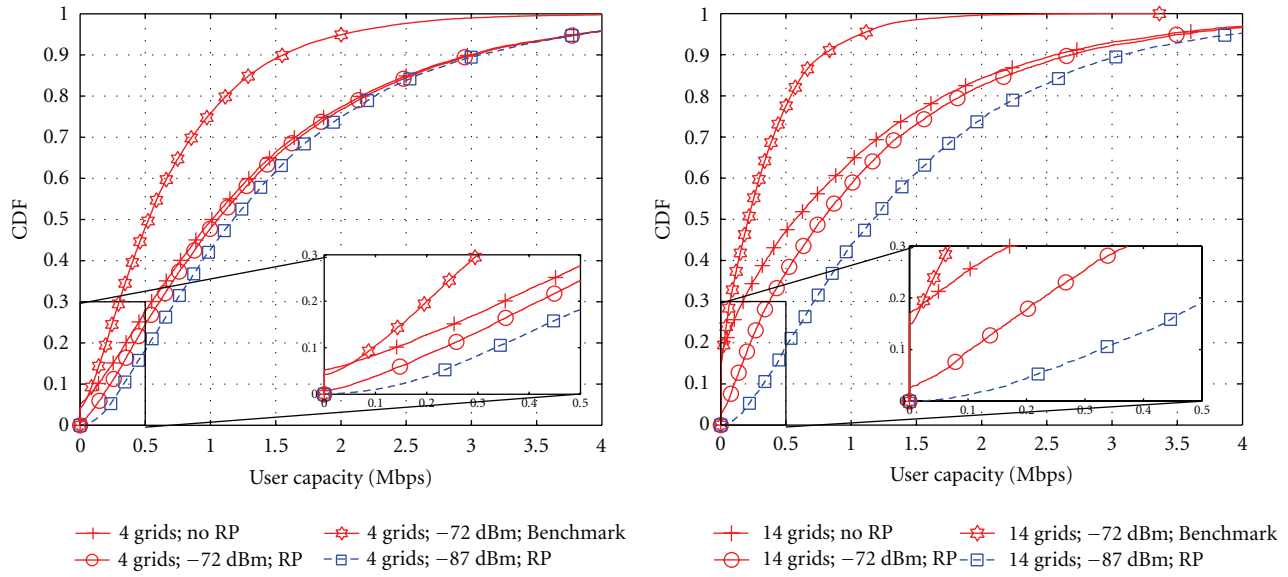

(a) 4 5 × 5 grids per macro-cell sector

(b) 14 5 × 5 grids per macro-cell sector

Figure 6: CDFs of the overall downlink macro user capacity for a system with and without resource partitioning, compared against the benchmark system with no femto-cell deployment.

Figure 6 reveals that there is a higher resource partitioning gain in the lower capacity regime (lower percentiles of the CDF). This is due to affected macro UEs that severely suffer from interference originating from nearby HeNBs. In the higher capacity regime, resource partitioning gains diminish because macro UEs achieving high capacities typically lie outdoors, well protected from interfering HeNBs through walls, so that the dominant interference for such macro UEs originates from other eNBs.

It is observed that the user capacity of the system with 14 grids per macro-cell sector shown in Figure 6(b) is consistently worse than the performance of the system with lower grid density shown in Figure 6(a). This is expected as increasing the grid density increases the amount of interference originating from the femto layer. For the benchmark, a higher grid density means that the same amount of resources in the macro-cell have to be shared among a higher number of users, thus compromising user capacity. Interestingly, it is observed that when $I_{\text{th}} = -87$ dBm, the performance of the systems with either grid density are almost identical. This is attributed to the fact that in either case, the number of macro UEs remains the same, and the high value of I_{th} then ensures that the majority of HeNBs partition resources. As a result, the amount of femto interference stays largely independent of the grid density. Of note is that a decreasing I_{th} enhances the attainable gains in macro UE capacity.

It is clear from Figure 6 that augmenting a cellular network with femto-cell deployment yields tremendous capacity gains over the benchmark system. These gains are attributed to two reasons. First, in the benchmark system, all former femto UEs are served by the outdoor eNB, where high wall penetration losses result in a highly attenuated signal. The second reason is that in the benchmark system, all UEs must share the macro resources, so that each UE is assigned fewer RBs compared to the case with femto-cell deployment. For four apartment blocks per sector (Figure 6(a)), with each apartment having a 10% probability of containing an active HeNB, each sector contains, on average, ten femto UEs in addition to the ten macro UEs. This means that in the benchmark system, each macro UE is allocated half the number of RBs in comparison to the system with femto-cell deployment. The situation is obviously worsened in the 14 grid per sector case, as shown in Figure 6(b). This is also responsible for the benchmark system showing the highest outage. In this context, a UE goes into outage if the achieved SINR on all RBs is less than γ_{min}.

Finally, in the very low capacity regime (<0.1 Mbps in either case), the benchmark system outperforms the system without resource partitioning. This is due to excessive femto-to-macro interference experienced by macro UEs trapped within the coverage area of femto-cells.

Figure 7 shows the overall femto user capacity on the downlink. Results are gathered for all femto UEs, regardless of whether they are in the vicinity of a vulnerable macro UE. In general, very high capacities are achieved in femto-cells. This is due to the very short transmission distances within femto-cells, as well as outdoor interference protection through high wall penetration losses. We observe that in all cases, user capacities saturate at 39.6 Mbps, due to the upper bound of the link-to-system mapping (4). According to (4), the maximum achievable spectral efficiency is capped at $\overline{C}_{\text{max}} = 4.4$ bit/s/Hz, and because HeNBs only serve one femto UE, with all available resources $\mathcal{N}$ being allocated to this UE, this equates to a maximum downlink capacity of 39.6 Mbps.

Figure 7 also reveals that femto-cells must sacrifice some capacity when resource partitioning is in place. This is obvious because the affected HeNBs are forbidden from

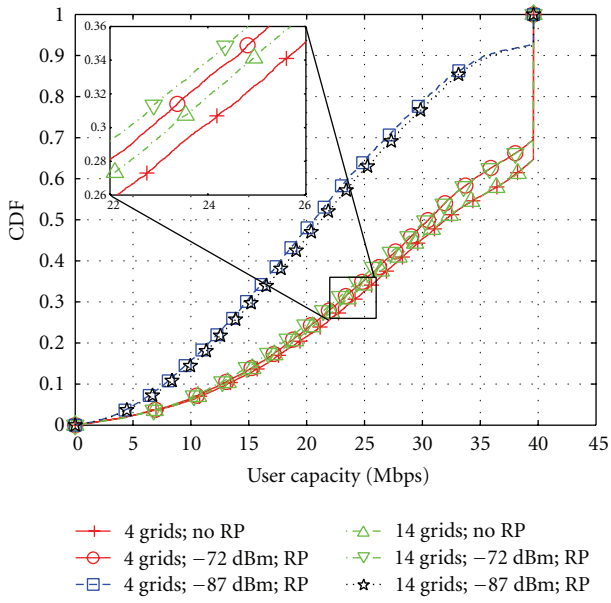

Figure 7: CDFs showing femto downlink user capacity for a system with resource partitioning compared against a system without resource partitioning.

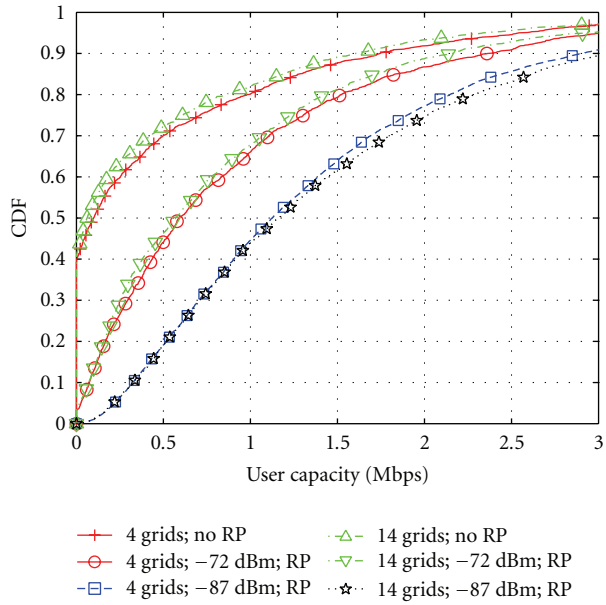

Figure 8: CDFs showing downlink user capacity only for affected macro UEs for a system with resource partitioning compared against a system without resource partitioning.

using RBs allocated to nearby macro UEs. Moreover, the lower the threshold I_{th} the higher the partitioning of femto-cell resources, and thus the lower the proportion of femto UEs that approach the maximum capacity. For $I_{\text{th}} = -72$ dBm, the degradation in femto user capacity is in the order of 1 Mbps. On the other hand, when $I_{\text{th}} = -87$ dBm, the degradation increases to approximately 10 Mbps. It is important to note that owing to the full buffer assumption, the degradation in femto user capacities reflects a worst case scenario. In case femto-cells are not assigned all available resources, the degradation due to resource partitioning is obviously lower.

A trade-off between the improvement in macro capacity and degradation of femto capacity exists. Optimization of this trade-off depends on the acceptable degradation of macro-cell capacity (see Figure 6), in particular at the low percentiles of the corresponding CDF. This enables the determination of the appropriate threshold I_{th}, which in turn results in a certain degradation of femto-cell performance.

Figures 8 and 9 concentrate on affected macro and femto UEs. Figure 8 shows the capacity performance of affected macro UEs. It is observed that resource partitioning delivers a significant gain to the downlink performance of affected macro UEs. It is seen that regardless of the grid density, with $I_{\text{th}} = -72$ and -87 dBm, a five and, respectively, tenfold capacity increase of affected macro UEs is observed.

Figure 9 shows that the sacrifice in downlink capacity that affected femto UEs incur due to resource partitioning. It is observed that UEs associated with HeNBs that must partition resources incur a reduction in capacity of approximately 25% with $I_{\text{th}} = -72$ dBm and 39% with $I_{\text{th}} = -87$ dBm. It is important to note that for a sacrifice of 39% of femto capacity, the affected macro UEs are rewarded with a tenfold

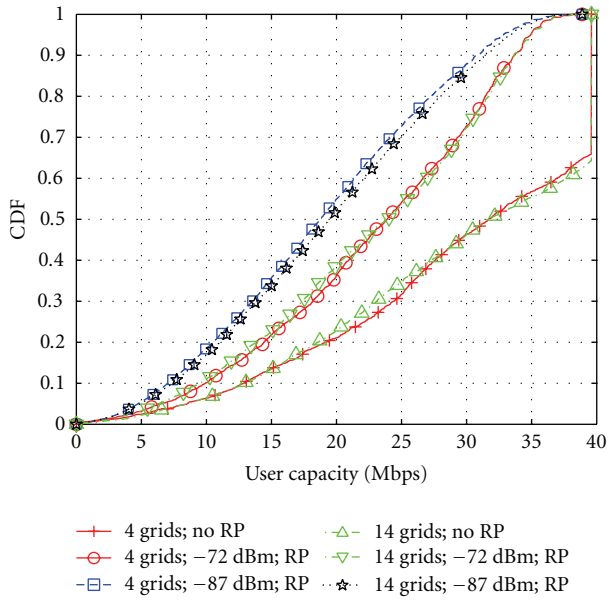

Figure 9: CDF showing downlink user capacity only for affected femto UE for a system with resource partitioning compared against a system without resource partitioning.

capacity increase. We note that with either grid density, the affected macro and femto UE performance is almost identical because in both cases, the macro UE density remains the same and therefore, every HeNB must partition the same proportion of resources.

The sum system capacity in the downlink normalized per macro sector shows some interesting trends. With

Table 4: Femto UE capacity degradation and macro UE capacity improvement.

I_{th} value	Overall femto UE degradation	Affected macro UE improvement	Affected femto UE degradation
−72 dBm	1 Mbps	5x	25%
−87 dBm	10 Mbps	10x	39%

a grid density of 4 grids per macro-cell sector and $I_{th} = -72$ dBm, the use of resource partitioning results in an affected macro UE capacity increase of 6.4% at the cost of a 2.8% degradation in femto capacity. However, when $I_{th} = -87$ dBm, a 14.2% increase in macro capacity is accompanied by a 29.6% decrease in femto capacity. The situation is different for the case when the grid density is increased to 14 grids per macro sector. When $I_{th} = -72$ dBm, a 15.7% increase in macro capacity is attained at a the expense of a 2.8% decrease in femto capacity. For $I_{th} = -87$ dBm, resource partitioning results in a 53.2% increase in affected macro UE capacity with a 25.1% decrease in femto capacity. This shows that with decreasing grid densities, a relatively high interference threshold I_{th} becomes more effective.

For convenience, the femto UE degradation and macro UE improvement in capacity through the use of resource partitioning are listed in Table 4.

6. Summary and Conclusion

Femto-cell deployment poses a viable complement to cellular networks. Operators need to bear low cost in their deployment because they are installed directly by the users themselves. Furthermore, because they share both, the radio access scheme and the frequency band with eNBs, they are compatible with legacy UEs. Aside from these benefits, a cellular network stands to significantly gain in overall system throughput through the widespread deployment of HeNBs. Not only do HeNBs improve indoor coverage, bringing broadband-like experience directly to the handset, but they also offload resources from the eNB that can be utilized to improve coverage to outdoor users.

It has been seen that in a closed-access system, macro UEs lying in the proximity of femto-cells experience at least as much downlink interference from HeNBs as they do from eNBs. It has been demonstrated that by introducing LTE-specific resource partitioning, the capacity of such macro UEs can be boosted by a factor of ten. The cost incurred by femto UE in doing so is minimal as they lose less than half of their capacity (which is more than one order of magnitude higher than macro UE downlink capacity). Users therefore experience a very high throughput inside femto-cells due to the favorable channel conditions and continue to do so even in the presence of resource partitioning. Introducing resource partitioning to a closed-access system with femto-cell deployment substantially boosts the sum system capacity while ensuring reliable macro-cell operation.

Acknowledgments

Initial parts of this work were supported by **DFG Grant** HA 3570/2-1 as part of program SPP-1163 (adaptability in heterogeneous communication networks with wireless access—AKOM) while some latter parts of this work have been performed within the framework of the CELTIC project CP5-026 WINNER+. Harald Haas acknowledges the Scottish Funding Council support of his position within the Edinburgh Research Partnership in Engineering and Mathematics between the University of Edinburgh and Heriot Watt University.

References

[1] M.-S. Alouini and A. J. Goldsmith, "Area spectral efficiency of cellular mobile radio systems," *IEEE Transactions on Vehicular Technology*, vol. 48, no. 4, pp. 1047–1066, 1999.

[2] T. Nihtilä, "Increasing femto cell throughput with HSDPA using higher order modulation," in *Proceedings of the IEEE International Networking and Communications Conference (INCC '08)*, pp. 49–53, Lahore, Pakistan, May 2008.

[3] V. Chandrasekhar, J. G. Andrews, and A. Gatherer, "Femtocell networks: a survey," *IEEE Communications Magazine*, vol. 46, no. 9, pp. 59–67, 2008.

[4] Z. Bharucha, I. Ćosović, H. Haas, and G. Auer, "Throughput enhancement through femto-cell deployment," in *Proceedings of the 7th IEEE International Workshop on Multi-Carrier Systems & Solutions (MC-SS '09)*, pp. 311–319, Herrsching, Germany, May 2009.

[5] Z. Bharucha, H. Haas, A. Saul, and G. Auer, "Throughput enhancement through femto-cell deployment," *European Transactions on Telecommunications*, vol. 21, no. 4, 2010.

[6] M. Etoh, T. Ohya, and Y. Nakayama, "Energy consumption issues on mobile network systems," in *Proceedings of the International Symposium on Applications and the Internet (SAINT '08)*, pp. 365–368, IEEE, Turku, Finland, July-August 2008.

[7] H. Haas and G. J. R. Povey, "Capacity analysis of a TDD underlay applicable for UMTS," in *Proceedings of the 10th IEEE International Symposium on Personal, Indoor and Mobile Radio Communications (PIMRC '99)*, p. A6-4, Osaka, Japan, September 1999.

[8] H. Haas and G. J. R. Povey, "A capacity investigation on UTRA-TDD utilising underused UTRA-FDD uplink resources," in *Proceedings of the IEE Colloquium on UMTS Terminals and Software Radio*, pp. 1–7, Glasgow, Scotland, April 1999, Ref. no. 1999/055.

[9] P. K. Jain, H. Haas, and S. McLaughlin, "Capacity enhancement using ad hoc pico-cells and TDD underlay," in *Proceedings of the 17th IEEE International Symposium on Personal, Indoor and Mobile Radio Communications (PIMRC '06)*, pp. 1–5, Helsinki, Finland, September 2006.

[10] X. Yang, G. Feng, and C. K. Siew, "Call admission control for multi-service mobile networks with bandwidth asymmetry between uplink and downlink," in *Proceedings of the IEEE Global Telecommunications Conference (GLOBECOM '04)*, vol. 5, pp. 3285–3289, November-December 2004.

[11] 3GPP, "Physical Channels and Modulation (Release 8)," 3GPP TS 36.211 V 8.2.0, March 2008, http://www.3gpp.org/ftp/Specs.

[12] D. López-Pérez, A. Valcarce, G. De La Roche, and J. Zhang, "OFDMA femtocells: a roadmap on interference avoidance,"

IEEE Communications Magazine, vol. 47, no. 9, pp. 41–48, 2009.

[13] H. Claussen, "Performance of macro- and co-channel femtocells in a hierarchical cell structure," in *Proceedings of the 18th IEEE International Symposium on Personal, Indoor and Mobile Radio Communications (PIMRC '07)*, pp. 1–5, Athens, Greece, September 2007.

[14] L. T. W. Ho and H. Claussen, "Effects of user-deployed, co-channel femtocells on the call drop probability in a residential scenario," in *Proceedings of the 18th IEEE International Symposium on Personal, Indoor and Mobile Radio Communications (PIMRC '07)*, pp. 1–5, Athens, Greece, September 2007.

[15] V. Chandrasekhar and J. Andrews, "Uplink capacity and interference avoidance for two-tier femtocell networks," *IEEE Transactions on Wireless Communications*, vol. 8, no. 7, pp. 3498–3509, 2009.

[16] 3GPP, "X2 General Aspects and Principles (Release 8)," 3GPP TS 36.420 V8.0.0, December 2007, http://www.3gpp.org/ftp/Specs.

[17] 3GPP, "X2 Application Protocol (X2AP) (Release 8)," 3GPP TS 36.423 V8.2.0, June 2008, http://www.3gpp.org/ftp/Specs.

[18] T. S. Rappaport, *Wireless Communications: Principles and Practice*, Prentice Hall, Upper Saddle River, NJ, USA, 2nd edition, 2001.

[19] 3GPP, "Evolved Universal Terrestrial Radio Access (E-UTRA); Radio Frequency (RF) System Scenarios," 3GPP TR 36.942 V 8.2.0, May 2009, http://www.3gpp.org/ftp/Specs.

[20] A. Persson, T. Ottosson, A. Saul, G. Auer, and M. Afgani, "On the performance of inter-sector scheduling in OFDMA systems," in *Proceedings of the 11th International OFDM Workshop (InOWo '06)*, Hamburg, Germany, August 2006.

[21] ITU-R Working Party 5D (WP5D)—IMT Systems, "Report of correspondence group for IMT.EVAL," Tech. Rep. 124, Dubai, United Arab Emirates, May 2008.

[22] W. Wang, T. Ottosson, M. Sternad, A. Ahlén, and A. Svensson, "Impact of multiuser diversity and channel variability on adaptive OFDM," in *Proceedings of the 58th IEEE Vehicular Technology Conference (VTC '03)*, pp. 547–551, Orlando, Fla, USA, October 2003.

[23] NTT DOCOMO, "New Evaluation Models (Micro Cell, Indoor, Rural/High-Speed)," 3GPP TSG RAN WG1 R1-082713, July 2008, http://www.3gpp.org/ftp/tsg_ran/WG1_RL1/TSGR1_53b/Docs.

[24] 3GPP, "Simulation Assumptions and Parameters for FDD HeNB RF Requirements," 3GPP TSG RAN WG4 R4-092042, May 2008, http://www.3gpp.org/ftp/Specs.

[25] S. Sesia, I. Toufik, and M. Baker, Eds., *LTE—The UMTS Long Term Evolution: From Theory to Practice*, John Wiley & Sons, New York, NY, USA, 1st edition, 2009.

[26] 3GPP, "Evolved Universal Terrestrial Radio Access (E-UTRA); Physical Layer Procedures (Release 8)," 3GPP TS 36.213 V 8.8.0, September 2009, http://www.3gpp.org/ftp/Specs.

Hindawi Publishing Corporation
EURASIP Journal on Wireless Communications and Networking
Volume 2010, Article ID 690161, 14 pages
doi:10.1155/2010/690161

Research Article

Best Signal Quality in Cellular Networks: Asymptotic Properties and Applications to Mobility Management in Small Cell Networks

Van Minh Nguyen,[1] François Baccelli,[2] Laurent Thomas,[1] and Chung Shue Chen[2]

[1] *Network and Networking Department, Bell Labs, Alcatel-Lucent, 91620 Nozay, France*
[2] *TREC (Research Group on Network Theory and Communications), INRIA-ENS, (École Normale Supérieure), 75214 Paris, France*

Correspondence should be addressed to Van Minh Nguyen, van_minh.nguyen@alcatel-lucent.com

Received 15 October 2009; Revised 17 February 2010; Accepted 21 March 2010

Academic Editor: Ozgur Oyman

The quickly increasing data traffic and the user demand for a full coverage of mobile services anywhere and anytime are leading mobile networking into a future of small cell networks. However, due to the high-density and randomness of small cell networks, there are several technical challenges. In this paper, we investigate two critical issues: *best signal quality* and *mobility management*. Under the assumptions that base stations are uniformly distributed in a ring-shaped region and that shadowings are lognormal, independent, and identically distributed, we prove that when the number of sites in the ring tends to infinity, then (i) the maximum signal strength received at the center of the ring tends in distribution to a Gumbel distribution when properly renormalized, and (ii) it is asymptotically independent of the interference. Using these properties, we derive the distribution of the best signal quality. Furthermore, an optimized random cell scanning scheme is proposed, based on the evaluation of the optimal number of sites to be scanned for maximizing the user data throughput.

1. Introduction

Mobile cellular networks were initially designed for voice service. Nowadays, broadband multimedia services (e.g., video streaming) and data communications have been introduced into mobile wireless networks. These new applications have led to increasing traffic demand. To enhance network capacity and satisfy user demand of broadband services, it is known that reducing the cell size is one of the most effective approaches [1–4] to improve the spatial reuse of radio resources.

Besides, from the viewpoint of end users, full coverage is particularly desirable. Although today's macro- and micro-cellular systems have provided high service coverage, 100%-coverage is not yet reached because operators often have many constraints when installing large base stations and antennas. This generally results in potential coverage holes and dead zones. A promising architecture to cope with this problem is that of small cell networks [4, 5]. A small cell only needs lightweight antennas. It helps to replace bulky roof top base stations by small boxes set on building facade, on public furniture or indoor. Small cells can even be installed by end users (e.g., femtocells). All these greatly enhance network capacity and facilitate network deployment. Pervasive small cell networks have a great potential. For example, Willcom has deployed small cell systems in Japan [6], and Vodafone has recently launched home 3G femtocell networks in the UK [7].

In principle, high-density and randomness are the two basic characteristics of small cell networks. First, reducing cell size to increase the spatial reuse for supporting dense traffic will induce a large number of cells in the same geographical area. Secondly, end users can set up small cells by their own means [2]. This makes small cell locations and coverage areas more random and unpredictable than traditional mobile cellular networks. The above characteristics have introduced technical challenges that require new studies beyond those for macro- and micro-cellular networks. The main issues concern spectrum sharing and interference mitigation, mobility management, capacity analysis, and network self-organization [3, 4]. Among these, the *signal quality*, for example, in terms of signal-to-interference-plus-noise ratio (SINR), and *mobility management* are two critical issues.

In this paper, we first conduct a detailed study on the properties of *best signal quality* in mobile cellular networks. Here, the best signal quality refers to the maximum SINR received from a number of sites. Connecting the mobile to the best base station is one of the key problems. The best base station here means the base station from which the mobile receives the maximum SINR. As the radio propagation experiences random phenomena such as fading and shadowing, the best signal quality is a random quantity. Investigating its stochastic properties is of primary importance for many studies such as capacity analysis, outage analysis, neighbor cell scanning, and base station association. However, to the best of our knowledge, there is no prior art in this area.

In exploring the properties of best signal quality, we focus on cellular networks in which the propagation attenuation of the radio signal is due to the combination of a distance-dependent path-loss and of lognormal shadowing. Consider a ring B of radii $R_{\min}$ and R_B such that $0 < R_{\min} < R_B < \infty$. The randomness of site locations is modeled by a uniform distribution of homogeneous density in B. Using extreme value theory (c.f., [8, 9]), we prove that the maximum signal strength received at the center of B from n sites in B converges in distribution to a Gumbel distribution when properly renormalized and it is asymptotically independent of the total interference, as $n \to \infty$. The distribution of the best signal quality can thus be derived.

The second part of this paper focuses on applying the above results to mobility support in dense small cell networks. Mobility support allows one to maintain service continuity even when users are moving around while keeping efficient use of radio resources. Today's cellular network standards highlight mobile-assisted handover in which the mobile measures the pilot signal quality of neighbor cells and reports the measurement result to the network. If the signal quality from a neighbor cell is better than that of the serving cell by a handover margin, the network will initiate a handover to that cell. The neighbor measurement by mobiles is called *neighbor cell scanning*. Following mobile cellular technologies, it is known that small cell networking will also use mobile-assisted handover for mobility management.

To conduct cell scanning [10–12], today's cellular networks use a *neighbor cell list*. This list contains information about the pilot signal of selected handover candidates and is sent to mobiles. The mobiles then only need to measure the pilot signal quality of sites included in the neighbor cell list of its serving cell. It is known that the neighbor cell list has a significant impact on the performance of mobility management, and this has been a concern for many years in practical operations [13, 14] as well as in scientific research [15–18]. Using neighbor cell list is not effective for the scanning in small cell networks due to the aforementioned characteristics of high density and randomness.

The present paper proposes an optimized *random cell scanning* for small cell networks. This random cell scanning will simplify the network configuration and operation by avoiding maintaining the conventional neighbor cell list while improving user's quality-of-service (QoS). It is also implementable in wideband technologies such as WiMAX and LTE.

In the following, Section 2 describes the system model. Section 3 derives the asymptotic properties and the distribution of the best signal quality. Section 4 presents the optimized random cell scanning and numerical results. Finally, Section 5 contains some concluding remarks.

2. System Model

The underlying network is composed of cells covered by base stations with omnidirectional antennas. Each base station is also called a *site*. The set of sites is denoted by $\Omega \subset \mathbb{N}$. We now construct a model for studying the maximum signal strength, interference, and the best signal quality, after specifying essential parameters of the radio propagation and the spatial distribution of sites in the network.

As mentioned in the introduction, the location of a small cell site is often not exactly known even to the operator. The spatial distribution of sites seen by a mobile station will hence be treated as completely random [19] and will be modeled by an homogeneous Poisson point process [20] with intensity λ.

In the following, it is assumed that the downlink pilot signal is sent at constant power at all sites. Let $R_{\min}$ be some strictly positive real number. For any mobile user, it is assumed that the distance to his closest site is at least $R_{\min}$ and hence the path loss is in the far field. So, the signal strength of a site i received by a mobile at a position $\mathbf{y} \in \mathbb{R}^2$ is given by

$$P_i(\mathbf{y}) = A(|\mathbf{y} - \mathbf{x}_i|)^{-\beta} X_i, \quad \text{for } |\mathbf{y} - \mathbf{x}_i| \geq R_{\min}, \tag{1}$$

where $\mathbf{x}_i \in \mathbb{R}^2$ is the location of site i, A represents the base station's transmission power and the characteristics of propagation, β is the path loss exponent (here, we consider $2 < \beta \leq 4$), and the random variables $X_i = 10^{X_i^{\mathrm{dB}}/10}$, which represent the lognormal shadowing, are defined from $\{X_i^{\mathrm{dB}}, i = 1, 2, \ldots\}$, an independent and identically distributed (i.i.d.) sequence of Gaussian random variables with zero mean and standard deviation σ_{dB}. Typically, σ_{dB} is approximately 8 dB [21, 22]. Here, we consider that fast fading is averaged out as it varies much faster than the handover decision process.

Cells sharing a common frequency band interfere one another. Each cell is assumed allocated no more than one frequency band. Denote the set of all the cells sharing frequency band kth by Ω_k, where $k = 1, \ldots, K$. So $\Omega_k \cap \Omega_{k'} = \emptyset$ for $k \neq k'$, and $\bigcup_{k=1}^{K} \Omega_k = \Omega$. The SINR received at $\mathbf{y} \in \mathbb{R}^2$ from site $i \in \Omega_k$ is expressible as

$$\zeta_i(\mathbf{y}) = \frac{P_i(\mathbf{y})}{N_0 + \sum_{j \neq i, j \in \Omega_k} P_j(\mathbf{y})}, \quad \text{for } i \in \Omega_k, \tag{2}$$

where N_0 is the thermal noise average power which is assumed constant. For notational simplicity, let $A := A/N_0$. Then $\zeta_i(\mathbf{y})$ is given by

$$\zeta_i(\mathbf{y}) = \frac{P_i(\mathbf{y})}{1 + \sum_{j \neq i, j \in \Omega_k} P_j(\mathbf{y})}, \quad \text{for } i \in \Omega_k. \tag{3}$$

In the following, we will use (3) instead of (2).

3. Best Signal Quality

In this section, we derive the distribution of the best signal quality. Given a set of sites $S \subset \Omega$, the *best signal quality* received from S at a position $\mathbf{y} \in \mathbb{R}^2$, denoted by $Y_S(\mathbf{y})$, is defined as

$$Y_S(\mathbf{y}) = \max_{i \in S} \zeta_i(\mathbf{y}). \tag{4}$$

Let us first consider a single-frequency network (i.e., $K = 1$).

Lemma 1. *In the cell set S of single-frequency network, the site which provides a mobile the maximum signal strength will also provide this mobile the best signal quality, namely,*

$$Y_S(\mathbf{y}) = \frac{M_S(\mathbf{y})}{1 + I(\mathbf{y}) - M_S(\mathbf{y})}, \quad \forall \mathbf{y} \in \mathbb{R}^2, \tag{5}$$

where

$$M_S(\mathbf{y}) = \max_{i \in S} P_i(\mathbf{y}) \tag{6}$$

is the maximum signal strength received at $\mathbf{y}$ from the cell set S, and

$$I(\mathbf{y}) = \sum_{i \in \Omega} P_i(\mathbf{y}) \tag{7}$$

is the total interference received at $\mathbf{y}$.

Proof. Since $\zeta_i(\mathbf{y}) = P_i(\mathbf{y})/\{1 + I(\mathbf{y}) - P_i(\mathbf{y})\}$ and $P_i(\mathbf{y}) < I(\mathbf{y})$, (5) follows from the fact that no matter which cell $i \in \Omega$ is considered, $I(\mathbf{y})$ is the same and from the fact that $x/(c - x)$ with c constant is an increasing function of $x < c$. □

Let us now consider the case of multiple-frequency networks. Under the assumption that adjacent-channel interference is negligible compared to cochannel interference, cells of different frequency bands do not interfere one another. Thus, for a given network topology $\mathcal{T}$, the SINRs received from cells of different frequency bands are independent. In the context of a random distribution of sites, the SINRs received from cells of different frequency bands are therefore conditionally independent given $\mathcal{T}$. Write cell set S as

$$S = \bigcup_{k=1}^{K} \{S_k : S_k \subset \Omega_k\}, \tag{8}$$

with S_k the subset of S allocated to frequency k. Let

$$Y_{S_k}(\mathbf{y}) = \max_{i \in S_k} \zeta_i(\mathbf{y}) \tag{9}$$

be the best signal quality received at $\mathbf{y}$ from sites which belong to S_k. The random variables $\{Y_{S_k}(\mathbf{y}), k = 1, \ldots, K\}$ are conditionally independent given $\mathcal{T}$. As a result,

$$\mathbf{P}\{Y_S(\mathbf{y}) \le \gamma \mid \mathcal{T}\} = \prod_{k=1}^{K} \mathbf{P}\{Y_{S_k}(\mathbf{y}) \le \gamma \mid \mathcal{T}\}. \tag{10}$$

Remark 1. For the coming discussions, we define

$$I_S(\mathbf{y}) = \sum_{i \in S} P_i(\mathbf{y}), \tag{11}$$

which is the interference from cells in set S. In the following, for notational simplicity, the location variable $\mathbf{y}$ appearing in $Y_S(\mathbf{y})$, $M_S(\mathbf{y})$, $I_S(\mathbf{y})$, and $I(\mathbf{y})$ will be omitted in case of no ambiguity. We will simply write Y_S, M_S, I_S, and I. Note that $I_S \le I$ since $S \subset \Omega$.

Following Lemma 1, the distribution of Y_S can be determined by the joint distribution of M_S and I, which is given below.

Corollary 1. *The tail distribution of the best signal quality received from cell set S is given by*

$$\overline{F}_{Y_S}(\gamma) = \int_{u=0}^{\infty} \int_{v=u}^{((1+\gamma)/\gamma)u-1} f_{(I,M_S)}(v,u)\,dv\,du, \tag{12}$$

where $f_{(I,M_S)}$ is the joint probability density of I and M_S.

Proof. By Lemma 1, we have

$$\begin{aligned} \mathbf{P}\{Y_S \ge \gamma\} &= \mathbf{P}\left\{\frac{M_S}{(1 + I - M_S)} \ge \gamma\right\} \\ &= \mathbf{P}\left\{I \le \frac{1+\gamma}{\gamma} M_S - 1\right\} \\ &= \int_{u=0}^{\infty} \int_{v=u}^{((1+\gamma)/\gamma)u-1} f_{(I,M_S)}(v,u)\,\mathrm{d}v\,\mathrm{d}u. \end{aligned} \tag{13}$$

□

In view of Corollary 1, we need to study the properties of the maximum signal strength M_S as well as the joint distribution of M_S and I. As described in the introduction, in dense small cell networks, there could be a large number of neighbor cells and a mobile may thus receive from many sites with strong enough signal strength. This justifies the use of extreme value theory within this context.

For some $R_{\min}$ and R_B such that $0 < R_{\min} < R_B < \infty$, let $B \subset \mathbb{R}^2$ be a ring with inner and outer radii $R_{\min}$ and R_B, respectively. In this section, we will establish the following results.

(1) The signal strength P_i received at the center of B belongs to the *maximum domain of attraction* (MDA) of the Gumbel distribution (c.f., Theorem 1 in Section 3.1).

(2) The maximum signal strength and the interference received at the center of B from n sites therein are *asymptotically independent* as $n \to \infty$ (c.f., Corollary 3 in Section 3.1).

(3) The distribution of the best signal quality is derived (c.f., Theorem 2 in Section 3.3).

3.1. Asymptotic Properties. To begin with, some technical details need to be specified. Given a ring B as previously defined, we will study metrics (such as e.g., signal strength, interference, etc.) as seen at the center of B for a set $S \subset \Omega$ of n sites located in B. We will use the notation M_n, Y_n, and I_n instead of M_S, Y_S, and I_S, respectively, with

$$M_n = \max_{i=1,i\in S}^{n} P_i, \qquad I_n = \sum_{i=1,i\in S}^{n} P_i, \qquad Y_n = \max_{i=1,i\in S}^{n} \zeta_i. \quad (14)$$

Lemma 2. *Assume that $0 < R_{\min} < R_B < \infty$, that sites are uniformly distributed in B, and that the shadowing X_i follows a lognormal distribution of parameters $(0, \sigma_X)$. Then the cdf of the signal strength P_i received at the center of B from a site located in B is given by*

$$F_P(x) = c\Big\{a^{-2/\beta}G_1(x) - b^{-2/\beta}G_2(x) - e^{\nu}x^{-2/\beta}G_3(x) + e^{\nu}x^{-2/\beta}G_4(x)\Big\}, \quad (15)$$

where $a = AR_B^{-\beta}$, $b = AR_{\min}^{-\beta}$, $c = A^{2/\beta}(R_B^2 - R_{\min}^2)^{-1}$, $\nu = 2\sigma_X^2/\beta^2$, and G_j, $j = 1,\ldots,4$, refers to the cdf of a lognormal distribution of parameters (μ_j, σ_X), in which

$$\mu_1 = \log a, \qquad \mu_3 = \mu_1 + \frac{2\sigma_X^2}{\beta}, \qquad \mu_2 = \log b, \qquad \mu_4 = \mu_2 + \frac{2\sigma_X^2}{\beta}. \quad (16)$$

Proof. See Appendix A. □

Under the studied system model, $\{P_i, i = 1, 2, \ldots\}$ are independent and identically distributed (i.i.d.), and so the cdf F_{M_n} and probability density function (pdf) f_{M_n} of M_n are directly obtained as follows.

Corollary 2. *Under the conditions of Lemma 2, the cdf and the pdf of M_n are given, respectively, by*

$$F_{M_n}(x) = F_P^n(x), \quad (17)$$

$$f_{M_n}(x) = n f_P(x) F_P^{n-1}(x), \quad (18)$$

where $F_P(x)$ is given by (15)*, and f_P is the pdf of P_i, $f_P(x) = dF_P(x)/dx$.*

Since M_n is the maximum of i.i.d. random variables, we can also study its asymptotic properties by extreme value theory. Fisher and Tippett [9, Theorem 3.2.3] proved that under appropriate normalization, if the normalized maximum of i.i.d. random variables tends in distribution to a nondegenerate distribution H, then H must have one of the three known forms: Fréchet, Weibull, or Gumbel distribution. In the following, we prove that P_i belongs to the MDA of a Gumbel distribution. First of all, we establish the following result that is required to identify the limiting distribution of M_n.

Lemma 3. *Under the conditions of Lemma 2, the signal strength received at the center of B from a site located in B has the following tail equivalent distribution:*

$$\overline{F}_P(x) \sim \kappa \frac{\exp\left(-(\log x - \mu_2)^2/(2\sigma_X^2)\right)}{(\log x - \mu_2)^2/(2\sigma_X^2)} \quad (19a)$$

$$\sim \kappa \frac{2\sqrt{2\pi}\sigma_X \overline{G}_2(x)}{\log x - \mu_2}, \quad \text{as } x \longrightarrow \infty, \quad (19b)$$

where $\overline{G}_2(x) = 1 - G_2(x)$, and $\kappa = (\sigma_X/\sqrt{2\pi}\beta)(R_{\min}^2/(R_B^2 - R_{\min}^2))$.

Proof. See Appendix B. □

Equation (19b) shows that the tail distribution of the signal strength P_i is close to that of G_2, although it decreases more rapidly. The fact that G_2 determines the tail behavior of F_P is in fact reasonable, since G_2 is the distribution of the signal strength received from the closest possible neighboring site (with $b = AR_{\min}^{-\beta}$ and σ_X). The main result is given below.

Theorem 1. *Assume that $0 < R_{\min} < R_B < \infty$, that sites are uniformly distributed in B, and that shadowings are i.i.d. and follow a lognormal distribution of parameters $(0, \sigma_X)$ with $0 < \sigma_X < \infty$. Then there exists constants $c_n > 0$ and $d_n \in \mathbb{R}$ such that*

$$c_n^{-1}(M_n - d_n) \xrightarrow{d} \Lambda \quad \text{as } n \longrightarrow \infty, \quad (20)$$

where Λ is the standard Gumbel distribution:

$$\Lambda(x) = \exp\{-e^{-x}\}, \quad x \in \mathbb{R}, \quad (21)$$

and $\xrightarrow{d}$ represents the convergence in distribution. A possible choice of c_n and d_n is

$$c_n = \sigma_X (2\log n)^{-1/2} d_n,$$

$$d_n = \exp\left\{\mu_2 + \sigma_X\left(\sqrt{2\log n} + \frac{-\log\log n + \log\kappa}{\sqrt{2\log n}}\right)\right\}, \quad (22)$$

with κ given by Lemma 3.

Proof. See Appendix C. □

By Theorem 1, the signal strength belongs to the MDA of the Gumbel distribution, denoted by MDA(Λ). From [23, 24], we have the following corollary of Theorem 1.

Corollary 3. *Let σ_P^2 be the variance and μ_P be the mean of signal strength P_i. Let $\widetilde{I}_n = (I_n - n\mu_P)/(\sqrt{n}\sigma_P)$. Let $\widetilde{M}_n = (M_n - d_n)/c_n$, where c_n and d_n are given by* (22)*. Under the conditions of Theorem 1,*

$$\left(\widetilde{M}_n, \widetilde{I}_n\right) \xrightarrow{d} (\Lambda, \Phi) \quad \text{as } n \longrightarrow \infty, \quad (23)$$

where Λ is the Gumbel distribution and Φ the standard Gaussian distribution, and where the coordinates are independent.

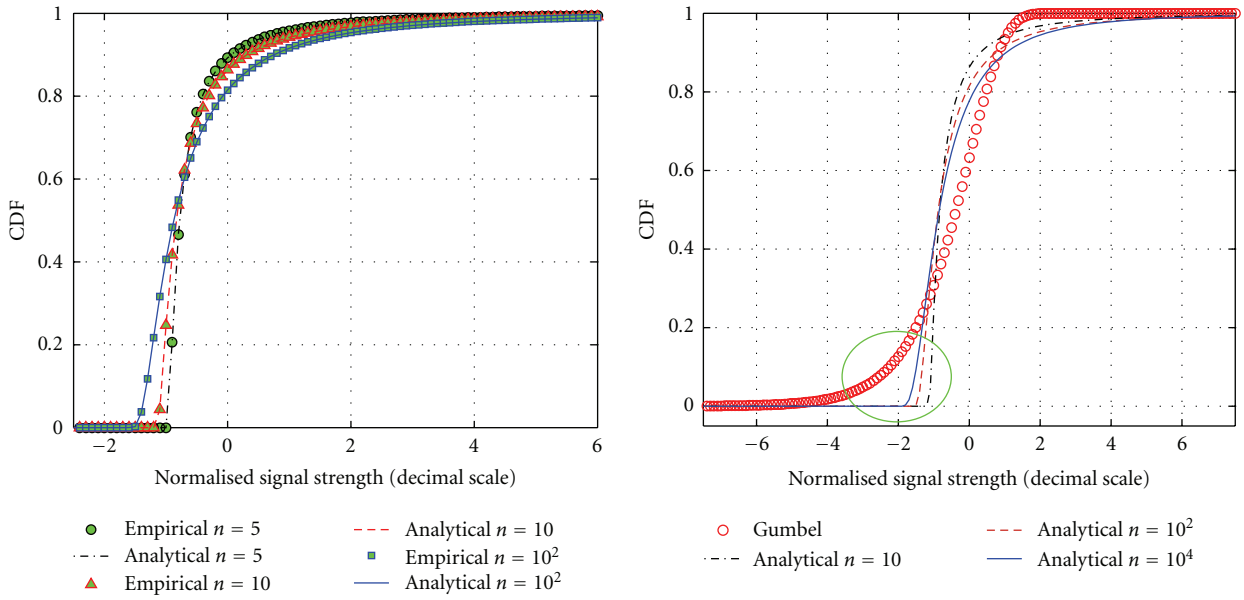

(a) Comparison between analytical and empirical CDFs

(b) Comparison between analytical and limiting CDFs

Figure 1: CDF of $\widetilde{M}_n$ under different n: $\sigma_{\text{dB}} = 8$, $\beta = 3$.

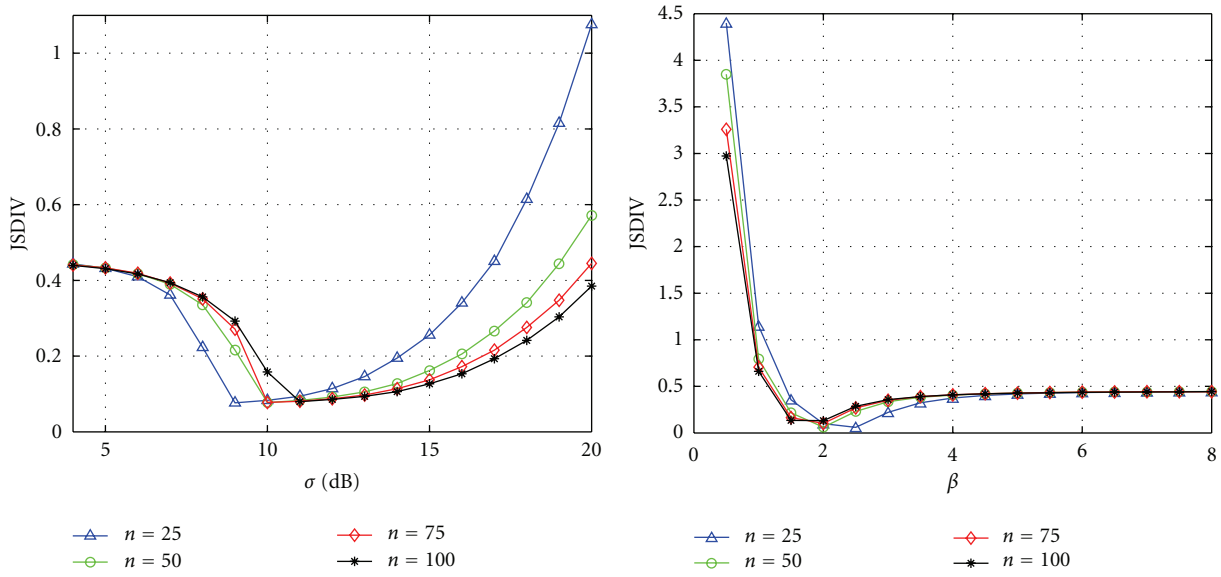

(a) Under different σ_{dB}: $\beta = 3$

(b) Under different β: $\sigma_{\text{dB}} = 8$

Figure 2: Jensen-Shannon divergence between $\widetilde{M}_n$ and Λ.

Proof. Conditions $0 < R_{\min}$ and $\sigma_X < \infty$ provide $\sigma_P^2 \leq \text{var}\{AR_{\min}^{-\beta} X_i\} < \infty$. Then the result follows by Theorem 1 and [23, 24]. □

Note that the total interference I can be written as $I = I_n + I_n^c$ where I_n^c denotes the complement of I_n in I. Under the assumptions that the locations of sites are independent and that shadowings are also independent, I_n and I_n^c are independent. The asymptotic independence between M_n and I_n thus induces the asymptotic independence between M_n and I. This observation is stated in the following corollary.

Corollary 4. *Under the conditions of Theorem 1, M_n and I are asymptotically independent as $n \to \infty$.*

This asymptotic independence facilitates a wide range of studies involving the total interference and the maximum signal strength. This result will be used in the coming

sub-section to derive the distribution of the best signal quality.

Remark 2. The asymptotic properties given by Theorem 1 and Corollaries 3 and 4 hold when the number of sites in *a bounded area* tends to infinity. This corresponds to a network densification process in which more sites are deployed in a given geographical area in order to satisfy the need for capacity, which is precisely the small cell setting.

3.2. Convergence Speed of Asymptotic Limits. Theorem 1 and Corollaries 3 and 4 provide asymptotic properties when $n \to \infty$. In practice, n is the number of cells to be scanned, and so it can only take moderate values. Thus, it is important to evaluate the convergence speed of (20) and (23). We will do this based on simulations and will measure the discrepancy using a symmetrized version of the Kullback-Leibler divergence (the so-called Jensen-Shannon divergence (JSdiv)).

Let us start with some numerical evaluations of the convergence of $\widetilde{M}_n$ to its limiting distribution. Figure 1(a) shows $F_{\widetilde{M}_n}$ for different n and compares to empirical simulation results. As expected the analytical distributions obtained by (17) of Corollary 2 match with the empirical distributions for all n. Figure 1(b) plots the analytical distribution and its limiting distribution, that is, the Gumbel distribution Λ. There is a discrepancy in the negative regime (see the circled region in Figure 1(b)). It is worth pointing out that as a maximum of signal strengths, $M_n \geq 0$ and thus $\widetilde{M}_n \geq -d_n/c_n = -\sqrt{2\log n}/\sigma_X$ since $\widetilde{M}_n = (M_n - d_n)/c_n$. This means that $F_{\widetilde{M}_n}(x) = 0$, $\forall x \leq -\sqrt{2\log n}/\sigma_X$, whereas $\Lambda(x) > 0$, $\forall x > -\infty$. This explains the gap observed for small n. This dissimilarity should have limited impact as long as we only deal with positive values of M_n (resp., $\widetilde{M}_n \geq -\sqrt{2\log n}/\sigma_X$).

We now study the symmetrized divergence between the analytical and limiting distributions of $\widetilde{M}_n$ for some moderate values of n and under different σ_{dB} and β. The convergence is best for σ_{dB} around 10 dB and β around two to four. For practical systems, σ_{dB} is approx. 8 dB and $2 < \beta \leq 4$. We compute the Jensen-Shannon divergence for $\beta = 3$ and $\sigma_{\text{dB}} = 8$ and plot the results in Figures 2(a) and 2(b), respectively. For these (and other) values (within the range given above) of σ_{dB} and β, $\widetilde{M}_n$, and Λ have low divergence.

Let us now measure the (dis)similarity between the empirical joint distribution, $\mathbf{P}\{\widetilde{M}_n \leq u, \widetilde{I}_n \leq v\}$, and the product of the empirical marginal distributions, $\mathbf{P}\{\widetilde{M}_n \leq u\} \times \mathbf{P}\{\widetilde{I}_n \leq v\}$. Figure 3 shows an example with $n = 50$, $\beta = 3$, and $\sigma_{\text{dB}} = 8$. We see that these two density functions are very similar. Figure 4 compares these two density functions for different values of σ_{dB} and β. Within the range defined above, the divergence between the two distributions is again small. Comparing Figure 2 and Figure 4, one can conclude that even if the convergence of $\widetilde{M}_n \xrightarrow{d} \Lambda$ remains slow, $\widetilde{M}_n$ and $\widetilde{I}_n$ quickly become uncorrelated. Thus, the independence between M_n and I_n holds for moderate values of n, that is,

$$f_{(M_n,I_n)}(u,v) \approx f_{M_n}(u) \times f_{I_n}(v), \tag{24}$$

and so the same conclusion holds for the independence between M_n and I.

3.3. Distribution of the Best Signal Quality. From the above results, we have the distribution of M_n and the asymptotic independence between M_n and I. In order to derive the distribution of the best signal quality, we also need the distribution of the total interference.

Lemma 4. *Assume that shadowings are i.i.d. and follow a lognormal distribution of parameters $(0, \sigma_X)$, $\beta > 2$, and that sites are distributed according to a Poisson point process with intensity λ outside the disk of radius $R_{\min} > 0$. Let I be the interference received at the disk center, and ϕ_I be the characteristic function of I. Then:*

(1)

$$\phi_I(w) = \exp\left\{-\pi\lambda\alpha(A|w|)^\alpha \int_0^{A|w|/R_{\min}^\beta} \frac{1-\phi_X(\text{sign}(w)t)}{t^{\alpha+1}}dt\right\}, \tag{25}$$

where $\alpha = 2/\beta$, and ϕ_X is the characteristic function of X_i;

(2) *$|\phi_I(w)|^p \in \mathbb{L}$ for all $p = 1, 2, \ldots$, where $\mathbb{L}$ is the space of absolutely integrable functions;*

(3) *If $AR_{\min}^{-\beta}$ is large, then ϕ_I admits the following approximation:*

$$\phi_I(w) \approx \exp\left(-\delta|w|^\alpha\left[1 - j\,\text{sign}(w)\tan\left(\frac{\pi\alpha}{2}\right)\right]\right), \tag{26}$$

where $\delta = \pi\lambda A^\alpha \exp((1/2)\alpha^2\sigma_X^2)\Gamma(1-\alpha)\cos(\pi\alpha/2)$, with $\Gamma(\cdot)$ denoting the gamma function.

Proof. See Appendix D. □

Theorem 2. *Under the assumptions of Lemma 4, let B be the ring of inner and outer radii $R_{\min}$ and R_B, respectively. Denote the best signal quality received at the center of B from n sites in B by Y_n. Assume that $0 < \sigma_X < \infty$, $0 < R_{\min} < R_B < \infty$, that $AR_{\min}^{-\beta}$ is large, and that $\pi\lambda(R_B^2 - R_{\min}^2) > n$, with high probability, where n is some positive integer. Then the tail distribution of Y_n can be approximated by*

$$\overline{F}_{Y_n}(\gamma) \approx \int_\gamma^\infty \left\{ f_{M_n}(u) \int_0^\infty \frac{2}{\pi w} e^{-\delta w^\alpha} \sin\left(w\frac{u-\gamma}{2\gamma}\right) \times \cos\left(wu + w\frac{u-\gamma}{2\gamma} - \delta w^\alpha \tan\frac{\pi\alpha}{2}\right) dw \right\} du. \tag{27}$$

Proof. See Appendix E. □

The approximation proposed in Theorem 2 will be used in Section 4 below. It will be validated by simulation in the context considered there.

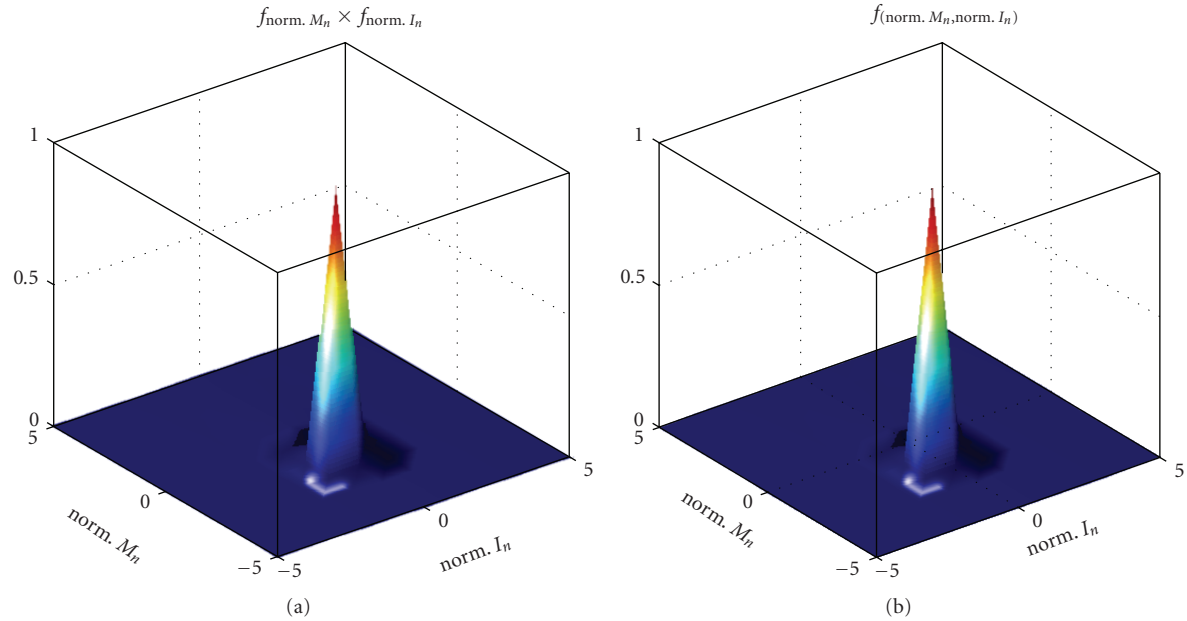

FIGURE 3: Example of joint densities of $\widetilde{M}_n$ and $\widetilde{I}_n$: $n = 50$, $\sigma_{\text{dB}} = 8$, $\beta = 3$. Here, norm. M_n refers to $\widetilde{M}_n$, while norm. I_n refers to $\widetilde{I}_n$.

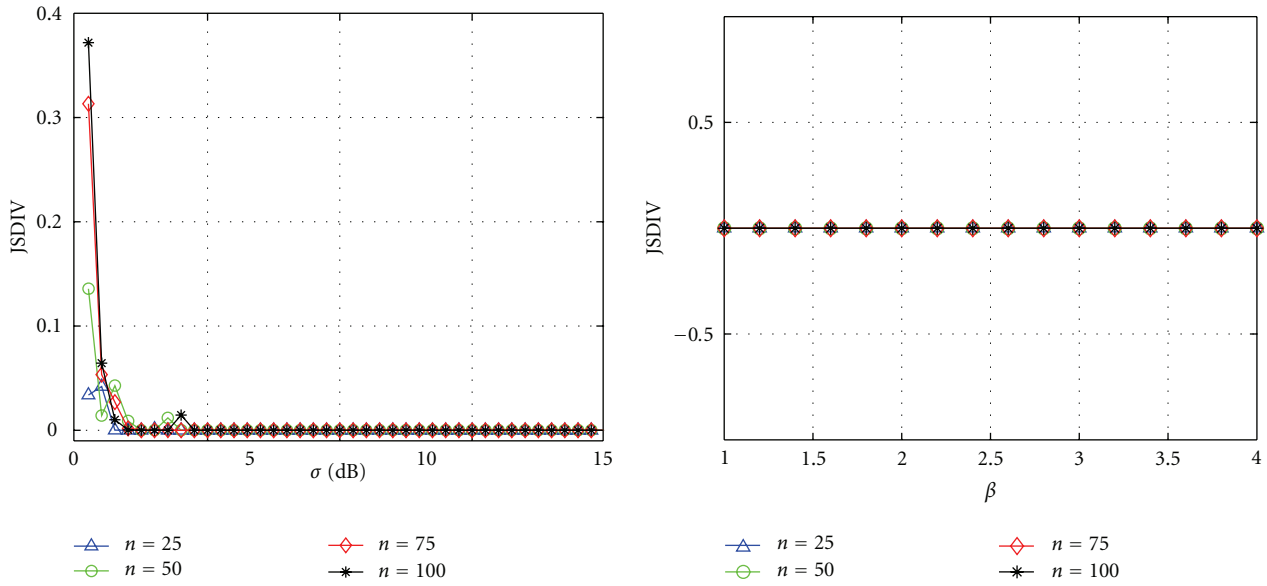

(a) Under different σ_{dB}: $\beta = 3$

(b) Under different β: $\sigma_{\text{dB}} = 8$

FIGURE 4: Jensen-Shannon divergence between $f_{(\widetilde{M}_n, \widetilde{I}_n)}$ and $f_{\widetilde{M}_n} \times f_{\widetilde{I}_n}$.

4. Random Cell Scanning for Data Services

In this section, the theoretical results developed in Section 3 are applied to random cell scanning.

4.1. Random Cell Scanning. Wideband technologies such as WiMAX, WCDMA, and LTE use a predefined set of codes for the identification of cells at the air interface. For example, 114 pseudonoise sequences are used in WiMAX [25], while 504 physical cell identifiers are used in LTE [26]. When the mobile knows the identification code of a cell, it can synchronize over the air interface and then measure the pilot signal quality of the cell. Therefore, by using a predefined set of codes, these wideband technologies can have more autonomous cell measurement conducted by the mobile. In this paper, this identification code is referred to as cell synchronization identifier (CSID).

In a dense small cell network where a large number of cells are deployed in the same geographical area, the mobile

can scan any cell as long as the set of CSIDs used in the network is provided. This capability motivates us to propose *random cell scanning* which is easy to implement and has only very few operation requirements. The scheme is detailed below.

(1) When a mobile gets admitted to the network, its (first) serving cell provides him/her the whole set of CSIDs used in the network. The mobile then keeps this information in its memory.

(2) To find a handover target, the mobile randomly selects a set of n CSIDs from its memory and conducts the standardized scanning procedure of the underlying cellular technology, for example, scanning specified in IEEE 802.16 [25], or neighbor measurement procedure specified in 3G [27] and LTE [12].

(3) The mobile finally selects the cell with the best received signal quality as the handover target.

In the following, we determine the number of cells to be scanned which maximizes the data throughput.

4.2. Problem Formulation. The optimization problem has to take into account the two contrary effects due to the number of cells to be scanned. On one hand, the larger the set of scanned cells, the better the signal quality of the chosen site, and hence the larger the data throughput obtained by the mobile. On the other hand, scanning can have a linear cost in the number of scanned cells, which is detrimental to the throughput obtained by the mobile.

Let us quantify this using the tools of the previous sections.

Let W be the average cell bandwidth available per mobile and assume that it is a constant. Under the assumption of additive white Gaussian noise, the maximum capacity ξ_n that the mobile can have by selecting the best among n randomly scanned cells is

$$\xi_n = W \log(1 + Y_n). \tag{28}$$

Hence

$$\begin{aligned} \mathbf{E}\{\xi_n\} &= W\mathbf{E}\{\log(1 + Y_n)\} \\ &= W \int_{\gamma=0}^{\infty} \log(1+\gamma) f_{Y_n}(\gamma) \mathrm{d}\gamma, \end{aligned} \tag{29}$$

where f_{Y_n} is the pdf of Y_n. By an integration by parts of $\log(1+\gamma)$ and $f_{Y_n}(\gamma)\mathrm{d}\gamma = -\mathrm{d}\overline{F}_{Y_n}(\gamma)$, this becomes

$$\mathbf{E}\{\xi_n\} = W \int_{\gamma=0}^{\infty} \frac{\overline{F}_{Y_n}(\gamma)}{1+\gamma} \mathrm{d}\gamma. \tag{30}$$

Note that $\mathbf{E}\{\xi_n\}$ is the expected throughput from the best cell. Since Y_n is the maximum signal quality of the n cells, Y_n increases with n and so does ξ_n. Hence, the mobile should scan as many cells as possible. However, on the other hand, if scanning many cells, the mobile will consume much time in scanning and thus have less time for data transmission with the serving cell. A typical situation is that where the scanning time increases proportionally with the number of cells scanned and where the data transmission is suspended. This for instance happens if the underlying cellular technology uses a *compressed mode* scanning, like for example, in IEEE 802.16 [25] and also inter-frequency cell measurements defined by 3GPP [12, 27]. In this mode, scanning intervals, where the mobile temporarily suspends data transmission for scanning neighbor cells, are interleaved with intervals where data transmission with the serving cell is resumed.

Another scenario is that of *parallel scanning-transmission*: here scanning can be performed in parallel to data transmission so that no transmission gap occurs; this is the case in, for example, intrafrequency cell measurements in WCDMA [27] and LTE [12].

Let T be the average time during which the mobile stays in the tagged cell and receives data from it. Let s be the time needed to scan one cell (e.g., in WCDMA, the mobile needs $s = 25$ ms if the cell is in the neighbor cell list and $s = 800$ ms if not [28], whereas in WiMAX, $s = 10$ ms, i.e., two 5-ms frames). Let $L(n)$ be the duration of the suspension of data transmission due to the scanning of the n cells:

$$L(n) = \begin{cases} s \times n & \text{if } \textit{compressed mode} \text{ is used,} \\ 0 & \text{if } \textit{parallel scan.-trans.} \text{ is enabled.} \end{cases} \tag{31}$$

Finally, let $\mathbf{E}\{\xi_0\}$ be the average throughput received from the serving cell when no scanning at all is performed (this would be the case if the mobile would pick as serving site one of the sites of set S at random).

The gain of scanning n cells can be quantified by the following metric, that we will call the *acceleration*

$$\begin{aligned} \rho_n &\triangleq \frac{T \cdot \mathbf{E}\{\xi_n\}}{T \cdot \mathbf{E}\{\xi_0\} + L(n) \cdot \mathbf{E}\{\xi_0\}} \\ &= \frac{T}{T + L(n)} \times \frac{\mathbf{E}\{\xi_n\}}{\mathbf{E}\{\xi_0\}}. \end{aligned} \tag{32}$$

In this definition, $T \cdot \mathbf{E}\{\xi_n\}$ (resp., $T \cdot \mathbf{E}\{\xi_0\} + L(n) \cdot \mathbf{E}\{\xi_0\}$) is the expected amount of data transmitted when scanning n cells (resp., doing no scanning at all). We aim at finding the value of n that maximizes the acceleration ρ_n.

It is clear that $T/(T + L(n)) = 1$ when (i) $T \to \infty$, that is, the mobile stays in and receives data from the tagged cell forever, or (ii) $L(n) = 0$, that is, parallel scanning-transmission is enabled. In these cases, ρ_n increases with n and the mobile "should" scan as many cells as possible. However, ρ_n is often concave and the reward of scanning then decreases. To characterize this, we introduce a *growth factor* g defined as follows:

$$g_n \triangleq \frac{\rho_n}{\rho_{n-1}} = \frac{T + L(n-1)}{T + L(n)} \times \frac{\mathbf{E}\{\xi_n\}}{\mathbf{E}\{\xi_{n-1}\}}. \tag{33}$$

Special cases as those considered above can be cast within a general framework which consists in finding the value of n that maximizes ρ_n under the constraint that $g_n \geq 1 + \Delta_g$, where $\Delta_g > 0$ is a threshold.

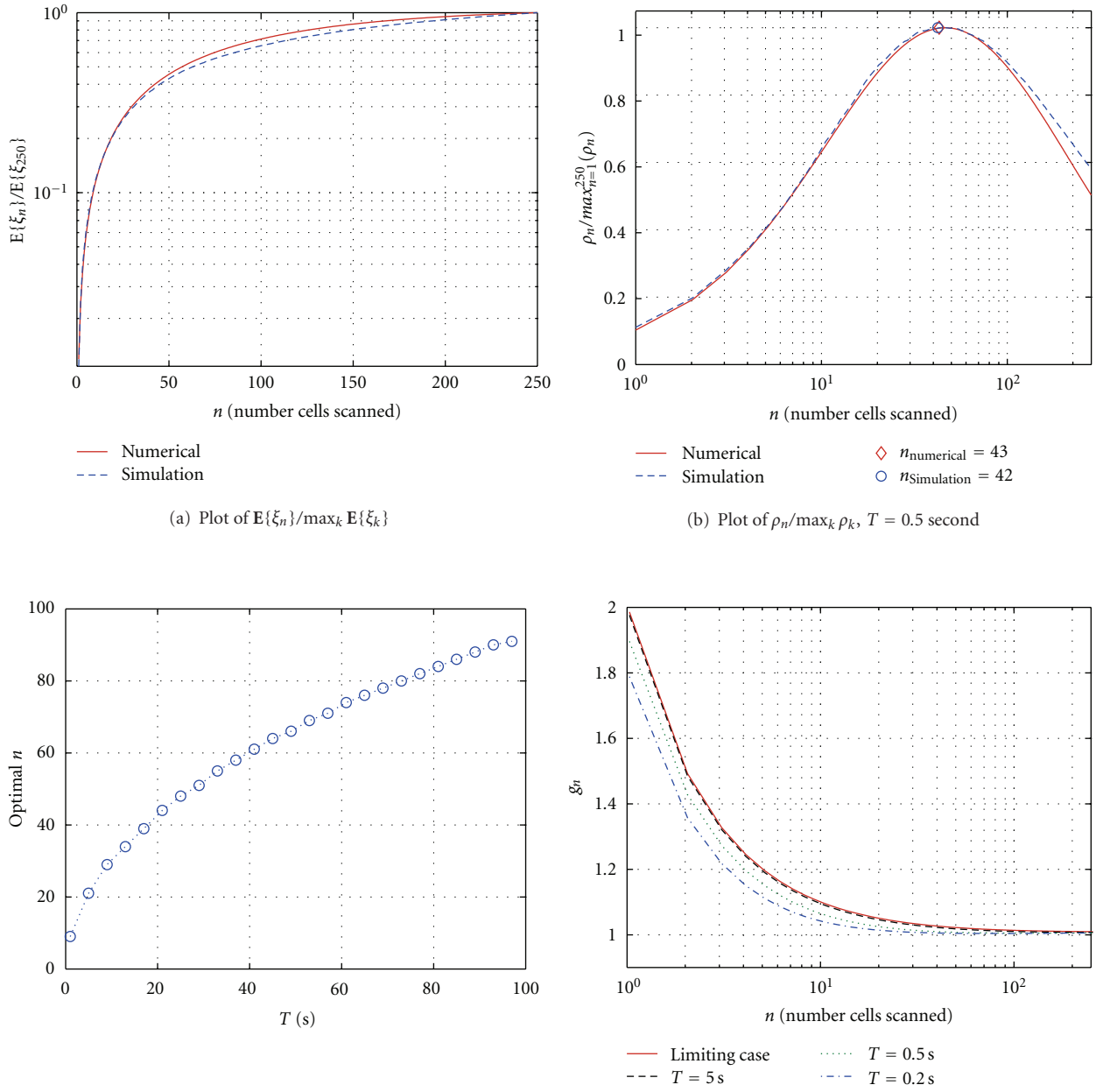

(a) Plot of $\mathbf{E}\{\xi_n\}/\max_k \mathbf{E}\{\xi_k\}$

(b) Plot of $\rho_n/\max_k \rho_k$, $T = 0.5$ second

(c) Optimal number of cells to be scanned

(d) Growth factor g_n under different T

FIGURE 5: Numerical results in the random cell scanning optimization.

4.3. Numerical Result. In the following, we show how to apply the above results to find the optimal n. We adopt WCDMA as the underlying cellular network technology. 100 omnidirectional small cell base stations are deployed in a square domain of 1 km × 1 km. The network density is thus equal to

$$\lambda = 10^{-4} \text{ small base stations/m}^2. \quad (34)$$

It is assumed that any cell synchronization identifier can be found in a radius $R_B = 1$ km. We take $R_{\min}$ equal to 2 meters. The propagation path loss is modeled by the picocell path loss model [29]:

$$PL_{[\text{dB}]}(d) = 37 + 30\log_{10}(d) + 18.3 f^{((f+2)/(f+1)-0.46)}, \quad (35)$$

where d is the distance from the base station in meters, f the number of penetrated floors in the propagation path. For indoor office environments, $f = 4$ is the default value [22]; however, here, the small cell network is assumed to be deployed in a general domain including outdoor urban areas where there are less penetrated walls and floors. So, we use $f = 3$ in our numerical study.

It is assumed that the total transmission power including the antenna gain of each small cell base station is $P_{\mathrm{Tx},[\mathrm{dBm}]} = 32\,\mathrm{dBm}$. Shadowing is modeled as a random variable with lognormal distribution with an underlying Gaussian distribution of zero mean and 8 dB standard deviation. The signal strength received at any distance d from a base station i is expressible as

$$P_{i,[\mathrm{dBm}]}(d) = P_{\mathrm{Tx},[\mathrm{dBm}]} - PL_{[\mathrm{dB}]}(d) + X_i^{\mathrm{dB}}. \tag{36}$$

By (35), we have

$$P_{i,[\mathrm{dBm}]}(d) = P_{\mathrm{Tx},[\mathrm{dBm}]} - 37 - 18.3 f^{((f+2)/(f+1)-0.46)} - 30\log_{10}(d) + X_i^{\mathrm{dB}}. \tag{37}$$

The parameters A and β appearing in $P_i = Ad^{-\beta}X_i$ can be identified from (37) after converting the received signal strength from the dBm scale to the linear scale:

$$\beta = 3, \qquad A_{[\mathrm{mW}]} = 10^{(P_{\mathrm{Tx},[\mathrm{dBm}]} - 37 - 18.3 f^{((f+2)/(f+1)-0.46)})/10}. \tag{38}$$

The received noise power N_0 is given by

$$N_{0,[\mathrm{mW}]} = k_{\mathrm{B}} T_{\mathrm{Kelvin}} \times NF_{[\mathrm{W}]} \times W_{[\mathrm{Hz}]} \times 10^3, \tag{39}$$

where the effective bandwidth $W_{[\mathrm{Hz}]} = 3.84 \times 10^6\,\mathrm{Hz}$, k_{B} is the Boltzmann constant, and T_{Kelvin} is the temperature in Kelvin, $k_{\mathrm{B}} T_{\mathrm{Kelvin}} = 1.3804 \times 10^{-23} \times 290\,\mathrm{W/Hz}$ and $NF_{[\mathrm{dB}]}$ is equal to 7 dB.

It is assumed that the mobile is capable of scanning eight identified cells within 200 ms [28]. So, the average time needed to scan one cell is given by $s = 25\,\mathrm{ms}$.

In order to check the accuracy of the approximations used in the analysis, a simulation was built with the above parameter setting. The interference field was generated according to a Poisson point process of intensity λ in a region between $R_{\min}$ and $R_\infty = 100\,\mathrm{km}$. For a number n, the maximum of SINR received from n base stations which are randomly selected from the disk B between radii $R_{\min}$ and R_B was computed. After that the expectation of the maximal capacity $\mathbf{E}\{\xi_n\}$ received from the n selected BSs was evaluated.

In Figure 5(a), the expectation of the maximal throughput $\mathbf{E}\{\xi_n\}$ for different n is plotted, as obtained through the analytical model and simulation. The agreement between model and simulation is quite evident. As shown in Figure 5(a), $\mathbf{E}\{\xi_n\}$ increases with n, though the increasing rate slows down as n increases. Note that in Figure 5(a), $\mathbf{E}\{\xi_n\}$ is plotted after normalization by $\mathbf{E}\{\xi_{250}\}$.

Figure 5(b) gives an example of acceleration ρ_n for $T = 0.5$ second and $L(n) = n \times 25$ ms. In the plot, ρ_n is normalized by its maximum. Here, an agreement between model and simulation is also obtained. We see that ρ_n first increases rapidly with n, attains its maximum at $n = 42$ by simulation and $n = 43$ by model, and then decays.

Next, using the model we compute the optimal number of cells to be scanned and the growth factor g_n for different T. Note that in (32), the factor $T/(T + L(n))$ can be rewritten as

$$\frac{T}{T + L(n)} = \frac{1}{1 + n \times s/T} \quad \text{for} \begin{cases} T < \infty, \\ L(n) = n \times s. \end{cases} \tag{40}$$

It is clear that this factor also depends on the ratio T/s. Figure 5(c) plots the optimal n for different values of T/s. Larger T/s will drive the optimal n towards larger values. Since T can be roughly estimated as the mobile residence time in a cell, which is proportional to the cell diameter divided by the user speed, this can be rephrased by stating that the faster the mobile, the smaller T and thus the fewer cells the mobile should scan.

Finally, Figure 5(d) plots the growth factor g_n with different T. In Figure 5(d), the "limiting case" corresponds to the case when $T \to \infty$ or $L(n) = 0$. We see that g_n is quite stable w.r.t. the variation of T. Besides, g_n flattens out at about 30 cells for a wide range of T. Therefore, in practice this value can be taken as a recommended number of cells to be scanned in the system.

5. Concluding Remarks

In this paper, we firstly develop asymptotic properties of the signal strength in cellular networks. We have shown that the signal strength received at the center of a ring shaped domain B from a base station located in B belongs to the maximum domain of attraction of a Gumbel distribution. Moreover, the maximum signal strength and the interference received from n cells in B are asymptotically independent as $n \to \infty$. The above properties are proved under the assumption that sites are uniformly distributed in B and that shadowing is lognormal. Secondly, the distribution of the best signal quality is derived. These results are then used to optimize scanning in small cell networks. We determine the number of cells to be scanned for maximizing the mean user throughput within this setting.

Appendices

A. Proof of Lemma 2

Let $d_i = |\mathbf{y} - \mathbf{x}_i|$ be the distance from a site located at $\mathbf{x}_i \in \mathbb{R}^2$ to a position $\mathbf{y} \in \mathbb{R}^2$. Under the assumption that site locations are uniformly distributed in B, the distance d_i from a site located in B, that is, $\mathbf{x}_i \in B$, to the center of B has the following distribution:

$$F_D(d) = \mathbf{P}[d_i \le d] = \frac{\pi d^2 - \pi R_{\min}^2}{\pi R_B^2 - \pi R_{\min}^2} = \frac{d^2 - R_{\min}^2}{R_B^2 - R_{\min}^2}. \tag{A.1}$$

Let $U_i = Ad_i^{-\beta}$, for $\beta > 0$, its distribution is equal to

$$F_U(u) = -c\left(u^{-2/\beta} - a^{-2/\beta}\right), \quad \text{for } u \in [a, b], \tag{A.2}$$

where $c = A^{2/\beta}(R_B^2 - R_{\min}^2)^{-1}$, $a = AR_B^{-\beta}$, and $b = AR_{\min}^{-\beta}$. The density of U_i is given by $f_U(u) = (2c/\beta)u^{-1-2/\beta}$.

Thus, the distribution F_P of the power P_i is equal to

$$F_P(x) = \int_{u=a}^{b} F_X\left(\frac{x}{u}\right) f_U(u)\mathrm{d}u. \tag{A.3}$$

Substituting F_X with lognormal distribution of parameters $(0, \sigma_X)$ and f_U given above into (A.3), after changing the variable such that $t = \log(x/u)$, we have

$$\begin{aligned} F_P(x) = \frac{c}{\beta} x^{-2/\beta} \Bigg(& \int_{\log(x/b)}^{\log(x/a)} e^{2t/\beta}\mathrm{d}t \\ & + \int_{\log(x/b)}^{\log(x/a)} e^{2t/\beta} \operatorname{erf}\left(\frac{t}{\sqrt{2}\sigma_X}\right)\mathrm{d}t \Bigg), \end{aligned} \tag{A.4}$$

where the first integral is straightforward. By doing an integration by parts of $\operatorname{erf}(t/\sqrt{2}\sigma_X)$ and $e^{2t/\beta}\mathrm{d}t$ for the second integral, we get

$$\begin{aligned} F_P(x) = \frac{c}{\beta} x^{-2/\beta} \frac{\beta}{2} \Bigg[& e^{2t/\beta} + e^{2t/\beta} \operatorname{erf}\left(\frac{t}{\sqrt{2}\sigma_X}\right) \\ & - e^{2\sigma_X^2/\beta^2} \operatorname{erf}\left(\frac{t}{\sqrt{2}\sigma_X} - \frac{\sqrt{2}\sigma_X}{\beta}\right) \Bigg] \Bigg|_{t=\log(x/b)}^{\log(x/a)}. \end{aligned} \tag{A.5}$$

After some elementary simplifications, we can obtain

$$\begin{aligned} F_P(x) = c \Bigg\{ & a^{-2/\beta} \left(\frac{1}{2} + \frac{1}{2} \operatorname{erf}\left(\frac{\log x - \mu_1}{\sqrt{2}\sigma_X}\right)\right) \\ & - b^{-2/\beta} \left(\frac{1}{2} + \frac{1}{2} \operatorname{erf}\left(\frac{\log x - \mu_2}{\sqrt{2}\sigma_X}\right)\right) \\ & + e^{\nu} x^{-2/\beta} \Bigg[-\frac{1}{2} - \frac{1}{2} \operatorname{erf}\left(\frac{\log x - \mu_3}{\sqrt{2}\sigma_X}\right) \\ & + \frac{1}{2} + \frac{1}{2} \operatorname{erf}\left(\frac{\log x - \mu_4}{\sqrt{2}\sigma_X}\right) \Bigg] \Bigg\}, \end{aligned} \tag{A.6}$$

where $\nu = 2\sigma_X^2/\beta^2$, $\mu_1 = \log a$, $\mu_3 = \mu_1 + 2\sigma_X^2/\beta$, $\mu_2 = \log b$, and $\mu_4 = \mu_2 + 2\sigma_X^2/\beta$. Let $G_j, j = 1, \ldots, 4$, be the lognormal distribution of parameters $(\mu_j, \sigma_X), j = 1, \ldots, 4$, F_P can be rewritten as (15).

B. Proof of Lemma 3

Let $\overline{G}_j(x) = 1 - G_j(x)$ and note that $c(a^{-2/\beta} - b^{-2/\beta}) = 1$, we have from (15)

$$\begin{aligned} F_P(x) = 1 - c \Big\{ & a^{-2/\beta} \overline{G}_1(x) - b^{-2/\beta} \overline{G}_2(x) \\ & - e^{\nu} x^{-2/\beta} \overline{G}_3(x) + e^{\nu} x^{-2/\beta} \overline{G}_4(x) \Big\}. \end{aligned} \tag{B.1}$$

This yields the tail distribution $\overline{F}_p = 1 - F_P$:

$$\begin{aligned} \overline{F}_p(x) = c \Big\{ & a^{-2/\beta} \overline{G}_1(x) - b^{-2/\beta} \overline{G}_2(x) \\ & - e^{\nu} x^{-2/\beta} \overline{G}_3(x) + e^{\nu} x^{-2/\beta} \overline{G}_4(x) \Big\}. \end{aligned} \tag{B.2}$$

For (B.2), we have $\overline{G}_j(x) = (1/2)\operatorname{erfc}\{(\log x - \mu_j)/(\sqrt{2}\sigma_X)\}$. An asymptotic expansion of $\operatorname{erfc}(x)$ for large x [30, 7.1.23] gives us:

$$\begin{aligned} \overline{G}_3(x) & \underset{\infty}{\sim} \frac{\sigma_X}{\sqrt{2\pi}(\log x - \mu_3)} \exp\left\{ -\frac{(\log x - \mu_3)^2}{2\sigma_X^2} \right\} \\ & = \frac{\sigma_X}{\sqrt{2\pi}(\log x - \mu_1 - 2\sigma_X^2/\beta)} \\ & \quad \times \exp\left\{ -\frac{(\log x - \mu_1 - 2\sigma_X^2/\beta)^2}{2\sigma_X^2} \right\} \\ & = \frac{\sigma_X a^{-2/\beta} e^{-\nu} x^{2/\beta}}{\sqrt{2\pi}(\log x - \mu_1)} \exp\left\{ -\frac{(\log x - \mu_1)^2}{2\sigma_X^2} \right\} \\ & \quad \times \frac{1}{1 - 2\sigma_X^2/\beta(\log x - \mu_1)}, \end{aligned} \tag{B.3}$$

in which after a Taylor expansion of the last term on the right-hand side, we can have

$$\begin{aligned} & e^{\nu} x^{-2/\beta} \overline{G}_3(x) \\ & \underset{\infty}{\sim} a^{-2/\beta} \left[\overline{G}_1(x) + \sqrt{\frac{2}{\pi}} \frac{\sigma_X^3}{\beta} \frac{\exp\left(-(\log x - \mu_1)^2/2\sigma_X^2\right)}{(\log x - \mu_1)^2} \right]. \end{aligned} \tag{B.4}$$

This implies that

$$\begin{aligned} & a^{-2/\beta} \overline{G}_1(x) - e^{\nu} x^{-2/\beta} \overline{G}_3(x) \\ & \underset{\infty}{\sim} -\sqrt{\frac{2}{\pi}} \frac{a^{-2/\beta}\sigma_X^3}{\beta} \frac{\exp\left(-(\log x - \mu_1)^2/2\sigma_X^2\right)}{(\log x - \mu_1)^2}. \end{aligned} \tag{B.5}$$

In the same manner, we have

$$\begin{aligned} & b^{-2/\beta} \overline{G}_2(x) - e^{\nu} x^{-2/\beta} \overline{G}_4(x) \\ & \underset{\infty}{\sim} -\sqrt{\frac{2}{\pi}} \frac{b^{-2/\beta}\sigma_X^3}{\beta} \frac{\exp\left(-(\log x - \mu_2)^2/2\sigma_X^2\right)}{(\log x - \mu_2)^2}. \end{aligned} \tag{B.6}$$

A substitution of (B.5) and (B.6) into (B.2) results in

$$\begin{aligned} \overline{F}_p(x) \underset{\infty}{\sim} \sqrt{\frac{2}{\pi}} \frac{c\sigma_X^3}{\beta} \Bigg\{ & b^{-2/\beta} \frac{\exp\left(-(\log x - \mu_2)^2/(2\sigma_X^2)\right)}{(\log x - \mu_2)^2} \\ & - a^{-2/\beta} \frac{\exp\left(-(\log x - \mu_1)^2/(2\sigma_X^2)\right)}{(\log x - \mu_1)^2} \Bigg\}. \end{aligned} \tag{B.7}$$

Moreover, $b > a$ yields $\mu_2 - \mu_1 = \log(b/a) > 0$. Then, we have the following result for large x:

$$\begin{aligned} & \frac{\exp\left(-(\log x - \mu_1)^2/2\sigma_X^2\right)/(\log x - \mu_1)^2}{\exp\left(-(\log x - \mu_2)^2/2\sigma_X^2\right)/(\log x - \mu_2)^2} \\ & = \left(\frac{\log x - \mu_2}{\log x - \mu_1}\right)^2 \exp\left(\frac{\mu_2^2 - \mu_1^2}{2\sigma_X^2}\right) x^{-(\mu_2 - \mu_1)/\sigma_X^2} \underset{x \to \infty}{\longrightarrow} 0. \end{aligned} \tag{B.8}$$

Taking this into account in (B.7), finally we have

$$\overline{F}_p(x) \underset{\infty}{\sim} \kappa \frac{\exp\left(-(\log x-\mu_2)^2/(2\sigma_X^2)\right)}{\left((\log x-\mu_2)/(\sqrt{2}\sigma_X)\right)^2} \underset{\infty}{\sim} 2\sqrt{2\pi}\sigma_X\kappa\frac{\overline{G}_2(x)}{\log x-\mu_2}, \quad \kappa=\frac{\sigma_X}{\sqrt{2\pi}\beta}\frac{R_{\min}^2}{R_B^2-R_{\min}^2}. \tag{B.9}$$

C. Proof of Theorem 1

We will use Lemma 3 and the following two lemmas to prove Theorem 1.

Lemma 5 (Embrechts et al. [9]). *Let Z_i be i.i.d. random variables having distribution F, and $\Psi_n = \max_{i=1}^n Z_i$. Let g be an increasing real function, denote $\widetilde{Z}_i = g(Z_i)$, and $\widetilde{\Psi}_n = \max_{i=1}^n \widetilde{Z}_i$. If $F \in MDA(\Lambda)$ with normalizing constant c_n and d_n, then*

$$\lim_{n\to\infty} \mathbf{P}\left(\widetilde{\Psi}_n \le g(c_n z + d_n)\right) = \Lambda(z), \quad z\in\mathbb{R}. \tag{C.1}$$

Lemma 6 (Takahashi [31]). *Let F be a distribution function. Suppose that there exists constants $\omega > 0$, $l > 0$, $\eta > 0$, and $r \in \mathbb{R}$ such that*

$$\lim_{x\to\infty}\frac{(1-F(x))}{(lx^r e^{-\eta x^\omega})} = 1. \tag{C.2}$$

For $\mu \in \mathbb{R}$ and $\sigma > 0$, let $F_* = F((x-\mu)/\sigma)$. Then, $F_* \in MDA(\Lambda)$ with normalizing constants $c_n^* = \sigma c_n$ and $d_n^* = \sigma d_n + \mu$, where

$$c_n = \frac{(\log n/\eta)^{1/\omega-1}}{\omega\eta}, \qquad d_n = \left(\frac{\log n}{\eta}\right)^{1/\omega} + \frac{\eta^{1/\omega}}{\omega^2}\frac{r(\log\log n-\log\eta)+\omega\log l}{(\log n)^{1-1/\omega}}. \tag{C.3}$$

Let $g(t) = e^{\sqrt{2}\sigma_X t+\mu_2}$ be a real function defined on $\mathbb{R}$, g is increasing with t. Let Q_i be the random variable such that $P_i = g(Q_i)$. By (19a) of Lemma 3, the tail distribution $\overline{F}_Q$ is given by

$$\overline{F}_Q(x) = \overline{F}_P\left(e^{\sqrt{2}\sigma_X x+\mu_2}\right) \sim \kappa x^{-2}e^{-x^2}, \quad \text{as } x\longrightarrow\infty. \tag{C.4}$$

By (C.4), F_Q satisfies Lemma 6 with constants $l = \kappa$, $r = -2$, $\eta = 1$, and $\omega = 2$. So, $F_Q \in \mathrm{MDA}(\Lambda)$ with the following normalizing constants:

$$c_n^* = \frac{(\log n/\eta)^{1/\omega-1}}{\omega\eta} = \frac{1}{2}(\log n)^{-1/2}, \qquad d_n^* = \left(\frac{\log n}{\eta}\right)^{1/\omega} + \frac{\eta^{1/\omega}}{\omega^2}\frac{r(\log\log n-\log\eta)+\omega\log l}{(\log n)^{1-1/\omega}} = (\log n)^{1/2} + \frac{1}{2}\frac{(-\log\log n+\log\kappa)}{(\log n)^{1/2}}. \tag{C.5}$$

Then, by Lemma 5, we have

$$\lim_{n\to\infty}\mathbf{P}(M_n \le g(c_n^* x + d_n^*)) = \Lambda(x), \quad x\in\mathbb{R}. \tag{C.6}$$

By a Taylor expansion of $\exp(\sqrt{2}\sigma_X c_n^* x)$, we have

$$\lim_{n\to\infty}\mathbf{P}\left\{e^{-(\sqrt{2}\sigma_X d_n^*+\mu_2)}M_n \le 1+\sqrt{2}\sigma_X c_n^* x + o(c_n^*)\right\} = \Lambda(x). \tag{C.7}$$

Since $c_n^* \to 0$ when $n\to\infty$, we have

$$\frac{M_n - e^{\sqrt{2}\sigma_X d_n^*+\mu_2}}{\sqrt{2}\sigma_X c_n^* e^{\sqrt{2}\sigma_X d_n^*+\mu_2}} \xrightarrow{d} \Lambda, \quad \text{as } n\longrightarrow\infty. \tag{C.8}$$

Substituting c_n^* and d_n^* from (C.5) into (C.8), we obtain c_n and d_n for (22). The conditions $R_{\max} < \infty$, $R_{\min} > 0$ and $\sigma_X > 0$ provide $\kappa > 0$. This leads to $d_n > 0$, and consequently, $c_n > 0$.

D. Proof of Lemma 4

Under the assumptions of the lemma, the interference field can be modeled as a shot noise defined on $\mathbb{R}^2$ excluding the inner disk of radius $R_{\min}$. Hence, using Proposition 2.2.4 in [20], the Laplace transform of I is given by

$$\mathcal{L}_I(s) = \exp\left\{-2\pi\lambda\int_{R_{\min}}^{\infty}\left(1-\mathbf{E}\left\{e^{-sAX_i/r^\beta}\right\}\right)r\,\mathrm{d}r\right\}. \tag{D.1}$$

Noting that

$$\phi_I(w) = \mathcal{L}_I(-jw), \quad w\in\mathbb{R}, \tag{D.2}$$

we have from (D.1) that

$$\phi_I(w) = \exp\left\{-2\pi\lambda\int_{R_{\min}}^{\infty}\left(1-\mathbf{E}\left\{e^{jwAX_i/r^\beta}\right\}\right)r\,\mathrm{d}r\right\}. \tag{D.3}$$

Using the change of variable $t = |w|Ar^{-\beta}$, we obtain

$$\int_{R_{\min}}^{+\infty}\left(1-\mathbf{E}\left\{e^{jwAX_i/r^\beta}\right\}\right)r\,\mathrm{d}r = \frac{(A|w|)^{2/\beta}}{\beta}\int_0^{A|w|/R_{\min}^\beta}\frac{1-\mathbf{E}\left\{e^{j\,\mathrm{sign}(w)tX_i}\right\}}{t^{2/\beta+1}}\mathrm{d}t, \tag{D.4}$$

where $\mathbf{E}\{e^{j\,\mathrm{sign}(w)tX_i}\} = \phi_X(\mathrm{sign}(w)t)$. So, substituting this into (D.3), we get the first part of the Lemma 4.

From (25), for all $p = 1, 2, \ldots$, we have

$$|\phi_I(w)|^p = \exp\left(-p\pi\lambda\alpha(A|w|)^\alpha\mathbf{E}\left\{\int_0^{A|w|/R_{\min}^\beta}\frac{1-\cos(tX_i)}{t^{\alpha+1}}\mathrm{d}t\right\}\right). \tag{D.5}$$

Since $1-\cos(tX_i)\ge 0$, $\forall t\in\mathbb{R}$, we have

$$\mathbf{E}\left\{\int_0^{A|w|/R_{\min}^\beta}\frac{1-\cos(tX_i)}{t^{\alpha+1}}\mathrm{d}t\right\} \ge 0. \tag{D.6}$$

Therefore

$$|\phi_I(w)|^p \le \exp(-c|w|^\alpha), \tag{D.7}$$

where c is some positive constant, and hence the right hand-side of this is an absolutely integrable function. This proves the second assertion of Lemma 4.

Under the assumption that $AR_{\min}^{-\beta} \approx \infty$, ϕ_I can be approximated by

$$\phi_I(w) \approx \exp\left(-\pi\lambda\alpha(A|w|)^\alpha \int_0^\infty \frac{1-\phi_X(\operatorname{sign}(w)t)}{t^{\alpha+1}}\mathrm{d}t\right). \tag{D.8}$$

For $0 < \alpha < 1$, we have

$$\begin{aligned}&\int_0^\infty \frac{1-e^{j\operatorname{sign}(w)tX_i}}{t^{\alpha+1}}\mathrm{d}t \\ &\quad = -\Gamma(-\alpha)\left|\operatorname{sign}(w)X_i\right|^\alpha e^{-j\operatorname{sign}(w)(\pi\alpha/2)}.\end{aligned} \tag{D.9}$$

Since $X_i \ge 0$, we can write $|\operatorname{sign}(w)X_i|^\alpha = X_i^\alpha$. Taking expectations on both sides, we get

$$\begin{aligned}&\int_0^{+\infty} \frac{1-\mathbf{E}\left\{e^{j\operatorname{sign}(w)tX_i}\right\}}{t^{\alpha+1}}\mathrm{d}t \\ &\quad = -\mathbf{E}\{X_i^\alpha\}\Gamma(-\alpha)e^{-j\operatorname{sign}(w)(\pi\alpha/2)} \\ &\quad = \mathbf{E}\{X_i^\alpha\}\frac{\Gamma(1-\alpha)}{\alpha}\cos\left(\frac{\pi\alpha}{2}\right)\left[1-j\operatorname{sign}(w)\tan\left(\frac{\pi\alpha}{2}\right)\right].\end{aligned} \tag{D.10}$$

Substituting this into (D.8) and noting that

$$\mathbf{E}\{X_i^\alpha\} = \exp\left(\frac{1}{2}\alpha^2\sigma_X^2\right), \tag{D.11}$$

for X_i lognormally distributed, we obtain (26).

E. Proof of Theorem 2

Under the assumption that sites are distributed as a homogeneous Poisson point process of intensity λ in B, the expected number of cells in B is $\pi\lambda(R_B^2 - R_{\min}^2)$. We assume that $\pi\lambda(R_B^2 - R_{\min}^2)$ is much larger than n, which ensures that there are n cells in B with high probability, so that Y_n is well defined.

Under the conditions of Theorem 2, M_n and I are asymptotically independent according to Corollary 4. So, by substituting (24) into (12), we have

$$\mathbf{P}\{Y_n \ge \gamma\} \approx \int_0^\infty f_{M_n}(u)\int_0^\infty h(v,u)f_I(v)\mathrm{d}v\,\mathrm{d}u, \tag{E.1}$$

where

$$\begin{aligned}h(v,u) &= 1_{(v\le(1+\gamma)u/\gamma-1)}1_{(v\ge u)} \\ &= \begin{cases}1 & \text{if } v \in \left[u, \dfrac{1+\gamma}{\gamma}u - 1\right],\ u > \gamma \\ 0 & \text{otherwise.}\end{cases}\end{aligned} \tag{E.2}$$

It is easily seen that $h(v,u)$ is square-integrable with respect to v, and its Fourier transform w.r.t. v is given by

$$\hat{h}\left(\frac{w}{2\pi},u\right) = \begin{cases}0 & \text{if } u \le \gamma, \\ \displaystyle\int_u^{((1+\gamma)/\gamma)u-1} e^{-jwv}\mathrm{d}v & \text{if } u > \gamma,\end{cases} \tag{E.3}$$

which yields:

$$\hat{h}\left(\frac{w}{2\pi},u\right) = \begin{cases}0 & \text{if } u \le \gamma, \\ \dfrac{1}{jw}\left(e^{-jwu} - e^{jw(1-((1+\gamma)/\gamma)u)}\right) & \text{if } u > \gamma.\end{cases} \tag{E.4}$$

Besides, according to Lemma 4 we have that $\phi_I \in \mathbb{L}$ and $\phi_I \in \mathbb{L}^2$, where $\mathbb{L}^2$ is the space of square integrable functions. And so, by Theorem 3 in [32, page 509], f_I is bounded continuous and square integrable. Hence, by applying the Plancherel-Parseval theorem to the inner integral of (E.1), we have

$$\int_0^\infty h(v,u)f_I(v)\mathrm{d}v = \int_{-\infty}^\infty \hat{h}(-w,u)\hat{f}_I(w)\mathrm{d}w, \tag{E.5}$$

where $\hat{f}_I(w)$ is the Fourier transform of $f_I(v)$. Take (E.4) into account for (E.5) and (E.1), we have

$$\overline{F}_{Y_n}(\gamma) = \int_\gamma^\infty \left\{f_{M_n}(u)\int_{-\infty}^\infty \hat{h}(-w,u)\hat{f}_I(w)\mathrm{d}w\right\}\mathrm{d}u, \tag{E.6}$$

where we further have

$$\begin{aligned}&\int_{-\infty}^\infty \hat{h}(-w,u)\hat{f}_I(w)\mathrm{d}w \\ &\quad = \frac{1}{2\pi}\int_{-\infty}^{+\infty}\hat{h}\left(-\frac{w}{2\pi},u\right)\hat{f}_I\left(\frac{w}{2\pi}\right)\mathrm{d}w \\ &\quad = \frac{1}{2\pi}\int_0^{+\infty}\left(\hat{h}\left(\frac{w}{2\pi},u\right)\hat{f}_I\left(\frac{-w}{2\pi}\right) + \hat{h}\left(\frac{-w}{2\pi},u\right)\hat{f}_I\left(\frac{w}{2\pi}\right)\right)\mathrm{d}w.\end{aligned} \tag{E.7}$$

Note that

$$\hat{f}_I\left(\frac{w}{2\pi}\right) = \phi_I(-w). \tag{E.8}$$

And under the assumption that $AR_{\min}^{-\beta} \approx \infty$, ϕ_I is approximated by (26). Thus, by (26) and (E.4), we have for $w \in [0,+\infty)$:

$$\begin{aligned}&\hat{h}\left(\frac{w}{2\pi},u\right)\hat{f}_I\left(-\frac{w}{2\pi}\right) \\ &\quad \approx \frac{e^{-\delta w^\alpha}}{jw}\left\{e^{j(-wu+\delta w^\alpha\tan(\pi\alpha/2))}\right. \\ &\qquad \left. - e^{-j(-w+w(((1+\gamma)/\gamma)u-\delta w^\alpha\tan(\pi\alpha/2))}\right\}, \\ &\hat{h}\left(-\frac{w}{2\pi},u\right)\hat{f}_I\left(\frac{w}{2\pi}\right) \\ &\quad \approx \frac{e^{-\delta w^\alpha}}{jw}\left\{-e^{-j(-wu+\delta w^\alpha\tan(\pi\alpha/2))}\right. \\ &\qquad \left. + e^{j(-w+w(((1+\gamma)/\gamma)u-\delta w^\alpha\tan(\pi\alpha/2))}\right\}.\end{aligned} \tag{E.9}$$

By (E.9), we get

$$\begin{aligned}
&\frac{1}{2\pi}\left[\hat{h}\left(\frac{w}{2\pi},u\right)\hat{f}_I\left(\frac{-w}{2\pi}\right)+\hat{h}\left(\frac{-w}{2\pi},u\right)\hat{f}_I\left(\frac{w}{2\pi}\right)\right]\\
&\quad\approx\frac{e^{-\delta w^\alpha}}{\pi w}\left[\sin\left(-wu+\delta w^\alpha\tan\frac{\pi\alpha}{2}\right)\right.\\
&\qquad\left.+\sin\left(-w+w\frac{1+\gamma}{\gamma}u-\delta w^\alpha\tan\frac{\pi\alpha}{2}\right)\right]\\
&\quad=\frac{2e^{-\delta w^\alpha}}{\pi w}\sin\left(w\frac{u-\gamma}{2\gamma}\right)\\
&\qquad\times\cos\left(wu+w\frac{u-\gamma}{2\gamma}-\delta w^\alpha\tan\frac{\pi\alpha}{2}\right).
\end{aligned}\tag{E.10}$$

Substitute the above into (E.7) and then into (E.6), we have (27).

References

[1] W. C. Y. Lee, "Smaller cells for greater performance," *IEEE Communications Magazine*, vol. 29, no. 11, pp. 19–23, 1991.

[2] H. Claussen, L. T. W. Ho, and L. G. Samuel, "Financial analysis of a pico-cellular home network deployment," in *Proceedings of the IEEE International Conference on Communications*, pp. 5604–5609, June 2007.

[3] V. Chandrasekhar, J. G. Andrews, and A. Gatherer, "Femtocell networks: a survey," *IEEE Communications Magazine*, vol. 46, no. 9, pp. 59–67, 2008.

[4] S. Saunders, S. Carlaw, A. Giustina, R. R. Bhat, V. S. Rao, and R. Siegberg, *Femtocells: Opportunities and Challenges for Business and Technology*, John Wiley & Sons, New York, NY, USA, 2009.

[5] A. Urie, "Keynote: the future of mobile networking will be small cells," in *Proceedings of the IEEE International Workshop on Indoor and Outdoor Femto Cells (IOFC '09)*, Tokyo, Japan, September 2009.

[6] Y. Chika, "Keynote: true BWA—eXtended Global Platform," in *Proceedings of the IEEE International Workshop on Indoor and Outdoor Femto Cells (IOFC '09)*, Tokyo, Japan, September 2009.

[7] P. Judge, *Vodafone Launches Home 3G Femtocell in the UK*, eWeekEurope, London, UK, 2009.

[8] M. R. Leadbetter, G. Lindgren, and H. Rootzén, *Extremes and Related Properties of Random Sequences and Processes*, Springer, New York, NY, USA, 1983.

[9] P. Embrechts, C. Klüppelberg, and T. Mikosch, *Modelling Extremal Events for Insurance and Finance*, Springer, New York, NY, USA, 1997.

[10] M. Nawrocki, H. Aghvami, and M. Dohler, *Understanding UMTS Radio Network Modelling, Planning and Automated Optimisation: Theory and Practice*, John Wiley & Sons, New York, NY, USA, 2006.

[11] WiMAX Forum, "Mobile System Profile," Approved Spec. Release 1.0, Revision 1.4.0, May 2007.

[12] 3GPP TS 36.331, "Evolved Universal Terrestrial Radio Access (EUTRA) Radio Resource Control (RRC): protocol Specification (Release 8)," Tech. spec. v8.8.0, December 2009.

[13] NGMN Alliance, "Next Generation Mobile Networks Use cases related to self-organising network, Overall description," Tech. Rep. v2.02, December 2008.

[14] NGMN Alliance, "Next Generation Mobile Networks Recommendation on SON and O&M requirements," Req. Spec. v1.23, December 2008.

[15] S. Magnusson and H. Olofsson, "Dynamic neighbor cell list planning in a micro cellular network," in *Proceedings of the Annual International Conference on Universal Personal Communications Record*, vol. 1, pp. 223–227, October 1997.

[16] R. Guerzoni, I. Ore, K. Valkealahti, and D. Soldani, "Automatic neighbor cell list optimization for UTRA FDD networks: theoretical approach and experimental validation," in *Proceedings of the Western Province Motor Club (WPMC '05)*, Aalborg, Denmark, 2005.

[17] D. Soldani and I. Ore, "Self-optimizing neighbor cell list for UTRA FDD networks using detected set reporting," in *Proceedings of the 65th IEEE Vehicular Technology Conference*, pp. 694–698, 2007.

[18] M. Amirijoo, P. Frenger, F. Gunnarsson, H. Kallin, J. Moe, and K. Zetterberg, "Neighbor cell relation list and measured cell identity management in LTE," in *Proceedings of the IEEE Network Operations and Management Symposium*, pp. 152–159, April 2008.

[19] M. Z. Win, P. C. Pinto, and L. A. Shepp, "A mathematical theory of network interference and its applications," *Proceedings of the IEEE*, vol. 97, no. 2, pp. 205–230, 2009.

[20] F. Baccelli and B. Błaszczyszyn, "Stochastic geometry and wireless networks volume 1: theory," *Foundations and Trends in Networking*, vol. 3, no. 3-4, pp. 249–449, 2009.

[21] 3GPP TR 36.942, "Evolved Universal Terrestrial Radio Access (EUTRA): Radio Frequency (RF) system scenarios (Release 8)," Tech. Rep. v8.2.0, May 2009.

[22] WiMAX Forum, "WiMAX systems evaluation methodology," Spec. v2.1, July 2008.

[23] T. Chow and J. Teugels, "The sum and the maximum of i.i.d. random variables," in *Proceedings of the 2nd Prague Symposium on Asymptotic Statistics*, pp. 81–92, 1978.

[24] C. W. Anderson and K. F. Turkman, "The joint limiting distribution of sums and maxima of stationary sequences," *Journal of Applied Probability*, vol. 28, no. 1, pp. 33–44, 1991.

[25] IEEE 802.16, "Air Interface for Broadband Wireless Access Systems," IEEE, Standard Std 802.16-2009, May 2009.

[26] 3GPP TS 36.300, "Evolved Universal Terrestrial Radio Access (EUTRA) and Evolved Universal Terrestrial Radio Access Network (EUTRAN)—Overall description: stage 2 (Release 8)," Tech. Spec. v8.11.0, December 2009.

[27] 3GPP TS 25.331, "Radio Resource Control (RRC): protocol Specification (Release 8)," Tech. Spec. v8.6.0, March 2009.

[28] 3GPP TS 25.133, "Requirements for support of Radio Resource Management FDD (Release 8)," Tech. Spec. v8.9.0, Dec. 2009.

[29] ETSI TR 101.112, "Selection procedures for the choice of radio transmission technologies of the UMTS," Tech. Rep. v3.2.0, April 1998.

[30] M. Abramowitz and I. A. Stegun, *Handbook of Mathematical Functions*, Dover, New York, NY, USA, 1965.

[31] R. Takahashi, "Normalizing constants of a distribution which belongs to the domain of attraction of the Gumbel distribution," *Statistics and Probability Letters*, vol. 5, no. 3, pp. 197–200, 1987.

[32] W. Feller, *An Introduction to Probability Theory and Its Applications*, vol. 2, John Wiley & Sons, New York, NY, USA, 2nd edition, 1971.